# A petrographic and geochemical study of mafic sills within the Transvaal Supergroup, east of the Bushveld Igneous Complex

**By**

**Thendo Netshidzivhe**




**Thesis presented in full fulfilment of the requirements for the degree of MSc Geology department, Earth Science, Stellenbosch University.**

**December 2017**

**Supervisor: Dr. Martin Klausen**

# DECLARATION

By submitting this thesis, I declare that the entirety of the work contained therein is my own original work under the supervision of Dr. Martin Klausen, and has not previously been submitted for any degree or examination for obtaining another qualification at any other university.

# Acknowledgements

My sincere and heartfelt gratitude goes to my Almighty God, for strengthening me throughout the duration of my MSc. This research was funded by the National Research Foundation (NRF) through a Grant to my supervisor, Dr. Martin Klausen whom I would like to express my deepest gratitude to, for mostly his patience, guidance, and supervision through this project until its completion, thank you for teaching me and encouraging me to understand everything and not merely take in things without fully understanding. I would also love to thank Dr. Klausen for his kindness, love for Geology and dedication to his work that is without limit. I'll like to extend my many thanks to the following people for their contribution to this project; Prof. Ulf Söderlund and his post-graduate students for teaching me everything I learnt about baddeleyite separation during my visit to his laboratory at Lund University (Sweden), Ashley Gumsley thank you for allowing me into your home during my stay in Lund and making sure I was comfortable for the duration of my visit, your hospitality is very much appreciated. Many thanks to my family (My siblings, Livha, Moses, Fhatuwani, Tshifhiwa, Ndidzu, Elekanyani, Hangwi and Hulisani) for your endless support, your love, encouragement and financial support. Many thanks to my Pastor Edwin Mukong and my prayer partner/bestfriend Ndivhuwo for all your encouragement and prayers when I needed them the most. To my amazing bestfriends/sisters Thendo Sigidi and Grace Maponya for their love and support, all the late nights in the post graduate lab while we were trying to put all our work together, and for being there for me without complaining. I would also like to thank my late parents (Hamilton and Matilda) for teaching me not to let anything discourage me and allowing me the opportunity to persevere in my studies before their departure.

# Abstract

The marginal sills that intruded into the Transvaal Supergroup have long been used to infer the parental magmas of the Rustenburg layered suite (RLS) due to their geochemical similarities which they share with the different zones of the RLS. New geochemical and petrographical data on mafic-ultramafic sills hosted within the sedimentary rocks across most of the Transvaal Supergroup, as well as below it (i.e., into the Archean basement) reveal a large group of 'boninitic norites' (BN) with primary mineral assemblage of euhedral orthopyroxene, subhedral plagioclase and interstitial plagioclase as well as tholeiitic dolerites (TDs) that have a primary mineral assemblage of euhedral plagioclase, clinopyroxene, and accessory Fe–Ti oxides. There are also some ultramafic sills that clearly formed through the accumulation of mainly olivine crystals, suggesting in situ fractional crystallisation within the sills. The slightly ultramafic and orthopyroxene-rich BN-sills are not believed to be cumulates, however, as testified by 'spinifex-textured' examples of similar compositions that may be regarded as quenched magmas.

In many cases both BN and TD type sill samples are severely altered or even metamorphosed into mainly amphibole-rich mineral assemblages (as well as serpentinized harzburgites), where normative calculations become the best way to interpret protolith modal compositions. It is not obvious to classify more altered/metamorphosed sills as being pre-Bushveld and more pristine samples as syn- to post-Bushveld, because local alteration, as opposed to regional contact metamorphism, may also have played a role.

Truly boninitic sills have relatively high MgO, Si, LREE and lower Fe-Ti and were emplaced throughout the sedimentary sequence, together with graphic quartz-feldspar dominated norites, which through their geochemistry are believed to have been more differentiated magmas within the same BN-suite. A comparison of geochemical signatures confirms a link between the BN rocks and the early B1 magmas of the Bushveld Complex. However, the wider stratigraphical distribution of BN sills argue against these clearly Bushveld related magmas to only have been injected from the large magma chamber that formed the RLS, but rather that many BN sills also were injected prior to the magma chamber's establishment as well as replenished it during the deposition of the RLS.

The geochemical characteristics of the tholeiitic dolerites (high Ti, low Si, Mg and LILE) do not match other proposed Bushveld-related B2 and B3 parental magmas, These TD sills also seem to cluster within the Silverton Formation, the Archean basement, as well as the Malmani Group (mainly cutting the Uitkomst Complex), and could therefore have formed during an entirely different magmatic event. A geochemical match suggests that most basement sills were fed by an intersecting Rykoppies dyke swarm, during the early deposition of the Wolkberg Group. A similar geochemical comparison cannot be made with overlying Transvaal Supergroup hosted lavas, where it seems plausible that many of the Silverton-hosted TD sills may have formed during the deposition of the Machadodorp Formation. However, geochemical similarities with the ~1.1 Ga Diabete dyke swarm also opens up for many of the TD suite being post-Bushveld (especially those that cut throughout the Uitkomst Complex).

# Table of content

# List of Figures

# 1 Introduction and purpose of the thesis

The Earth's history is marked by very large magmatic events where the mantle generated extremely large volumes of magma which then extruded onto the earth surface (Söderlund et al., 2016). According to Sheth (2007), the term Large Igneous Provinces (LIPs) should encompass all igneous provinces exposed over an area of >50000km$^2$, regardless of their composition and petrogenesis (independent of composition, tectonic setting or emplacement mechanism). However, Bryan and Ernst (2008) suggests a different classification criterion, they argue that using only the areal extent of igneous provinces will result in incorrect classifications. They suggest that in addition to the area of igneous provinces it is also important to look at their volumes, durations and the rates of emplacement, as well as geochemical signatures, which set LIP events apart from other igneous events on Earth. They continued to revise the definition of LIPs as follows: "Large Igneous Provinces are magmatic provinces with areal extents >0.1 Mkm$^2$, igneous volumes >0.1 Mkm$^3$ and maximum lifespans of ~50 Myr that have intraplate tectonic settings/geochemical affinities, and are characterised by igneous pulse(s) of short duration (~1–5 Myr), during which a large proportion (>75%) of the total igneous volume has been emplaced". They are dominantly mafic, but can also have significant ultramafic and silicic components, and some are dominated by silicic magmatism.

The current study is on the Bushveld igneous complex (BIC), which on the basis of its large volume and rapid emplacement is an excellent example of a LIP event, and may as such also be referred to as the Bushveld Large Igneous Province (BLIP). The BIC overall comprises an array of >30 magma bodies that were emplaced across most of the Kaapvaal Craton (KC). The estimated 65000 km$^3$ large Rustenburg Layered Suite (RLS) almost classifies as a LIP on its own, and this most dominant body is often referred to as the Bushveld Complex. The BIC is also compositionally bimodal, including felsic rocks such as 1) the Lebowa granite suite, which intruded above the RLS, 2) the Rashoop Granophyre Suite, which comprises both intrusive and metamorphic rocks along contacts between the Lebowa granite and the RLS, and 3) most lavas of the Rooiberg Group, known to have been an immediate precursor to the mafic intrusions of the RLS (Cawthorn et al., 2006).

This thesis will focus on the mafic-ultramafic part of the BIC, in order to make sense of how the accumulated dunites, pyroxenites, norites, gabbronorites and anorthosites to magnetite and apatite dominated diorites of the RLS relate to potential parental magmas preserved in its marginal zone, marginal sills and other satellite intrusions. Finally, the Paleoproterozoic emplacement age of the mafic parts of the BIC is now very precisely constrained through many U-Pb ages as emplaced between 2054 – 2058.9 ± 0.8 Ma, and thereby fulfil Bryan and Ernst's (2008) LIP-criteria. A compilation of all available good ages has already been done by, e.g., Rajesh et al., (2013) and Zeh et al., (2015) and a summary is provided below in table1.1.

Table 1.1: Compilation of available geochronological data from different rock units of the BLIP

| Age (Ma) | Method and location | Reference |
|---|---|---|
| 2015 ± 2.16 | Whole rock Rb-Sr isochron on lower zone marginal rocks | Harmer and Sharpe, 1985 |
| 2061 ± 2.7 | Mean Rb-Sr of Upper Zone | Walraven et al., 1990 |
| 2054.4 ± 1.8 | Nebo granites shrimp zircon age | Walraven and Hattingh, 1993 |
| 2055.6 ± 3.1 | SHRIMP method | de Waal and Armstrong, 2000 |
| 2058.9 ± 0.8 | Platreef precise U–Pb titanite age | Buick et al., 2001 |
| 2052 ± 6 | U–Pb zircon age marginal sill with B2-parentage | Curl, 2001 (unpublished thesis) |
| 2044 ± 8 | Uitkomst Complex, 207Pb/206Pb SHRIMP zircon age | de Waal et al.,2001 |
| 2054 ± 2 | Zircons and titanites from the Moshaneng granite | Mapeo et al., 2004 |
| 2054.8 ± 5.7 | Shrimp zircon $^{207}Pb/^{206}Pb$ dating of the spessartine Uitkomst | de waal et al., 2005 |
| 2054.8 ± 5.7 | Lindeques Drift | de Waal et al., 2005 |
| 2053.9 ± 9.2 | Roodekraal- quench-textured diorite, SHRIMP zircon 207Pb/206Pb | de Waal et al., 2005 |
| 2054.4 ± 1.4 | Zircon Concordia age of for the Merensky Reef in the lower-lying Critical Zone | Scoates and Friedman, 2008 |
| 2057.7 ± 1.6 | U–Pb Marginal Zone | Olsoon, 2010 |
| 2057 ± 1.6 | Marginal Zone | Olsson et al., 2010 |
| 2051 ± 9 Ma | Zircons from the Merensky Reef and the Upper Platreef located | Yudovskaya et al., 2013 |
| 2054.89 ± 0.37 | High-precision U–Pb geochronology on zircon | Zeh et al., 2015 |
| 2058.4 ± 1.3 | U–Pb baddeleyite ages from B-1 sills | Wabo et al., 2016 |
| 2054.5 ± 6.9 | U–Pb baddeleyite ages Uitkomst Complex | Wabo et al., 2016 |

## 1.1 Parental magmas

The study of igneous layered intrusions has over the years provided valuable insights into the processes of igneous differentiation through fractional crystallization as well as the formation of magmatic ore deposits. Apart from estimating melt compositions from the accumulating minerals' compositions, that these were in equilibrium with, as well as looking at incompatible element ratios, whose absolute concentrations depend on the proportion of interstitial melt remaining between accumulating crystals, it is difficult to estimate the parental magma compositions that gave rise to layered sequences, like Bushveld's RLS. Wager and Brown (1968) first proposed that repeated injections (replenishments) of a tholeiitic parental magma were responsible for generating the lower most zones of the RLS. Hamilton (1977) found that each zone of the layered suite was characterised by a different initial Sr isotopic ratios and this led him to propose that each zone could have been derived from an isotopically distinct parental magma.

Since then, BIC researchers have long been trying to identify the exact parental magma composition of the intrusion. Parent magma compositions of a layered intrusion are traditionally determined by the chemistry of chilled margins and associated sills (Frick, 1973) and dykes (Hoover 1989; Greenwood et al., 1990), that do not have any accumulated minerals like the RLS. Such samples also offer our best means to geochemically investigate how parental magmas formed in the first place as primary mantle-derived melts (i.e., petrogenesis), and thereby provide clues as to how/why entire LIPs, like the BIC/BLIP, formed (Barnes et al., 2010). As it is furthermore uncertain how such potential parental melts evolved and more or less mixed into a long-lived magma chamber; the cumulate mineral chemistry of any layer is still our best means of determining what magma compositions could potentially have replenished the magma chamber, while variations in cumulate mineral compositions provide our best means to constrain its evolution during fractional crystallisation and accumulation of the RLS.

Chill zone rocks are regarded as true estimators of the parental magma composition of any layered intrusions and, studying these would give a better insight because they represent the true composition of the magma that initially filled the magma chamber. However chilled margins are not always preserved as outcrops due to events such as chemical and thermal erosion of initial chills. It is also possible that such chill samples are poorly representative, due to local wall rock assimilation and in situ fractionation. Thus, more peripheral minor intrusions may become better representative, although it is often more difficult to confidently determine if any preserved marginal satellite intrusion is coeval, either through field relationships or, preferably, absolute ages. One main reason that has attracted researchers to study the mafic sills related to the BIC is their usefulness for estimating the compositions of the magmas that formed the RLS (Cawthorn et al., 1981; Sharpe, 1981; Harmer and Sharpe, 1985; Sharpe and Hulbert, 1985; Barnes et al., 2010). Since the RLS is so large, however, it is difficult to relate a sill (or other possible representative of a parental magma) to any specific stage in the evolution of the magma chamber, from which the accumulating crystals formed, let alone be certain that it was coeval with the BLIP.

## 1.2 Aims

As reviewed above, field relationships, petrography and geochemistry have previously been used to genetically link Transvaal Supergroup hosted sills to the BIC's RLS. Especially, their chemical compositions seem to be a more useful classification tool when the original petrography has been altered through weathering and/or metamorphism, and also provide more detailed trace element constraints on their magma petrogenesis (e.g., Barnes et al., 2010). The initial aims of this thesis were to fully present field relationships as well as petrographic, and geochemical characteristics of 85 mafic and ultramafic sills, as well as produce U-Pb baddeleyite ages on selected sills, from the Eastern Limb of the RLS in the Mpumalanga area. This is done in order to both intensify and expand on the previous study of these mafic sills and thereby hopefully contribute with new results and interpretations. However, while most of previous studies focused on the BIC's most proximally located marginal sills, this thesis also incorporates more distal sills that are hosted stratigraphically deeper into- and even below the Transvaal Supergroup.

More specifically, the first step will be to present and describe field observations, in order to constrain field relationships relative to the RLS and study any emplacement and crystallisation features, such as the stratigraphical distribution of different sill types and any indications of igneous layering or chills. Collected samples will then be described and classified petrographically, in order to study the primary crystallisation of these sills in even greater detail, as well as any secondary alteration. Finally, bulk rock compositions provide a means to further classify even altered rocks on the basis of both normative mineral proportions and different geochemical signatures. All of these results can then be used to 1) evaluate if the sampled sills belong to a previously identified B1-UM, B1, B2, B3 types (comparing to previously published data); 2) determine which types might belong to the same suite through differentiation and/or accumulation; 3) evaluate whether suites are coeval to the BIC; 4) discuss which suites could be parental to the RLS' different stratigraphical units; and finally 5) investigate how primary melts for the different suites may have been generated.

# 2 Geological setting

The ~3.60 to 3.10 Ga Kaapvaal Craton is one of the World's oldest and best preserved granite-greenstone cratonic terranes, and forms the basement of much of South Africa, Swaziland, Lesotho and parts of Botswana. It has been suggested that the amalgamation of its larger terrane blocks happened during continent-continent collisions at ~3.23 and 2.9 Ga along firstly the prominent ENE-WSW trending Barberton greenstone belt, then along the more northerly located Murchison-Thabazimbi suture zone, and final the N-S trending Colesberg lineament in the west (Anhaeusser, 2006). Subsequent to the craton's stabilisation it was eroded and covered by an almost complete Mesoarchean to Paleoproterozoic supracrustal record (Anhaeusser, 2006). These supracrustal sequences still cover ~85% of the Kaapvaal Craton and host numerous volcanic formations as well as mafic to ultramafic intrusions, which formed during several large magmatic events (e, g., Klausen et al., 2010). The emplacement of the BIC was arguably the most unusual and economically important of these magmatic events, intruding and extruding across much of the central parts of the craton. As no coeval feeder dykes have so far been identified, it is thought that much of the complex was fed by mantle-derived magmas along major trans-crustal shear zones (Zeh et al., 2015), including the Murchison Thabazimbi suture zone. The main RLS magma intruded into the alternating quartzite and shale formations of the Pretoria group (upper part of the Transvaal Supergroup). Current exposure of the RLS shows that it is characterized by 5 limbs, which are the far western limb, the western limb, the northern limb (where the Platreef is found), the Eastern Limb and the southeastern Bethal limb, the latter of which lies beneath Karoo sediments and is only known from borehole drilling (Eales, 2001).

## 2.1 The Rustenburg Layered Suite

The initial emplacement of parental magmas must have occurred within a relatively short time, in order for magmas to have remained molten, collect into such a large lopolith and accumulate such an extensive and thick RLS. Zeh et al., (2015) recently reported that the ~9 km thick cumulate pile of the RLS crystallized within ~1 Ma. During that time, magmas were emplaced as a large transgressive lopolith into a thick package of sedimentary rocks of the ~2.06 Ga old Transvaal Supergroup at a relatively shallow crustal level of <12 km (<0.4 GPa). It covers an area of 65,000 $km^2$ and preserves a volume of mafic-ultramafic rocks estimated to be ~600,000 $km^3$ (Eales and Cawthorn, 1996; Cawthorn and Walraven, 1998) and is partially surrounded by a chilled margin referred to as the Marginal Zone (MZ). Outside the MZ, there are pre- to syn-Bushveld sills (reviewed in more detail below) as well as cross cutting post–Bushveld dykes and sills (Willemse, 1969; Frick, 1973; Sharpe, 1981; Cawthorn et al., 1981). The MZ ranges in thickness from 0 to 800 m, and consists of medium-grained poorly layered norite with minor pyroxenites (Harmer and Sharpe 1985; Cawthorn and Walraven, 1998). Its transgressive and often scree-covered contact is mainly exposed against the Magaliesburg quartzite and in some places also the Vermont Formation of the Transvaal Supergroup. Along the Eastern Limb, at the well exposed Dwars Rivier Pass, intermingling pale noritic and dark pyroxenitic layers are complexly sheath folded (Clarke et al., 2005). Its pyroxenitic parts are characterised by quench-textured elongate orthopyroxes. The RLS is further subdivided into the following 4 major zones:

1) The Lower Zone (LZ) is primarily made up of chromite-bearing ultramafic cumulates, consisting of a Lower orthopyroxenitic (bronzitic) subzone (LLZ) and an Upper subzone (ULZ) with up to nine macrocyclic dunite (±chromite) – harzburgite – orthopyroxenite units (Cameron, 1978). Most orthocumulates typically have intercumulus plagioclase and/or clinopyroxene, as well as traces of sulphides. The rhythmic layering seen in this zone is most likely produced by at least nine repetitive magma replenishments (Kruger, 1992). Cawthorn et al (2006) agree with Teigler and Eales (1996), in that the top of the LZ coincides with its uppermost olivine-bearing unit, which also coincides with a major lowering of initial $^{87}Sr/^{86}Sr$ (Kruger, 1994).

2) The Critical Zone (CZ) is subdivided into a Lower Critical Zone (LCZ) and Upper Critical Zone (UCZ), marked by a first appearance of cumulus plagioclase and is

located at the base of the lowermost anorthositic layer of the RLS. Together with its lowermost pyroxenites, which some authors include in the LZ, the LCZ primarily contains orthopyroxenite cumulates with a thickness of ~800m, characterised by rare interbedded olivine bearing units as well as chromitite layers. Otherwise, the layering is not very pronounced within the predominantly orthopyroxenitic LCZ. From the first appearance of cumulus plagioclase at its base, modal layering becomes much more distinct up through the UCZ (Eales and Cawthorn, 1996). Thus there are many cyclic units of more or less complete chromitite – hartzburgite– orthopyroxenites – norite – anorthosite. Seven Lower Group, four Middle Group and two-three upper group chromite layers are more continuous and labelled within this zone. Amongst these, the PGE-rich UG2 is being mined, together with the pyroxenitic and PGE-rich Merensky Reef. The Merensky Reef is located close to the top of the CZ, as defined by the Bastard Reef's termination of the UCZ's cyclic layering.

3) Main Zone (MZ) is characterised by a complete absence of cumulate olivine and chromite, and constitute a massive sequence of poorly layered noritic and gabbroic rocks. The MZ is said to have accumulated from a final major magma recharge into the Bushveld magma chamber, as indicated by relatively constant $^{87}Sr/^{86}Sr$ up through the sequence (although lowered once at a lone pyroxenite marker near the top of the MZ). However, cryptic reversals of Mg# of pyroxene and anorthite contents of plagioclase have been recorded within this zone. Kruger (1994) reported that incompatible trace element ratios as well as initial Sr and Nd isotope composition of the MZ are dissimilar to that of the underlying orthopyroxene-dominated zones, and resemble that of a tholeiitic basalt rather than a high Mg andesitic basalt parent magma.

4) Upper Zone (UZ) forms the roof of the RLS which is consistent with its late saturation within Fe-enriched tholeiitic magmas. This is reflected by the introduction of cumulate magnetite (even as massive layers), the re-appearance of fayalitic cumulate olivines, as well as apatite-bearing quartz- diorites towards the top of the zone. There are between 20-30 thick monominerallic magnetitite layers, which could be explained by magma replenishment, even if there are no changes in $^{87}Sr/^{86}Sr$ (Tegner, 2006). The UZ is subdivided into three subzones, where UZb is defined by the accumulation of Fe-rich fayalite and UZc by the accumulation of apatite. The cumulate minerals

become Fe and Na-rich towards the top of the sequence, in consistence with the RLS representing a cumulate sequence that was primarily deposited from the bottom up.

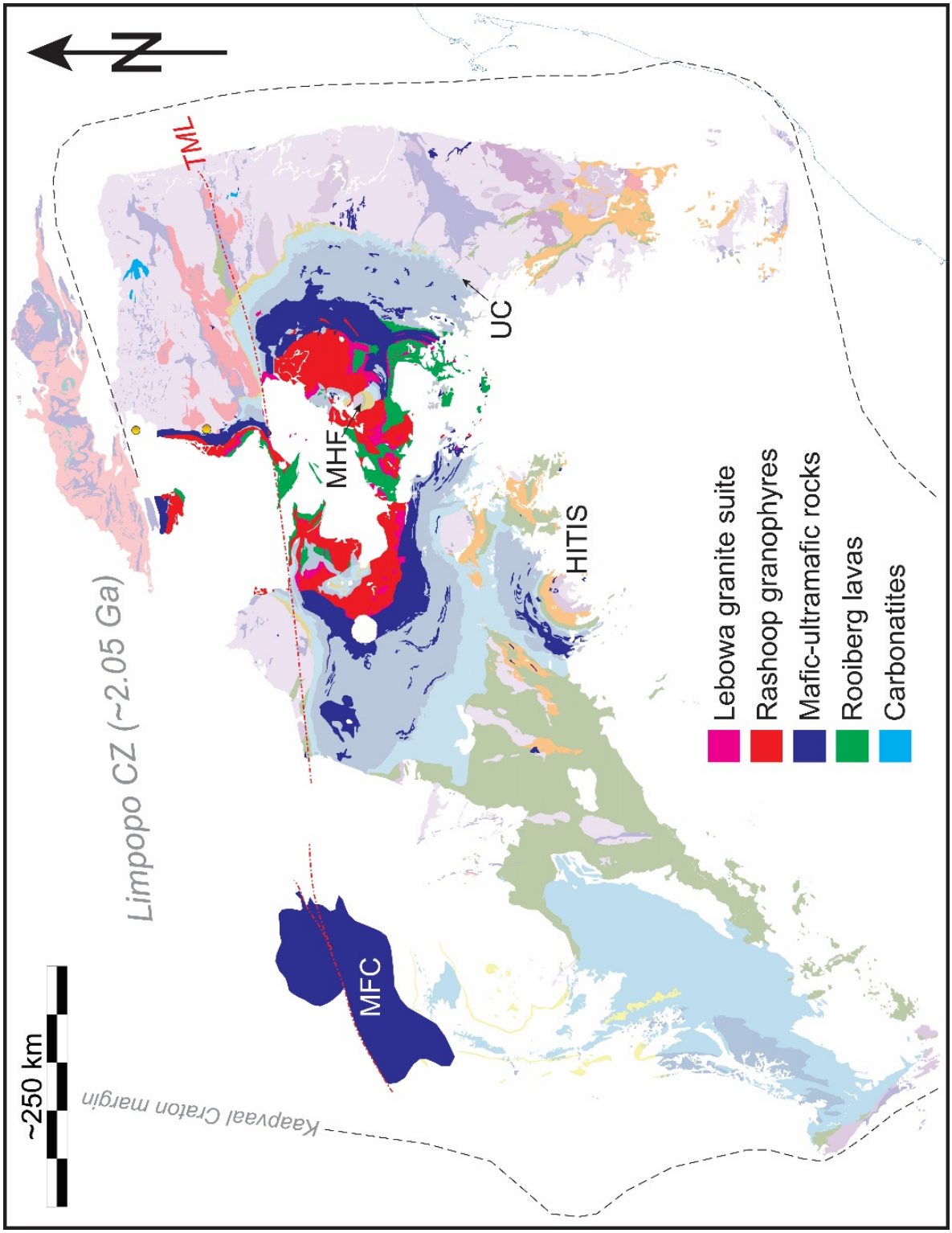


**Figure 2.1:** Geological map of the units that form the Bushveld Large Igneous Province that shows all exposed host rocks (undifferentiated), all units that are older than the BIC have been subdued 50%. The Thabazimbi-Murchison lineament (TML) is included along with the satellite intrusions reviewed in this thesis including Molopo Farms Complex (MFC), High Titanium Igneous Suites (HITIS), Marble Hall Formation (MHF) and Uitkomst Complex (UC).

## 2.2 Satellite intrusions

The BIC/BLIP incorporates a number of larger satellite complexes, formations and intrusions of similar age (Hall, 1932; Coetzee and Kruger, 1989), which include the Molopo Farms, Moshaneng, Okwa, Uitkomst, Roodekraal, Lindequesdrift, Rietfontein and Heideberg (cf., Fig 2.1 for locations). In this section, the 1) Uitkomst Complex; 2) Marble Hall Formation; 3) Molopo Farms Complex and 4) High Ti igneous intrusions around the Vredefort Dome (de waal et al., 2006; de waal et al.,2008) are described in more detail below.

### 2.2.1 Uitkomst Complex

The Uitkomst Complex is situated 20 km north of Badplaas, in the Mpumalanga Province of South Africa (Gauert et al., 1995). Its basal gabbro is the best candidate as Uitkomst's parental magma composition because it likely represents an early chilled magma to the basal gabbro cumulates (Gauert et al., 1998). This otherwise layered basic to ultrabasic complex formed from an intrusion into the basal sedimentary rock of the Transvaal Supergroup, between the Black Reef Quartzite Formation (floor) and the Timeball Hill Formation (roof). The Uitkomst complex is relatively well studied due to its Ni-rich massive to disseminated magmatic sulphide ore deposits, as well as chromite layers, mined since 1996. The Complex' 2054.5 ± 6.9 Ma (Wabo et al., 2016b) age is coeval with the RLS and could therefore have formed from similar parental magmas.

The Complex is according to Kenyon et al (1986) and Gauert et al (1995) subdivided into 1) a mineralized Basal Group, which is further subdivided into 3 lithological units, overlain by 2) a lower ultramafic and 3) an upper mafic layered sequence, as shown in Figure 2.2. The Basal Group has 3 lithological units, starting with 1) a basal gabbro that ranges between 0 and 15m in thickness, and is not always developed along the base of the complex. The basal gabbro is overlain by progressively more evolved cumulate zones, referred to stratigraphically as 2) a lower hartzburgite reaching thicknesses up to 50m, and 3) an upper chromitiferous hartzburgite averaging 60m in thickness.

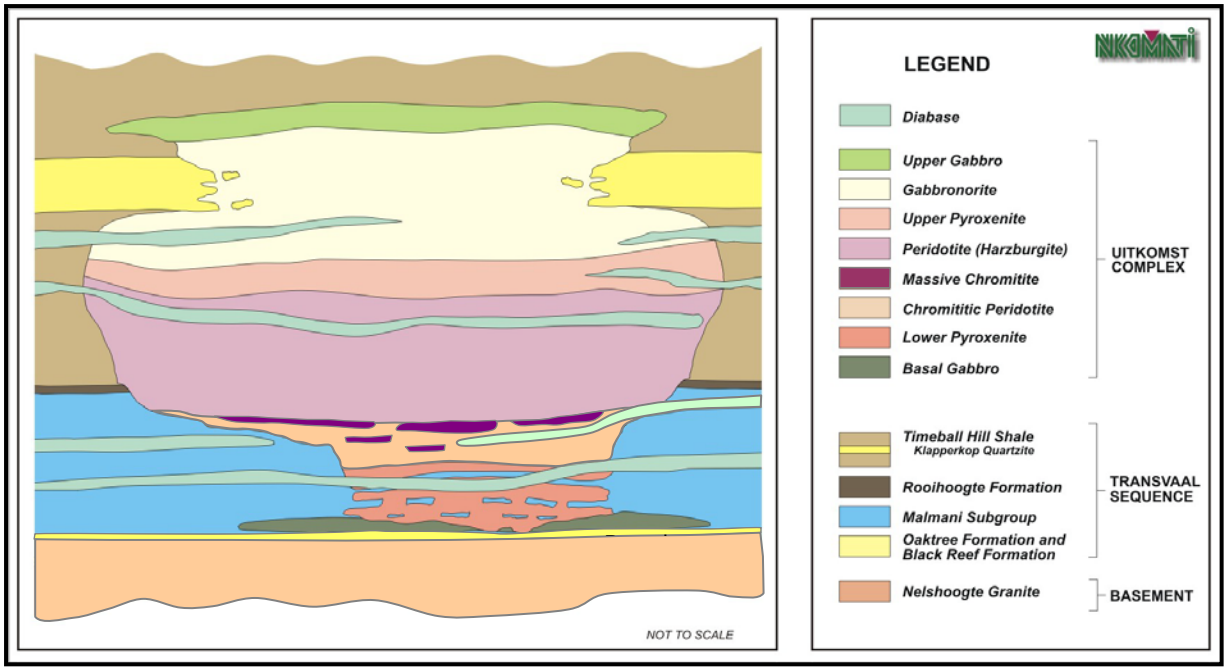


**Figure 2.2:** Schematic cross section through the layered Uitkomst Complex, hosted by basal sequences of the Transvaal Supergroup. Figure copied from an Nkomati Mine presentation in 2010. Note how the complex is cut by younger mafic sills, some of which were sampled for this thesis from a drill core, which included the basal gabbro.

Above the Basal Group, and separated by a 3 to 4 m thick massive chromitite layer, the ultramafic main group is made up of a lower < 330m thick main hartzburgite, and an upper ~ 60m thick pyroxenite, separated by a sharp contact. The upper pyroxenite is further subdivided into a lower olivine-orthopyroxenite subunit, overlain by an orthopyroxenite with accessory chromite and sulphide. The ultramafic main group is finally overlain by a 250m thick upper group of norite to gabbronorite rock units, which are made up of plagioclase, clinopyroxene and minor quartz. This is a phase layer transition between the ultramafic main group and the mafic upper group, as olivine disappears and plagioclase appears. Much less secondary alteration appears to have affected the gabbronorites, compared to Uikomst's more ultramafic rocks.

### 2.2.2 Marble Hall Formation

The Marble Hall Formation is situated 150km north east of Pretoria, near the town of Marble Hall, in the Mpumalanga Province of South Africa. From the study carried out by de Waal et al., 2008 they recorded a concordant zircon SHRIMP age for the Marble Hall sills to be 2055.6 ±3.1Ma as well as a 2053 ± 3.1 Ma age for some breccia's. The diorites are mainly sills that hosted within a large abducted(?) fragment of the

Transvaal Supergroup, which is entirely surrounded by medium- to coarse-grained Nebo Granite of the Lebowa Granite Suite (Snyman, 1958; de Waal, 1963; 1970), and are thereby comparable to the sills studied in this thesis. The high $Na_2O$, $K_2O$ and $TiO_2$ concentrations of the Marble Hall diorites, as well as enrichment in incompatible trace elements, are consistent with more evolved magmas ranging from olivine tholeiite to a mildly alkaline composition (de Waal and Armstrong, 2000).

### 2.2.3 The Molopo Farms Complex (MFC)

The Molopo Farms Complex is a large layered ultramafic/mafic intrusion which is located farthest west within the known extent of the BLIP, and covers a ~1300 $Km^2$ area across the border between South Africa and Botswana. It is emplaced close to the western margin of the Kaapvaal Craton and is almost completely covered by younger sedimentary rocks and desert dunes, including a Carboniferous to Triassic glacial valley of tillites and mudstone. Mainly drill core studies on the Complex has revealed lithologies that bear close resemblance to the Bushveld Complex. (Walker et al., 2010)

The complex consists of an ultramafic to mafic layered sequence that in many ways resembles the RLS (Cawthorn et al., 2008). Thus, the ultramafic lower sequence of the Molopo Farm Complex is also made up of cyclic layers of minor chromite-bearing dunites – hartzburgites – pyroxenites. The overlying mafic sequence (aka Main Zone) is dominated by plagioclase-rich norites, with minor intermittent modal layers of feldspathic pyroxenite. Geochemical results from a study done by Reichhardt (1994) include Ti/Zr ratios between 40 and 70 (average = 50) of both the ultramafic and mafic sequence, lying within the range determined for the BIC (Harmer and Sharpe, 1985).

Whole rock Rb-Sr dating of the complex gave an errorchron of ~2050 Ma, while Kruger (1989) obtained a mineral isochron age of 2044 ± 24 Ma (Coetzee and Kruger, 1989), which is within error of the Bushveld Complex emplacement. The lower part of the ultramafic sequence is characterised by an initial $^{87}Sr/^{86}Sr$ value of 0.703 to 0.705 followed by a sudden increase to 0.707, close to the base of the mafic sequence, which – much like BIC's LZ and LCZ – is then followed by a decrease toward the top of the ultramafic sequence (Harmer and Sharpe, 1985). These authors propose the involvement of two isotopically different parental magmas to explain this temporal isotopic variation; i.e., an early ultramafic melt with initial Sr ratios between 0.703 to

0.705 followed by a later mafic magma with initial 0.709 ratios that formed the overlying main zone (Sharpe, 1985).

### 2.2.4 High Titanium Igneous Suite (HITIS)

Small outcrops of mafic-felsic rocks are scattered across a ~20,000km$^2$ large area including intrusions along the exposed northern rim of the Vredefort impact structure. This wide distribution of rocks has been tentatively grouped into a single high-Ti igneous suite (HITIS), including the Marble hall diorites, basal gabbro unit of the Uitkomst Complex, the Lindeques drift, Heidelberg intrusions and volcanic Roodekraal Complex. de Waal and Armstrong (2000) found all of these intrusions to be syn-Bushveld. de waal et al., (2006), focusing on the Lindeques drift intrusion, Heidelberg intrusion and Roodekraal Complex, showed that the Lindeques drift intrusion is a ~150-200m thick and up to 11 km wide, semi-concordant and aphyric to porphyritic spessartine sill, that – like the Uitkomst Complex – is hosted by the Malmani dolomites of the Transvaal Supergroup. Shrimp zircon $^{207}Pb/^{206}Pb$ dating of the spessartine gave a 2054.8 ± 5.7 Ma age (de Waal et al., 2006) that is indistinguishable from the RLS, as well as the Uitkomst Complex.

The Roodekraal Complex is made up from a series of gabbroic outcrops that cover an area of ~12-15km$^2$, 10km south of Potchefstroom, which were emplaced uncomformably on top of tilted quartzites, shales and Hekpoort lavas of the Pretoria group, along unsheared intrusive contacts (de Waal et al.,2006). These intrusions are therefore also comparable to the sills studied in this thesis. Pseudotachylites, related to the slightly younger Vredefort impact event (2023 Ma; Kamo et al., 1996), cut through these rocks.

Within the Heidelberg district, the Heidelberg intrusion outcrops beneath 45m thick sedimentary cover rocks of the Karoo Supergroup, ~95km south of Pretoria. The intrusion is predominantly made up of spessartine (a hornblende-phyric lamprophyre, or appinite), which differ from the reviewed satellite intrusions, as well as any sills studied in this thesis.

Petrographically, most of the HITIS members have relatively similar mineralogies, where the primary magmatic phases are clinopyroxene, Fe-Ti oxides (magnetite-ilmenite), amphiboles, olivine, orthopyroxene, and plagioclase. Magnetites have lamellae and more irregular exsolutions of ilmenite, where the ilmenite content is found

to increase in more evolved rocks. de Waal et al (2008) concluded that the most primitive HITIS rocks might represent transitional to alkali basaltic parental Bu magmas, which due to the presence of igneous amphiboles must have been relatively volatile rich. Such alkali basic magmas also represent relatively low fraction mantle melts, which could still have been derived from the same source as that of the more subalkaline B3 magma of the Bushveld complex. 2054.8 ± 5.7 Ma and 2053.9 ± 9.2 Ma ages of both the Lindeques Drift and Roodekraal intrusion, respectively, are all indistinguishable from that of the Bushveld Complex. Marble Hall breccia is known from de Waal et al's (2002) study to contain B1 type Bushveld sill clasts enclosed in their HITIS matrix as xenoliths. If the B1 magma is parental to the Lower Zone, this field relationship is consistent with a younger 2053 ± 3.1 Ma emplacement age for these breccias and thereby possibly the HITIS as a whole.

## 2.3 Marginal sills within the Transvaal Supergroup

Marginal Zone rocks and adjacent marginal intrusions along the eastern and western lobes of the Bushveld Complex have been mapped and investigated over the past years by several geologists, Frick (1973), Engelbrecht (1990), and Sharpe (1981, 1984). These authors argue for the existence of several petrographically and geochemically distinct marginal rock types along with sills that have been proposed as different parental magmas for the RLS. Thus, Sharpe (1981) inferred that so-called B1, B2 and B3 type marginal sills, represent feeders/parents to the RLS' (1) LZ to LCZ, (2) UCZ, and (3) MZ, respectively. The very special B1 magma is siliceous yet Mg-rich, and regarded to represent the earliest parental magmas of the RLS (Zintwana and Wilson, 2012). This was followed by parental magmas that formed the overlying zones; namely, B2 magmas forming a plagioclase-bearing UCZ, characterised by more norites and anorthosites, and B3 magmas forming a MZ of even more noritic and gabbroic rocks, as well as even more iron rich gabbroic and dioritic parental magmas of the UZ. Barnes et al (2010) also noted that besides the mafic sills that intruded the Transvaal super group there are ultramafic sills with a B1 affinity, which they termed B1-UM magma sills that simply represent olivine cumulates from a B1 magma, rather than a magma type of its own.

Hall (1913) originally speculated on a genetic relationship between the BIC and marginal sills that intruded sedimentary host rocks of the Transvaal Supergroup. This

was after finding an abundance of diabase sills with petrographic similarities (probably noritic), which in South Africa is otherwise unusual outside the BIC. The Great Dyke is also noritic and maybe a few SE-trending 2.98 Ga dykes across the Badplaas area. Thus, finding noritic sills close to an orthopyroxenitic and noritic RLS would make you suspect a link, simply based on their proximity and orthopyroxene being a common essential mineral that is not as common in other mafic intrusions, outside the Bushveld Complex as well as the Great Dyke of Zimbabwe.

Willemse (1959, 1969) later subdivided these mafic marginal sills into two main types based on a mineralogical and petrochemical study. The first one he named the Lydenburg type, which is characterised by gabbroic rocks, where clinopyroxene often is metamorphosed under hornblende-hornfels conditions to hornblende. He regarded this type as a truly uncontaminated parent magmas of the Bushveld Complex. The other one he called a Maruleng type, characterised by noritic rocks where orthopyroxene is the dominant phase.

Frick (1973) mapped an area west of Dullstroom-Lydenburg and divided the sills that intruded the Pretoria group into dioritic and doleritic groups. He found that less evolved dolerite sills are more abundant inside his mapping area and these are characterised by the presence of olivine, clinopyroxene and plagioclase cumulates. Closer to the Bushveld complex the same dolerites, appear to be contact metamorphosed to greenschist facies.

Sharpe (1981) elaborated on previous sub-divisions by distinguishing between pre- and syn-Bushveld sills, as based upon further detailed field evidence, petrography and geochemistry. He also recognised that the original igneous textures of sill outcrops located closer to the Bushveld complex appear to be more altered, presumably due to a greater degree of contact metamorphism, a process that also makes classifications difficult. Accordingly, Sharpe (1981) proposed the following detailed classification scheme for either metamorphosed pre-Bushveld or more pristine syn-Bushveld sills.

### 2.3.1 Pre-Bushveld (PB) sills

According to Sharpe (1984), pre-Bushveld (PB) sills equate to the Lydenburg type sills of Willemse (1959). They are found to be abundant above the Vermont Formation and have a highly variable petrography that is characterised by an abundance of amphiboles at the expense of fresh pyroxenes, consistent with greenschist facies

metamorphism. Sharpe (1982) further identified 2 main sub-types of PB sills, depending on whether the dominant amphibole is either hornblende or tremolite.

Hornblende>Tremolite PB sills include lithologies ranging from pure amphibolites, characterised by blocky hornblende that may be penetrated by tremolite, to more evolved leuco-amphibolites with plagioclase, biotite and quartz. These sills were found to be concentrated above the Magaliesburg formation (Sharpe, 1982). Hornblende grains are mostly euhedral, exhibit distinct cleavages and have compositionally zoned margins. The group's many more evolved rocks contain micrographic intergrowths between quartz and feldspar. In some cases, a sub-ophitic pseudomorph texture may be discerned, typical for dolerites. Some of the amphibolitic sills contain 20-50% tremolite pseudomorphing orthopyroxene and rarely clinopyroxene.

Tremolite>hornblende PB sills are typically dominated by fibrous grains of tremolite replacing primary orthopyroxenes, through an alteration process that is referred to as tremolitization (Sharpe, 1984). These sills often have low modal proportions of interstitial plagioclase and are therefore more or less ultramafic. When the rock is completely altered into fibrous tremolite they give rise to a rock called a tremolitite.

### 2.3.2 Syn-Bushveld sills

All relatively pristine sills (i.e., with a considerable proportion of pyroxenes, as opposed to amphiboles) are tentatively considered as related to the BIC. As will be scrutinized further, syn-Bushveld sills can be subdivided depending on the lithology parentages; i.e., the so called noritic B1 and more gabbroic B2 and B3 groups. However, this is a somewhat genetic classification scheme that assumes certain magmas derived from, or replenished, an evolving magma chamber during the formation of the RLS. Thus according to Sharpe (1984), sills are better classified more objectively on the basis of their pristine igneous petrography into the following likely syn-Bushveld groups:

#### 2.3.2.1. Pyroxenites

These can be further subdivided into quench textured micropyroxenites, ultramafic sills, ordinary orthopyroxenites, as well as more evolved feldspathic orthopyroxenites subtypes.

Quench-textured micropyroxenites represents a very special rock type. It was first mentioned by Frick (1967), after he discovered some sills west of Lydenburg that are

characterised by the presence of euhedral orthopyroxene and plagioclase in a matrix of dark devitrified glass. Barnes et al (2010) identified similar sills, characterised by elongate orthopyroxene phenocrysts and plagioclase rosettes also in a devitrified glass matrix. Sharpe (1978) mapped a uniquely textured and so-called cone-bearing diabase sill, just above the Magaliesburg quartzites in the Dullstroom-Lydenburg district, which appear similar to the sills that Frick (1967) also discovered, but are locally made up of very elongate spinifex-like orthopyroxenes that he also interpreted as formed through quench-like crystallisation. Although this spinifex-like quench-type texture is not very micropyroxenitic, its larger pyroxene and plagioclase crystals are still set within a devitrified glass matrix. Davies et al., (1980) also discovered similar cone-type sills within the western part of the Transvaal Basin, underlying the western lobe of the BIC. They and Cawthorn et al (1979, 1981) showed that the composition of these sills were all similar and argue that their bulk rock compositions represent true (non-accumulated) parental magma compositions for the RLS. Compositionally zoned euhedral orthopyroxene and plagioclase phenocrysts in a matrix of devitrified glass seems to be the most common petrographical characteristic of this special subgroup of likely quenched pyroxenitic sills.

Orthopyroxenites, feldspathic and orthopyroxenites were all found by Sharpe (1982) to be common closer to volcanic rocks of the Machadodorp Formation, as well as within the Lakenvalei Formation quartzite. Two orthopyroxenitic varieties are common: One with long orthopyroxene grains; whereas, another has stubbier orthopyroxene prisms. Micrographic intergrowths of feldspar and quartz are common in the feldspathic pyroxenites and less so in the pyroxenites. Orthopyroxenes are rarely altered and no clinopyroxenes are found in these sills.

2.3.2.2. Noritic sills

The noritic sills are typically more altered and have even longer lath-shaped orthopyroxene grains than the pyroxenites. Interstitial quartz and plagioclase micrographic intergrowths are also more common, reflecting a more Si-rich magma (yet still also Mg-rich as evidenced by large modal proportions of orthopyroxenes) and thereby *qtz*-normative.

#### 2.3.2.3. Gabbronorite and gabbroic sills

These are rare and never exceed 20m in thickness. These sill types appear to be restricted within the Steenkampsberg formation, where the magmas typically intruded along its quartzite bedding planes. Plagioclase, clinopyroxene, orthopyroxene as well as some minor magnetite and ilmenite, make up the mineralogy of these sills. B2 and B3 types are typically identified amongst such gabbroic sills, which can be further subdivided petrographically into microgabbroic, gabbronorites associated with the UCZ (B2) and gabbros associated with the MZ (B3). The latter two have somewhat similar mineralogies, however, and are more confidently distinguished from each other on the basis of their whole rock geochemistry, where Mg#, $TiO_2$, $K_2O$ and $P_2O_5$ tends to be higher in B2 than B3 sills. B2 have LREE enrichment with smooth REE patterns (La/Sm of 2.5) and Gd/Lu of 1.6. B3 sills have low REE compared to B2 sills. (Sharpe, 1981 and Barnes et al., 2010). Gabbronorites are rarer and appear to be restricted within the Steenkampsberg formation where sills intruded along its quartzite bedding planes. Plagioclase, clinopyroxene, orthopyroxene as well as some minor magnetite and ilmenite, make up the mineralogy of these sills.

#### 2.3.2.4. Ultramafic sills

Ultramafic sills are rare and are mostly found in close proximity to the marginal zone. Willemse (1959) reported on the best known ultramafic sills known as the Burgersfort and Wildebeestkraal peridotite bodies as well as the Wimbledon sill. Most of these and other studied ultramafic sills (all restricted above the Magaliesburg quartzite) are dunites, hartzburgites and orthopyroxenites with interstitial plagioclase and minor quartz (Sharpe and Hulbert, 1985). Barnes et al (2010) suggest that their B1-UM sills intruded as olivine crystal slurries (ultramafic olivine: liquid ratio of ~40:60) injected into the country rocks from the LZ during syn-magmatic tectonism (Sharpe and Hulbert, 1985).

## 2.4 Past petrogenetic models for Bushveld's parental melts

Many different tectono-magmatic and petrogenetic models have been proposed for the BLIP, in order to explain the generation of such large volumes of mantle derived mafic parental magmas within a relatively short time, including its early and relatively unusual boninitic norite B1 parents. Thus, a mantle plume was proposed by Hatton

(1985), who from looking at previous studies of the Bushveld Complex such as that of Willemse (1959) or Wager and Brown (1968), noted that boninitic B1 magmas could represent very large degree komatiitic mantle melts that had assimilated a lot of continental crust (>40 %). This has been suggested due to the B1's relatively high MgO and $SiO_2$, as well as enriched high Sr and Pb isotopic ratios and high $K_2O$ contents of the rocks (Hamilton 1977; Harmer and Sharpe 1985). Hatton (1995) also emphasised other supporting features, including Sharpe's (1981) discovery of a radial distribution of intrusive centres and satellite bodies. Alternatively, a depleted sub-continental mantle harzburgite (providing high Mg compositions) with eclogite components (providing higher aluminium through the melting of garnet), in addition to asthenospheric mantle melts, could all have played a role in the genesis of BIC's parental magmas.

Olsson et al., (2010) looked at another radiating mafic dyke swarm (NE and SE trending) east of the Transvaal, which also radiates conspicuously from the eastern lobe of the BIC but which they dated to be 2.70 and 2.66 Ga (600 Ma prior to emplacement of the BIC). They, nevertheless, used this radiating swarm pattern to locate the centre of a Neoarchean mantle plume head which introduced magmas in large volumes into both the crust and the base of the lithosphere during the so-called Ventersdorp event. The density of its deeper mafic rocks increased due to metamorphism into eclogite as well as subsequent cooling, resulting in the subsidence of the cratonic lithosphere, allowing to the deposition of the Transvaal basin. Mantle lithosphere delamination finally occurred and resulted in an inflow and a rapid rise of hot asthenospheric mantle, which melted due to decompression and could be used to explain the production of the voluminous Bushveld magmas.

Harris et al., (2005) reported on $\delta^{18}O$ values from plagioclase, pyroxene and olivine of the RLS. Throughout the layered suite, the 7.1‰ to 1.4 ‰ values were higher than what should be expected of a mantle-derived magma (typically values around 5.3-5.7‰) and this is suggestive of the assimilation of crustal rocks that have experienced alteration by meteoritic water (i.e., close to the surface). As no systematic change in $\delta^{18}O$ value with stratigraphic height is recorded, Harris et al. (2005) suggested that the contamination took place in a 'staging chamber' prior to the emplacement into the 'present chamber'. The extensive crustal contamination proposed by Harris et al., 2005 becomes a problem when considering that it would require a considerable

amount of heat, which led them to support Barnes' (1989) proposal of a mantle-derived magma with a komatiitic composition.

In order to determine whether the BLIP formed in response to a typically more enriched plume or from a more depleted asthenospheric upper mantle, Zirakparvar et al., (2014) measured zircon Hf isotope compositions from intrusions that make up a part of the BLIP. They found that these intrusions all display homogeneous $\varepsilon Hf_{2.06\ Ga}$ values around zero (i.e., unradiogenic), leading them to believe that any typically more radiogenic plume could only have acted as a heat source, which melted a less radiogenic sub-continental lithospheric mantle (SCLM) source. This SCLM could have included eclogites from previously subducted and altered oceanic crust (e.g., during the Limpopo orogen), in order to also explain the mentioned high $\delta^{18}O$ values of BIC rocks. This might also be consistent with the high $SiO_2$ and MgO content of the B1 Bushveld magmas, which have boninitic affinities (Barnes, 1989).

# 3 Analytical methodology

## 3.1 Sampling and sample processing

In the Mpumalanga Province, a total of 85 igneous samples were collected from within the Transvaal super group by Dr Martin B. Klausen in 2007 (samples BCS1-1 to -39), 2014 (samples BCS2-1 to -53), as well as a recent resampling in June 2017 of some new BCS1 hand specimens. Table 4.1 shows a full sample list with coordinates (localities are also shown on Fig. 4.1) as well as processing, analytical and other details. A stratigraphically sorted list (from top to bottom) of representative and available field photos have also been compiled (together with Dr Klausen) into Appendix A1, to which more detailed maps and cross sections are also added, Important field relationships, compiled from Dr Klausen's field notes, photographs and personal communication, will otherwise be further described in Chapter 4.

All BCS2 samples were processed in Stellenbosch University, whereas 17 BCS1 samples were processed for an Honours project at UKZN and the remainder (18) for an Honours project at Stellenbosch (Soorajlal, 2013). All samples were processed in the same fashion at both UKZN and Stellenbosch, using similar jaw crushers and swing mills, as used for processing of BCS2 samples. In preparation of 49 BCS2 geochemical analyses, samples were cleaned and weathered/contaminated parts of the rocks were removed using a rock saw. Fist sized cut pieces were washed and dried before being crushed in a carbon steel jaw crusher. The bean-sized, crushed material was then quarter-and-cone split before a portion was pulverised in a carbon steel swing mill. In between every sample, the processing equipment was thoroughly brushed, washed with water, and tissue-dried with acetone. For the swing-mill, pure quartz was processed in the equipment between samples, in order to reduce all contamination to the common Si.

## 3.2 Slab scanning and thin sections

Approximately 1 cm thick rock slabs were cut from 18 BCS2- samples. These slabs were then scanned on a flatbed scanner in 600-1200 dpi resolution. The images were cut into 4x2.5 cm rectangles and auto-adjusted in Photoshop. This was only done for the BCS2 samples, however, until similar scans could be made from some resampled BSC1 samples, collected in June 2017. Selected rock slabs were cut into 4x2.5 cm

blocks that were sent to thin section laboratories at UKZN (BCS1- by Jele, 2007), who only made covered slides, and Rhodes University for BCS2-, who produced polished thin sections. Thin sections were then scanned with a ION FILM2SD PRO slide scanner and also auto-adjusted in Photoshop. Appendix A2 lists all available slab and thin section scans stratigraphically (from top to bottom), together with pie charts that show normative mineral proportions (based on major element geochemistry derived from whole rock XRF analyses, described below).

## 3.3 Whole rock geochemical analysis at Stellenbosch

All 49 BCS2-powders were analysed for whole rock geochemistry by the Central Analytical Facility of Stellenbosch University, using the following procedures.

### 3.3.1 XRF

Glass disks were prepared for XRF analysis using 7 g of high purity trace element and Rare Earth Element-free flux ($LiBO_2$ = 32.83%, $Li_2B_4O_7$ = 66.67%, LiI = 0.50%) mixed with 0.7g of the powder sample. Whole-rock major element compositions were determined by XRF spectrometry on a PANalytical Axios Wavelength Dispersive spectrometer at the Central of Analytical Facilities, Stellenbosch University, South Africa. The spectrometer is fitted with a Rh tube and with the following analyzing crystals: LIF200, LIF220, PE 002, Ge 111 and PX1. The instrument is fitted with a gas-flow proportional counter and a scintillation detector. The gas-flow proportional counter uses a 90% Argon-10% methane mixture of gas. Major elements were analyzed on a fused glass disk using a 2.4kW Rhodium tube. Matrix effects in the samples were corrected for by applying theoretical alpha factors and measured line overlap factors to the raw intensities measured with the SuperQ PANalytical software. The concentration of the control standards that were used in the calibration procedures for major element analyses fit the range of concentration of the samples. Amongst these standards were NIM-G (Granite from the Council for Mineral Technology, South Africa) and BE-N (Basalt from the International Working Group).

### 3.3.2 Laser Ablation ICP-MS

#### 3.3.2.1 Instrumental Set-up

For ICPMS-LA a Resonetics 193nm Excimer laser connected to an Agilent 7500ce ICP-MS is used in the analysis of trace elements in bulk rock samples. Ablation is performed in He gas at a flow rate of 0.35L/min, then mixed with argon ICPMS-LA (0.9L/min) and Nitrogen (0.004L/min) just before introduction into the ICP plasma. For traces in fusions, 2 spots of 173µm is ablated on each sample using a frequency of 10Hz and 100mJ energy.

#### 3.3.2.2 Sample preparation

Fusion disks used for XRF analysis were coarsely crushed and a chip of sample mounted along with up to 12 other samples in a 2.4cm round resin disk. The mount was mapped, and then polished for analysis.

#### 3.3.2.3 Quantification

Trace elements are quantified using NIST 612 for calibration and the % $SiO_2$ from XRF measurement as internal standard, using standard – sample bracketing. Two replicate measurements are made on each sample. The calibration standard was run every 12 samples. A quality control standard is run in the beginning of the sequence as well as with the calibration standards throughout. BCR-2 or BHVO 2G, both basaltic glass certified reference standards produced by USGS (Dr Steve Wilson, Denver, CO 80225), is used for this purpose. A fusion control standard from certified basaltic reference material (BCR-2, also from USGS) is also analysed in the beginning of a sequence to verify the effective ablation of fused material. Data was processed using Glitter software, distributed by Access Macquarie Ltd., Macquarie University NSW 2109.

## 3.4 Whole rock geochemical analysis at UKZN

Jele's (2008) major and trace elements were analysed at University of KwaZulu-Natal following the procedure mentioned below:

### 3.4.1 XRF

Fused discs of 18 Samples (Table 1) were analysed at the University of KwaZulu-Natal's School of Geological Sciences. All samples were analysed for major and trace

elements on a X-ray fluorescence sequential spectrometer (Phillips PW1410 XRF) with Rh, Au, Cr and Sc/Mo tubes and PET, LiF200 and PX-1 crystals. The XRF count data was analysed by a revised version of Norris and Hutton's (1969) software program. These results were calibrated against international standards BCR-1(Basalt), BHVO-1 (Basalt from the United States Geological Survey, Reston) and monitors (Klausen et al., 2010).

### 3.4.2 ICPMS

18 samples (Table1) were analysed on an inductively-coupled mass spectrometer (PerkinElmer 6100 ICP-MS), using the Anton-Paar microwave digestion system calibrated against standard solutions (Klausen et al., 2010; Wilson, 2003).

| Sample ID | Lat | Long | Formation | Thin Sections | Cut slabs? | Other information | Analytical lab used |
|---|---|---|---|---|---|---|---|
| BCS1-01 | 25.30718 | 30.24274 | Vermont | Cover glass | No | Picked pieces >30 baddeleyite picked | UKZN School of Geoscience |
| BCS1-02 | 25.29361 | 30.23451 | Vermont top | Cover glass | No | | UKZN School of Geoscience |
| BCS1-03 | 25.41095 | 30.02801 | Steenkampsberg | No | No | | UKZN School of Geoscience |
| BCS1-04 | 25.41399 | 30.04418 | Steenkampsberg | No | No | | CAF Stellenbosch University |
| BCS1-05 | 25.41314 | 30.11361 | Steenkampsberg base | No | No | | UKZN School of Geoscience |
| BCS1-06 | 25.21656 | 30.47304 | Daspoort | Cover glass | No | | UKZN School of Geoscience |
| BCS1-07 | 25.237 | 30.48501 | Daspoort | Cover glass | No | | UKZN School of Geoscience |
| BCS1-08 | 25.23749 | 30.49392 | Daspoort/Strubenkop | Cover glass | No | | UKZN School of Geoscience |
| BCS1-09 | 25.25273 | 30.51491 | Strubenkop | No | No | | CAF Stellenbosch University |
| BCS1-10 | 25.2722 | 30.52778 | Strubenkop | No | No | | CAF Stellenbosch University |
| BCS1-11 | 25.28037 | 30.52810 | Strubenkop | Cover glass | No | | UKZN School of Geoscience |
| BCS1-12 | 25.31239 | 30.53983 | Strubenkop base | No | No | | CAF Stellenbosch University |
| BCS1-13 | 25.38229 | 30.44211 | Strubenkop | No | No | Picked pieces from crushed material, no baddeleyites found | CAF Stellenbosch University |
| BCS1-14 | 25.38515 | 30.43179 | Strubenkop | Cover glass | No | | UKZN School of Geoscience |
| BCS1-15 | 25.3853 | 30.42987 | Strubenkop | Cover glass | No | | UKZN School of Geoscience |

| | | | | | | | |
|---|---|---|---|---|---|---|---|
| BCS1-16 | 25.386 | 30.42870 | Strubenkop | Cover glass | No | Picked pieces from crushed material, 22 baddeleyites found | UKZN School of Geoscience |
| BCS1-17 | 25.38913 | 30.42596 | Strubenkop | No | No | | CAF Stellenbosch University |
| BCS1-18 | 25.38701 | 30.42168 | Strubenkop | No | No | | UKZN School of Geoscience |
| BCS1-19 | 25.3866 | 30.41408 | Strubenkop | No | No | | CAF Stellenbosch University |
| BCS1-20 | 25.39105 | 30.41174 | Strubenkop | No | No | | CAF Stellenbosch University |
| BCS1-21 | 25.39368 | 30.40917 | Strubenkop | No | No | Picked pieces from crushed material, 20 baddelyites found | CAF Stellenbosch University |
| BCS1-25 | 25.38796 | 30.40499 | Strubenkop | Cover glass | No | | UKZN School of Geoscience |
| BCS1-26 | 25.38795 | 30.40463 | Strubenkop | Cover glass | No | | UKZN School of Geoscience |
| BCS1-27 | 25.38189 | 30.40327 | Strubenkop | No | No | | CAF Stellenbosch University |
| BCS1-28 | 25.37811 | 30.39425 | Strubenkop | Cover glass | No | | UKZN School of Geoscience |
| BCS1-29 | 25.38054 | 30.38752 | Strubenkop | No | No | | CAF Stellenbosch University |
| BCS1-30 | 25.25703 | 30.37373 | Silverton | No | No | | CAF Stellenbosch University |
| BCS1-31 | 25.26669 | 30.37638 | Strubenkop | Cover glass | No | | CAF Stellenbosch University |
| BCS1-32 | 25.24709 | 30.39925 | Strubenkop | Cover glass | No | | UKZN School of Geoscience |
| BCS1-33 | 25.05313 | 30.69032 | Timeball(Klapperkop) | No | No | | CAF Stellenbosch University |
| BCS1-34 | 25.05674 | 30.69532 | Timeball(Klapperkop) | Cover glass | No | | CAF Stellenbosch University |
| BCS1-35 | 25.06724 | 30.70250 | Timeball(Klapperkop) | No | No | | CAF Stellenbosch University |
| BCS1-36 | 25.0665 | 30.70550 | Timeball(Klapperkop) | No | No | | CAF Stellenbosch University |
| BCS1-37 | 25.06648 | 30.70795 | Timeball(Klapperkop) | Cover glass | No | | CAF Stellenbosch University |

| | | | | | | | |
|---|---|---|---|---|---|---|---|
| BCS1-38 | 25.08498 | 30.71078 | Timeball | No | No | Picked pieces from crushed material, no baddeleyites found | CAF Stellenbosch University |
| BCS1-39 | 25.08885 | 30.72535 | Rooihoogte | Polished | No | | CAF Stellenbosch University |
| BCS2-01 | 25.2853 | 30.32852 | Silverton | No | yes | | CAF Stellenbosch University |
| BCS2-02 | 25.28745 | 30.32849 | Silverton | No | yes | | CAF Stellenbosch University |
| BCS2-03 | 25.29046 | 30.32902 | Silverton | No | yes | 2 slabs used, no baddeleyite found | CAF Stellenbosch University |
| BCS2-04 | 25.28844 | 30.32725 | Silverton | No | yes | 2 slabs used, no baddeleyite found | CAF Stellenbosch University |
| BCS2-05 | 25.28844 | 30.32725 | Silverton | No | yes | | CAF Stellenbosch University |
| BCS2-06 | 25.28829 | 30.32703 | Silverton | No | yes | | CAF Stellenbosch University |
| BCS2-07 | 25.28514 | 30.32540 | Silverton | No | yes | | CAF Stellenbosch University |
| BCS2-08 | 25.28485 | 30.32405 | Silverton | No | yes | | CAF Stellenbosch University |
| BCS2-09 | 25.28239 | 30.32443 | Silverton | No | yes | | CAF Stellenbosch University |
| BCS2-10 | 25.27481 | 30.32253 | Magaliesberg | No | yes | | CAF Stellenbosch University |
| BCS2-11 | 25.2758 | 30.32376 | Magaliesberg/Silverton | Polished | yes | | CAF Stellenbosch University |
| BCS2-12 | 25.29409 | 30.29446 | Magaliesberg | Polished | yes | | CAF Stellenbosch University |
| BCS2-13 | 25.29409 | 30.29446 | Magaliesberg | Polished | yes | | CAF Stellenbosch University |
| BCS2-14 | 25.28499 | 30.28443 | Vermont | No | yes | | CAF Stellenbosch University |
| BCS2-15 | 25.28718 | 30.27983 | Vermont | No | yes | | CAF Stellenbosch University |
| BCS2-16 | 25.28832 | 30.27829 | Vermont | Polished | yes | | CAF Stellenbosch University |
| BCS2-17 | 25.28929 | 30.27334 | Vermont | No | yes | | CAF Stellenbosch University |
| BCS2-18 | 25.3014 | 30.27247 | Vermont | No | yes | | CAF Stellenbosch University |
| BCS2-19 | 25.30058 | 30.26715 | Vermont | No | yes | | CAF Stellenbosch University |
| BCS2-20 | 25.29992 | 30.26397 | Vermont | No | yes | | CAF Stellenbosch University |
| BCS2-21 | 25.29962 | 30.26355 | Vermont | No | yes | | CAF Stellenbosch University |
| BCS2-22 | 25.29911 | 30.26170 | Vermont | Polished | yes | | CAF Stellenbosch University |
| BCS2-23 | 25.29823 | 30.26113 | Vermont | No | yes | 2 cut slabs used, no baddeleyite found | CAF Stellenbosch University |

| | | | | | | | |
|---|---|---|---|---|---|---|---|
| BCS2-24 | 25.29734 | 30.25525 | Vermont | Polished | yes | | CAF Stellenbosch University |
| BCS2-25 | 25.29372 | 30.25212 | Vermont | No | yes | | CAF Stellenbosch University |
| BCS2-26 | 25.08784 | 30.76263 | Malmani(Chuniespoort) | Polished | yes | 2 cut slabs used, no baddeleyite found | CAF Stellenbosch University |
| BCS2-29 | 25.03514 | 30.90267 | Sill | Polished | yes | | CAF Stellenbosch University |
| BCS2-30 | 25.01882 | 30.92979 | Sill | No | yes | | CAF Stellenbosch University |
| BCS2-31 | 25.00999 | 30.93002 | Sill | Polished | yes | | CAF Stellenbosch University |
| BCS2-32 | 25.00325 | 30.92450 | Sill | Polished | yes | | CAF Stellenbosch University |
| BCS2-33 | 24.98708 | 30.92962 | Sill | No | yes | | CAF Stellenbosch University |
| BCS2-34 | 24.97929 | 30.93383 | Sill | No | yes | | CAF Stellenbosch University |
| BCS2-35 | 24.91364 | 30.94154 | Sill | Polished | yes | | CAF Stellenbosch University |
| BCS2-36 | 24.85750 | 30.95634 | Dyke | No | yes | | CAF Stellenbosch University |
| BCS2-37 | 24.83950 | 30.96116 | Sill/dyke | No | yes | Cut slabs used, 3 baddeleyite found | CAF Stellenbosch University |
| BCS2-38 | 24.82089 | 30.96804 | Rykoppie Dyke | No | yes | | CAF Stellenbosch University |
| BCS2-40 | 24.81189 | 30.97516 | Sill/dyke | Polished | yes | | CAF Stellenbosch University |
| BCS2-41 | 25.25468 | 30.37495 | Silverton | No | yes | | CAF Stellenbosch University |
| BCS2-42 | 25.25034 | 30.37586 | Silverton | No | yes | | CAF Stellenbosch University |
| BCS2-44 | 25.24849 | 30.37626 | Silverton | No | yes | | CAF Stellenbosch University |
| BCS2-45 | 25.24533 | 30.37582 | Silverton | No | yes | | CAF Stellenbosch University |
| BCS2-46 | | | Malmani(Chuniespoort) | Polished | Drill core | | CAF Stellenbosch University |
| BCS2-47 | | | Malmani(Chuniespoort) | No | Drill core | | CAF Stellenbosch University |
| BCS2-48 | | | Malmani(Chuniespoort) | No | Drill core | | CAF Stellenbosch University |
| BCS2-49 | | | Malmani(Chuniespoort) | Polished | Drill core | | CAF Stellenbosch University |
| BCS2-50 | | | Malmani(Chuniespoort) | No | Drill core | | CAF Stellenbosch University |

| | | | | | | | |
|---|---|---|---|---|---|---|---|
| BCS2-51 | | | Malmani(Chuniespoort) | No | Drill core | | CAF Stellenbosch University |
| BCS2-52 | | | Malmani(Chuniespoort) | No | Drill core | | CAF Stellenbosch University |
| BCS2-53 | | | Malmani(Chuniespoort) | Polished | Drill core | Cut slabs used, 15 baddeleyites found | CAF Stellenbosch University |

Table 3.1: *Table showing full sample list, coordinates* (localities also shown on Fig. 4.1) as well as processing, analytical detail

# 4 Field Relationships

A total of eight days of field work was carried out in 2007, 2014 and 2017 by Dr Martin Klausen along a transect down through the ~9 km-thick Transvaal Supergroup, from Dullstroom in the west and eastwards through Lydenburg (Mashishing) and Sabie, and into the underlying Precambrian basement. From this field work, a total of 85 bulk rock samples were collected as shown on the digitized map in Figure 4.1 and lithological log in Figure 4.2. Complementing a past focus on Bushveld's ultramafic and mafic marginal sills in closer proximity to the BIC, this study therefore extends the investigation to stratigraphically deeper and more distally located intrusions in the <2.65 Ga Transvaal Supergroup, as well as some intrusions hosted within the underlying Archean basement (referred to hereafter as 'basement sills'). With the assistance of geological maps and Google earth, more easily accessible outcrops along roads and tracks were mainly described and sampled in such a fashion as to sample every sill, yet avoid sampling dykes or the same sill more than once. A photo for every sample locality is provided in Appendix A1, whereas this chapter provides a selective recollection of unpublished field notes, additional published field descriptions (e.g., Sharpe, 1984), and field relationships derived from Figures 4.1 and 4.2.

**Figure 4.1 (following page):** Geological map of the Transvaal Supergroup, east of the eastern lobe of the Rustenburg Layered Suite (Mpumalanga Province) digitized from 1:250000 geological map sheets 2430 Pilgrim's Rest (Walraven, 1986) and 2530 Barberton (Walraven & Harzer, 1986) using adobe illustrator, as well as Google earth. Mafic sills are emphasized in green and labelled sample localities are added (note that 8 samples from the Uitkomst Complex are derived from a drill core). Host rocks have been grouped into predominantly finer grained (mainly shale), coarser grained (mainly sandstone) clastic, volcanic and dolomitic rocks. E-W trending Rykoppies dyke swarm (Olsson et al., 2010, 2011) and SSW-NNE trending presumed Black Hills dyke swarm (Olsson et al., 2016) and NW-SE trending dykes of presumed Umkondo age (de Kock et al., 2014) are represented by thin black lines.

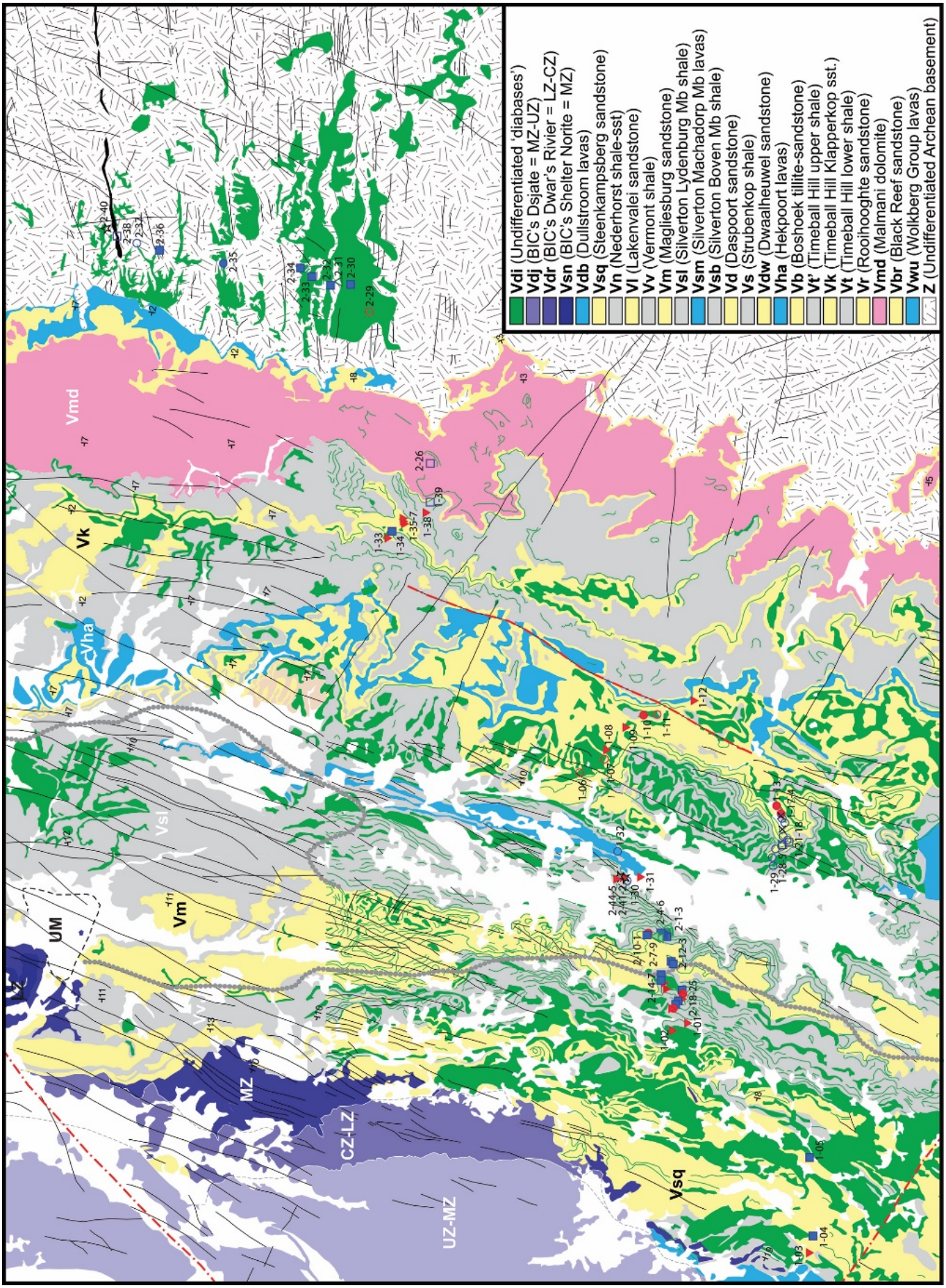

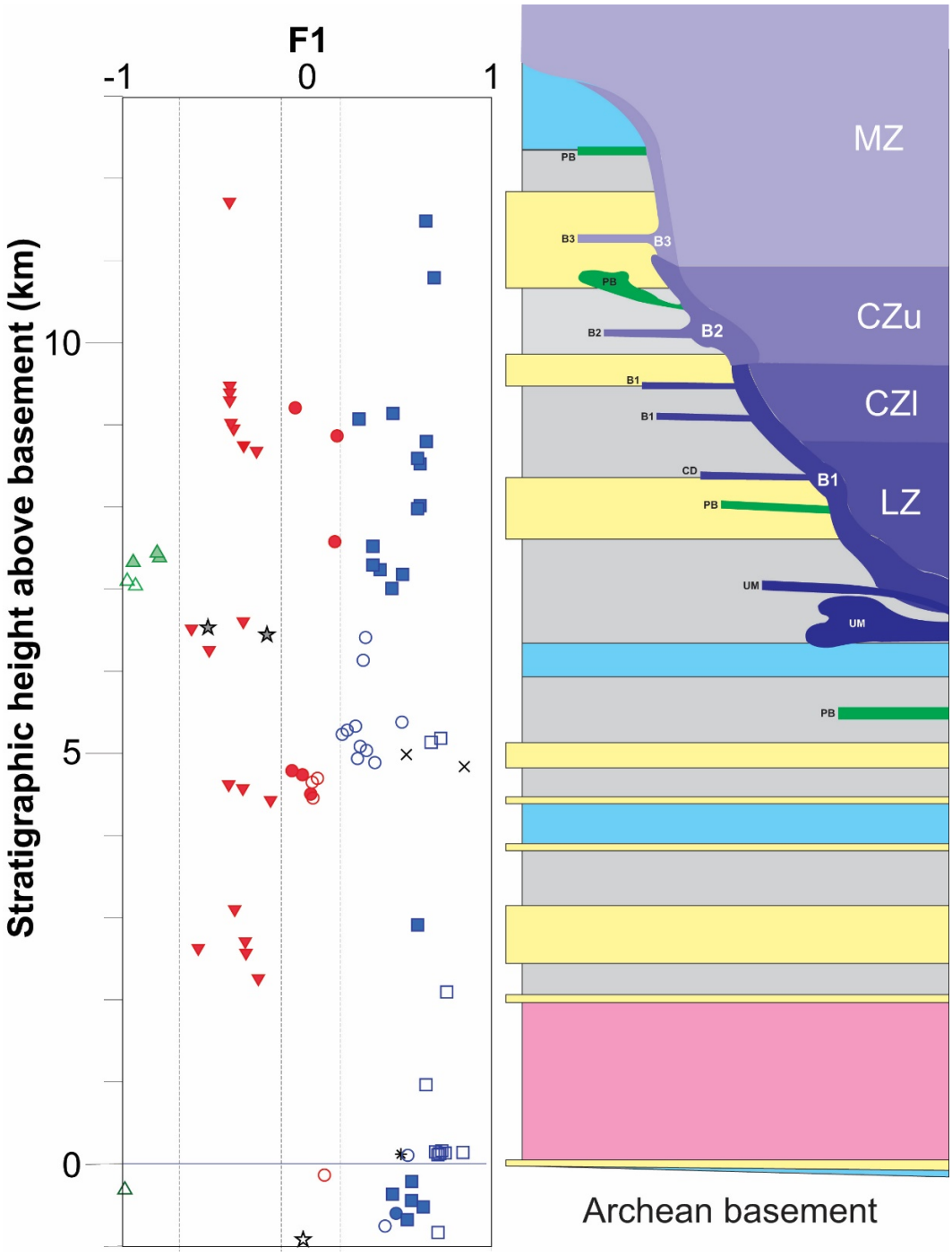


**Figure 4.2:** Samples roughly plotted against stratigraphical height and a statistical value that separates these into different first-order groups, as shown later in the thesis. This provides their location relative to a simplified stratigraphic log of the Bushveld Complex and host Transvaal Supergroup sequence (modified from Sharpe and Hulbert, 1985) to the right. The stratigraphic log overlies the Archean basement and illustrates how the Rustenburg Layered Suite transects the upper part of the sequence, as shown from north to south in Figure 4.1. F1 axis shows first principal component values from a correspondence analysis, which roughly subdivide samples into ultramafic (green), noritic (red triangles), intermediate (red circles) and more gabbronoritic rocks (blue), further subdivided as shown in Chapter 6.

## 4.1 Overview of sampling transects

Samples were collected from the top of the Transvaal Supergroup along six major sub-traverses, referred to as the Dullstroom, Lydenburg, Crocodile River, Road, Sabie and Basement transects. Each of these transects are briefly described below (note that there are field photos of most sample localities in Appendix A1), followed by another section that focuses on particularly interesting field relationships and sill characteristics.

The Dullstroom area includes Dullstroom basalts (base of the Rooiberg lavas; part of the Bushveld Complex), underlain by mudrocks and sandstones of the Houtenbek-Steenkampsberg-Nederhorst-Lakenvalei Formations. According to Figure 4.1, these units host a relatively high concentration of mafic sills. In the field, these units typically form a slightly undulating grass landscape where only three sill samples (BCS1-03 to -05) were collected from within the Steenkampsberg sandstones.

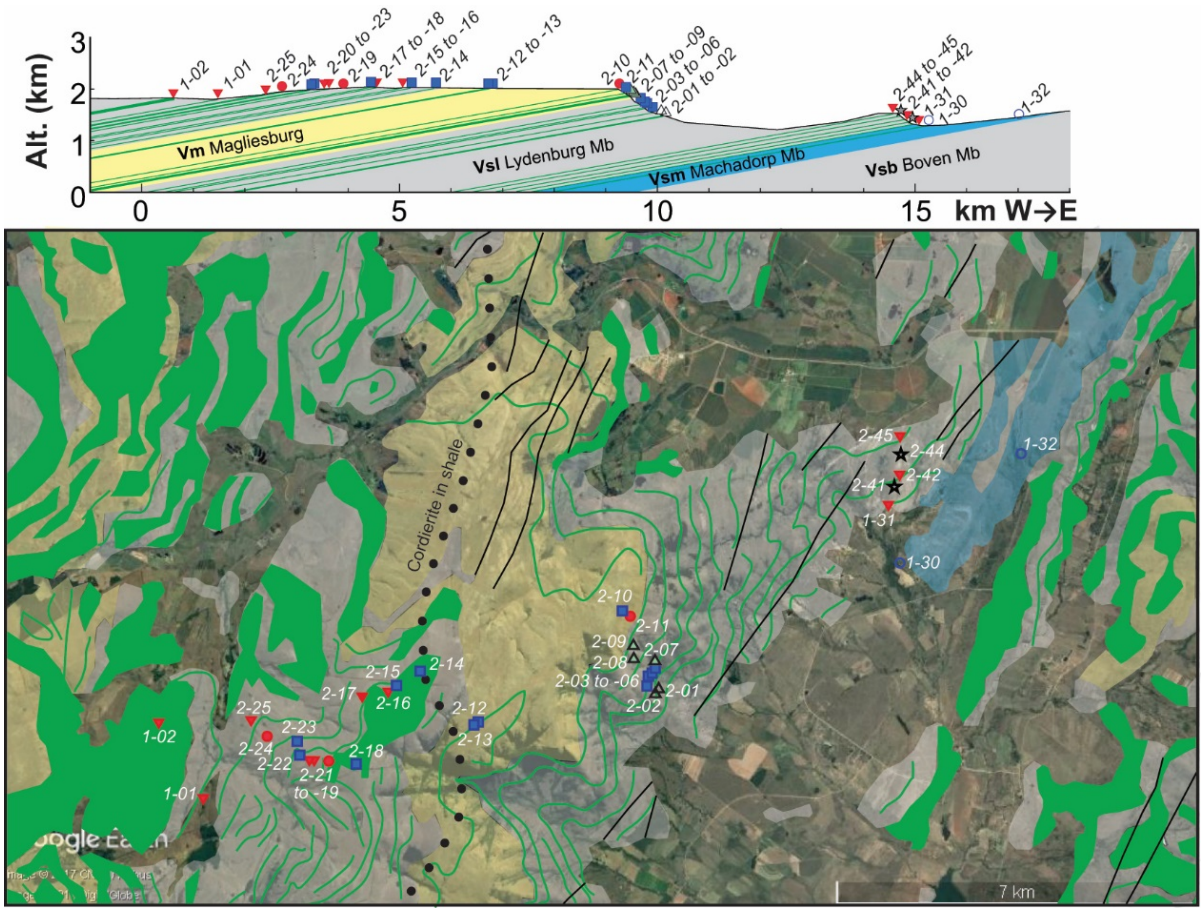


**Figure 4.3:** Cross section (above) and map (below) of Lydenburg transect (section taken from google Earth). Mafic sills are emphasized in green and labelled sample localities from this transect are added.

The Lydenburg transect starts with the uppermost BCS1-02 sample, collected from a main road cut. Including this, 14 samples were mainly collected from boulder ridges that weather out amongst a slightly undulating grass plateau of predominantly Vermont Formation mudrocks, inside the Elandspruit (107) and Rustenburg (108) farms. Very few mafic intrusions were found outcropping within the 225-550 m-thick Magaliesburg Formation sandstone, which forms the eastern edge of this plateau and uppermost cap rocks of a major escarpment. Although Sharpe (1978) mapped a characteristic cone-structured diabase sill along this escarpment top, no such cone-like chill textures were found along this transect.

The Lydenburg Shale Member (within the Silverton Formation) underlies the resistant Magaliesberg cap rocks as a steep escarpment, which exposed several sills that were mainly sampled along a recently cut 4x4 track on the Rietfontein Farm. The lower parts of these shales form the floor of a distinct valley, within which Lydenburg lies, with relatively fewer exposed mafic intrusions. However, several boulder ridges were sampled along a 4x4 track up a small hill on the Rietfontein game farm (courtesy by Buffaloland Safari Ltd), where a fire at the time had burnt down the grass.

**Figure 4.4:** BCS1-32 sample locality along main road cut exposing a ~1m-thick sill, hosted by Machadodorp Member shales. Note small dextral fault to the left of 2008 UKZN Honours students Nathi and Spha, as well as a minor overlapping dextral intrusive offset to the left of the telephone pole.

No samples are believed to have been collected from the volcanic Machadodorp Member. According to Lenhardt and Eriksson (2012), the Machadodorp Member (of the Silverton Formation) is made up of fine-grained tuffs to tuff-breccias volcaniclastic rocks, overlain by fine grained aphyric textured sheet-lavas, with deeply weathered pillow lavas; whereas, the BCS1-31 sample was collected from a distinct medium grained boulder ridge, whereas BCS1-32 was sampled from a 1m-thin sill along a long

road cut where both chilled margins and the surrounding shale hosts were well exposed (Fig 4.4).

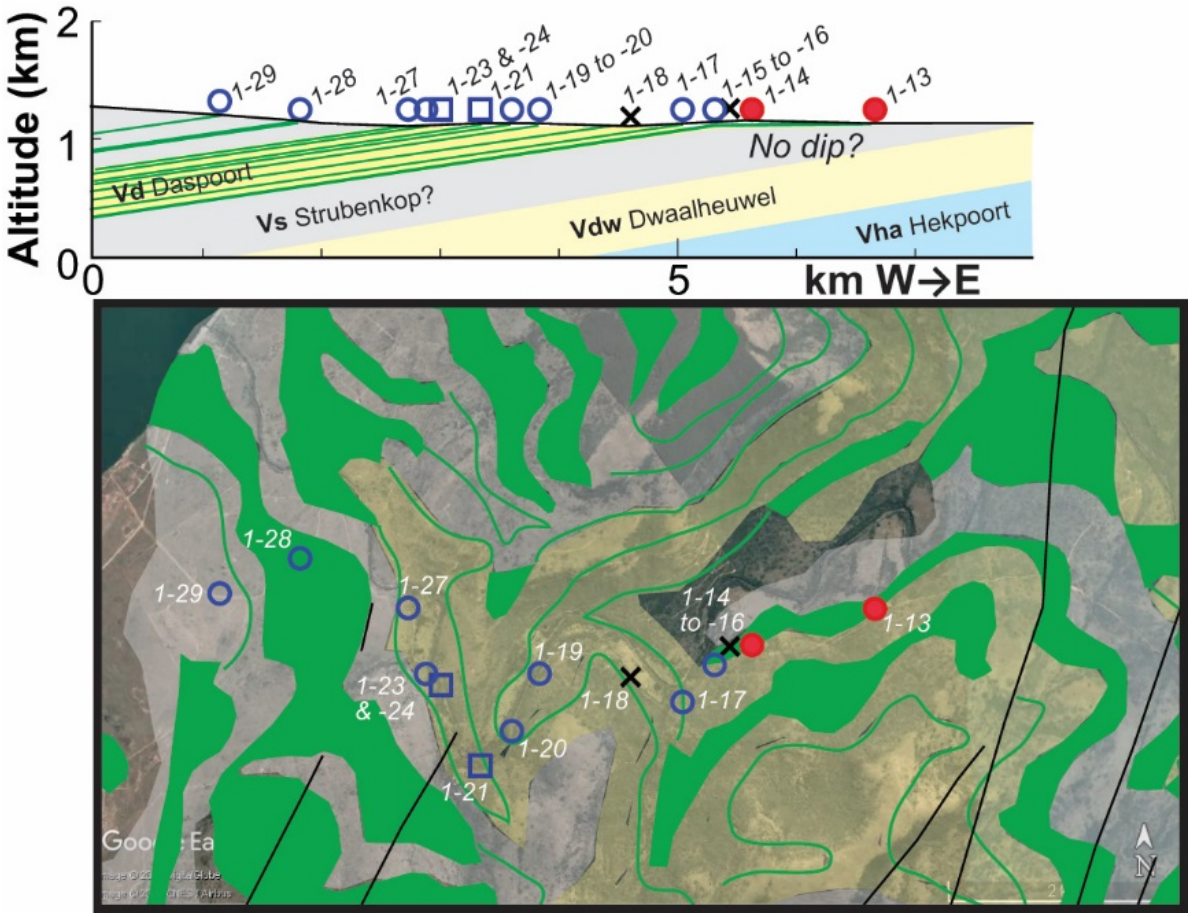


**Figure 4.5:** Cross section (above) and map (below) of Crocodile River transect.

Offset to the south of the relatively long Lydenburg transect, the Crocodile River transect continues stratigraphically below the volcanic Machadodorp Member, where the Boven Shale Member of the Silverton Formation appears to be heavily intruded by thick mafic sills (cf., Fig. 4.5). These sills were sampled along a game farm track along the southern side of the Crocodile River (BCS1-13 to -29), below the Kwena (Braam Raubenheimer) Dam. It is likely that several samples in 2007 were collected from the same sill in this area. Samples BCS1-13 to -21 were collected along a relatively flat section.

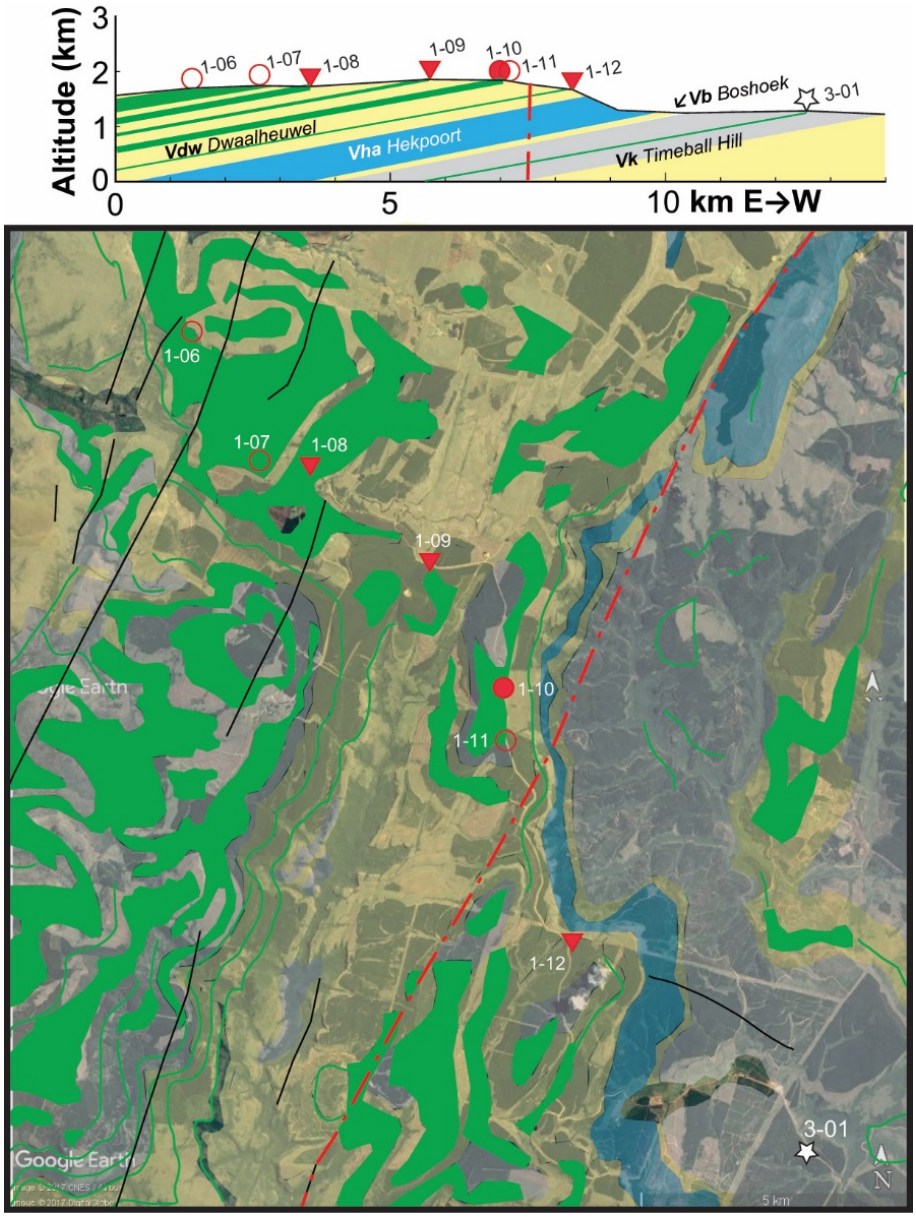


**Figure 4.6**: Cross section (above) and map (below) of Road transect.

Sill samples were in 2007 collected within the Daspoort-Strubenkop-Dwaalheuwel Formations, which form another prominent sandstone plateau that ultimately caps the next major escarpment. According to Figure 4.6, different thick sills were sampled mainly from isolated boulder localities that outcrop along the roadside (BCS1-06 to -12). It is also possible, however, that some of these samples were collected from the same thick sill, since it is difficult to see how these could have been mapped as shown in Figure 4.6. No samples were collected from the underlying volcanic Hekpoort Formation (made up of basalts and andesites, including many pyroclastic deposits), which is a relatively thin formation along this sampling transect.

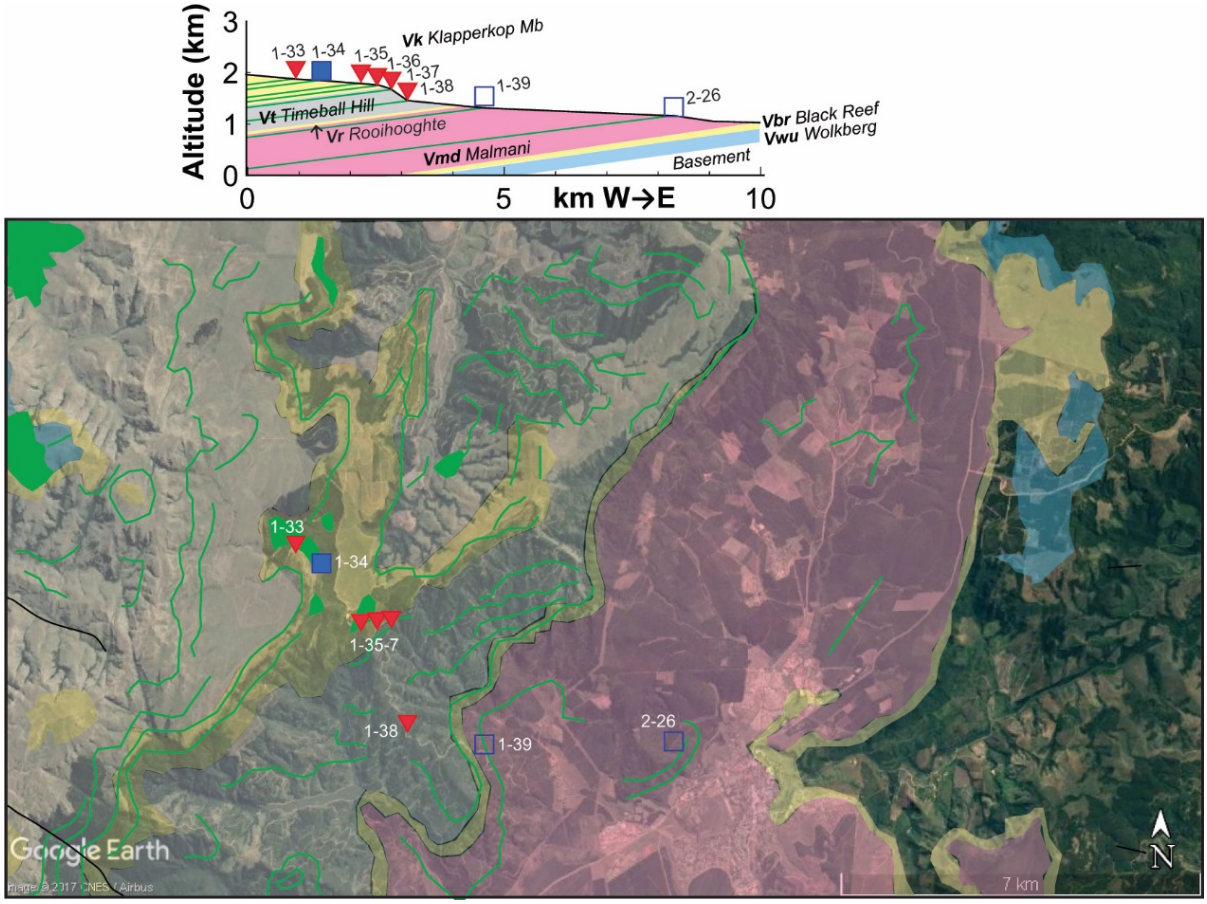


**Figure 4.7:** Cross section (above) and map (below) of Sabie transect.

From the southern termination of the Road traverse, the section is offset a few km, along the very resistant Boshoek Formation, to a traverse just ENE of Sabie. No sills were sampled from the upper parts of this forested escarpment, made up of Timeball Hill Formation shales and interspersed sandstones, even if some are indicated on Figure 4.7, because of logistical difficulties. Several sills were sampled along accessible forest roads going down the escarpment, however, from boulder outcrops in the lower parts of the formation (BCS1-33 to -39). According to Figure 4.7, the stratigraphically (and topographically) lowermost BCS1-39 and BCS2-26 sills were sampled below a thin Rooihoogte Formation quartzite-conglomerate, and inside the overlying dolomitic Malmani Formation of the Chuniespoort Group, which becomes progressively more deeply weathered and covered by talus. However, a few drill core samples (BCS2-46 to -50) were provided by the Nkomati Mine, ~125km south of Sabie, which include the basal gabbro of the Uitkomst Complex (BCS2-53).

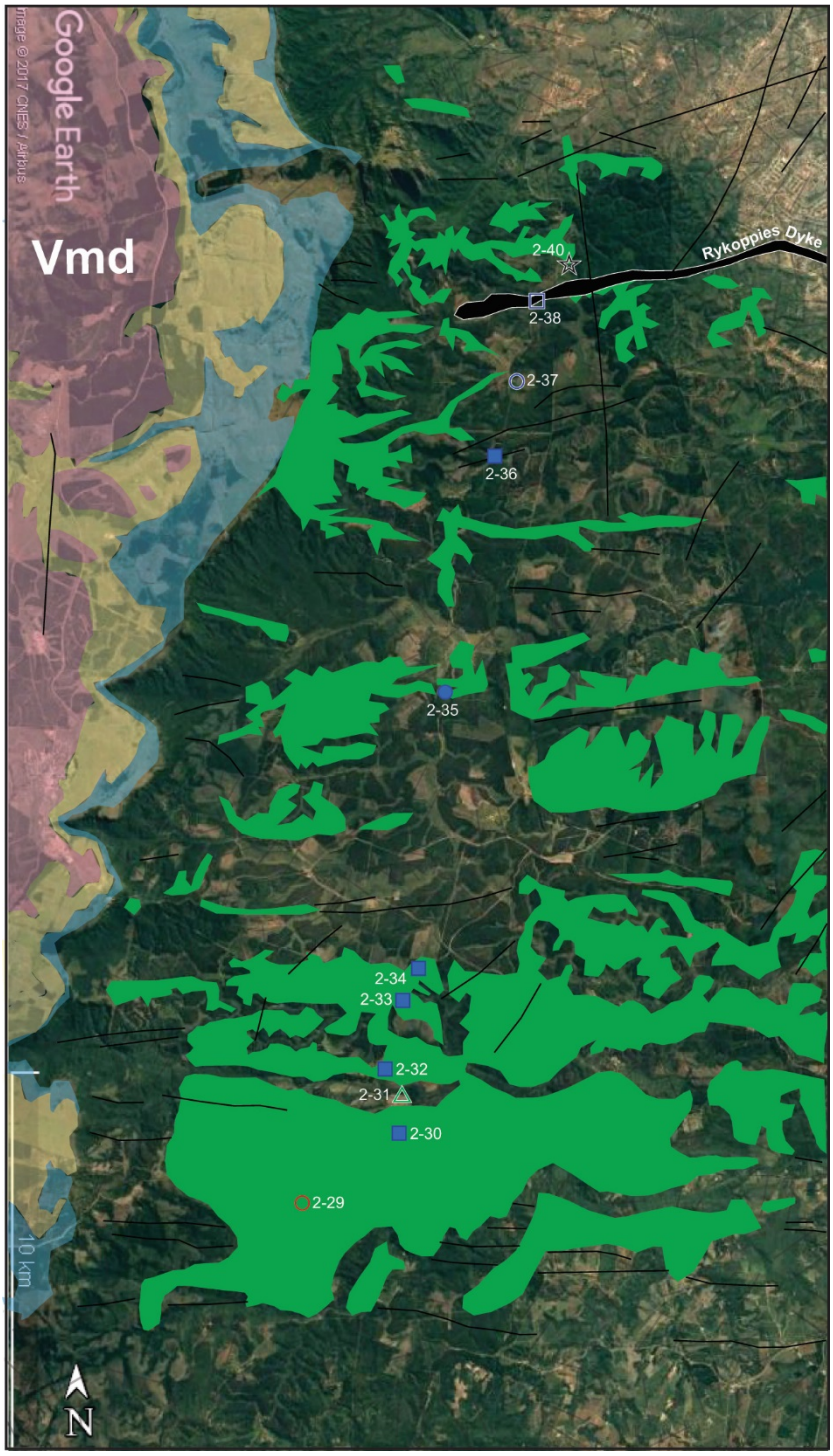


**Figure 4.8:** Map of Basement transect.

Protobasinal units, underlying the Transvaal Supergroup, only occur north of Sabie, referred to as the Wolkberg Group. No samples were collected from within this Group but several mafic rocks were sampled from sills mapped across the underlying Precambrian basement (Fig. 4.8), and along a transect that underlies the southern part of the volcanic Wolkberg group. Some of these samples could have been

collected from an E-W trending and ~2.68 Ga-old Rykoppies Dyke Swarm that is coeval with and therefore very likely feeders to Wolkberg-hosted volcanics (at least BCS2-36 and -38/39; cf., Olsson et al., 2011), and possibly even the sampled sills. According to Figure 4.8, boulder samples BCS2-35, -37 and -40 were each collected from a separate sill, although that may only be an artefact of erosion. Samples BCS2-29 to -34 appear on the other hand to have been collected from the same coherent sill, where at least the BSC2-29 outcrop exhibited distinct vertical cooling joints consistent with a sill intrusion. The rest of the samples, apart from one flat river outcrop at BCS2-32, were collected from relatively loose boulder outcrops.

## 4.2 Particularly interesting field features

In some cases, especially along road cuts and across steeper topography - exposed chilled margins, cooling joints and/or the extent of mafic rocks can help distinguish whether a mafic outcrop exposes a concordant sill or a discordant dyke. In other cases, (e.g., flatter and/or more vegetated terrains), however, this distinction becomes more uncertain. Amongst the more uncertain samples, some localities coincide with mapped sills and no sample localities coincide with any mapped dykes which also cut across this part of the Transvaal Supergroup (cf., black lines in Fig. 4.1). In the basement, however, 4 samples (BCS2-36, -37, -38, -40) were likely collected from what appear to be E-W trending basement-hosted dykes, which presumably all belong to the 2.68 Ga Rykoppies Dyke Swarm (Olsson et al., 2011). The rest of the basement-hosted intrusions were collected from more extensive outcrops. Across flatter terrains, it is also possible for more than one sample to have been collected from (the apophyses of) the same (thick) sill, as seems likely for the following sample pairs/groups:

- BCS1-06, 1-07 & 1-08;
- BCS1-10 &1-11;
- BCS1-13, 1-14,1-15 and 1-16;
- BCS 1-26-1-28, 1-19 & 1-20,
- BCS 1-16 &1-17;
- BCS2-01, 2-04, 2-05 & 2-06;
- BCS 2-10 &2-11;
- BCS 2-43 & 2-44.

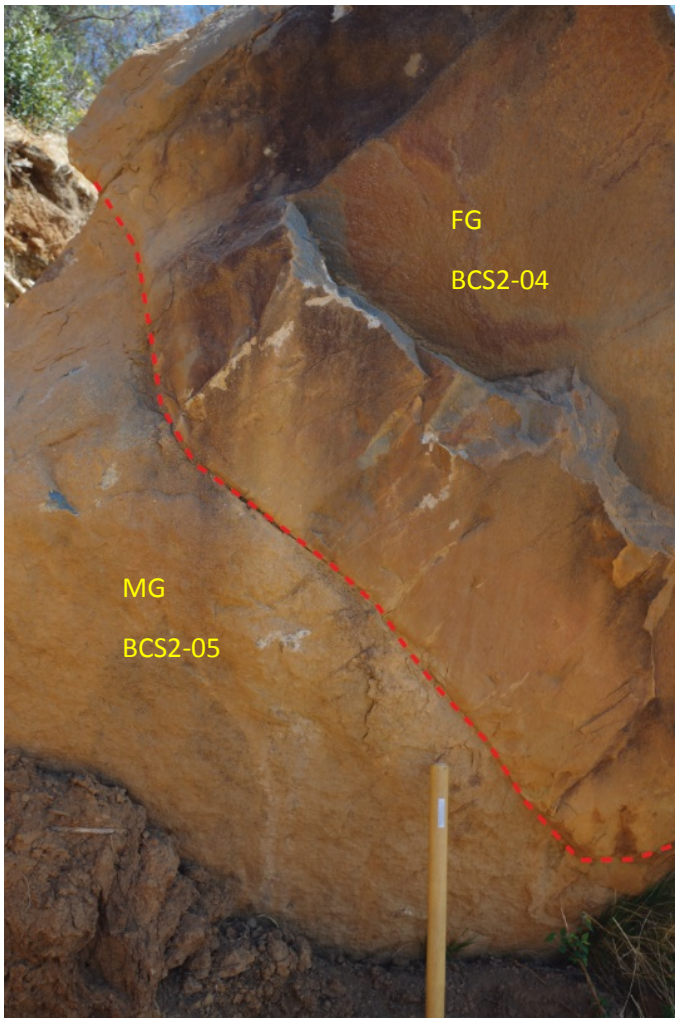


**Figure 4.9:** A large loose boulder along central parts of 4x4 track up through the Lydenburg Member shale escarpment, where one fine grained (FG) intrusion (BCS2-04 to the right) chills against another medium grained (MG) intrusion (BCS2-05 to the left), along the dashed red line. It is not possible to determine the original orientation of this boulder or its chilled contact, but it shows evidence of either multiple intrusion of two sills or a dyke-sill intersection within the Lydenburg Member of the Silverton Formation. Hammer shaft is ~5 cm wide.

At one locality, a chilled margin against another pre-existing mafic intrusion was observed in a loose boulder (Fig 4.9), suggesting that some intrusions may be multiple.

Most massive mafic intrusions appear as rusty brown and concentrically weathered smooth boulders in the field, where interior fresh surfaces often reveal a melanocratic, dark grey-green coloured rock below a mm-thin weathered crust. Most intrusions appear to be aphyric fine to coarser grained, where grain sizes typically (are assumed to) increase inwards from chilled margins (e.g., Fig 4.9). Some intrusions may also be porphyritic and include samples BCS2-19, -20, -22, -23, -26 and BCS2-38. Most of these are plagioclase-phyric but some also host mafic phenocrysts. In two fine-medium grained mafic rock outcrops, more resistant weathered-out ‘knobs’ (Fig 4.10 A-B) are tentatively interpreted to represent pyroxene oiko-/phenocrysts. There is no apparent systematic stratigraphical distribution of these porphyritic sills (cf., Fig. 4.1).


**Figure 4.10:** Similar looking fine-medium grained mafic rock outcrops with more resistant weathered-out 'knobs'. (a) Clearly aligned 'knobs' in BCS2-14 outcrop. (b) More dispersed randomly distributed 'knobs' in BCS2-21 outcrop. See text for interpretations. Camera cap is ~5 cm in diameter.

It is difficult to determine the matrix mineralogy of rocks in the field and by using hand specimens and slab scans along with petrography presented in the next chapter, one can confidently describe these rocks in more detail. Within the coarser grained rocks it is easy to note the more plagioclase or enstatite-dominated rock types which can later be shown to be more doleritic or noritic based on their petrography and chemistry. One outcrop along the basal parts of the Lydenburg member (Silverton Formation) exhibits some exceptionally long acicular mafic minerals in a rather chaotic texture (Fig 4.11), which in the field could be interpreted as elongated and presumed metamorphic amphiboles. However, Sharpe's (1978) report of similar acicular enstatite crystals within a so-called 'cone-type sill' (Fig 4.11A-B), shows that enstatite may grow unusually elongated and sometimes more chaotically. Whereas, the cone-type sill was emplaced along the basal parts of the Vermont Formation, just above the Magaliesberg quartzites, sample BCS2-42 sill outcropped stratigraphically deeper, within the base of the Lydenburg Member of the Silverton Formation. Sharpe (1978) interpret his cones as so-called 'quench rosettes', made up of both enstatite and plagioclase crystals that typically grew downwards from the sill's roof zone; i.e., a primary igneous quench textures that may be partly altered to amphiboles, and also interprets these as primary quench textures within ultramafic melts. "Spinifex" is adopted as a common descriptive term of such exceptionally elongated enstatites for the remainder of this thesis, even though this term is mainly used for olivines within komatiitic lava flows.

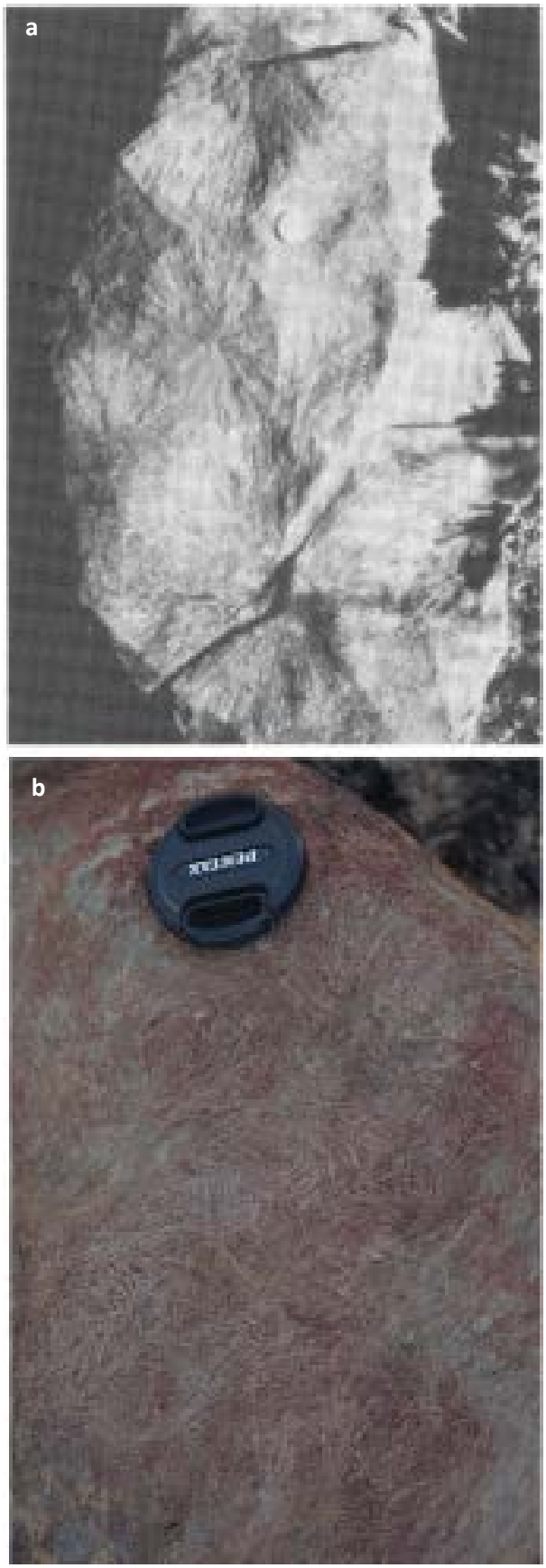


**Figure 4.11:** (A) So-called cone structures within sill on Beetgeskraal 19JT Farm (Sample CD002 scale is 24mm diameter) and hosted within the Silverton Formation (copied from Sharpe, 1978). (B) Weathered surface of sample BCS2-42 from within the Lydenburg shale-mudstone member (Silverton formation) exhibiting a more irregular pattern of elongated crystals. Such elongated enstatites will be referred to throughout this thesis as 'spinifex like'. Lens cap is 5 cm wide.

Although sills are more susceptible to gravitation crystal settling and accumulation than, e.g., dykes, obvious igneous layering was only observed at two localities. The first case was discovered in the lower road cuts at the base of the escarpment made up by the Lydenburg Formation, where cm-thick ultramafic layers weather out near the base of a sill (Fig 4.12 A-B). Figure 4.12 C (BCS2-01) is probably sampled from another sill where the upper part is exposed and the previous BCS2-02 exposes the basal part of the sill. The other case is that which was discovered in the Crocodile River outcrop described in Fig 4.13 where the layering was more variable. The latter sill locality was initially sampled in 2007. The leucocratic component may be mistaken as olivines, but appear to be pyroxene oiko/-phenocrysts.


**Figure 4.12:** (A-B) Subhorizontal protrusions of medium-coarse grained rocks along the base of a sill outcrop along the lower section of 4x4 track up through the Lydenburg Shale Member Escarpment. Later identified as olivine cumulates (BCS2-02) suggesting that these outcrops represent basal modal layers. (C) In-situ fresh dolerite boulders within an otherwise highly weathered outcrop stratigraphically below the previous layered outcrop (BCS2-01). (D) Scanned slab image of BCS2-01, showing a localized pegmatoidal concentration of white plagioclase that typically forms during the last crystallization of the upper central parts of sills (e.g., Pallisade sills, New York).

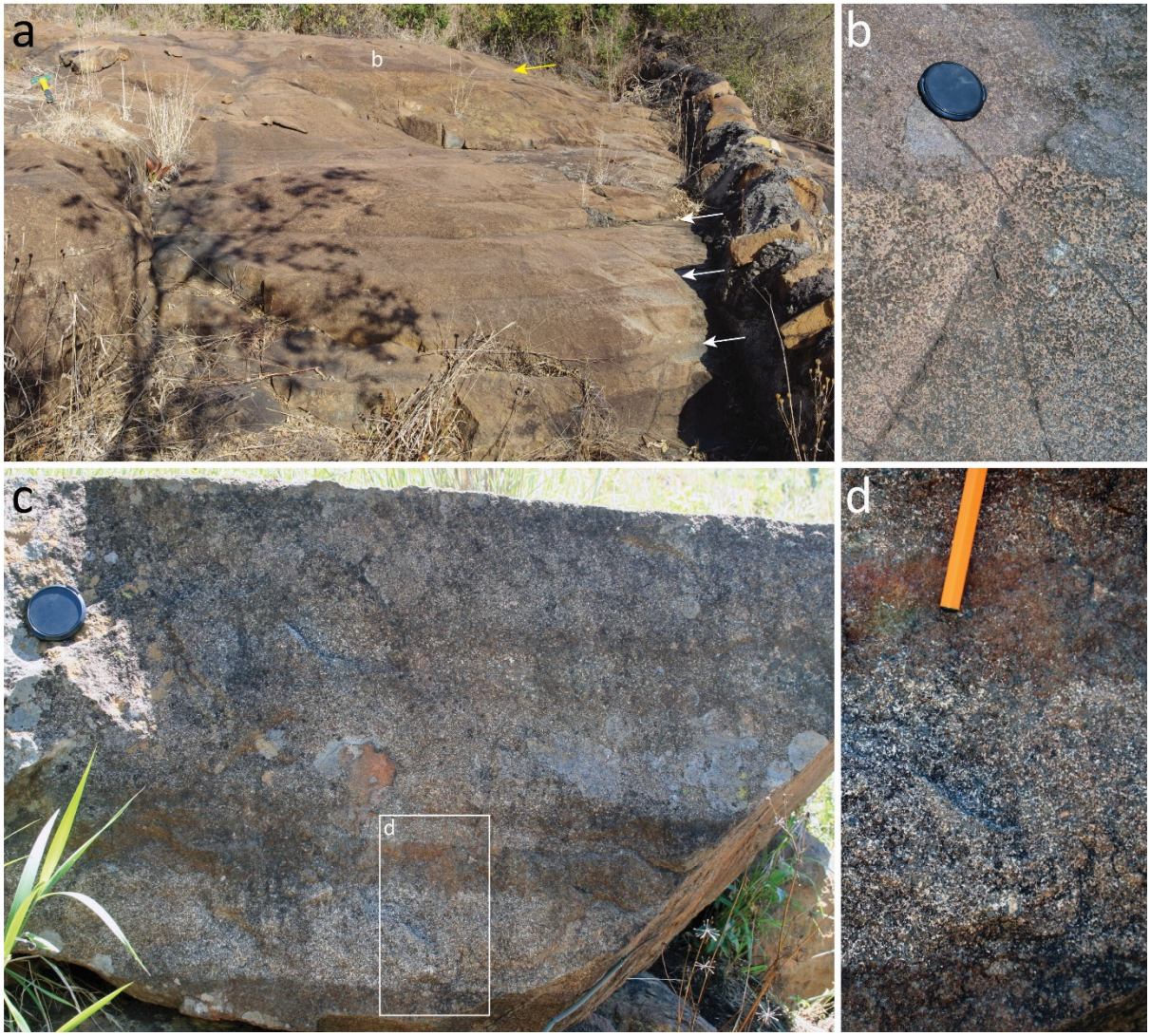


**Figure 4.13:** Layered sill in the Crocodile River (BCS1-22 to -26). (a) Main outcrop showing at least five rhythmic and sub-horizontal bands, indicated by arrows. Sledge hammer in upper right corner provides a scale. The contact indicated with a yellow arrow was in 2017 cut by a rock saw. (b) Detail of contact indicated by yellow arrow in (a), showing an upper darker layer above a paler layer with many rounded holes, initially interpreted in the field as eroded olivines. Lens cap is 5 cm wide. (c) Even more modal layering towards the deeper part of the sill, where (d) is a zoomed in portion of darker and lighter layers. Pen end for scale.

# 5 Petrography

Microscopic descriptions and identifications of textures and mineral phases was carried out using 35 thin sections and 49 cut and scanned slabs from the BCS-collection(Appendix A2). This is done in order to; 1) identify petrographic differences and similarities between sampled sills, 2) classify the rocks, 3) determine their degrees of alteration and metamorphism, and 4) understand how these igneous rocks crystallized. Nine (9) BCS1-samples could not be studied because there were no available hand specimens or thin sections of these. Only a selection of hand specimens, scanned cut surfaces and/or thin section photomicrographs are shown to illustrate main petrographic textures in this chapter (cf., Appendix A3).

## 5.1 Main textures observed.

In general, grain sizes predominantly range from fine to medium grained (<1mm-3mm) with only a few coarse grained (>3mm) samples. Most samples are dominated by similar mineral phases, which are sometimes variably altered. A few samples are so altered that the original igneous textures are no longer preserved and one has to resort to normative calculations in order to estimate proportions of igneous minerals.

The dominant silicate minerals in the rocks are igneous plagioclase and pyroxene (orthopyroxene and clinopyroxene), where pyroxenes are typically altered into amphiboles (either ortho-amphiboles or clino-amphiboles). Fresh plagioclases are identified on the basis of their subhedral shape and their albite twinning. Fresh orthopyroxenes are typically recognized on the basis of their euhedral-subhedral habits, 1$^{st}$ order birefringence colours and a parallel extinction; whereas clinopyroxenes are identified on the basis of their anhedral habit and 2$^{nd}$ order to 3$^{rd}$ order birefringence and inclined extinction. Ortho-amphiboles are identified on the basis of their straight extinction, 3$^{rd}$ order birefringence as well as their weak pleochroic character (brownish); whereas, clino-amphiboles are strongly pleochroic (greenish) and have inclined extinction. Olivine is only identified in two samples (BCS2-02 and BCS1-31) under the microscope and is typically altered. Interstitial quartz is common and typically found more or less intergrown with late-stage alkali feldspar. Accessory biotite and other mica (clay) minerals are all regarded as secondary phases.

As mentioned in the introduction (chapter 1), Sharpe (1984) identified pre-Bushveld, syn-Bushveld and post Bushveld sills on the basis of the presence or absence of metamorphic minerals. Thus, noritic pre-Bushveld samples are identified by the presence of amphiboles (typically hornblende and tremolite) and the absence of abundant fresh orthopyroxene grains, whilst syn-Bushveld sills are characterised by fresh to slightly altered orthopyroxene. However, this simple discrimination presumes that all (parts of) pre-existing sills were equally affected by the contact metamorphism of Bushveld's main intrusion (i.e., the current Rustenburg Layered Suite), purely as a function of its contact metamorphic aureole's temperature and pressure isograds. In reality, metamorphism is more locally dependent on the availability of water for solid-state reactions to equilibrate. Furthermore, post-Bushveld alteration and weathering may also affect sills variably and be difficult to distinguish from syn-Bushveld contact metamorphism, if both alteration processes result in similar amphibolitization of pyroxenes (i.e., uralitization). The samples will in this petrographic study primarily be divided into different groups based on igneous mineralogical and textural characteristics of fresher examples. Because most samples are altered to some degree, an igneous classification of such rocks should be attempted using corresponding ortho- and clino-amphiboles as indications of pre-existing enstatites and augites, respectively.

After examination of all available hand specimens, cut slab surfaces and thin sections, there are two major suites identified to which the sills can be classified into; namely a noritic and doleritic suite. Noritic sills are typically dominated by darker euhedral and lath shaped orthopyroxenes, which typically crystallized prior to paler coloured and more interstitial plagioclase, as seen in fresher samples BCS1-02, -35 BCS2-25, 20, -19, -17, -45 and BCS2-15 (Fig 5.1). Doleritic sills differ from noritic sills in that they are more dominated by euhedral plagioclase laths, tend to have a greater proportion of opaque oxides, and never any euhedral pyroxenes. These anhedral pyroxenes tend to be augites that crystallized between pre-existing plagioclase laths to form characteristic (sub-) ophitic textures. This suite includes BCS2-51, -50, -48, -47, -46, 1-39 (Fig. 5.2) and is mainly represented by samples from the Nkomati drill core

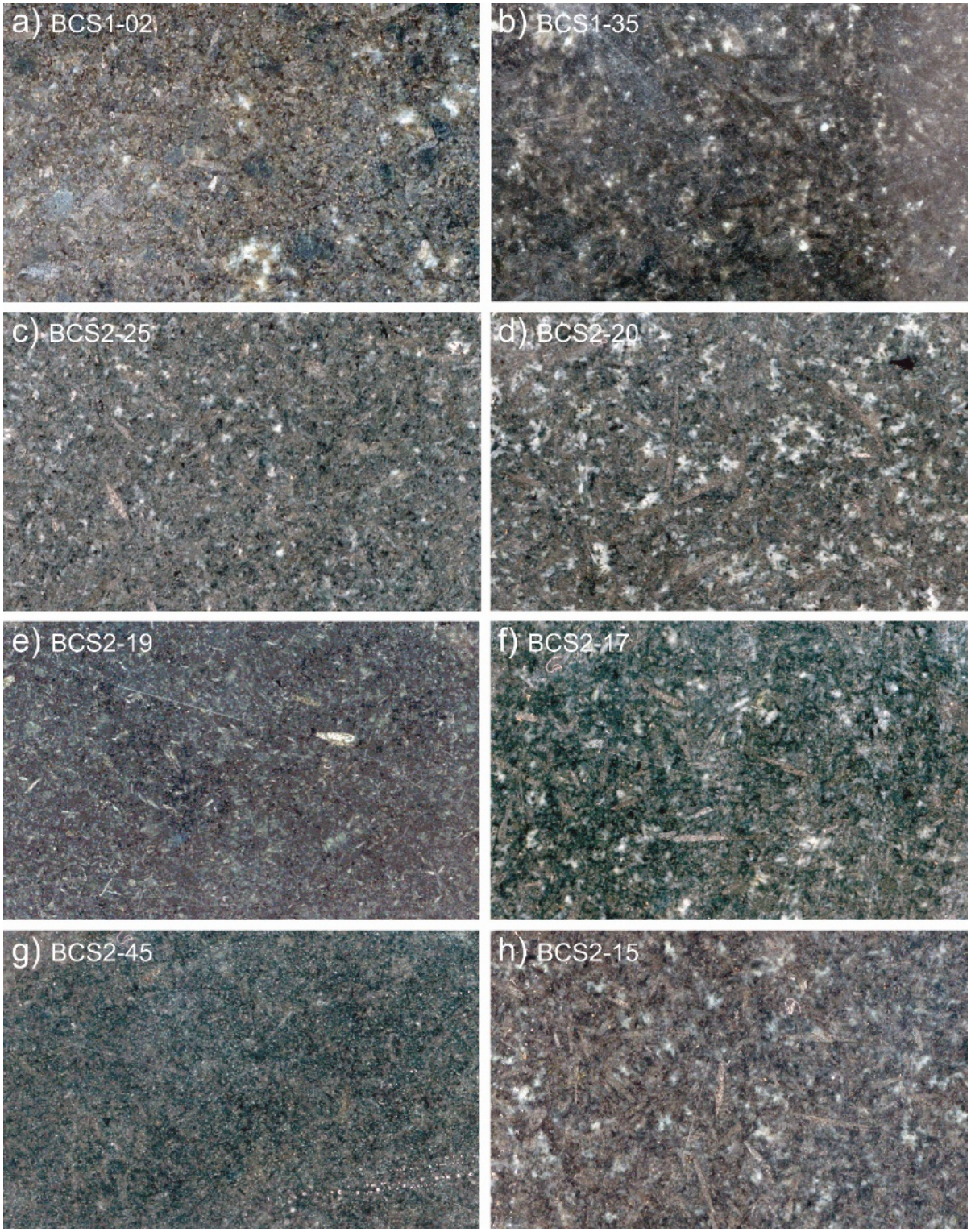


**Figure 5.1:** (A-H) slab scan images of fresh noritic samples showing the dominant euhedral opx grains.

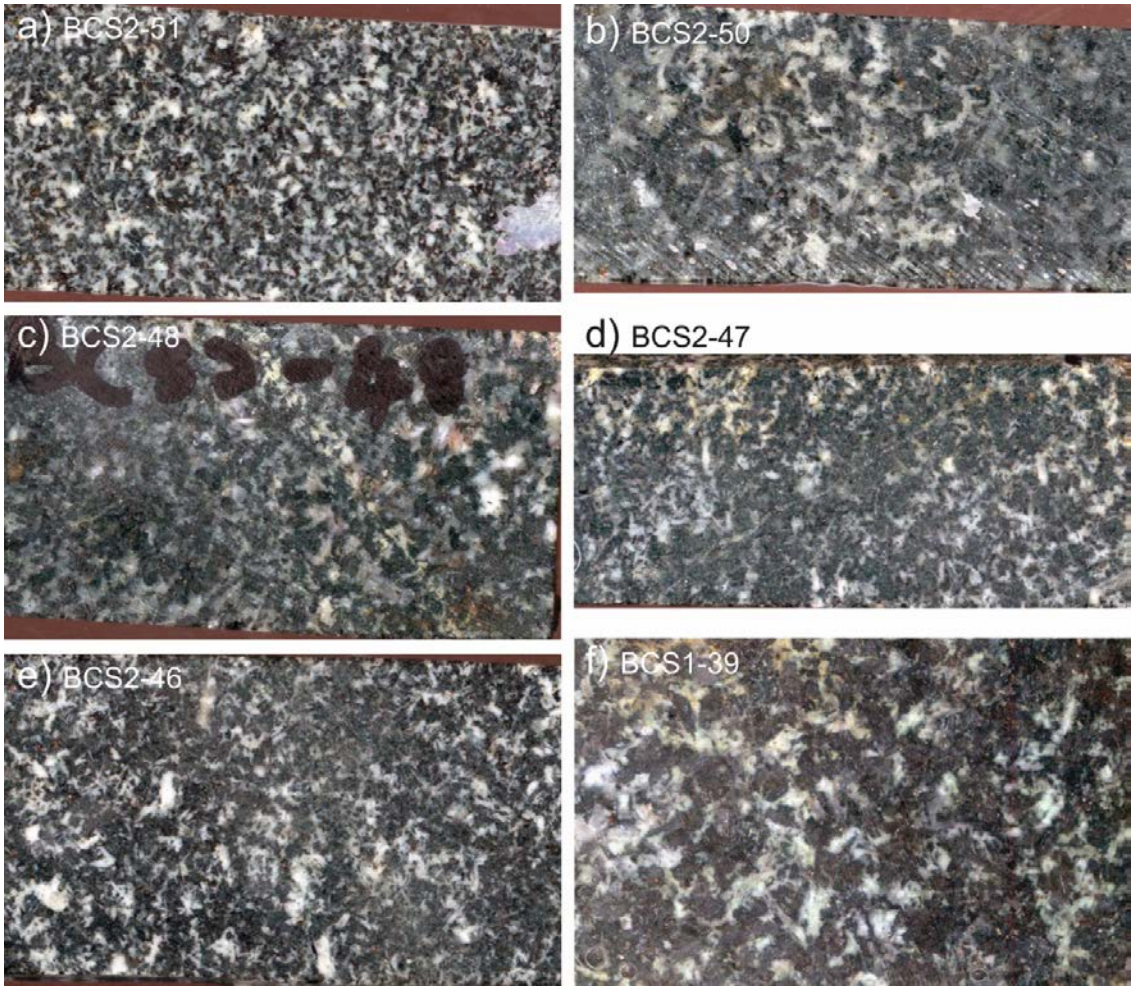


**Figure 5.2:** (a-f) slab scan images of gabbroic/doleritic rocks dominated by large plagioclase.

Each of these two major suites can be further subdivided into more overlapping subgroups of more or less evolved, or even cumulative varieties. More ultramafic cumulates may be difficult to directly relate to any of the above mentioned suites, and are therefore described in a separate section below. They have very little plagioclase, are medium to coarse grained, greenish in colour and a cumulate texture. This group is represented by samples BCS2-02, 2-07, 2-09, 2-03, 2-08 and 2-31(Fig 5.3). The 'spinifex' textured sills, recognised in the field (Fig. 4.11 B) is an exotic sub-member of the noritic suite, represented by two samples (BCS2-42 and BCS2-24) with radiating distributions of acicular enstatite crystals (Fig 5.4) that make them different from other noritic rocks. Finally, examples of increasing degrees of alteration are also presented for each of these two main groups, supported by normative classifications.

The petrographic descriptions for all 35 thin sections are more comprehensively summarized in Table 5.1 (at the end of this chapter) and in Appendix A3.

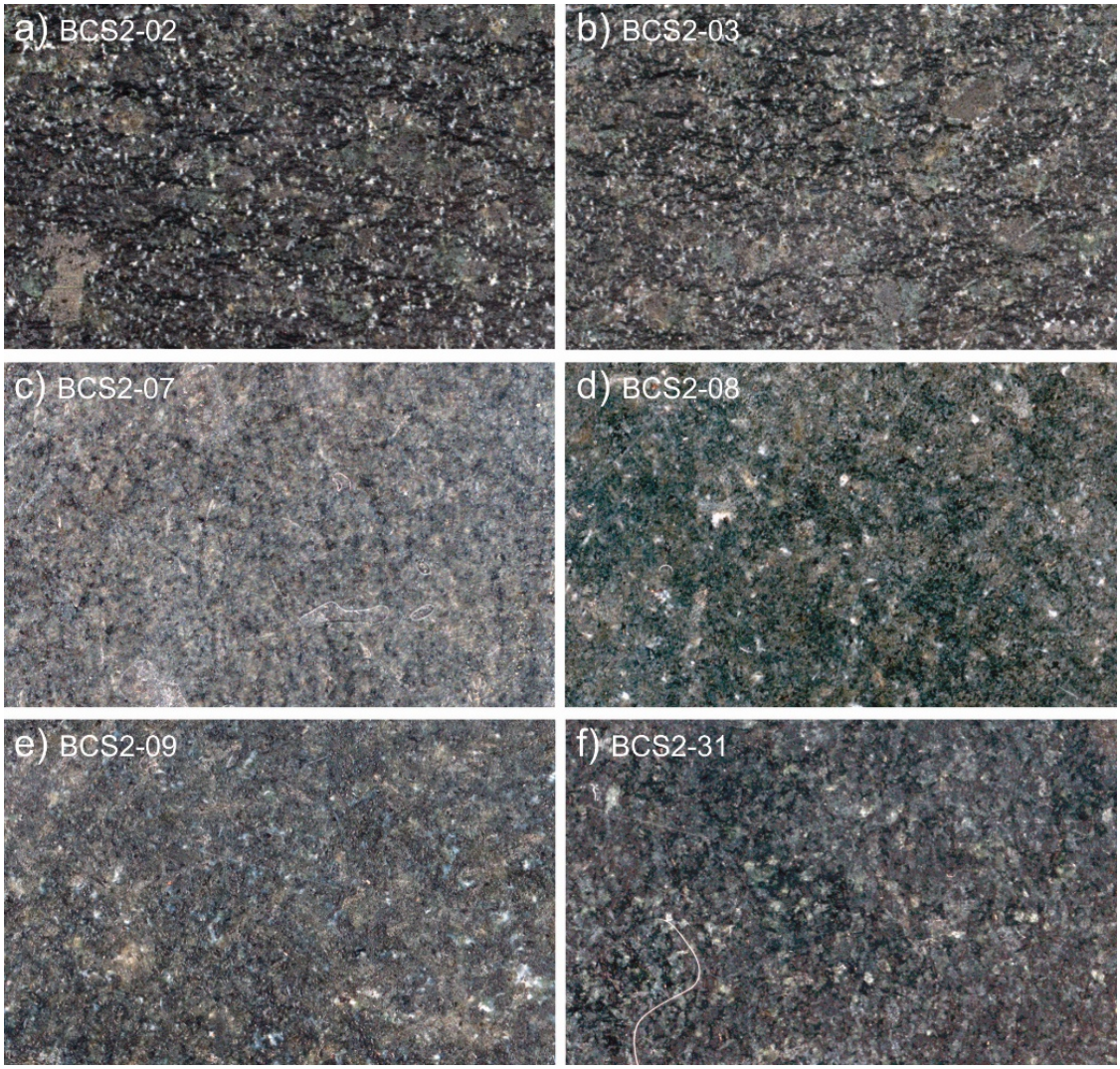


**Figure 5.3:** (a-f) slab scan images of greenish ultramafic cumulates.

**Figure 5.4:** Flat-bed scans of 'spinifex-textured' sample BCS2-42, collected near the base of the Lydenburg member of the Silverton Formation. This rock shows very long and acicular brownish-green enstatite crystals, which are also easily recognised in the field (e.g., Fig 4.11.b).

## 5.2 Noritic suite

### 5.2.1 Melanorites

22 out of 35 thin sections make this, by far, the most common type of sill based on this sample collection. The noritic group is characterised by the presence of euhedral and elongated grains of orthopyroxene ranging between (50-55%), subhedral plagioclase (20-25 %) and 10-15% interstitial clinopyroxene, 5-10% quartz and 5-10% opaques, calculated from normative calculations. Their euhedral habits testify to orthopyroxene being the earliest crystallising phase and the fact that the crystals often are in contact with one another could reflect that they may have accumulated. If so, the anhedral plagioclase is an intercumulus phase, together with less clinopyroxene and some quartz, and the rock may be regarded as an orthocumulate.

In the freshest examples, orthopyroxene of sample BCS1-01 (Fig 5.5 a-f) are more elongated than those found in BCS1-02 (Fig 5.5 c-d). Such habit variance for orthopyroxene appears to be real since there is no igneous lamination to suggest that these differences depend on different orientations of these thin sections. The slightly altered, fine grained BCS2-24 sample in Fig 5.5(e-f) has euhedral and elongated orthopyroxene, which in this case appear to have grown into a more radiating quench-like texture. Interstitial and saussuritized plagioclases surround the euhedral orthopyroxene crystals, together with minor quartz. Clinopyroxene is an accessory phase, which seems to be altered and is often found together with traces of oxides.


**Figure 5.5:** Microphotographs of noritic samples, where the field of view in each image is ~5.2 mm, and the left and right column show paired photographs taken under plane and crossed polars, respectively. (a-b) Least altered sample BCS1-02 of a noritic sill with euhedral opx, slightly subhedral but mainly interstitial plagioclase and minor interstitial clinopyroxene. Some secondary brown biotite and minute quartz-plagioclase symplectites may also be observed. Note the remarkably few opaques in both samples, typical for norites. (c-d) BCS1-01 noritic sill is slightly more altered (e.g., presence of brownish biotite) than BCS1-02 (a-b). Nevertheless, the low grade of alteration has not obscured its elongated euhedral opx and interstitial cpx and plagioclase, as well as some symplectites of quartz. (e-f) BCS2-24 is interpreted to represent an even more altered noritic sill than those in a-d. The elongated orthopyroxene crystals are more dirty looking under ppl, do not extinguish as single crystals under xpl, and may have altered to amphibole. Interstitial plagioclase also appears to be saussuritized. Clinopyroxene and little opaques are present as interstitial accessory phases.

### 5.2.2 Evolved norites

Under the microscope, more evolved norites are typically recognised by a larger abundance of both interstitial and micrographic quartz-feldspar intergrowths. There is a gradual transition, however, from small interstitial symplectites-looking examples less evolved and still quite orthopyroxene-rich noritic samples (Fig 5.5 a-f), to a greater abundance of larger and more obvious micrographic quartz - alkali feldspar intergrowths, found in even more evolved quartz-bearing noritic samples, represented by BCS2-22 (Fig. 5.6 a-b). Even so, these textures reflect progressively greater degree of silica-oversaturation during the latter stages of crystallization of noritic sills, consistent with this suite's early orthopyroxene, rather than olivine-crystallization. It will be shown later, on the basis of their whole rock geochemistry, that these samples represent more evolved differentiates of parental norites, described in Section 5.2.1, which forms a coherent noritic suite. In most evolved norites, their micrographic textures usually reside interstitially between greenish amphiboles with obvious 60/120 cleavage sets (Fig 5.6 c-d), which are presumed to be altered orthopyroxenes based on the euhedral habits of the amphiboles. Thus, even if this has never been discussed in the literature, petrographical observations cannot completely rule out that that more evolved norites crystallized primary igneous amphibole under higher $P_{H2O}$ and lower temperatures.

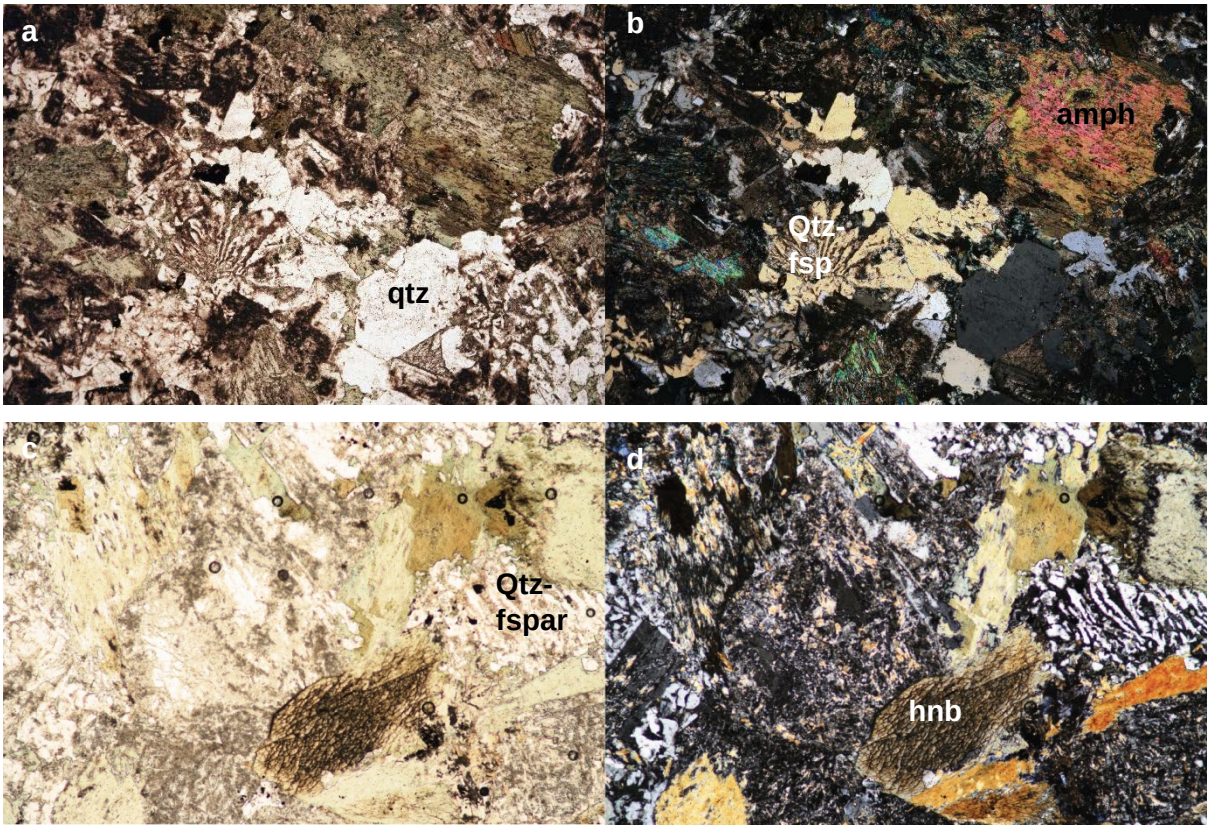


**Figure 5.6:** Microphotographs of more evolved norites, where the field of view in each image is ~5.2 mm, and the left and right column show paired photographs taken under plane and crossed polars, respectively. (a-b) BCS2-22 sample of a more evolved quartz-bearing norite, with stubby orthopyroxene altered to greenish ortho-amphiboles and interstitial pockets of micrographic plagioclase, alkali feldspar and quartz. (c-d) Highly altered norite sample BCS2-12 exhibits micrographic texture of quartz and plagioclase, in between greenish hornblende with the 120˚/60˚ double set cleavages (well displayed in the lower central part of photograph). The amphiboles were originally opx, and this makes them greenish ortho-amphiboles.

### 5.2.3 Norite alteration

Many samples are more or less altered and some are even found to have become obliterated beyond recognition, where original minerals as well as igneous textures can no longer be recognised. However, more euhedral pseudomorph amphibole outlines can tentatively be used to infer that these are hydrated pseudomorphs of primary orthopyroxene. The following examples in Figures 5.7 illustrates how variable this alteration/metamorphism is and how it may have progressed on presumed noritic protoliths, later supported by normative mineral proportions (cf., pie charts in Appendix A2).

Sample BCS1-37 (Fig 5.7a-b) shows a highly altered rock, yet with a clearly pseudomorphed texture that bears a resemblance to fresh melanoritic textures in Figure 5.5. This alteration type is somewhat unusual, however, and may resemble

bastite, which is what orthopyroxenes often alter to in more ultramafic rocks. In between the euhedral pseudomorphs, it is more difficult to determine the original interstitial mineralogy, which is now made up of quartz, amphibole and possibly some plagioclase. However, if BCS1-37 represents an altered melanorite, fresh melanorite suggest that plagioclase and clinopyroxene were original interstitial phases, and quartz may have been metasomatically added and/or left-over from metamorphic reactions.

In Figure 5.7(d-f), BCS2-29 and BCS1-31 also preserves similar pseudomorph melanoritic textures, which are most obvious under plane polarized light. In these cases, their euhedral and presumed orthopyroxene protominerals have been more or less amphibolitized, as evidenced by a slight pleochroism, relatively high interference colours, as well as common twinning. Sample BCS2-29 (Fig. 5.7c-d) is estimated to have been altered to an intermediate degree, where it becomes difficult to determine whether some of the high birefringent minerals might still be igneous clinopyroxenes rather than metamorphic amphiboles. However, based on the sample's pseodomorph texture and hypersthene-rich normative mineralogy (ranges between 45-50% plag, 40-45% cpx, 5-10% opx, 2% oxides), it is believed to have been orthopyroxenes that are entirely replaced by amphibole. In the apparently more altered melanorite sample BCS1-31 (Fig. 5.7e-f), pseudomorphs have been completely replaced by an abundance of fibrous (and thereby clearly metamorphic) amphibole crystals, which starts to make it difficult to distinguish from what could also be altered interstitial phases. More pervasive alteration, which starts to obliterate pseudomorphic textures, is regarded typical for the most altered (mela)norites.

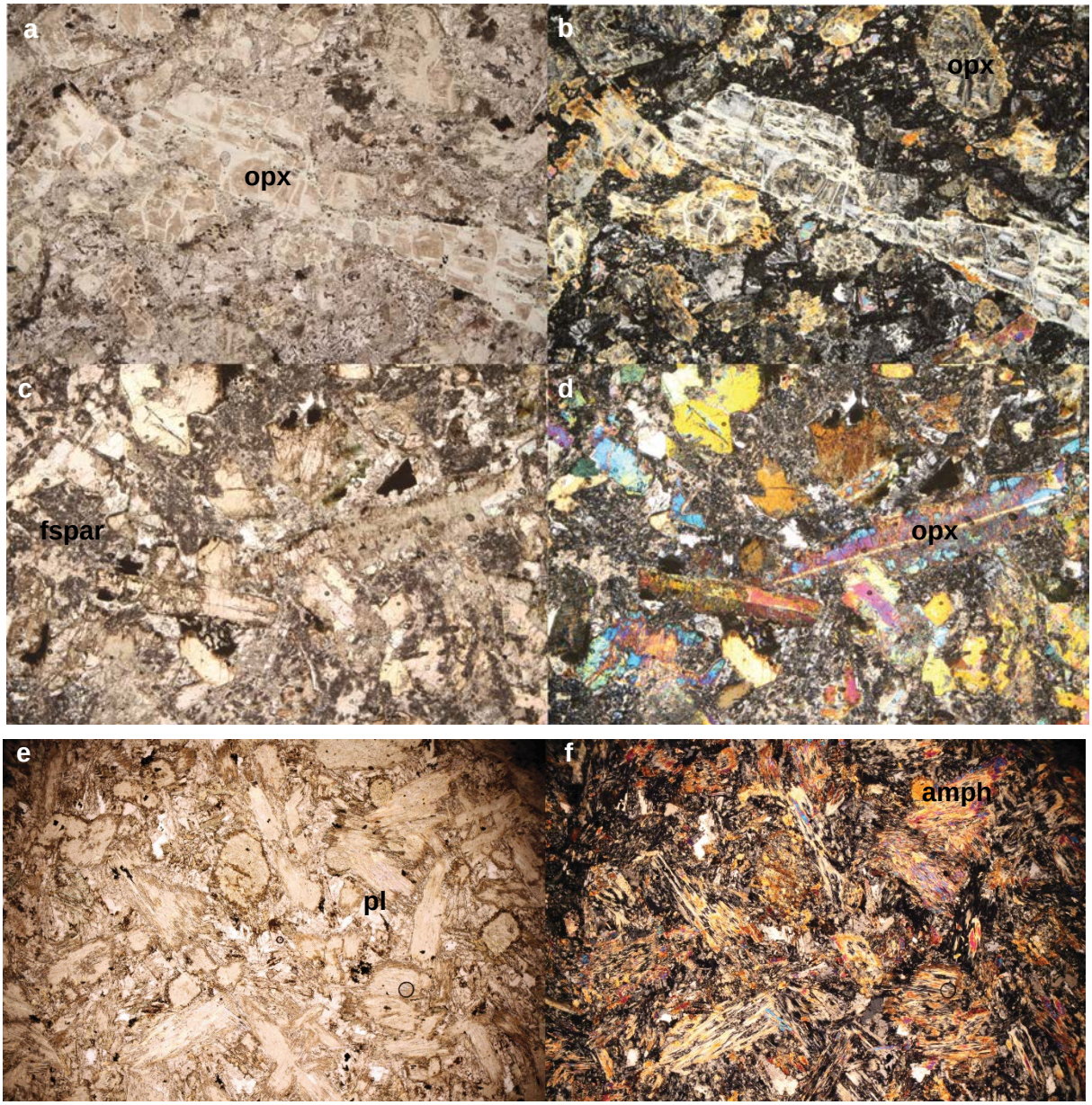


**Figure 5.7:** Microphotographs of more altered norites, where the field of view in each image is ~5.2 mm, and the left and right column show paired photographs taken under plane and crossed polars, respectively. (a-b) Sample BCS1-37, with pseudomorphed elongated opx, replaced by amphibole. Interstitial plagioclase. (c-d) More strongly altered BCS2-29 sample with large elongated and euhedral crystals of ortho-amphiboles which in ppl, tend to exhibit typical pinkish pleoichroism. Under xpl, the same crystals exhibit higher interference colours than orthopyroxene and are multiply twinned. Highly altered interstitial phases include feldspars with some quartz intergrowths, as well as accessory opaque phases. (e-f): Sample BCS1-31 is dominated by amphiboles; plagioclase is an interstitial phase but one can still see the pseudomorph outlines of what could have been primary opx.

## 5.3 Doleritic Suite

Amongst the 11 thin sections from this group, fresher samples typically display euhedral plagioclase laths amongst interstitial clinopyroxene, forming (sub-) ophitic textures (also noted in some hand specimens). Sample BCS2-53 from an Nkomati Mine drill core (Fig. 5.8 a-b), is the freshest example with such a typical doleritic mineralogy and texture, where large additional interstitial opaques of presumed (Fe+Ti)-oxides appear to be the last crystallizing phase. It is also conspicuous how doleritic samples tend to have a greater modal percentage of oxides than noritic samples.

BCS1-39 is an example of an even more altered dolerite with large skeletal opaques, which are interpreted as left-over ilmenite lamellas within subhedral oxides from which magnetite components have weathered out (Fig 5.8 e-f). Figure 5.9 shows sample BCS2-13, which is characterised by lath-shaped plagioclase microcrystals set in what could have been highly altered interstitial clinopyroxene within an ophitic dolerite but could also be set in a finer grained matrix of a porphyritic rock. Euhedral and sharply twinned plagioclase grains as well as a large greenish amphibole phenocrysts may argue for the latter interpretation. It is at least unusual with such large mafic phenocrysts within dolerites and its elongated habit may suggest that it was a primary amphibole, rather than a pyroxene.

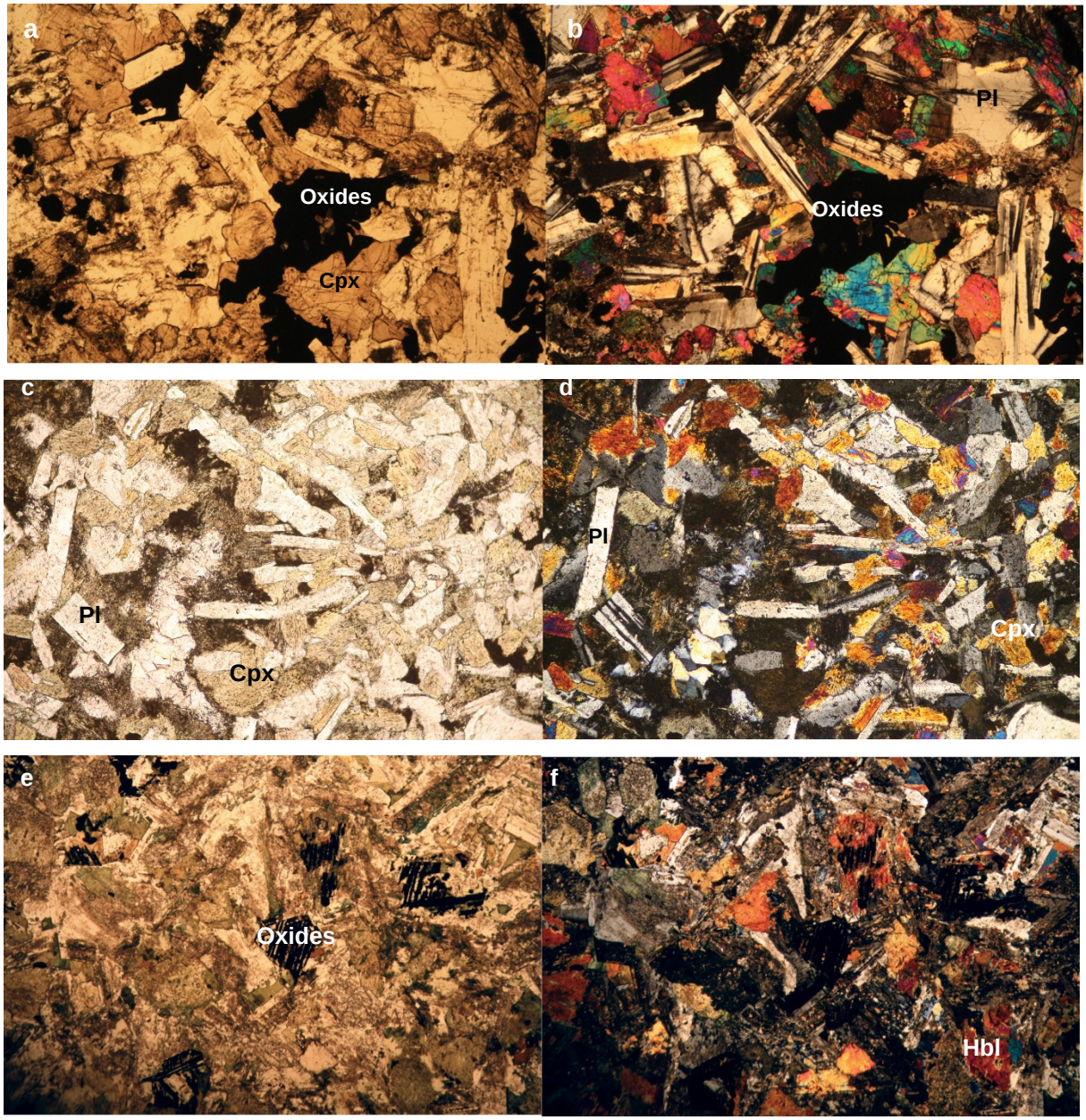


**Figure 5.8:** Microphotographs of relatively pristine dolerites, where the field of view in each image is ~5.2 mm, and the left and right column show paired photographs taken under plane and crossed polars, respectively. (a-b) BCS2-53 A sub-ophitic textured dolerite, with fresh eu-subhedral plagioclase, sub- to anhedral clinopyroxene and large anhedral opaques being most interstitial. (c-d) slightly altered dolerite, where the field of view in each image is ~5.2 m, BCS1-32 is slightly altered dolerite, dominated by euhedral plagioclase laths and interstitial augite. (e-f) Sample BCS1-39 is a highly altered hornblende and tremolite dominated rock, with saussuritized interstitial plagioclase and skeletal looking opaques, which collectively preserve a pseudomorph doleritic texture. Left and right photo taken under plane and crossed polarized light, respectively.

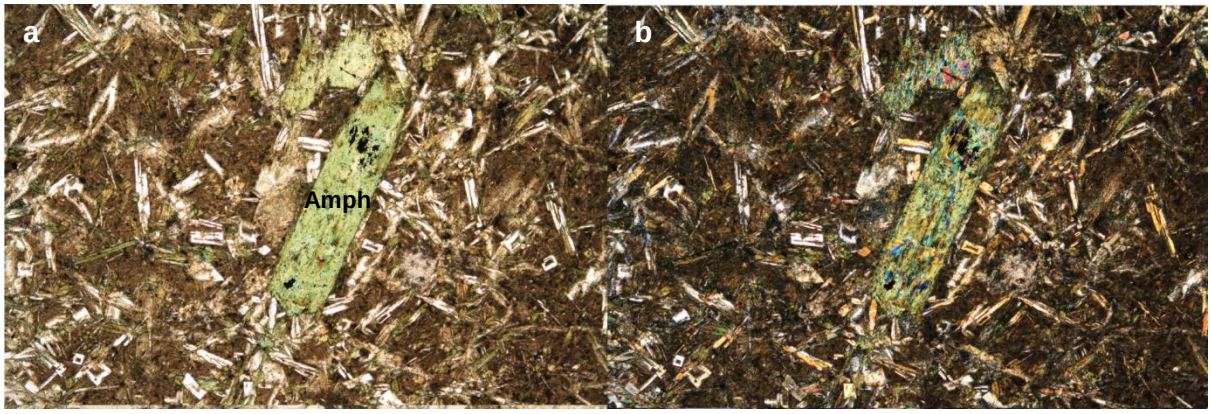


**Figure 5.9:** Microphotographs, where the field of view in each image is ~5.2 mm. (a-b) In sample BCS2-13, the main identifiable mineral phases are pale plagioclase laths and larger greenish amphiboles, set in a brownish fine grained and presumably altered 'matrix' of more uncertain origin. Left and right photo taken under plane and crossed polarized light, respectively.

Figure 4.13 shows an outcropping layered sill, from which scanned image of a cut contact between two layers is shown in Figure 5.10(a). The absence of any obvious chilled contact in Figure 5.10(a) and the sills' many centimetre to decimetre thick layers in Figure 4.13 indicates that the sill is rhythmically layered. Another cut surface (Fig. 5.10(b)) through the upper more melanocratic layer shows relatively little white plagioclase but it is otherwise difficult to identify the mafic minerals or discern any textures without a thin section. The cut surface in Figure 5.10(c) is from another more leucocratic layer in the lower parts of the sill, characterized by <2 cm large dark spots inside an otherwise plagioclase-rich gabbro that resembles the lower layer in Figure 5.10(a). It is worth noting, however, that the rock has euhedral plagioclases that are parallel orientated and could represent igneous lamination, which is typically found in layered gabbros.

Unfortunately, there is some uncertainty relating to the sample locations of BCS1-26 and BCS1-25, because the Honours student's field note book got displaced in 2008. However, their supervisor noted that the orientated BCS1-22 and BCS1-23 samples were collected from the layered sequence in Figure 4.13(a) and it is most likely that the subsequent two chemical analyses (and accompanying thin sections) represent samples from a more melanocratic and gabbroic part of this layered sill. This assumption agrees with a more melanocratic and gabbroic appearance of BCS1-26 and BCS1-25, respectively (no chemistry or thin section exist for BCS1-24), as well as a relatively confident location of subsequent samples (BCS1-27 to -32) as indicated on Figures 4.4 and 4.5. Nevertheless, doubt starts creeping in when it is noted that

these two presumed samples from the layered sills then represent an olivine meladoleritic gabbroic (BCS1-26) and a noritic (BCS1-25) layer (cf. normative pie charts in Appendix A2), seemingly co-existing within the same composite layered sill. As will become more apparent later on, this is very unexpected because the doleritic and noritic suites are not related to the same parent and can therefore not represent different layers within the same sill. So far, only new samples have been collected in 2017, while more time and funding is needed to produce critical geochemical analyses and thin sections from these.

Regardless of whether or not BCS1-26 and BCS1-25 are representative of a more melanocratic and more gabbroic layer, respectively, within this obvious rhythmic layered sill, it is first noted that both samples are highly altered, as indicated by skeletal oxides and greenish amphiboles (cf., Fig. 5.11). This makes it very difficult to recognize any primary igneous minerals or even pseudomorph textures, which could help explain whether they are doleritic or noritic, as well as truly cumulate rocks or not.

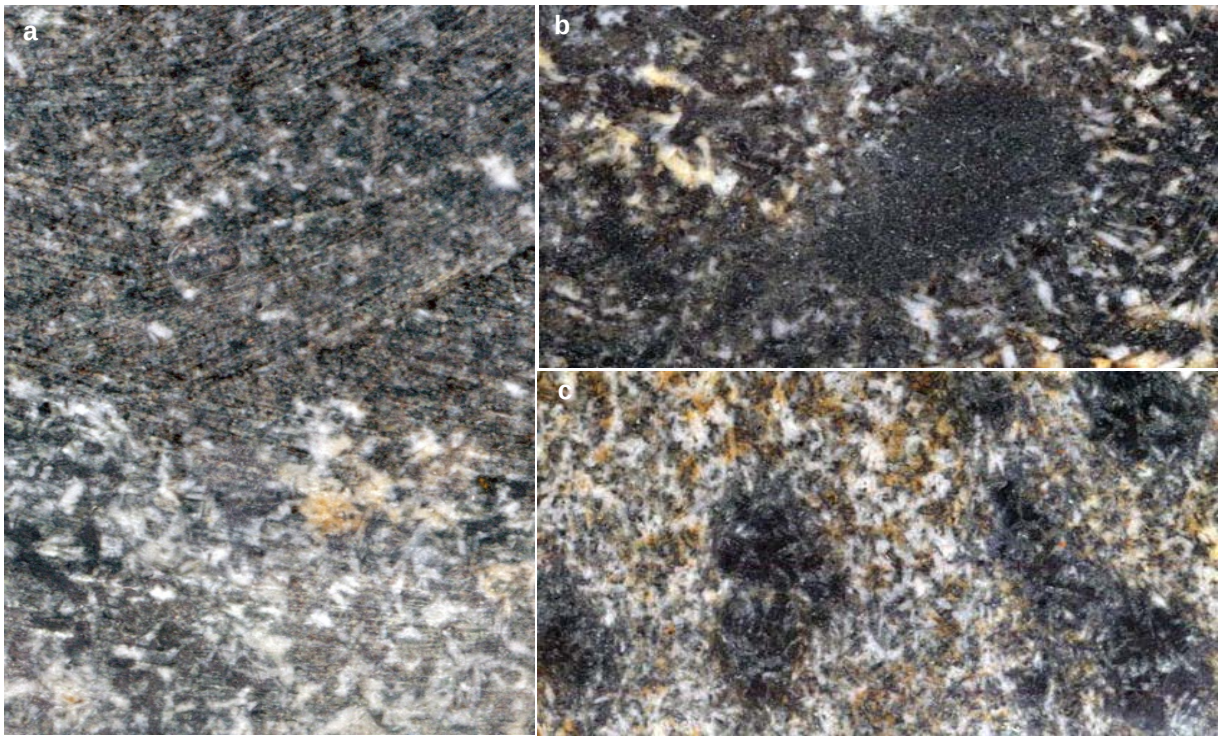


**Figure 5.10:** Scanned samples from layered sill in Figure 4.13 (a) the contact between an upper more melanocratic and a lower more normal gabbroic layer is without evidence of a fine grained chill. (b) BCS1-25 showing a fine grained dark enclave in the more melanocratic upper layer in (a). (c) spotted gabbroic BCS1-26 from a lower leucocratic part of the layered sill, dominated by more plagioclases. Darker spots may be pyroxene oikocrysts.

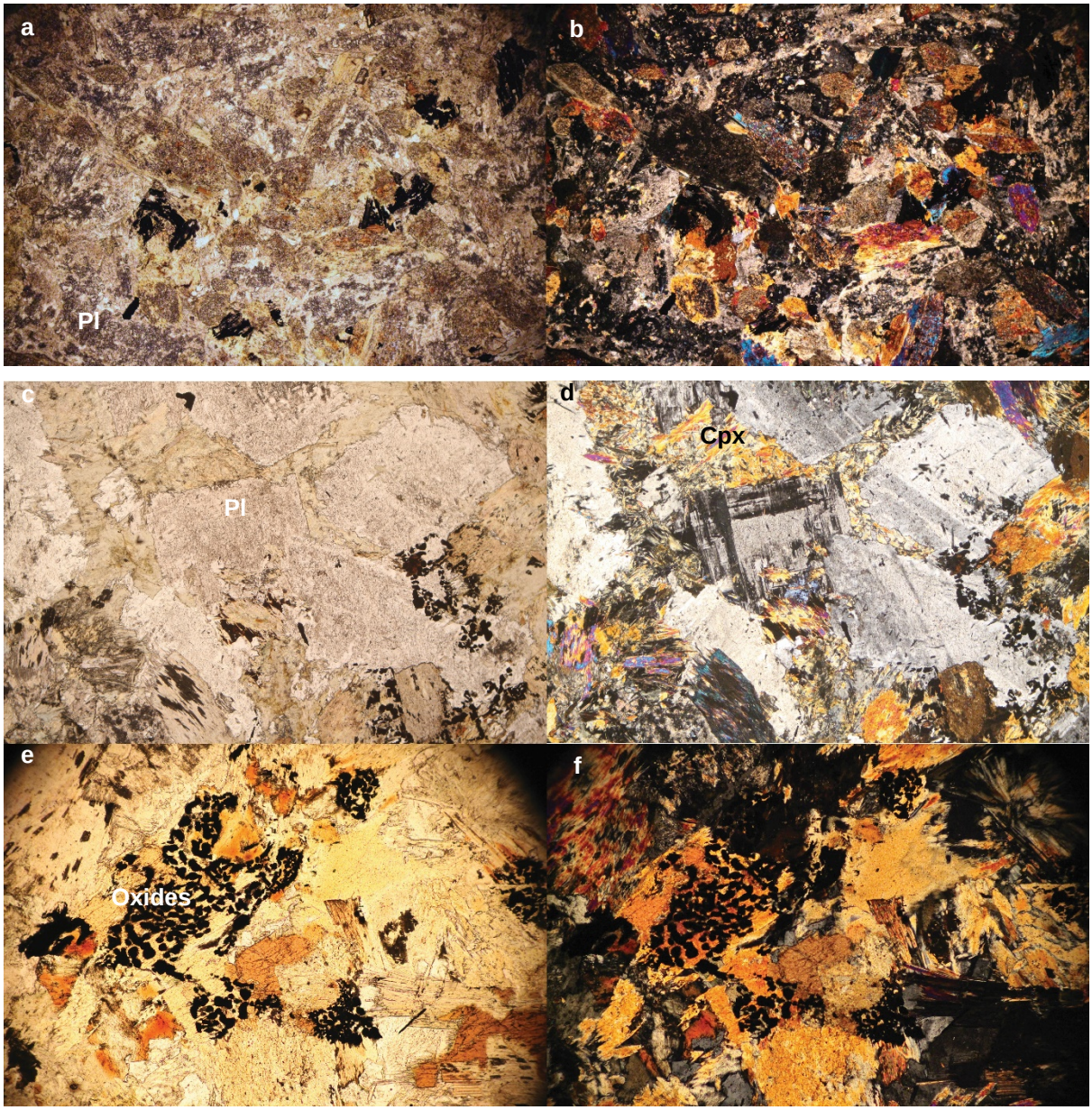


**Figure 5.11:** Microphotographs of two different units within a rhythmically layered sill, where the field of view in each image is ~5.2 mm, and the left and right column show paired photographs taken under plane and crossed polars, respectively. (a-b) sample BCS1-25 exhibiting the doleritic textures with plagioclase laths surrounded by clusters of fibrous pyroxenes. The original dolerite's pseudomorphic sub-ophitic texture was retained and this is seen in sample BCS1-39 (Fig 5.8 e-f). (c-f) BCS 1-26 shows a rock that exhibit patches of more subhedral plagioclase, with irregular fibrous patterns of clino-amphiboles.

Six more samples from the collection are more ultramafic and obvious cumulates, than the previous two altered samples from the rhythmically layered sill, where BCS2-07, -08, -09 and BCS2-02; and -03 may each have been collected from the same sill in the upper and lower part, respectively, of the Silverton Formation (Fig. 4.13), whereas BCS2-31 was obviously collected from a basement sill (Fig. 4.8). Their cumulate

origins are often supported by well-developed layering in the field (cf., Fig 4.12). Only two thin sections were made of these cumulate samples (BCS2-02 and 2-31):

The BCS2-02 sample was collected from the layered outcrops in Figure 4.12. Figure 5.12(a-b) shows that these rocks are made up of an abundance of up to 2 mm-large and rounded olivines, which are (sub) poikilitically, surrounded by either larger opx oikocrysts or sub-grained portions of interstitial plagioclase. It is obvious from this poikolitic texture that olivines accumulated before intercumulus opx grew around these. The thin section also reveals a few euhedral opaques with square habit, which most likely are primary chromites that accumulated together with the olivines from a relatively primitive magma. This rock is pervasively fractured along a preferred plane, along which the different minerals have experienced most of their different degrees and types of alteration. The more altered sample BCS2-31 Fig 5.12 (c-d) exhibits a pseudomorphed poikilitic texture, like that shown in BCS2-02, and is made up of serpentinized olivines with strands of opaques, left over from the serpentine reaction along previous olivine cracks. There is clearly <10 % intercumulus plagioclase, which classifies this as an ultramafic rock.

The BCS2-31 sample was collected from a basement sill outcrop that did not exhibit any obvious layering. Figure 5.12(c-d) shows that the rock is much more altered, yet possibly made up of totally serpentinized euhedral olivine pseudomorphs, which may have been less resorbed than the olivines enclosed by orthopyroxene in BCS2-02. It is uncertain, however, whether there were any similar opx oikocrysts in this heavily altered sample, which might then be altered into fibrous ortho-amphibole. In this case, it is better to resort to normative mineral proportions (e.g., pie charts in Appendix A2), which clearly show an over-abundance of both olivine and hypersthene and <20 % plagioclase, and makes it a plagioclase-bearing harzburgite.

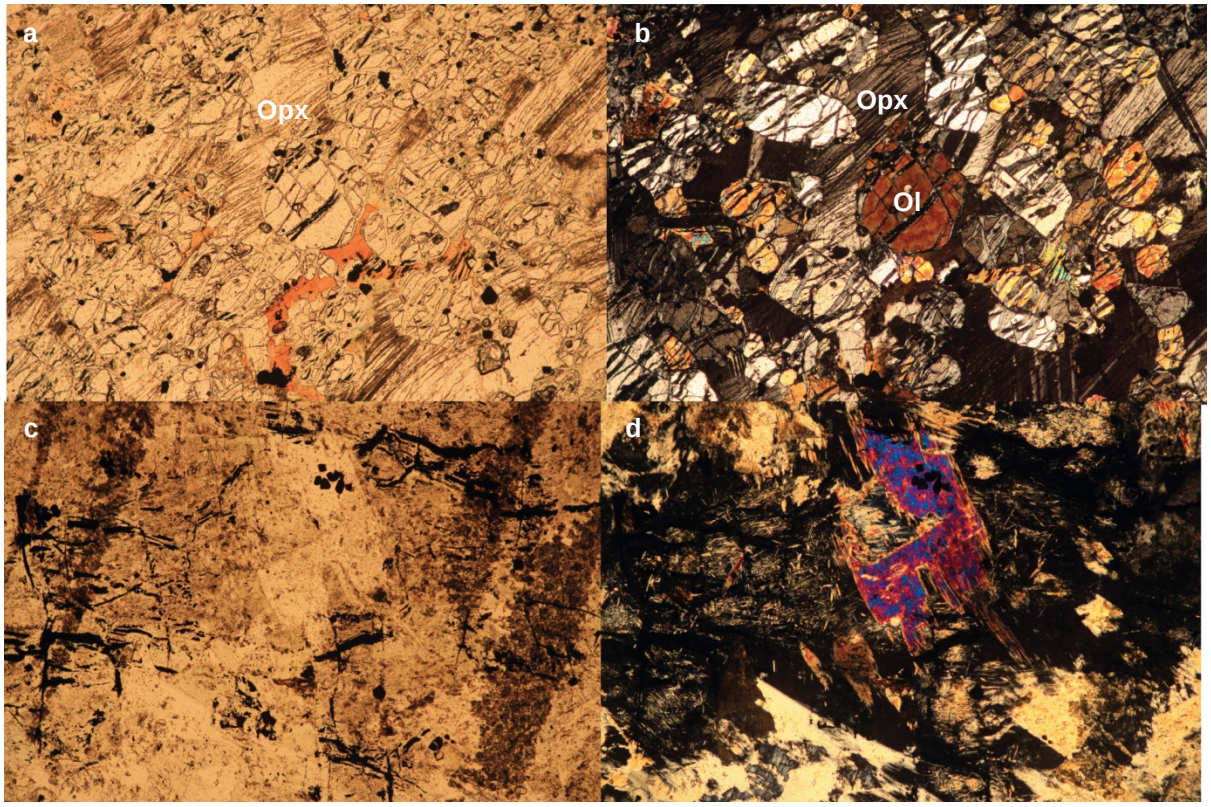


**Figure 5.12:** Microphotographs of ultramafic cumulates, where the field of view in each image is ~5.2 mm, and the left and right column show paired photographs taken under plane and crossed polars, respectively. (a-b) Sample BCS2-02, showing a poikilitic texture where orthopyroxene encloses euhedral olivine crystals (identified by its lack of cleavage and irregular fractures). The rock is pervasively fractured and olivines are preferentially serpentinized along these fractures, leaving behind opaque Fe-oxide bands inside the olivines and not inside the surrounding orthopyroxene oikocrysts. Additional euhedral and square-like opaques are interpreted to be cumulate chromite grains. Interstitial brownish biotite is also believed to be secondary. (c-d) Sample BCS2-31 is too altered to clearly display any cumulate minerals or textures, apart from likely serpentised olivines, if elongated opaques represent Fe-oxide along previously serpentinized cracks.

**Table 5.1:** Summary of petrography of available BCS2 and BCS1 thin sections.

| Sample ID | Group | L.O.I. | Sample description | Alteration |
|---|---|---|---|---|
| **BCS1-02** | Norites | 0.12 | Euhedral opx, inter cpx + plag (norite) | Fresh |
| **BCS1-01** | Norites | 0.77 | Euhedral opx, inter cpx + plag (norite) | V slight |
| **BCS2-25** | Norites | 2.85 | Euhedral Opx, lath plag (norite) | Slight |
| **BCS2-24** | Norites | 0.62 | Quench textured Euhedral opx + radiating plag (norite) | Mod-strong |
| **BCS2-12** | Evolved Norites | 1.49 | micrographic quartz-fsp, skeletal opaques (quartz-norite) | Moderate |
| **BCS2-22** | Evolved Norites | 1.65 | plg+px+graphic qtz (Qtz-norite) | Mod-strong |
| **BCS2-32** | Evolved Norites | 1.94 | Elong twinned orthoamphiboles, in altered plg, micrographic qtz-fspar (qtz-norite) | Mod-Strong |
| **BCS2-04** | Evolved Norites | 1.49 | much fresh euhedral plag,int fibrous replacement of opx?, quartz, Int hbl? | Mod-strong |
| **BCS2-11** | Evolved Norites | 2.00 | Eu-subhedral orthoamphiboles (pseudomorph opx?), subhedral plag, micrographic quartz-fsp. subhedral opaques (qtz norite) | V strong |
| **BCS2-01** | Norites | 1.18 | Euhedral opx, inter cpx + plag | Mod |
| **BCS1-15** | Altered norites | 1.42 | Eu-subhedral ortho-amphiboles (altered rims), much altered subhedral plag laths. | Mod-strong |
| **BCS1-14** | Altered norites | 1.46 | Eu-subhedral lath-shaped elongated ortho-amphiboles, Interstitial 'matrix' of | Mod-strong |

| | | | | |
|---|---|---|---|---|
| | | | hornblende, plag & quartz, large subhedral opaques. | |
| **BCS2-29** | Altered norites | 2.07 | Slightly skeletal opaques, eu-subhedral, very elongated twinned amphiboles, int plag (noritic) | Mod altered |
| **BCS1-26** | Altered dolerites | 2.48 | Irregular fibrous amphibole, mod skeletal opaques. patches of more eu-subhedral plagioclase | strong |
| **BCS1-31** | Altered norites | 3.87 | amphiboles (pseudomorph outlines of what could have been primary opx); int plagioclase | Heavily & pervasive |
| **BCS1-06** | Altered norites | 2.55 | Eu-subhedral mafics (ortho-amphibole), interstitial quartz (& plag?), moderate subhedral opaques. | Mod-strong |
| **BCS1-07** | Altered norites | 2.37 | Eu-subhedral mafics (ortho-amphibole), interstitial quartz (& plag?), moderate subhedral opaques. | Mod-strong |
| **BCS1-11** | Altered norites | 2.60 | Eu-subhedral mafics (ortho-amphibole), interstitial quartz (& plag?), moderate subhedral opaques. | V strong |
| **BCS1-08** | Altered norites | 2.32 | Large euhedral ortho-amphiboles (opx pseudomorphs), chaotic 'matrix' of subhedral & altered plag, clino-amphibole, int quartz | strong |
| **BCS1-37** | Altered norites | 3.34 | Euhedral opx laths appear to have first been serpentinized (bastite?) plag, clino-amphibole, micrographic qtz intergrowths (noritic) | Pseudomorph |

| | | | | |
|---|---|---|---|---|
| **BCS1-34** | Altered norites | 2.55 | Traces of euhedral px? Matrix obliterated | Pseudomorph |
| **BCS2-53** | Doleritic | -0.40 | Fresh sub-ophitic, Ti-rich augites around plag (much large int opaques) | Fresh |
| **BCS2-35** | Doleritic | 0.33 | subhedral cpx, moderate int opaques | Slight |
| **BCS2-40** | Doleritic | 1.67 | Euhedral mafic(high birefringence), Int plag(doleritic) | Slight-mod |
| **BCS1-28** | Doleritic | 2.29 | Altered sub-ophitic texture (cpx/amph?) & mod interstitial opaques (dolerite) | Altered |
| **BCS1-32** | Doleritic | 1.72 | Euhedral fresh plag & subhedral greenish augite/amph? (mod interstitial opaques), some long 'skeletal' plag (doleritic) | Weak |
| **BCS1-16** | Altered dolerites | 1.30 | Euhedral hornblende (+/- altered augites), more int but heavily alterted plag, large skeletal opaques. No qtz (doleritic) | Altered |
| **BCS1-39** | Altered dolerites | 1.76 | Eu-subhedral, plag with altered cores, interstitial green and pleichroic hbl (altered olivines?), large highly skeletal opaques. No quartz | Strong |
| **BCS1-25** | Altered norite | 1.90 | plagioclase laths surrounded by enclaves made by fibrous orthoamphiboles (originally pyroxenes) | strong |
| **BCS2-46** | Altered dolerites | 1.15 | eu-subhedral plag with alterted cores, interstitial hbl and bio, slightly skeletal opaques. No quartz (few greenish | V.strong alteration |

| | | | | |
|---|---|---|---|---|
| | | | patches with opaque dust = altered olivines?) | |
| **BCS2-49** | Altered dolerites | **6.06** | Greenish-isotropic, (epidote?) microcrystalline matrix. subhedral plag, opaques | Strong & sheared |
| **BCS2-02** | cumulates | **4.09** | Ol-opx cumulate | moderate |
| **BCS2-31** | cumulates | **6.84** | serpentinized olivines, opaque Fe-oxides strands along previous cracks | pervasive |

# 6 Bulk rock geochemistry

## 6.1 Rock alteration

Based on the previous petrographical observations in Chapter 5, the sampled intrusions range between fresh (where pristine igneous mineral have undergone very little to no alteration), through moderately altered (where original igneous minerals can still be identified) to strongly altered (where original igneous textures have been completely obliterated and primary minerals have been replaced by secondary alteration minerals).

As alteration often entails the hydration of mafic phases (typically amphibolitization of pyroxenes as well as olivine serpentinization), such alteration can roughly be monitored by a geochemical analyses' so-called Loss On Ignition (LOI). LOI values of all samples are listed in Table 5.1 and range between 0.06 - 6.84, where values above 1-2 wt% are tentatively regarded as anomalously high and possibly reflecting addition of $H_2O$ during alteration. The rest of the geochemical data used for this chapter are attached on appendix A4. These high LOI values do not necessarily correlate with petrographically more altered samples, however, with the exception of three pervasive altered samples (BCS2-31, 2-49 and BCS1-31) that also have the highest LOI values. In some instances, the samples with the lowest LOI contents are associated with the strongly altered rocks (BCS2-25 and BCS1-32, 1-15).

Alternatively, by plotting LOI against more fluid-mobile elements, it might be possible to more quantitatively test whether or not there is any relationship between alteration and LOI. Figure 6.1(a-d) plots CaO, $K_2O$, $Na_2O$ and Rb against LOI which all show that there exists no systematic correlation between LOI and these LILEs. The element scattering shown in the four diagrams plotted between LILE and LOI may be used to suggest that the bulk rock geochemical composition of samples was not severely modified by post magmatic alterations. Whole rock geochemical compositions of all samples from BCS1 and BCS2 collection are attached in appendix A4.

Finally, as will become evident later, different sill groups have too consistent geochemical signatures to have been seriously affected by any alteration, except for perhaps a few inconsistent samples that are not included in any of group that this study focuses on.

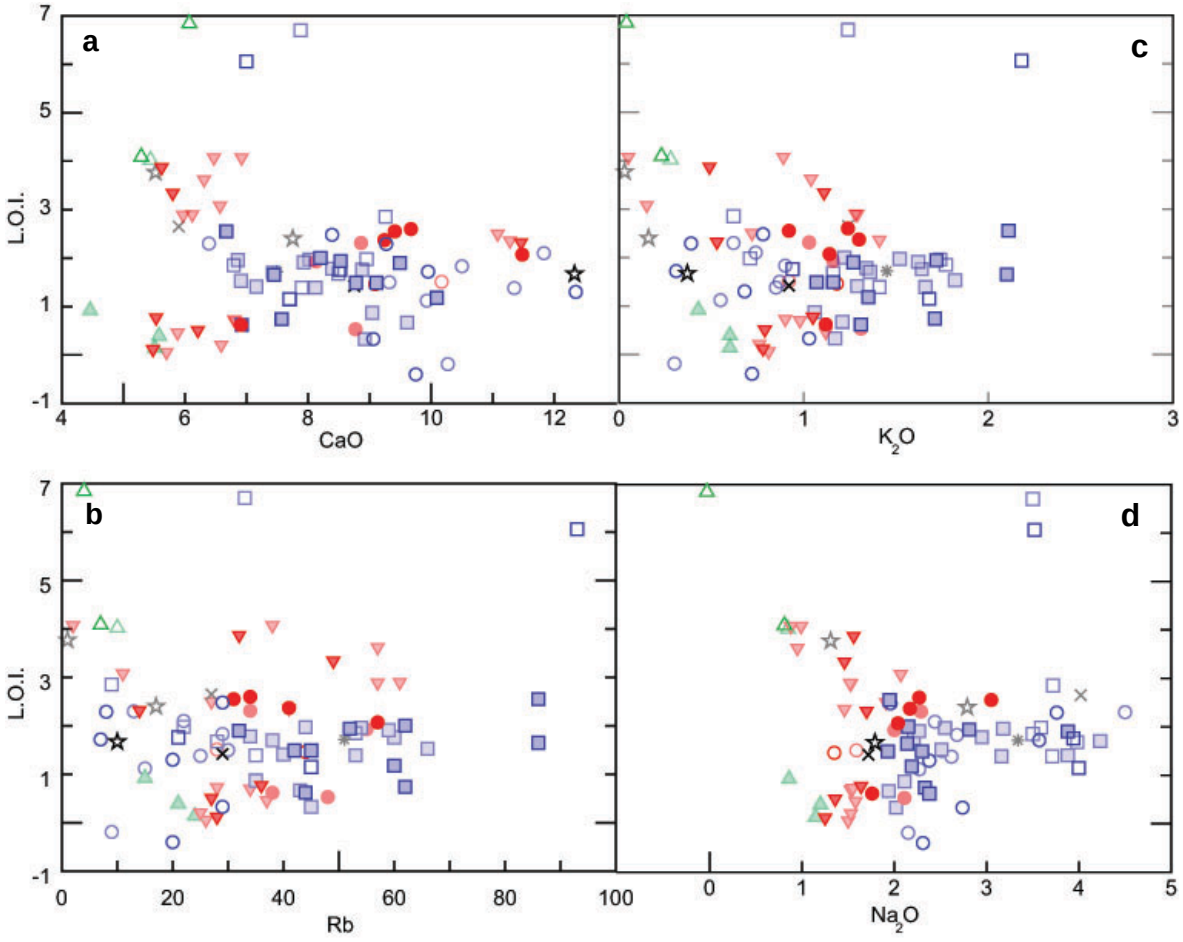


**Figure 6.1:** Four selected LILEs plotted against LOI, where the samples with no thin sections are plotted with faded colours. All LILEs show a scattered non-systematic relationship with LOI, suggesting that samples chemistries are relatively unaffected by alteration.

## 6.2 CIPW normative mineralogies.

CIPW norms were calculated by Kurt Hollocher's excel spread sheet (both into weight-% and volume-%), as well as through IgPet's bulk calculator, using an $Fe^{3+}/Fe^{2+}$ ratio of 0.1 for all of these mafic-ultramafic rocks. The relative proportions of different normative minerals are shown for each sample in Appendix A2, as pie charts, providing an alternative means to classify rocks petrographically, which is particularly useful for more altered samples. However, it also assumes an original dry mineral assemblage. Figure 6.2(a-c) shows four slightly different ternary diagrams, of which two are combined. For all cases, their two 'base' values are always normative *hy* and *di*, because these different pyroxenes are good discriminators between more noritic and gabbroic rock types, believed to be the two main magmatic suites in the study area.

A classification is most correctly done by plotting both pyroxene types – like in an IUGS opx-cpx-plag classification diagram for mafic rocks – against normative $plag_{2.7}$, which is calculated according to Barron (1980) by consistently adding 2.7 times more of the available *ab* to normative *an*. In Figure 6.2(b), both the normative pyroxenes are plotted against either normative *qtz* or *ol*, which are mutually exclusive CIPW minerals. This composite ternary diagram shows which samples are more or less *qtz*- or *ol*-normative and thereby indicate magmas that were silica-oversaturated to -under saturated, respectively. Finally, in Figure 6.2(c), the two normative pyroxenes are plotted against normative oxides (5 x *mt* +*ilm*), in order to distinguish between more or less Fe- and Ti-rich subgroups, as will be elaborated upon below.

As can be seen from Figure 6.2(a), as well as individual pie charts in Appendix A2, there is a smaller group of more noritic samples with relative high *hy* and less $plag_{2.7}$ as opposed to a majority of gabbronoritic rocks with higher plag. With the exception of a few harzburgitic cumulates, which plot together with the norites in Figure 6.2(a), the norites are all *qtz*-normative in Figure 6.3(b). On the contrary, gabbronorites range from highly *qtz*- to *ol*-normative types, where *ol*-normative types also tend to be more gabbroic than noritic. Many of these *ol*-normative gabbronorites have distinctly higher proportions of oxides (Fig 6.2c), as reflected by higher modal proportions of opaques (cf., Chapter 5 and Appendix A2).

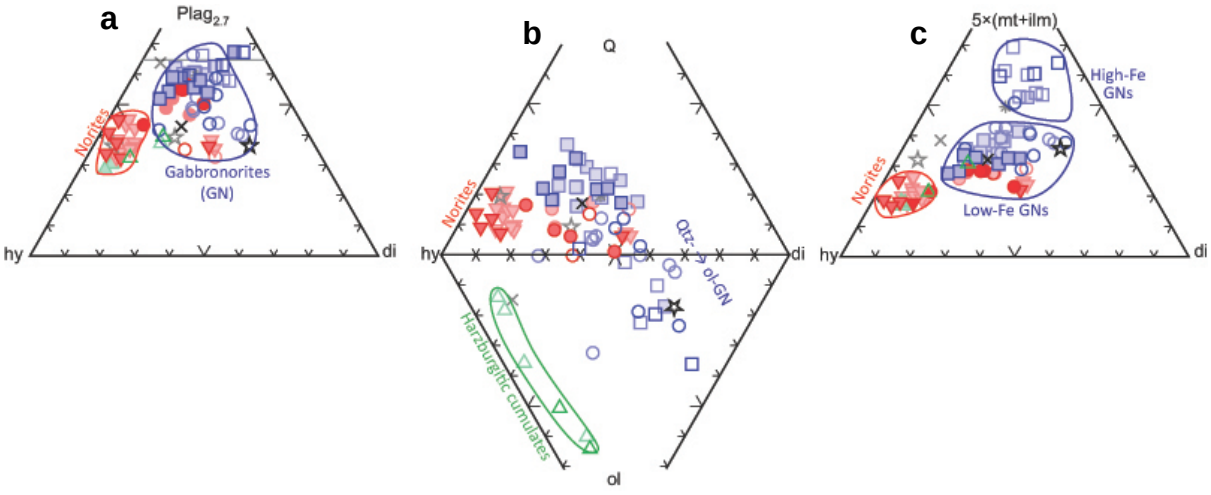


**Figure 6.2:** Four ternary plots of calculated CIPW normative mineral proportions, where hypersthene (*hy* = enstatite) and diopside (*di* = augite) are plotted against (a) plagioclase (*Plag* $_{2.7}$, which is an plus 2.7 times more of the available *ab* being allocated in plagioclase than together with *or* in alkali feldspar; cf., Barron 1980); (b) Mutually exclusive quartz (*qtz*) and olivine (*ol*), and (c) magnetite and ilmenite (5 x *mt* + *ilm*).

When classified in a TAS diagram after Le Maitre et al., (1989), the samples show a considerable major element chemical variation amongst all samples, within the subalkaline fields for basalts, basaltic andesites, andesites, and even a few more trachytic varieties (Fig 6.3 a). The latter more alkaline group may belong to a separate suite (mainly including samples shown as open blue squares) with a general predominance of $Na_2O$ over $K_2O$ (The $K_2O$ content of these alkaline sills range between 1.6 and 2.18 wt% and $Na_2O$ between 3.5 and 4 wt%). There also appears to be a very low-alkaline suite, including most harzburgitic cumulate samples (green triangles) as well as the more noritic samples (red triangles) with euhedral Opx, which do not fall on the more typical subakali trend defined by most of the other samples (i.e., open blue circles, filled red circles and filled blue squares). This is somewhat consistent with Figure 6.2(a), where ol-normative gabbronorites also are more basaltic (or alkaline) and more *qtz*-normative gabbronorites are more andesitic. The black star and black crosses of what is referred to as the “inconsistent group” show no consistent behaviour between different plots; i.e. neither belong to either the noritic or doleritic suite and are in Figure 6.3(a) distributed within the basalt-basaltic andesite fields of the TAS classification.

The open symbols of the more ol-normative samples also stand out by having higher Fe# as well as lower $SiO_2$ (Figure 6.3b), which indicate that these are more tholeiitic (or in the case of the squares, more alkaline). In contrast, most of the *qtz*-normative filled symbols (micrographic quartz- fspar dominant) have higher $SiO_2$ and relatively low Fe#, typical for more calc-alkaline suites but also consistent with their lower normative proportions of (Fe,Ti)-oxides (Fig 6.2c). The noritic samples (red triangles) stand out, together with the harzburgitic cumulates (green triangles), by having the lowest Fe#.

Furthermore, by using MgO as a differentiation index, rather than $SiO_2$, Figure 6.3(c-d) shows that the harzburgites and many mela-norites are even more MgO-rich than a common primary oceanic basalt (typically <12 wt% MgO). In the case of the hartzburgites such high MgO is consistent with their layering (Fig 4.3) and cumulate olivine (Fig 5.13); whereas, potential quenched textures of some mela-norites (Fig 5.5 e-f) suggest that their high MgO might resemble their primary melt compositions. If so, their relatively high MgO and $SiO_2$ resemble those for boninitic melts (cf., dashed

classification box in Fig 6.3c-d). This is also consistent with the norites' relatively low $TiO_2$ (Fig 6.3d), which in most cases also fall below the upper 0.5 wt% $TiO_2$ limit for boninitic melts, or, at least, are distinctly lower than *ol*-normative gabbronorites (open symbols).

Turning to the other samples, $TiO_2$ appears to be a very good discriminator, which much like Fe# in Figure 6.3(b) identifies 2-3 different magma suites, referred to as a (1) "hiTi" suite of primarily ol-normative and more alkaline gabbronorites (open blue squares); (2) "meTi" suite of primarily ol-normative yet more subalkaline and tholeiitic gabbronorites; and (3) "loTi" suite of most qtz-normative sills, including both norites and gabbronorites (and maybe even cumulate harzburgites). As argued for Fe#, these different suites cannot be related through fractional crystallization. Other major element variation diagrams may test this further, as well as put greater constraints on bulk fractionating phase assemblages.

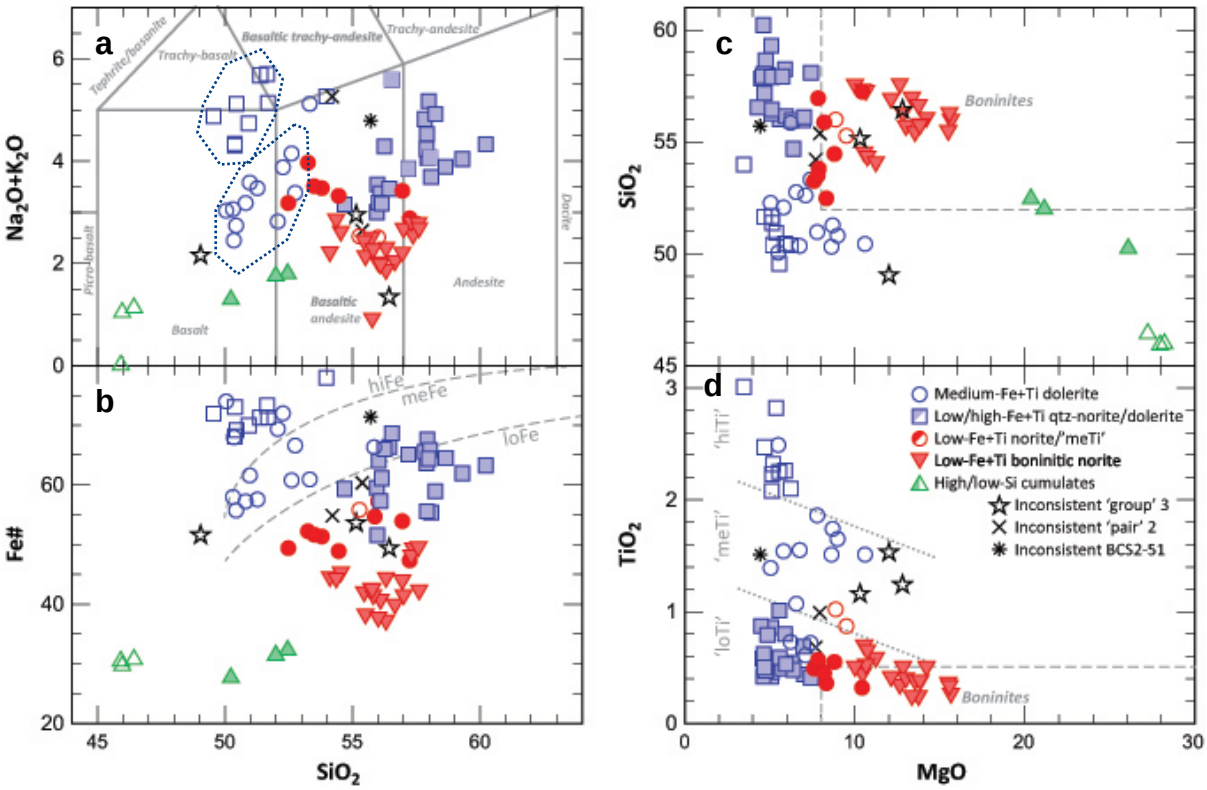


**Figure 6.3:** Four major element classification diagrams: a) Total alkalis vs Silica diagram of Le Maitre et al (1989) distinguishing between different rock types. b) Fe# vs $SiO_2$ distinguishing between loFe (calc-alkaline) >< hiFe (tholeiitic) suites. This Fe# plot is a revised version of (Myiashiro, 1974; Arculus, 2003), as a substitute for the AFM-diagram. c) MgO vs $SiO_2$, as a good discriminator between the more $SiO_2$ rich noritic suite and a doleritic suite with lower $SiO_2$. The field for high-MgO (>8 wt%) & $SiO_2$ (>52 wt%) boninites are shown by dashed lines. d) MgO vs $TiO_2$, from which three different levels referred to as LoTi, MeTi, and hiTi are unlikely to be related through fractional crystallization. Boninites have <0.5 wt% $TiO_2$.

Variation diagrams of selected major oxides are in Figure 6.4 plotted against Mg# (calculated as [(MgO/(MgO+(0.9*FeO*)) *100]), as a proxy for magma evolution, and are used to identify possible fractionation trends. At least two trends appear in Figure 6.4 (a-b and d), which are mainly made up of the noritic and doleritic suites and may each be related to fractional crystallisation from the same parental magma. In this case (1) the qtz-normative noritic suite, including norites and hartzburgite cumulates (green symbols), could also be referred to as the boninitic norite (BN) suite and (2) the ol-normative doleritic suite, including both more subalkaline and alkaline gabbronorites, could also be referred to as tholeiitic dolerite (TD) suite.

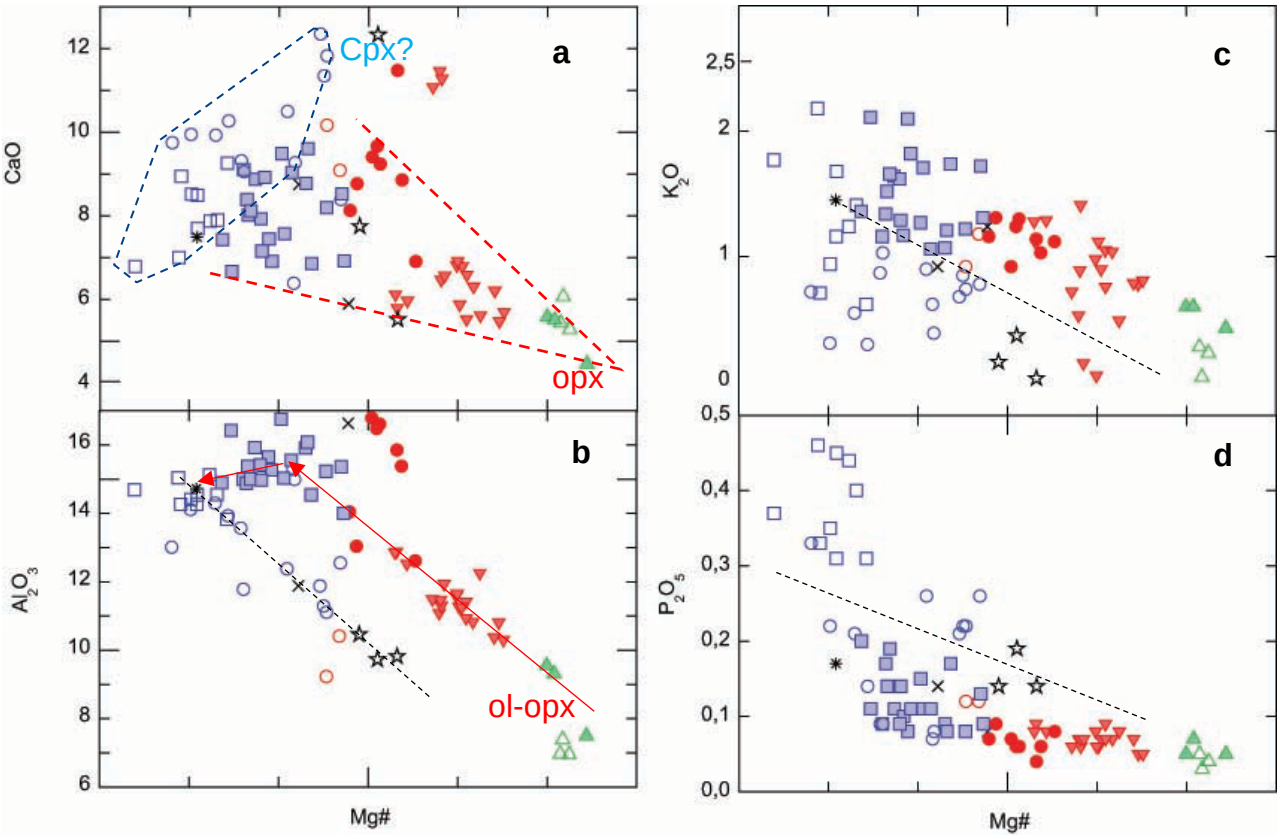


**Figure 6.4:** Major oxides (in wt%) plotted against Mg# as a differentiation index. In a-b, different trend lines roughly indicate how major oxides change with differentiation (possibly by fractionation of opx, ol or cpx) for different suites. In c-d, the dashed lines roughly separates two main suites, indicated by open or filled symbols. Symbols as in Figure 6.3.

More specifically, CaO concentrations for the BN-suite increase in a rather scattered fashion against decreasing Mg# (Fig. 6.4a); whereas, the TD-suite defines a steep positive trend. In Figure 6.4(b), both suites define sub-parallel trends of $Al_2O_3$ increasing against decreasing Mg#, which argues against plagioclase fractionation

during the differentiation of both suites. However, there may be a slight decline amongst the more evolved norites (indicated with a red arrow in Fig 6.4b), which could reflect a relatively late onset of plagioclase fractionation. This, furthermore, suggests that augite was the main fractionating phase for the TD-suite, explaining their CaO-decline against decreasing Mg#.

In addition to the BN-suite being overall more $Al_2O_3$-rich than the TD-suite, Figures 6.4(c-d) show that the BN-suite also has higher $K_2O$, yet lower $P_2O_5$ than the TD-suite, which collectively support the previous notion that these two suites are not related through fractional crystallization from a common parent. In the case of $P_2O_5$, its overall lower concentrations compare with the BN-suite's lower Fe# and $TiO_2$; i.e., is relatively depleted in high field strength elements, as opposed to LILEs like $K_2O$. In all of these cases, these elements increase incompatibly against decreasing Mg#, as a differentiation index, arguing against any (Fe,Ti)-oxide or apatite fractionation during the evolution of both suites.

## 6.3 Trace Elements

Both the Cr and Ni in Figure 6.5 a-b exhibit remarkably well defined decreasing curved trends against decreasing Mg#, where concentrations fall from 3736 to only 9 ppm Cr and 1400 to 4 ppm Ni. This, together with the decreasing Mg#, is consistent with the fractionation of chromite, olivine, and/or orthopyroxene. However, values greater than what is expected from a primary mantle melt (e.g., >1000 ppm Cr and >250-400 ppm Ni) more likely formed through the accumulation of such phases, and this interpretation is supported by the fact that hartzburgitic cumulates also have the highest abundance of Cr (>2616 ppm) and Ni (>700 ppm); consistent with the cumulate chromites olivines observed in BCS2-02 (Fig 5.13). One may note the high Cr- and Ni-contents of three 'inconsistent' samples (open black stars in Fig 6.5a-b), which do not conform to the overall curved trend, and may reflect chromite+olivine accumulation in these more samples even if these do not have as high Mg# as the harzburgitic cumulates. Cobalt (Co) is another element with a high partitioning coefficient for olivine, but does not show as distinct compatible trend as Ni and Cr, but rather a wide decreasing scatter against decreasing Mg# for both suites.

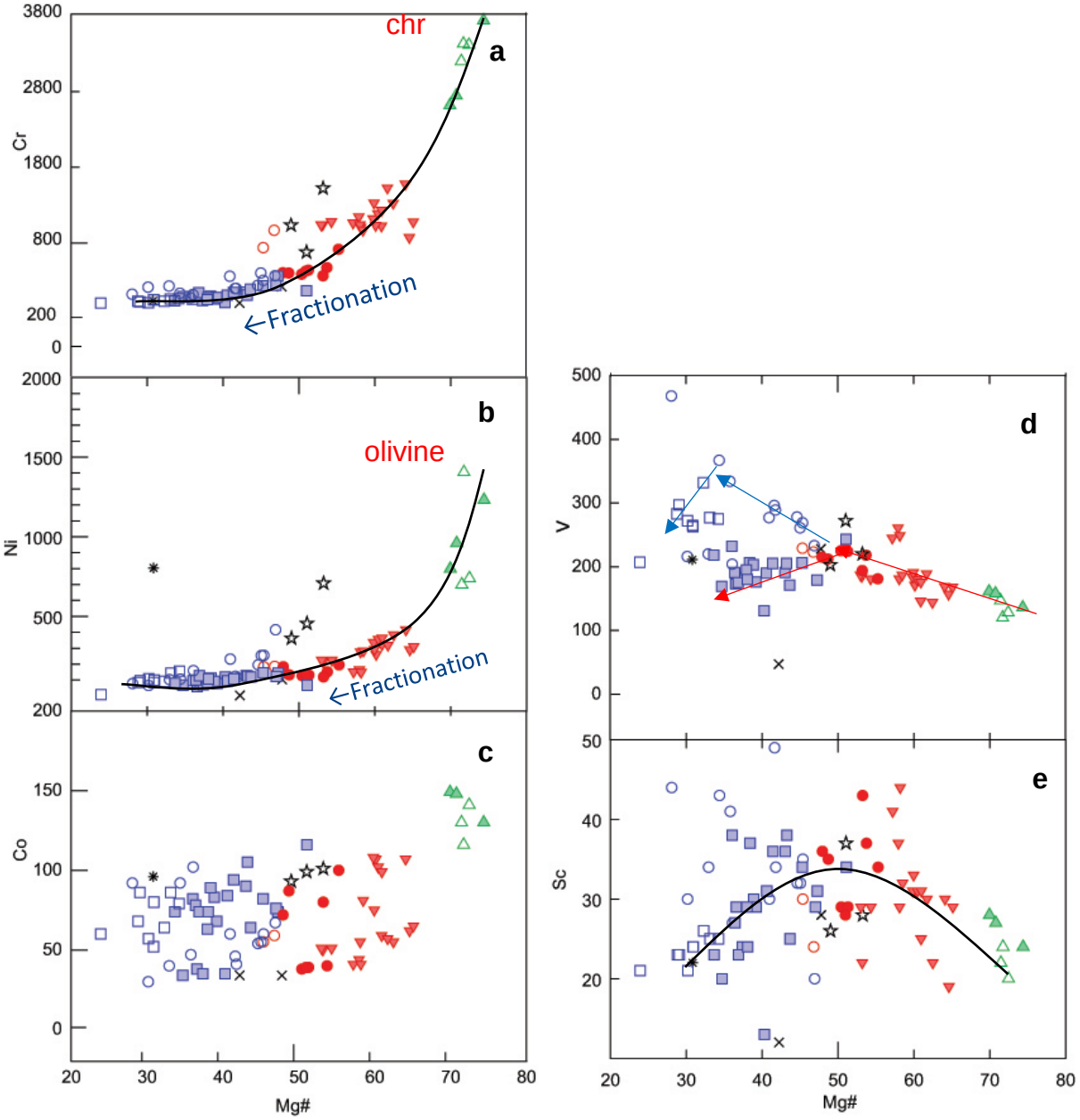


**Figure 6.5:** Selected more compatible trace elements (in ppm) ploted against Mg# as a differentiation index. Red lines and arrows indicate trends for the BN-suite; whereas, blue lines and arrows apply to the TD-suite. Black lines apply to both suites. Symbols as in Figure 6.3.

Against decreasing Mg#, Vanadium (V; Fig 6.5d) exhibits a kinked trend for the BN-suite, which first increases from the most primitive cumulates and through the boninitic norites (red triangles; Mg# >50) and then changes to a decreasing trend through the more evolved quartz norites (Mg# <50). The TD-suite may also exhibit a similar, kinked trend, but with its elbow closer to a Mg# of 35. Thus, behaving both incompatibly and then compatibly against decreasing Mg#, and because of V's high partitioning

coefficient for ilmenite may record the onset of (Fe,Ti)-oxides at Mg# ~ 50 and ~35 for each suite, respectively. However, ilmenite fractionation is not supported by similar kinked $TiO_2$-trends in Figure 6.3(d), rendering this interpretation uncertain. Scandium (Sc;) is often regarded as having particularly high partitioning coefficients for pyroxene and as its scattered distribution in Figure 6.5(e) roughly mimics the V-trend in Figure 6.5(d), this may argue for the onset of pyroxene, rather than ilmenite, fractionation (requiring that V is also compatible in pyroxene).

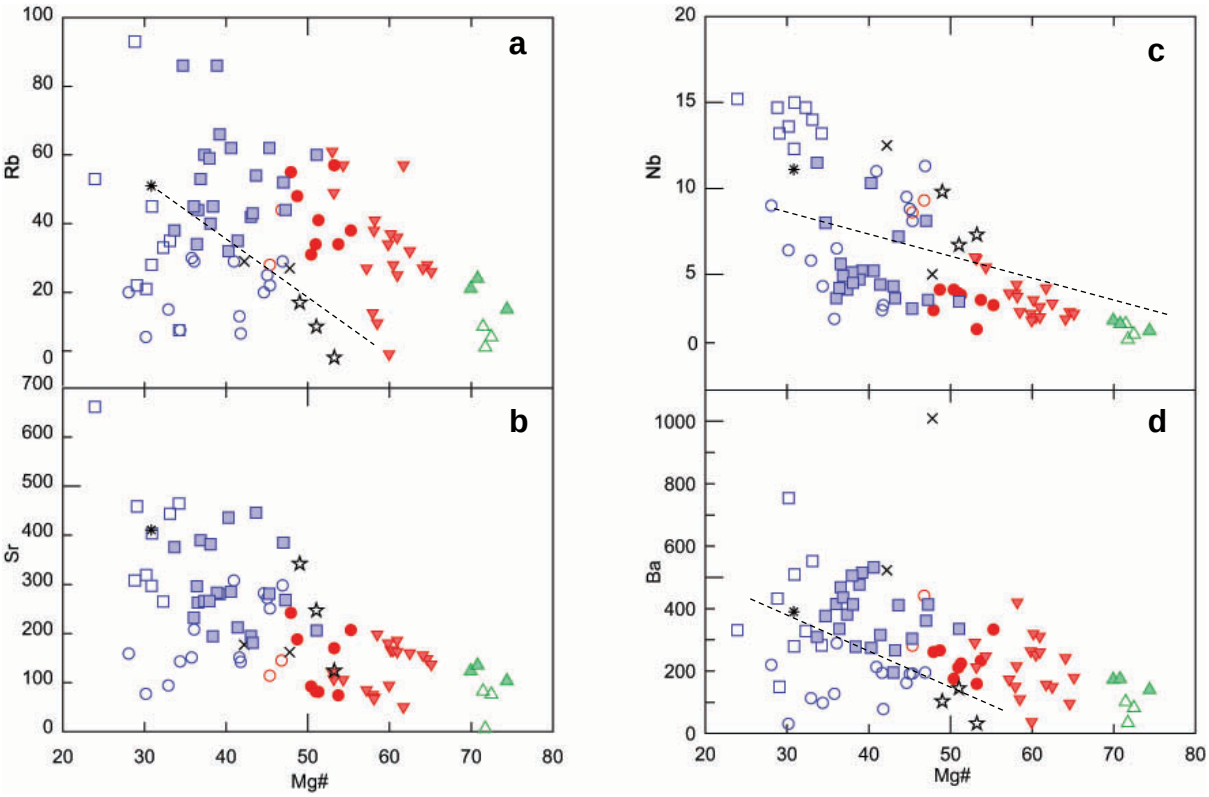


**Figure 6.6:** Selected more incompatible trace elements (in ppm) plotted against Mg# as a differentiation index. Dashed lines roughly separate BN- from TD-suites, as in Figure 6.4c-d. Symbols as in Figure 6.3.

Turning the attention to typically more incompatible trace elements, both suites exhibit increasing Nb with decreasing Mg#, but where the TD-suite has overall higher concentrations than the BN-suite, consistent with previous inferences that the TD-suite generally has higher HFSE (e.g., $TiO_2$ in Fig. 6.3d). Niobium is a particularly important element, however, since it is often anomalously low in subduction zone settings. In contrast, the BN-suite has relatively higher LILEs, including Ba, Rb and Sr, shown in Figure 6.6(b-d), although this distinction between more mobile elements that are susceptible to alteration is not as clear as for Nb. It is interesting, however, that both

anomalously low Nb and relatively higher LILE/HFSE are typical for subduction zone setting, and will be discussed further in the following chapter.

## 6.4 Rare Earth Elements

The rare-earth elements (REE) group is a special group of incompatible trace elements, with the same $3^+$ charge and only slightly smaller atomic radius with increasing atomic number up through the Lanthanide series. This allows for subtle differences to be recorded, which typically relate to the composition, depths and degree of partial melting of the mantle source, as well as the proportions and types of subsequent fractionating minerals. Thus, slightly more incompatible lighter REEs (LREEs with lower atomic numbers) tend to become more enriched than heavier REEs (HREEs) and thereby produce negatively sloping REE-patterns, except when the mantle source is so depleted that the opposite might become the case (e.g., classical N-MORB patterns). Furthermore, the presence of both oxidized $Eu^{3+}$ and reduced $Eu^{2+}$ allows plagioclase fractionation to produce negative Eu-anomalies.

REEs are usually plotted against chondritic values (e.g., McDonough and Sun, 1989 used here), not only to remove systematically higher concentrations of elements with even atomic numbers, inherited from our solar nebula but also to see how much more enriched magmas have become, relative to what the newly accreted Earth started as. In Figure 6.7, such chondrite-normalized REE patterns are first plotted for each of the two major suites in this study, which reveals the following differences:

The REE patterns of the BN-suite (Fig 6.7a), (primitive norites in red and evolved norites in blue) including hartzburgitic cumulates (in green), are all almost parallel to each other and characterised by relatively steep REE-patterns, with distinct enrichments of LREE over HREE. The overall mela-noritic sills have La concentrations that are 40 to 100 times chondrite; whereas, harzburgitic cumulates have lower patterns with La concentration between 10 and 40 times chondrite. The REE pattern of the BN-suite, expressed as Eu/Eu* values in Figure 6.8, range between 1.15 (slightly positive) to 0.45 (distinctly negative). The Eu/Eu* values in Figure 6.8 are plotted against $Al_2O_3$ as an index of plagioclase fractionation, during which $Al_2O_3$ is expected to decrease. However, there is no obvious correlation in this plot and this is consistent with the limited indication of plagioclase fractionation in Figure 6.4(a) as

well as the absence of euhedral plagioclases in more primitive noritic rocks. Samples BCS2-02 shows a negative Tb spike and BCS2-09 shows a negative Ho and Tm, which cannot be attributed to any geological process and might be due to analytical errors.

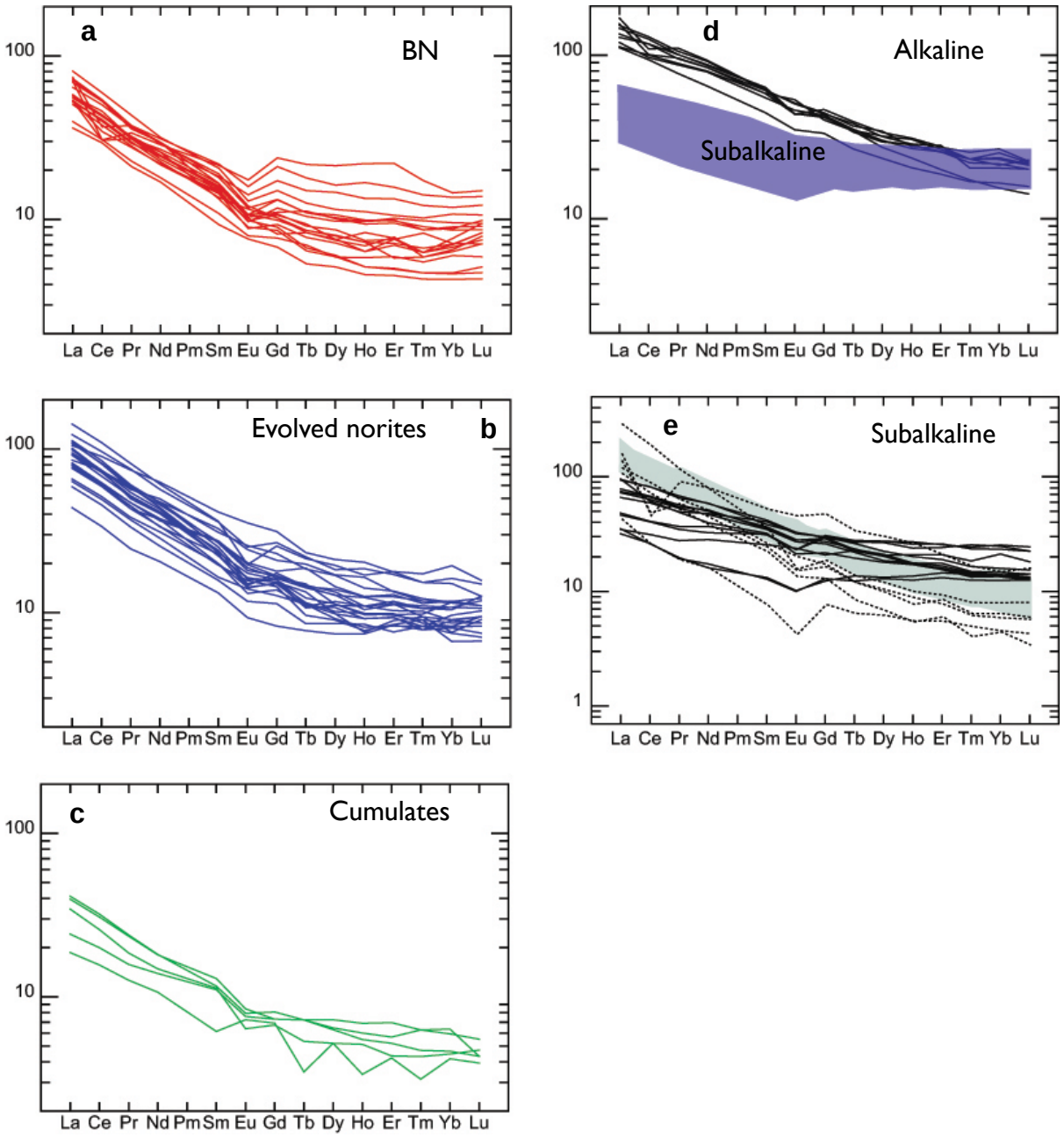


**Figure 6.7:** Chondrite normalised REE plots for a-b) BN-suite (both parental and evolved norites), c) cumulates and d-e) TD-suite (alkaline and subalkaline, where the background of the other plot is shown for comparison in each diagram). Note the flatter LREE-patterns for the subalkaline TD-suite. Normalization factors from McDonough and Sun (1989).

In contrast, the TD-suite (Fig 6.7d-e), including both more alkaline (plotted at the top with the subalkaline compositional range in the background) and sub-alkaline sub-groups, they exhibit less enriched REE-patterns, with especially higher HREE-concentrations than most BN-suite samples. In detail, the more alkaline sub-group is more LREE enriched, with La concentrations that are 100 to 200 times chondrite and relatively flat HREEs ($(Er/Yb)_N$ ratios of ~1.1) that are 20 and 30 times chondrite. The more subalkaline sub-group exhibit less LREE-enriched and almost flat REE patterns. There are some negative Eu anomalies amongst these sub-alkali samples, but no systematic variations that could relate to plagioclase fractionation, even if these sub-ophitic rocks do have euhedral plagioclases. This is supported by Figure 6.8, where there is no systematic decrease in Eu/Eu* against decreasing $Al_2O_3$, as would be expected during plagioclase fractionation from a common parent. Sample BCS1-29 found within the subalkali gabbronorites, shows a flat REE pattern (this could be from a more depleted source). Plotted along with the sub-alkali dolerites are the samples representing the “inconsistent” subgroup (dotted lines). Their REE patterns appear steeper than the almost flat TD suite.

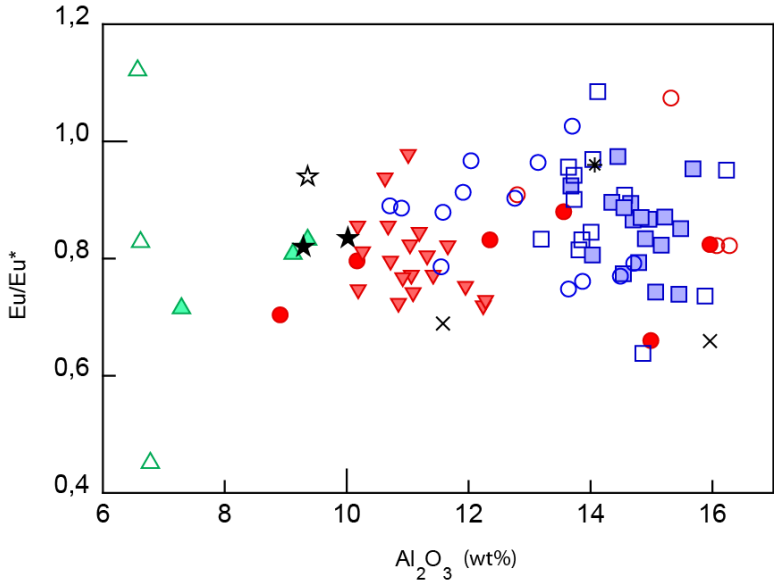


**Figure 6.8:** A plot of $Al_2O_3$ vs Eu anomalies (Eu/Eu* calculated in Igpet as 2*Eu/(Sm+Gd)N) showing no (Eu/Eu* = 1) to relatively negative (Eu/Eu* < 1) Eu-anomalies, but not necessarily against decreasing $Al_2O_3$. There is also no obvious discrimination between the two suites.

## 6.5 Multi-elements plot (spider grams)

On a spidergram normalized according to McDonough and Sun (1995) by a primitive-mantle-, all BN-suite samples demonstrate overall steep slopes, which decrease from primarily LILEs (e.g., Cs up to 600 times the primitive mantle) to primarily HFSEs, and especially HREEs (e.g., Lu down to 1.5 times the primitive mantle). All of these BN-rocks most notably have pronounced negative Nb-Ta spikes, together with distinct positive Pb spikes and relatively high LILE-HFSE ratios, as particularly diagnostic subduction zone signatures. This does not mean that these rocks formed above a subduction zone, however, because mafic magmas can also be sourced from a lithospheric mantle that has been metasomatized above an ancient subduction zone, and/or incorporate older subduction-generated crustal rocks. These various options will be discussed further in Chapter 7. In addition to their 'subduction zone' signatures, the BN-suite also exhibits distinctly negative and Ti anomalies, which can be attributed to preceding apatite and ilmenite fractionation, respectively. As this contradicts the incompatible behaviour displayed by their inverse correlations with Mg# (Figs 6.3d and 6.4d), however, this may also reflect the compositional characteristics of this BN-suite's source and/or assimilant. The harzburgitic cumulates plotted in Figure 6.9c, show concentrations of LILE lesser than those of the other boninitic norite sills.

The differences between the more alkaline and sub-alkaline subgroups of the TD suite is noted from their non-parallel incompatible elements patterns They exhibit an overall different slope to that of the BN where they tend to generally be shallow, flatter and decrease slightly from low LILE values (e.g., Cs up to 200 the primitive mantle) to slightly higher HREE values (e.g., Lu values down to 4.5 time the primitive mantle) in figure 6.9b. In general, these rocks are poorer in LILE/HFSE and richer in HREE. The Nb-Ta spikes are absent in this suite which, along with the absence of any pronounced anomalies is evident of no pronounced mineral fractionation during differentiation (with the exception of slight negative Sr spikes seen in the sub-alkaline dolerites). It is important to note the shaded backgrounds representing Barnes et al's (2010) compositions which will be discussed further in chapter 7.

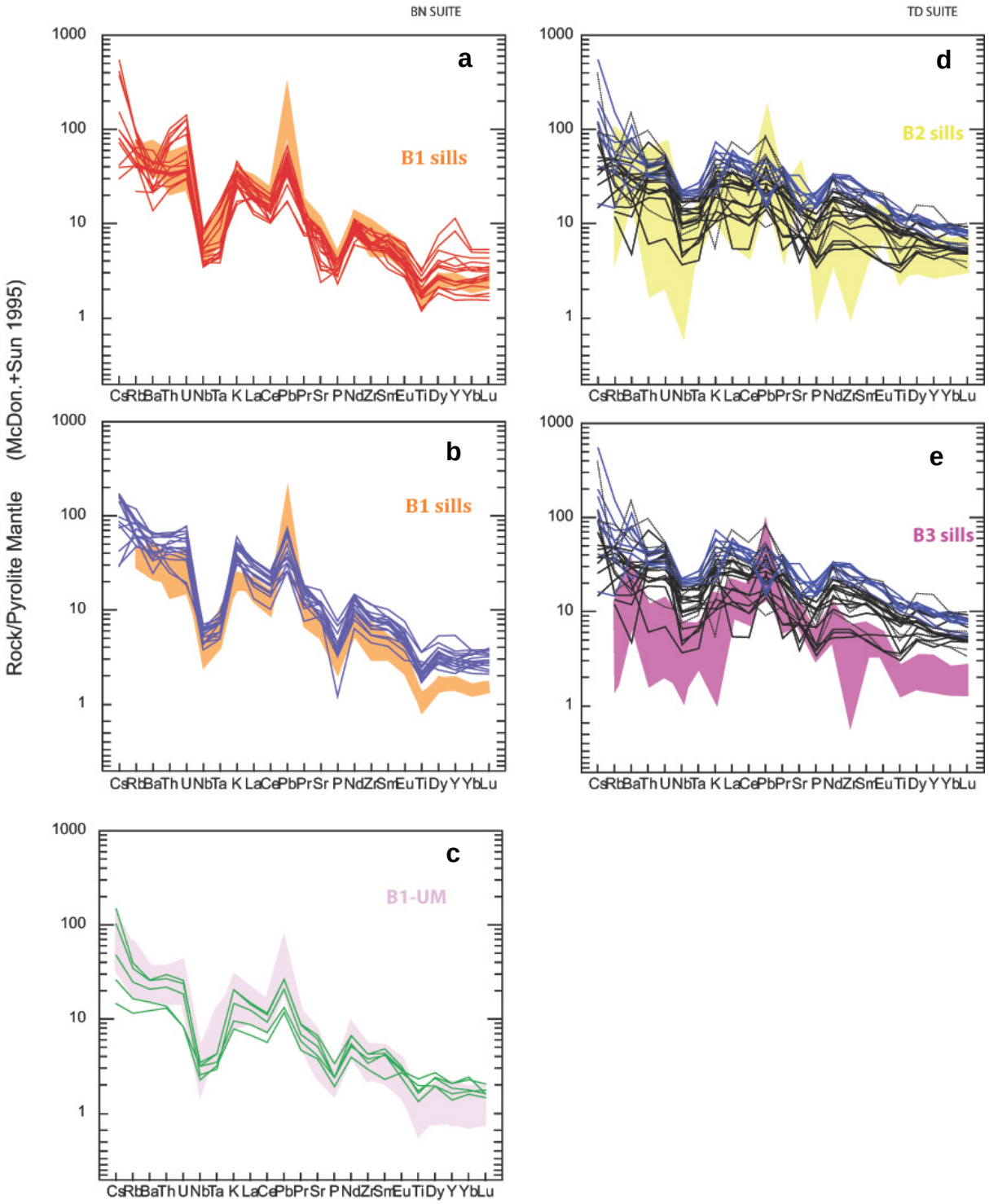


Figure 6.9: Primitive-mantle-normalized spider gram after McDonough and Sun (1995) for a-b) the BN-suite, c) harzburgitic cumulates and d-e) the TD-suite. It is important to note the shaded backgrounds for all plots representing Barnes et al's (2010) compositions.

# 7 Discussion

## 7.1 Linking sills to the Bushveld Complex and other igneous events on the Kaapvaal Craton

It has been shown in this study of the mafic sills that intruded into, and below, the sedimentary rocks of the Transvaal Supergroup that these belong to either a gabbroic or a noritic suite. It is also possible, in the field, to recognise noritic sills, when these have particularly elongated and occasionally spinifex textured enstatite crystals. However, this first order distinction is mainly based on petrographical differences in rare fresh samples (i.e., sub-ophitic gabbros versus norites with euhedral enstatite) and most convincingly through bulk rock geochemistry, where one can clearly make a similar distinction between a more Fe-rich tholeiitic and more Si-rich boninitic suite, respectively. It is, perhaps, less easy to determine which of these two main suites the hartzburgitic cumulates belong to. Finally, distinctly different geochemical signatures (e.g., Fig. 6.9) clearly show that the identified tholeiitic dolerite (TD) and the boninitic norite (BN) suite have been derived from different sources and thereby differentiated from distinctly different parents. In this section a discussion is made on how these different suites, and any sub-groups within these, may or may not be related to the Bushveld Complex. In the case where they are not related to the BIC, an attempt to see which magmatic event they may be related to is made.

The highest concentration of the sills is found within the Silverton Fm and closer to the contact of the RLS (Fig 4.1 and 4.2), which is also the reason why previous workers have made a direct stratigraphical correlation to B1, B2 and B3 magmas being parental to the LZ-LCZ, UCZ, and MZ-UZ, respectively (Cawthorn et al., 1981; Sharpe, 1981; Harmer and Sharpe, 1985; Sharpe and Hulbert, 1985; Barnes et al., 2010). However, this extended stratigraphical study of sills, all the way to down into the basement, has shown that BN-sills occur throughout the Transvaal Supergroup. Thus, the initial concept of how these unique BN-magmas were emplaced only along the level of transgressing LZ-LCZ has to be revised. The TD-sills are less abundant and cluster as more sub-alkaline dolerites within the shales of the Silverton Bowen Fm and as more alkaline dolerites within the Malmani dolomites (i.e., cutting across the Uitkomst Complex). More importantly, these do not occur at the same stratigraphical level as the UCZ-MZ-UZ, where more gabbroic B2 and B3 sills have been sampled by

others. While it seems reasonable for early B1 magmas to have been injected at several stratigraphical levels before a large magma chamber had been established and the RLS began accumulating, it seems less likely for B2-3 magmas to also have been emplaced at lower stratigraphical levels after a feeder system is likely to have been established to this magma chamber. Thus, based only on their spatial distributions, TD-sills could have formed during an entirely different magmatic event which will be explored further below in this chapter.

Finally, cumulates are mainly found as harzburgites along the base of the Magaliesburg Fm, but also in a basement sill, as well as some layered rocks in the lower Silverton Fm. It is difficult to find a particular reason for this, because there may be many such harzburgitic cumulates along the hidden bases of other sills, but it is visible that the Magaliesburg cumulates correlate stratigraphically to a large concentration of similar ultramafic cumulates within the Burgersfort Dome (Fig.4.1; Harmer and Hulbert, 1985). Thus, it may very well be that certain sills can be more directly related to the RLS and could even have formed through the injection of cumulate mushes, rather than accumulated in situ with a sill. Such a link with RLS-cumulates has been strengthened by the discovery of similar harzburgitic cumulates, as well as associated ‘quenched’ spinifex rocks, both below the RLS farther to the north and inside the RLS in the western lobe of the Bushveld Complex (Wilson, 2012; Maier et al., 2016).

In the following section, a comparison between the sills under current study and the recognised B1, B2 and B3 magmas (mainly Barnes et al., 2010), in an attempt to first see how many sills could have been emplaced during the formation of the Bushveld Complex, as potential feeders/parents to the RLS’ (1) LZ to LCZ, (2) UCZ, and (3) MZ, respectively.

It can be observed that the geochemical signatures of the BN sills (both primitive and more evolved) have characteristics that compare well with Barnes et al’s (2010) B1 sills. In particular, their sub-parallel incompatible element patterns that are LILE/HFSE-enriched and have relatively low HREE (Fig 6.9a), as well as distinctly similar negative Nb-Ta, Ti, P and positive Pb spikes. As such special BN-signatures are not recognised within any other magmatic event that is younger than the rock that these sills are hosted within, it becomes almost certain that all the sills belonging to the BN-suite must have been emplaced during the emplacement of the Bushveld Complex.

According to previous workers, more specifically, as parental magmas for the formation of the orthopyroxenitic LZ-LCZ. The lower most located TD-sills do not completely share similar incompatible element signatures with Barnes et al's (2010) B2 and B3 type magmas (Fig. 6.9b). Thus, B2 rocks are LILE, Th, Zr and LREE poorer and more enriched in Ti, P, HREE, Y than the TD-sills; whereas, B3 rocks are too depleted in REE, Y, Ti, P, and V. The B-2 and B3 magmas also exhibit stronger negative Zr anomalies which is not exhibited by any of the TD rocks. Based on these geochemical differences, I cannot with confidence interpret the TD-sills as B2 or B3 type magmas even if they share the same gabbroic textures. So, unless other types of tholeiitic magmas could also have been feeding the Bushveld Complex, it is suspected that these TD-sills formed during another magmatic event.

Figure 7.1 is used in an attempt to fit the TD-suite into any magmatic events which could be related to the Transvaal and are characterised by tholeiitic dolerite eruptions. It is obvious that whatever magmatic event gave rise to the TD-sills, these must have been younger than the host rock within which they are hosted. Thus, for the uppermost TD-sills in the Silverton Fm, these can only be related to Machadodorp Fm lavas (Fig 7.1 c) or younger events, which include the Bushveld, but also younger trans-Kalahari (ref; Olsson et al., 2016), Umkondo (de Kock et al., 2014) and Karoo (Jourdan et al., 2007) events. The TD-sills that cut across the Uitkomst Complex are most likely even younger than the Bushveld Complex (Figure 7.1 g); whereas the basement sills, could be related to both older Hekpoort Fm lavas as well as lavas within the protobasinal Wolkberg Group (Fig 7.1 b). As SW-NE trending dykes from the 1875-1835 Ma Black Hills dyke swarm (Olsson et al., 2016), as well as a few WNW-ESE trending and presumed 1.1 Ga Umkondo dykes (de Kock et al., 2014) cut across the eastern part of the Transvaal Supergroup (Fig 4.1), and the E-W trending (~2683–2686 Ma) Rykoppies dyke swarm (Olsson et al., 2010; Fig 4.8) coincide with the basement sills, it seems relevant to first compare respective TD-sills with these intrusions.

**Figure 7.1a-g: (following pages):** A schematic N-S cross section showing different stages, between known volcanic events (ages of published data are also shown for comparison), where sills could have been emplaced. Transects are roughly added showing sampled sills that may tentatively be related to a certain stage. The stratigraphic Transvaal Supergroup log, overlying the Archean basement and transected by the Rustenburg Layered Sequence is stretched and modified version of Figure 4.2 (modified from Sharpe and Hulbert, 1985).

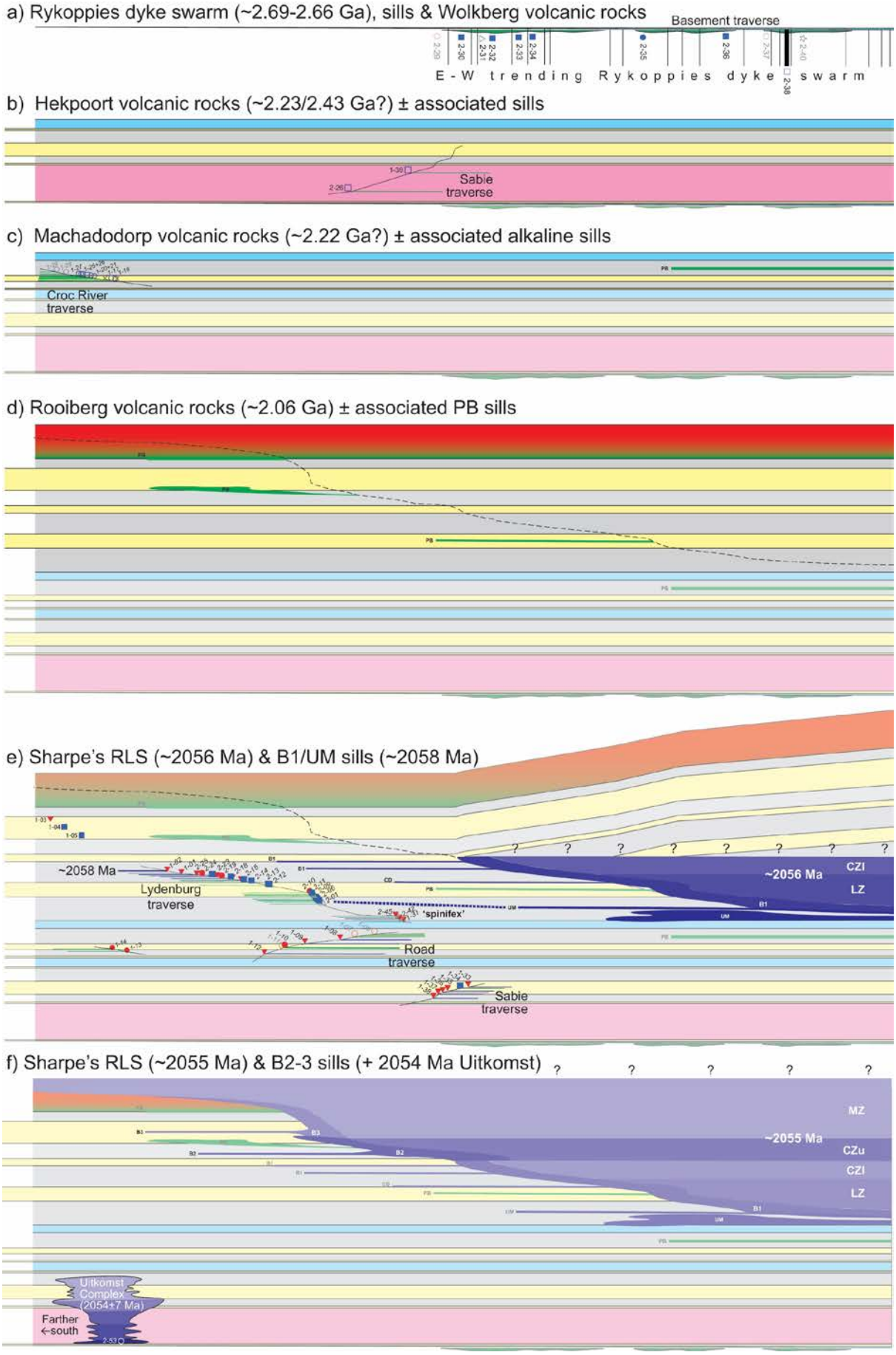

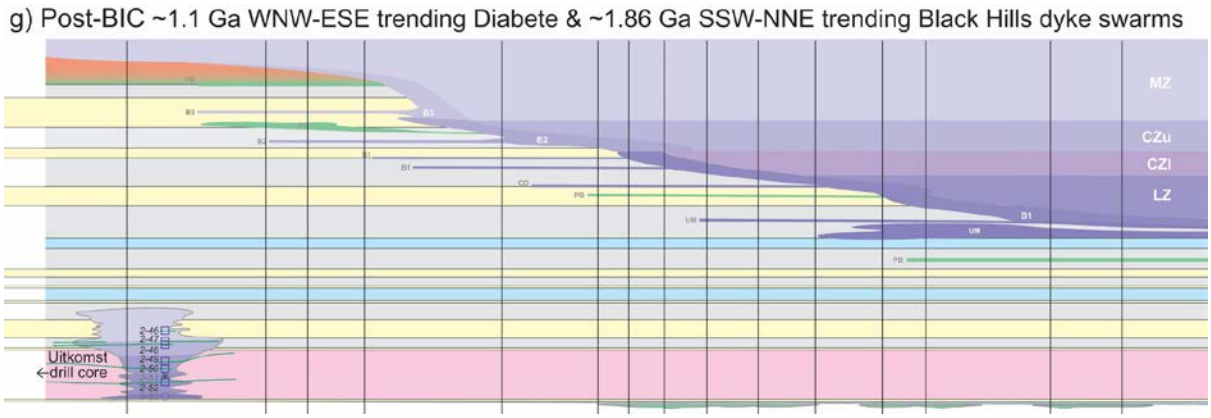


A comparison is made between the basement hosted TD-sills with the E-W trending 2683-2686 Ma Rykoppies dyke swarm (Olsson et al., 2011) in figure 7.2(a) where it is observed that their geochemical signatures have well correlated characteristic with the dykes' HREE enrichment, negative Ti, P and positive Pb spikes. It is also worth noting that sample BCS2-38 which was sampled from the Rykoppies dyke swarm does not fit in as well as other basement samples. Figure 7.1(b) plots selected Uitkomst Complex and Daspoort- Bowen Fm hosted TD-sills, compared to the 1875-1835 Ma Black Hills dyke swarm (Olsson et al., 2016) and the Diabete high-Ti 1.1 Ga Umkondo dykes (de Kock et al., 2014) without observing any overlap between them, which leads me to think that these TD sills are not related to any of the younger magmatic events mentioned above. One may consider comparing the uppermost Silverton Fm hosted TD-sills to the Machadodorp and the basement hosted sills to the Hekpoort lavas, but the limited available geochemical data of both lavas would be a disadvantage. This as shown in Figure 7.2a, could be compared with the Rykoppie dyke swarm, Hekpoort rocks (samples along the Sabie transect Fig 4.7), Machadodorp volcanic rocks (sills sampled along the Crocodile River transect) and even younger intrusions such as the Black Hills dyke swarm.

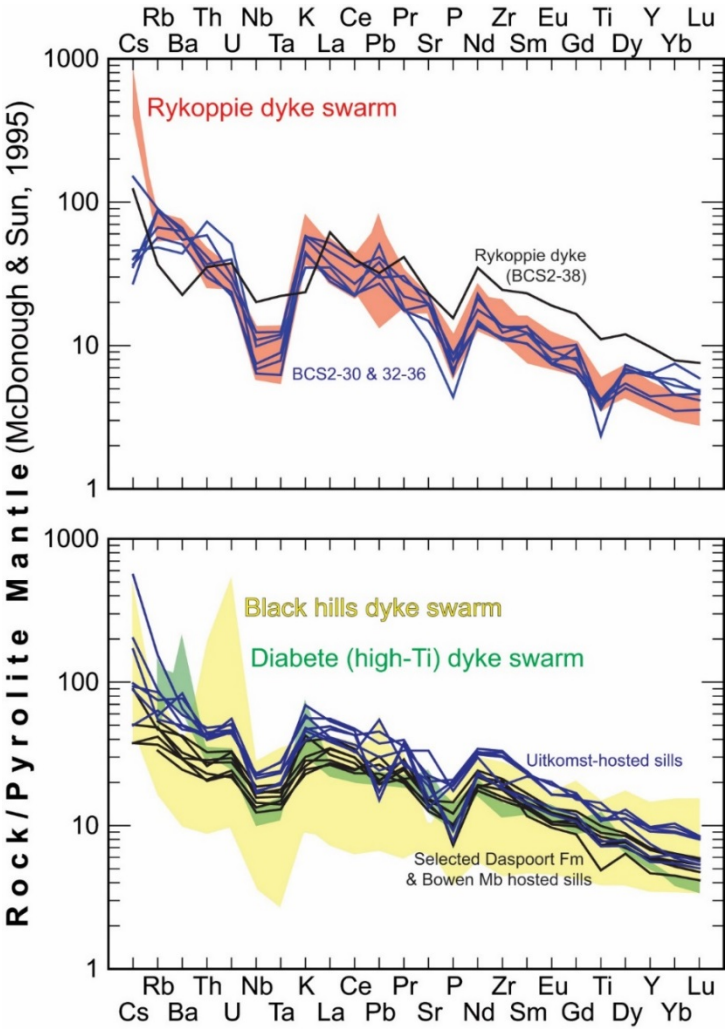


**Figure 7.2**: Primitive-mantle-normalized spider gram after McDonough and Sun 1995 for a) selected basement TD-sills with the E-W trending 2683-2686 Ma Rykoppies dyke swarm (Olsson et al., 2011) and (b) selected TD-sills from the Uitkomst Complex and Daspoort-Bowen compared to the ~1875-1835 Ma Black Hills in background (Olsson et al., 2016) and the Diabete 1.11 Ga Umkondo dyke swarms (de Kock et al., 2014).

## 7.2 Crystal Fractionation

From most of the variation diagrams plotted in Figures 6.3 - 6.7, it is observed that both suites follow trends, which in some cases are distinctly different from each other. This is most obvious for Mg# plotted against CaO (Fig. 6.4a), $Al_2O_3$ (Fig 6.4b) and V (Fig 6.5d), which clearly underpin that these two main suites cannot have derived from a common parent through fractional crystallization. There is a considerable variation in the major and trace element abundances in both suites, however, indicating that magmas differentiated and most likely through fractional crystallization. Below, the evidence for such crystal fractionation is discussed for each of the two suites, possible parental magmas and corresponding cumulates for each suite are defined. Finally, the possibility of sub-suites amongst these two main suites is investigated.

Starting with the dominant BN-suite, believed to either be feeding or being derived from the magma chamber that gave rise to at least the LZ-LCZ of the RLS, it is noted that enstatite is most commonly euhedral and therefore the most likely fractionating phase. This even applies to the most evolved norites wherein a greater abundance of micrographic quartz - alkali feldspar is entirely interstitial (Fig 5.6 a-b). Enstatite fractionation is consistent with decreasing Mg# (used as a differentiation index) as well as decreasing Cr and Ni (Fig. 6.5a-b), which also partition into enstatite, but could of coarse also have fractionated along with Cr-spinel and even some early olivine. In contrast, roughly increasing trends of both CaO and $Al_2O_3$ (Fig 6.4a-b) argue for opx fractionation within the BN suite. One may argue for a slight $Al_2O_3$-decline amongst the more evolved norites (indicated by a small oblique red arrow in Fig 6.4b), suggesting a very late onset of plagioclase fractionation, but this is of little significance compared to the overall trend. Vanadium (V) vs Mg# (Fig 6.5d) records a distinct kinked (or elbowed) trend for the BN suite, suggesting that V initially behaved incompatibly and then compatibly against decreasing Mg#. Because of V's high partitioning coefficient for ilmenite, this may record the onset of (Fe,Ti)-oxides at Mg# ~ 50 for the BN suite, were it not for the fact that no similar kinked $TiO_2$-trends is evident in Figure 6.3(d). Thus, it may be that V and Sc may have a relatively high partitioning coefficient for enstatite or another unknown phase that starts fractionating at Mg# ~ 50.

One of the noritic sills within the Silverton Formation exhibits a spinifex-texture dominated by acicular elongated orthopyroxene grains with a branching habit towards one preferred direction (right), which is tentatively interpreted as their growth direction from a cooling surface (Fig 5.4 a). This texture can be compared to that of Wilson (2012) sampled from the Lower Zone of the Eastern Bushveld Complex. Similar spinifex-textured pyroxenites have also been found inside the western lobe of the Bushveld Complex (Maier et al., 2016), suggesting that this rock type may have a more regional extent, the implications of which are still unclear.

For this study, spinifex-like quench textures within the melanorite BCS2-24 (Fig 5.5 e-f) attest to this sample representing a truly ultramafic parental melt; whereas more primitive samples (i.e., with higher Mg#) can be regarded as more or less cumulate rocks. This is important because it shows that the BN-suite formed from unusually Mg-rich parental melts, compared to the TD-suite.

The TD suite differs from the BN suite in having normative olivine, even if that is rarely (if ever) observed in thin sections (probably due to alteration). Dolerites also seem to have significantly more magnetite-ilmenite, which is consistent with their higher total Fe and Ti (BCS1-39, Fig 5.10 a-b). This is typical for tholeiitic magmas, believed to have differentiated under relatively low $P_{H2O}$ conditions, where plagioclase start fractionating at an earlier stage, before Fe-Ti-oxides. This is also consistent with a common sub-ophitic texture, where euhedral plagioclase laths are overgrown by more interstitial augite and opaque oxides. Nevertheless, it is still difficult to see any decline in $Al_2O_3$ against decreasing Mg# (Fig 6.4b) to support an earlier plagioclase fractionation, yet where declining CaO suggest early augite fractionation. This conundrum can only be explained by earlier augite fractionation (going against petrographical evidence) and/or plagioclase accumulation, at the expense of interstitial augite. As for the BN-suite, V vs Mg# (Fig 6.5d) also records a kinked (or elbowed) trend for the TD suite, but just at a lower Mg# of ~35. Consistent for a tholeiitic suite, this is very late in the evolution of the TD-suite, and, like for the BN-suite, is not reflected by $TiO_2$ (Fig 6.3d), which rises up to 3 wt % $TiO_2$ across the limited MgO-range from ~10-14 wt %. Thus, I do not think that much ilmenite fractionated from these TD-magmas, as supported by the opaque oxides' interstitial habits. Remarkable curved trends of decreasing Cr and Ni concentration against Mg# (Fig 6.5 a-b), for both doleritic and noritic suites, show evidence for early Cr-spinel, olivine and/or pyroxene fractionation for both suites. However, values greater than what is expected from a primary mantle melt (e.g., >1000 ppm Cr and >250-400 ppm Ni) more likely formed through the accumulation of such phases, and this interpretation is supported by the fact that hartzburgitic cumulates also have the highest abundance of Cr (>2616 ppm) and Ni (>700 ppm) which therefore is consistent with the cumulate chromites olivines observed in BCS2-02 (Fig 5.14).

## 7.3 Petrogenesis

It is very difficult to determine from what source and how primary melts for these sills may have formed. However, one could at least speculate on how two such radically different suites may have initially been generated. It is obvious from both suites' mafic-ultramafic characters that they were both derived through partial melting on an ultramafic mantle source, but whereas the TD-suite can be more easily related to a more typical mantle source, the source for the BN-suite is much more unusual. Much of the following discussion will first focus on this more enigmatic BN-suite, is mainly based on incompatible element signatures and follow upon Barnes et al's (2010) petrogenetic interpretation of their B1-samples.

Firstly, the boninitic character of the BN-suite must be emphasized, and this is according to Le Maitre (2002), constrained as a rock that has $SiO_2$> 52%, MgO>8% and is strongly depleted in $TiO_2$ (<0.5%). As can be seen in Figure 6.3(c-d) only the most primitive non-cumulate BN-samples satisfy this criteria, with more evolved BN-samples representing differentiates of such parents. However, such boninitic rocks are usually found in much younger oceanic (back-)arc settings, like the Bonin Island arc from where its name originates (Crawford 1989, Piercey et al., 2001). The petrogenesis of boninites within such a relatively simple setting (i.e., without additional interference from a continental lithosphere) are still not fully understood, however, but seems to require a silica-enriched, and thereby an orthopyroxene-rich, mantle source (Benard et al., 2017), where the silica-enrichment may stem from a partially melted oceanic slab.

Similar adakitic slab melts have also been inferred for the petrogenesis of Archean TTG gneisses (e.g., Martin et al., 2005) and it therefore makes sense that similar continental boninitic melts may be produced through the mixture of both high degrees of partial mantle melting (producing the high MgO) and the assimilation of large volumes (>40%) of TTG-crust (e.g., Cawthorn et a 2006). This is consistent with the BN-suite's steep LREE-enriched patterns (and relatively low HREE), as well as strong arc-like signatures (e.g., high LILE/HFSE and negative Nb-Ta), which could all have been inherited from the TTG gneiss. However, this requires komatiitic primary melts, which almost cease to exist after the Archean, and possibly also superheated in order

to fully assimilate so much crustal rocks before crystallizing (a process which there is little evidence of in the form of crustal xenoliths).

As an alternative explanation, Hall and Hughes (1990) proposed that continental boninitic primary melts may be generated more directly from a depleted (i.e., harzburgitic) sub-continental lithospheric mantle (SCLM) source, which had been locally enriched by adakitic slab melts during the Archean. This is very similar to Benard et al's (2017) explanation for oceanic boninites, and could have been a common metasomatic process during the Archean, where deplete SCLMs were silica-enriched and transformed into orthopyroxenitic mantle sources that upon partial melting more directly formed continental boninites. In fact, such Archean metasomatism could explain why all continental boninites are restricted to between 2.7 Ga (e.g., Stillwater Complex) and 2.0 Ga (e.g., the Bushveld Complex), as reviewed by Srivastava (2006), when Earth's earliest Superia supercontinent broke up and its SCLM was partially melted to produce, amongst other magma types, continental boninites like the BN-sills.

To further put a constraint on the composition of the BN primary melts, one may consider the isotopic signatures based on previously published data (Hamilton 1977; Kruger and Marsh, 1982; Harmer and Sharpe, 1985; Harris et al., 2005; Richardson and Shirey 2008; Zirakparvar et al., 2014) which enables for a better assessment of the interactions between the crust and the mantle during magma genesis. Sr isotopic values of Harmer and Sharpe (1985) revealed a crustal signature of these magmas. The initial large range of Sr isotopic values from 0.7063 in the Lower zone to 0.70769 at the top of the UZ $(^{87}Sr/^{86}Sr)_i$ are in support of a komatiite melt that had already assimilated lower crustal material (TTG) of the Kaapvaal Craton as evidenced from $(^{87}Sr/^{86}Sr)_i$ compositions. With an overall upward decreasing $(^{87}Sr/^{86}Sr)_i$ in the RLS sequence indicating a progressively higher involvement of mantle melts and a lower crustal influence with stratigraphy.

Along with B1 type sills Barnes et al (2010) termed their most ultramafic sills B1-UM and interpreted them to not have been a representative of a different magma type but instead represent olivine cumulates from a B1 magma. They are characterised by a lesser concentration of LILE than the main B1 sills and this is interpreted to be because incompatible elements were squeezed out with the intercumulus melts in cumulate rocks. The hartzburgitic cumulates correlate well with the B1-UM rocks with their sub

parallel patterns, an enrichment in LILE, positive Pb spikes and are depleted in Ti, P and Nb (Fig 6.9 a) and this is consistent with a similar parentage similar to that of the BN suite.

The TD-suite, on the other hand, requires a much more common primary melt, which can more easily be explained by the partial melting of a more normal mantle source. However, their slight arc-like signatures may still indicate some lithospheric influence, as more applied for, e.g., the Black Hills dyke swarm (Olsson et al., 2016).

# 8 Conclusion

This study sought to highlight and determine the relationship between Transvaal Supergroup hosted mafic sill intrusions and the BLIP. From petrographical and geochemical differences, it is concluded that sills can be subdivided into two major groups; namely the TD suite and the BN-Suite, which cannot be petrogenetically related through crystal fractionation.

The BN-suite is represented by 51 out of 85 sampled sills and their orthopyroxene-rich mineralogy and unique boninitic signatures are primarily what relate these sills to the Bushveld Complex. Especially, since there are no other similar boninitic norite events recorded across the Kaapvaal Craton. I do not think that these BN-sills were derived exclusively from the Lower and Lower Critical Zone of the RLS as Sharpe (1981) suggest for his similar B1 sills; i.e., injected into the same stratigraphical level (Fig 7.1 e). This is because BN sills are now found throughout the Transvaal Supergroup, stratigraphically below and above the Silverton and Lakenvalei Formations that host Sharpe's (1981) B1 sills. This is further supported by Wabo et al's (2016a) 2058.4±1.3 Ma and 2058.1±6Ma ages for BN sills (including sample BCS1-02), which is ~2 million years older than the RLS (Zeh et al., 2015). Instead, it is believed that most BN sills were injected into the Transvaal Supergroup prior to the formation of the RLS, which was also subsequently fed by similar parental magmas.

In contrast, the TD-suite shows no direct evidence that link these to the Bushveld Complex. Especially, since none of these 22 out of 85 sampled sill from the TD-suite have geochemical signatures that match the B2 and B3 magmas, postulated to have been injected from the Upper Critical to main Zone of the RLS (e.g., Sharpe, 1981). Instead, there are many other tholeiitic dolerite events that could equally well have given rise to the TD-suite. As summarised by Figure 7.1, these include the ~2.69-2.66 Ga Rykoppies dyke swarm which can be geochemically fitted to 6 basement hosted TD-sills; the ~2.23 Ga Hekpoort rocks and stratigraphically younger Machadodorp rocks, which, unfortunately, cannot be compared due to unavailable geochemical data; as well as sills having been injected from any cross cutting dyke swarms that are younger than the Bushveld Complex (e.g., the 1.1 Ga Diabete that show the most similar geochemical signatures to many of the TD samples (Fig. 7.2b).

# References

Barnes, S. J. (1989). Are Bushveld U-type parent magmas boninites or contaminated komatiites? Contributions to Mineralogy and Petrology, 101(4), 447-457.

Barnes, S. J., & Maier, W. D. (2002). Platinum-group element distributions in the Rustenburg layered suite of the Bushveld Complex, South Africa. The geology, geochemistry, mineralogy and mineral beneficiation of platinum-group elements, 54, 431-458.

Barnes, S. J., Maier, W. D., & Curl, E. A. (2010). Composition of the marginal rocks and sills of the Rustenburg Layered Suite, Bushveld Complex, South Africa: implications for the formation of the platinum-group element deposits. Economic Geology, 105(8), 1491-1511.

Barron, L. M. (1980). Feldspar compositions and amounts from a CIPW norm. Geochemical Journal, 14(1), 33-40.

Benard, A., Arculus, R. J., Nebel, O., Ionov, D. A., & McAlpine, S. R. B. (2017). Silica-enriched mantle sources of subalkaline picrite-boninite-andesite island arc magmas. Geochimica et Cosmochimica Acta, 199, 287-303.

Bryan, S. E., & Ernst, R. E. (2008). Revised definition of large igneous provinces (LIPs). Earth-Science Reviews, 86(1), 175-202.

Buick, I. S., Maas, R., & Gibson, R. (2001). Precise U–Pb titanite age constraints on the emplacement of the Bushveld Complex, South Africa. Journal of the Geological Society, 158(1), 3-6.

Cameron, E. N. (1978). The lower zone of the eastern Bushveld Complex in the Olifants River trough. Journal of Petrology, 19(3), 437-462.

Cawthorn, R. G., Davies, G., Clubley-Armstrong, A., & McCarthy, T. S. (1981). Sills associated with the Bushveld Complex, South Africa: an estimate of the parental magma composition. Lithos, 14(1), 1-16.

Cawthorn, R. G., & Walraven, F. (1998). Emplacement and crystallization time for the Bushveld Complex. Journal of Petrology, 39(9), 1669-1687.

Cawthorn, R. G., Lee, C. A., Schouwstra, R. P., & Mellowship, P. (2002). Relationship between PGE and PGM in the Bushveld Complex. The Canadian Mineralogist, 40(2), 311-328.

Cawthorn, R. G., Eales, H. V., Walraven, F., Uken, R., & Watkeys, M. K. (2006). The Bushveld Complex. In Johnson, M.R., Anhaeusser, C.R. and Thomas, R.J. (Eds.). The Geology of South Africa, Geological Society of South Africa, Johannesburg/Council of Geoscience, Pretoria, 261-281.

Coetzee, H., & Kruger, F. J. (1989). The geochronology, Sr-and Pb-isotope geochemistry of the Losberg Complex, and the southern limit of Bushveld Complex magmatism. South African Journal of Geology, 92(1), 37-41.

Clarke, B. M., Uken, R., Watkeys, M. K., & Reinhardt, J. (2005). Folding of the Rustenburg layered suite adjacent to the Steelpoort pericline: implications for syn-Bushveld tectonism in the eastern Bushveld Complex. South African Journal of Geology, 108(3), 397-412.

Crawford, A. J. (1989). Boninites and Related Rocks. Unwin Hyman, London, 465 pp.

Curl, E. A. (2001). Parental magmas of the Bushveld Complex, South Africa. PhD thesis, Monash University, Dept. of Earth Sciences.

Davies, G., Cawthorn, R. G., Barton, J. M., & Morton, M. (1980). Parental magma to the Bushveld Complex. Nature, 287(5777), 33-35.

de Kock, M. O., Ernst, R., Söderlund, U., Jourdan, F., Hofmann, A., Le Gall, B., and Moseki, L. M. (2014). Dykes of the 1.11 Ga Umkondo LIP, Southern Africa: clues to a complex plumbing system. Precambrian Research, 249, 129-143.

de Waal, SA (1970). Interference folding of Bushveld Complex age in the Transvaal System north of Marble Hall. Spec. Publ. geol. Soc. S. Afr., 1,283-298.

de Waal, S. A., & Armstrong, R. A. (2000). The age of the Marble Hall diorite, its relationship to the Uitkomst Complex, and evidence for a new magma type associated with the Bushveld igneous event. South African Journal of Geology, 103(2), 128-140.

de Waal, S. A., Graham, I. T., & Armstrong, R. A. (2006). The Lindeques Drift and Heidelberg Intrusions and the Roodekraal Complex, Vredefort, South Africa:

comagmatic plutonic and volcanic products of a 2055 Ma ferrobasaltic magma. South African Journal of Geology, 109(3), 279-300.

de Waal, S., Schweitzer, J. K., Graham, I., Gauert, C., & Ripley, E. (2008). A Bushveld-related high-Ti igneous suite (HITIS) derived from an alkali to transitional basaltic magma, South Africa. South African Journal of Geology, 111(2-3), 201-224.

Eales, H. V., & Cawthorn, R. G. (1996). The Bushveld Complex. Developments in Petrology, 15, 181-229.

Eales, H. V. (2001). A first introduction to the geology of the Bushveld complex and those aspects of South African geology that relate to it. Pretoria: Council for geoscience, Geol. survey of South Africa.

Engelbrecht, J. P. (1990). Contact metamorphic processes related to the aureole of the Bushveld Complex in the Marico District, western Transvaal, South Africa. South African journal of geology, 93(2), 339-349.

Frick, C. (1967). The margin of the Bushveld Complex in the vicinity of De Berg, north of Dullstroom. MSc thesis, University of Pretoria.

Frick, C. (1973). Intergrowths of orthopyroxene and ilmenite from Frank Smith Mine, near Barkly West, South Africa. South African Journal of Geology, 76(3), 195-200.

Gauert, C. D. K. (1998). The petrogenesis of the Uitkomst Complex, Mpumalanga Province, South Africa. PhD thesis, University of Pretoria.

Godel, B., Barnes, S. J., & Maier, W. D. (2011). Parental magma composition inferred from trace element in cumulus and intercumulus silicate minerals: An example from the Lower and Lower Critical Zones of the Bushveld Complex, South-Africa. Lithos, 125(1), 537-552.

Greenwood, R. C., Donaldson, C. H., & Emeleus, C. H. (1990). The contact zone of the Rhum ultrabasic intrusion: evidence of peridotite formation from magnesian magmas. Journal of the Geological Society, 147(2), 209-212.

Hall, A. L. (1913). The Geology of the Country South-west of Lydenburg. SA Geological Survey.

Hall, A. L. (1932). The Bushveld igneous complex of the central Transvaal (No. 28). The Government printer.

Hall, R. P., & Hughes, D. J. (1990). Noritic magmatism. In Early Precambrian basic magmatism. Springer Verlag, Netherlands. 83-110.

Hamilton, J. O. (1977). Sr isotope and trace element studies of the Great Dyke and Bushveld mafic phase and their relation to early Proterozoic magma genesis in southern Africa. Journal of Petrology, 18(1), 24-52.

Harmer, R. E., & Sharpe, M. R. (1985). Field relations and strontium isotope systematics of the marginal rocks of the eastern Bushveld Complex. Economic Geology, 80(4), 813-837.

Harris, C., Pronost, J. J., Ashwal, L. D., & Cawthorn, R. G. (2004). Oxygen and hydrogen isotope stratigraphy of the Rustenburg Layered Suite, Bushveld Complex: constraints on crustal contamination. Journal of Petrology, 46(3), 579-601.

Hatton, C. J., & Von Gruenewaldt, G. (1987). The geological setting and petrogenesis of the Bushveld chromitite layers. Van Nostrand Reinhold Company, New York. 109-143.

Hatton, C. J. (1995). Mantle plume origin for the Bushveld and Ventersdorp magmatic provinces. Journal of African Earth Sciences, 21(4), 571-577.

Hatton, C. J. (1995). The Bushveld Complex, a product of interaction among magmas derived from a mantle plume. Communications Geological Survey, Namibia, 10, 93-98.

Hoover, J. D. (1989). The chilled marginal gabbro and other contact rocks of the Skaergaard intrusion. Journal of Petrology, 30(2), 441-476.

James, D. E., Fouch, M. J., VanDecar, J. C., & Van Der Lee, S. (2001). Tectospheric structure beneath southern Africa. Geophysical research letters, 28(13), 2485-2488.

Johnson, M. R., Anhauesser, C. R., & Thomas, R. J. (2006). The Geology of South Africa. Geological Society of South Africa.

Jourdan, F., Bertrand, H., Schärer, U., Blichert-Toft, J., Féraud, G., & Kampunzu, A. B. (2007). Major and trace element and Sr, Nd, Hf, and Pb isotope compositions of the Karoo large igneous province, Botswana–Zimbabwe: lithosphere vs mantle plume contribution. Journal of Petrology, 48(6), 1043-1077.

Kamo, S. L., Reimold, W. U., Krogh, T. E., & Colliston, W. P. (1996). A 2.023 Ga age for the Vredefort impact event and a first report of shock metamorphosed zircons in pseudotachylitic breccias and granophyre. Earth and Planetary Science Letters, 144(3-4), 369-387.

Kenyon, A. K., Attridge, R. L., & Coetzee, G. L. (1986). The Uitkomst Nickel-Copper deposit, Eastern Transvaal. Mineral Deposits of Southern Africa. Geological Society of South Africa, Johannesburg, South Africa, II, 1009-1019.

Kinnaird, J. A. (2005). The Bushveld large igneous province. Review Paper, The University of the Witwatersrand, Johannesburg, South Africa, 39 pp.

Klausen, M. B., Söderlund, U., Olsson, J. R., Ernst, R. E., Armoogam, M., Mkhize, S. W., & Petzer, G. (2010). Petrological discrimination among Precambrian dyke swarms: eastern Kaapvaal craton (South Africa). Precambrian Research, 183(3), 501-522.

Kruger, F. J., & Marsh, J. S. (1982). Significance of $^{87}Sr/^{86}Sr$ ratios in the Merensky cyclic unit of the Bushveld Complex. Nature, 298(5869), 53-55.

Kruger, F. J. (1992). The origin of the Merensky cyclic unit: Sr-isotopic and mineralogical evidence for an alternative orthomagmatic model. Australian Journal of Earth Sciences, 39(3), 255-261.

Kruger, F. J. (1994). The Sr-isotopic stratigraphy of the western Bushveld Complex. South African Journal of Geology, 97(4), 393-398.

Large, R. R., Gemmell, J. B., Paulick, H., & Huston, D. L. (2001). The alteration box plot: A simple approach to understanding the relationship between alteration mineralogy and lithogeochemistry associated with volcanic-hosted massive sulfide deposits. Economic geology, 96(5), 957-971.

Le Maitre, R. W. B., Dudek, P., Keller, A., Lameyre, J., Le Bas, J., Sabine, M. J., & Zanettin, A. R. (1989). A classification of igneous rocks and glossary of terms:

Recommendations of the International Union of Geological Sciences, Subcommission on the Systematics of Igneous Rocks (No. 552.3 CLA). International Union of Geological Sciences.

Le Maitre, R. W., Streckeisen, A., Zanettin, B., Le Bas, M. J., Bonin, B., Bateman, P., & Lameyre, J. (2002). Igneous rocks: A classification and glossary of terms; Recommendations of the International Union of Geological Sciences. In Subcommission on the Systematics of Igneous rocks. Cambridge University Press.

Lenhardt, N., & Eriksson, P. G. (2012). Volcanism of the Palaeoproterozoic Bushveld Large Igneous Province: the Rooiberg Group, Kaapvaal Craton, South Africa. Precambrian Research, 214, 82-94.

Martin, H., Smithies, R. H., Rapp, R., Moyen, J. F., & Champion, D. (2005). An overview of adakite, tonalite–trondhjemite–granodiorite (TTG), and sanukitoid: relationships and some implications for crustal evolution. Lithos, 79(1), 1-24.

McDonough, W. F., & Sun, S. S. (1995). The composition of the Earth. *Chemical geology*, *120*(3-4), 223-253.

Miyashiro, A. (1975). Classification, characteristics, and origin of ophiolites. The journal of geology, 83(2), 249-281.

Norrish, K., & Hutton, J. T. (1969). An accurate X-ray spectrographic method for the analysis of a wide range of geological samples. Geochimica et cosmochimica acta, 33(4), 431-453.

Olsson, J. R., Söderlund, U., Klausen, M. B., & Ernst, R. E. (2010). U–Pb baddeleyite ages linking major Archean dyke swarms to volcanic-rift forming events in the Kaapvaal craton (South Africa), and a precise age for the Bushveld Complex. Precambrian Research, 183(3), 490-500.

Olsson, J. R., Söderlund, U., Hamilton, M. A., Klausen, M. B., & Helffrich, G. R. (2011). A late Archaean radiating dyke swarm as possible clue to the origin of the Bushveld Complex. Nature Geoscience, 4(12), 865.

Olsson, J. R., Klausen, M. B., Hamilton, M. A., März, N., Söderlund, U., & Roberts, R. J. (2016). Baddeleyite U–Pb ages and gechemistry of the 1875–1835 Ma

Black Hills Dyke Swarm across north-eastern South Africa: part of a trans-Kalahari Craton back-arc setting?. GFF, 138(1), 183-202.

Piercey, S. J., Murphy, D. C., Mortensen, J. K. and Paradis, S. (2001). Boninite magmatism in a continental margin setting, Yukon-Tanana terrane, southeastern Yukon, Canada. Geology 29, 731–734.

Rajesh, H. M., Chisonga, B. C., Shindo, K., Beukes, N. J., & Armstrong, R. A. (2013). Petrographic, geochemical and SHRIMP U–Pb titanite age characterization of the Thabazimbi mafic sills: Extended time frame and a unifying petrogenetic model for the Bushveld Large Igneous Province. Precambrian Research, 230, 79-102.

Reichhardt, F. J. (1994). The Molopo Farms complex, botswana: history, stratigraphy, petrography, petrochemistry and Ni-Cu-PGE mineralization. Exploration and Mining Geology, 3(3), 263-284.

Scoates, J. S., & Friedman, R. M. (2008). Precise age of the platiniferous Merensky Reef, Bushveld Complex, South Africa, by the U-Pb zircon chemical abrasion ID-TIMS technique. Economic Geology, 103(3), 465-471.

Sharpe, M. R. (1978). Cone-type" diabases from the eastern Transvaal—representatives of a quenched magma. Trans Geol Soc Afr, 81, 373-378.

Sharpe, M. R. (1981). The chronology of magma influxes to the eastern compartment of the Bushveld Complex as exemplified by its marginal border groups. Journal of the Geological Society, 138(3), 307-326.

Sharpe, M. R. (1982). Petrography, classification and chronology of intrusion of mafic sills beneath the eastern Bushveld Complex. University of Pretoria Institute for Geological Research on the Bushveld Complex.

Sharpe, M. R., & Chadwick, B. (1982). Structures in Transvaal sequence rocks within and adjacent to the eastern Bushveld Complex: Geological Society of South Africa Transactions, 85. 29-42.

Sharpe, M. R. (1984). Petrography, classification and chronology of mafic sill intrusions beneath the eastern Bushveld Complex (No. 77). Dept. of Mineral and Energy Affairs Geological Survey.

Sharpe, M. R. (1985). Strontium isotope evidence for preserved density stratification in the main zone of the Bushveld Complex, South Africa. Nature, 316(6024), 119-126.

Sharpe, M. R., & Hulbert, L. J. (1985). Ultramafic sills beneath the eastern Bushveld Complex; mobilized suspensions of early lower zone cumulates in a parental magma with boninitic affinities. Economic Geology, 80(4), 849-871.

Sheth, H. C. (2007). 'Large Igneous Provinces (LIPs)': Definition, recommended terminology, and a hierarchical classification. Earth-Science Reviews, 85(3), 117-124.

Snyman, C. P. (1958). n Gneis,'n Koepelstruktuur en die metamorfose van die Sisteem Transvaal suid van Marble Hall, Transvaal. South African Journal of Geology, 61(1), 225-262.

Söderlund, U., & Johansson, L. (2002). A simple way to extract baddeleyite (ZrO2). Geochemistry, Geophysics, Geosystems, 3(2).

Söderlund, U., Klausen, M. B., Ernst, R. E., & Bleeker, W. (2016). New advances in using large igneous provinces (LIPs) to reconstruct ancient supercontinents, Gff, 138(1), 1-5.

Soorajlal, R. (2013). A petrographic and geochemical study of mafic sills up through the Transvaal Supergroup: Searching for parental melts around the eastern lobe of the Bushveld Complex. unpublished Honours thesis, Stellenbosch University.

Spandler, C. J., Eggins, S. M., Arculus, R. J., & Mavrogenes, J. A. (2000). Using melt inclusions to determine parent-magma compositions of layered intrusions: Application to the Greenhills Complex (New Zealand), a platinum group minerals–bearing, island-arc intrusion. Geology, 28(11), 991-994.

Srivastava, R. K. (2006). Geochemistry and petrogenesis of Neoarchaean high-Mg low-Ti mafic igneous rocks in an intracratonic setting, Central India craton: Evidence for boninite magmatism. Geochemical Journal, 40(1), 15-31.

Teigler, B., & Eales, H. V. (1996). The Lower and Critical Zones of the western limb of the Bushveld Complex as intersected by the Nooitgedacht boreholes. Bulletin-Republiek van Suid-Afrika, geologiese opname.

Teigner, C., Cawthorn, R. G., & Kruger, F. J. (2006). Cyclicity in the Main and Upper Zones of the Bushveld Complex, South Africa: crystallization from a zoned magma sheet. Journal of Petrology, 47(11), 2257-2279.

VanTongeren, J. A., Zirakparvar, N. A., & Mathez, E. A. (2016). Hf isotopic evidence for a cogenetic magma source for the Bushveld Complex and associated felsic magmas. Lithos, 248, 469-477.

Wabo, H., De Kock, M. O., Klausen, M. B., Söderlund, U., & Beukes, N. J. (2016a). Paleomagnetism and chronology of B-1 marginal sills of the Bushveld Complex from the eastern Kaapvaal Craton, South Africa. Gff, 138(1), 133-151.

Wabo, H., Olsson, J. R., De Kock, M. O., Humbert, F., Söderlund, U., & Klausen, M. B. (2016b). New U–Pb age and paleomagnetic constraints from the Uitkomst Complex, South Africa: clues to the timing of intrusion. Gff, 138(1), 152-163.

Wager, L. E. (8). R. and Brown, GM (1968). Layered Igneous Rocks. Oliver and Boyd, Edinburgh, 57.

Walker, A. S. D., Key, R. M., Pouliquen, G., Gunn, G., Sharrock, J., McGeorge, I., & Farr, J. (2010). Geophysical modelling of the Molopo Farms Complex in southern Botswana; implications for its emplacement within the~ 2 Ga large igneous provinces of southern and central Africa. South African Journal of Geology, 113(4), 381-400.

Walraven, F., & Hattingh, E. (1993). Geochronology of the Nebo Granite, Bushveld Complex. South African Journal of Geology, 96(1-2), 31-41.

Willemse, J. (1959). The ‘floor’ of the Bushveld Igneous Complex. Proceedings of the Geological Society of South Africa, LXII, xxi–lxxx.

Willemse, J. (1969). The geology of the Bushveld Igneous Complex, the largest repository of magmatic ore deposits in the world. In a Symposium on Magmatic Ore Deposits. Econ. Geol. Monogr. 4, 1-22.

Wilson, A. H. (2003). A new class of silica enriched, highly depleted komatiites in the southern Kaapvaal Craton, South Africa. Precambrian Research, 127(1), 125-141.

Wood, D. A., Joron, J. L., Treuil, M., Norry, M., & Tarney, J. (1979). Elemental and Sr isotope variations in basic lavas from Iceland and the surrounding ocean floor. Contributions to Mineralogy and Petrology, 70(3), 319-339.

Yudovskaya, M., Kinnaird, J., Naldrett, A. J., Rodionov, N., Antonov, A., Simakin, S., & Kuzmin, D. (2013). Trace-element study and age dating of zircon from chromitites of the Bushveld Complex (South Africa). Mineralogy and Petrology, 107(6), 915-942.

Zeh, A., Ovtcharova, M., Wilson, A. H., & Schaltegger, U. (2015). The Bushveld Complex was emplaced and cooled in less than one million years–results of zirconology, and geotectonic implications. Earth and Planetary Science Letters, 418, 103-114.

Zintwana, M., & Wilson, A. H. (2012, April). The Petrography and Geochemistry of the Marginal and Lower Zones, Eastern Bushveld Complex, South Africa. In EGU General Assembly Conference Abstracts Vol. 14, p. 2020.

Zirakparvar, N. A., Mathez, E. A., Scoates, J. S., & Wall, C. J. (2014). Zircon Hf isotope evidence for an enriched mantle source for the Bushveld Igneous Complex. Contributions to Mineralogy and Petrology, 168(3), 1050.

# Appendix A1

## Field photos and Maps

Representative photos of sample localities, which are sorted stratigraphically from the top to bottom of the Traansvaal Supergroup





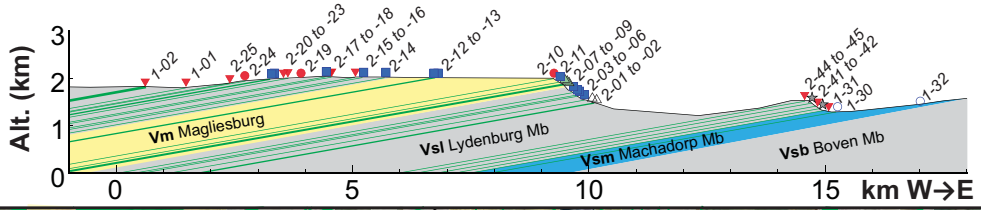


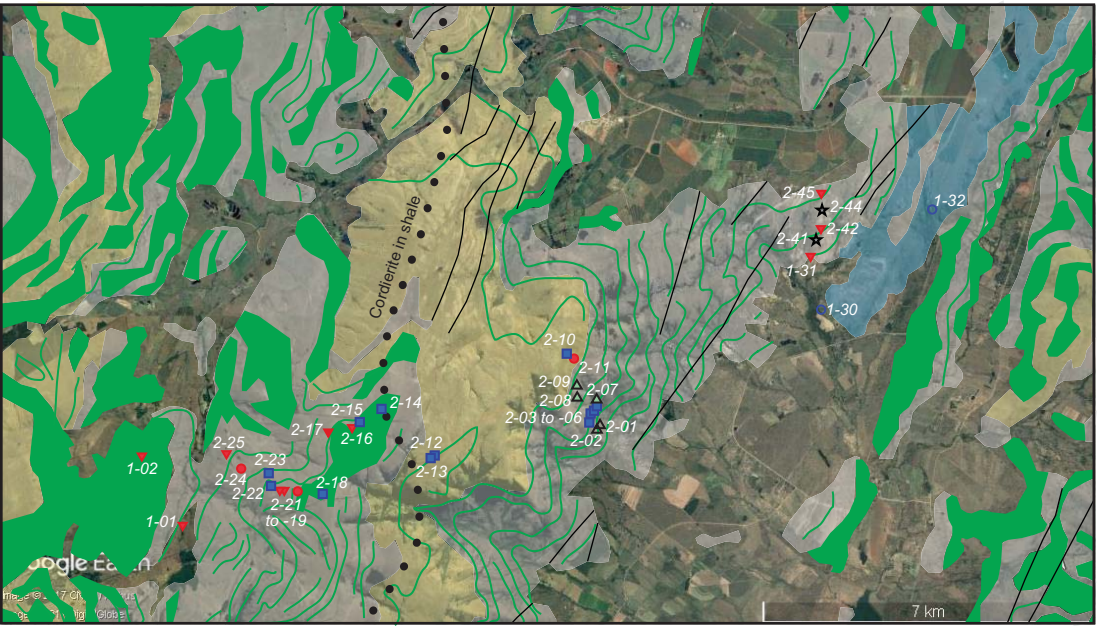


<BCS1-01 & BCS2-24 to -22


<BCS2-20 to -19





<BCS2-13 to -10





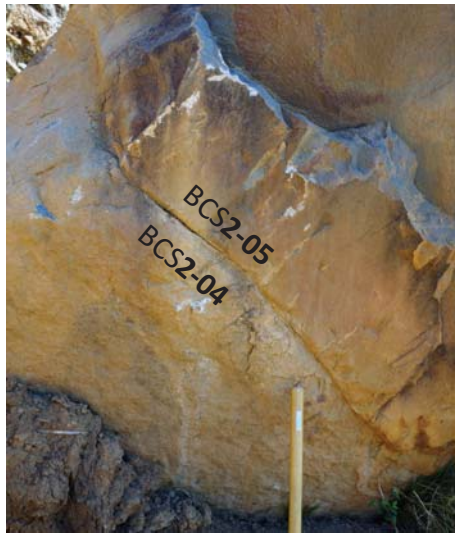



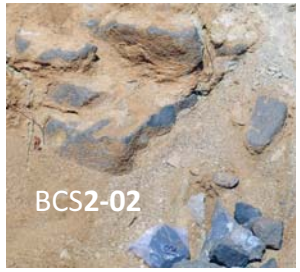



<BCS2-46





<BCS1-30


BCS1-32
~1.3 m

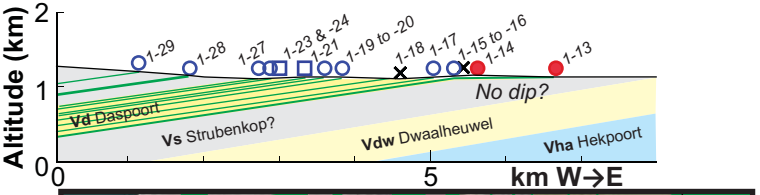
Altitude (km)
2
1
0
0
5
km W→E
1-29
1-28
1-27
1-23 & -24
1-21
1-19 to -20
1-18
1-17
1-15 to -16
1-14
1-13
No dip?
Vd Daspoort
Vs Strubenkop?
Vdw Dwaalheuwel
Vha Hekpoort

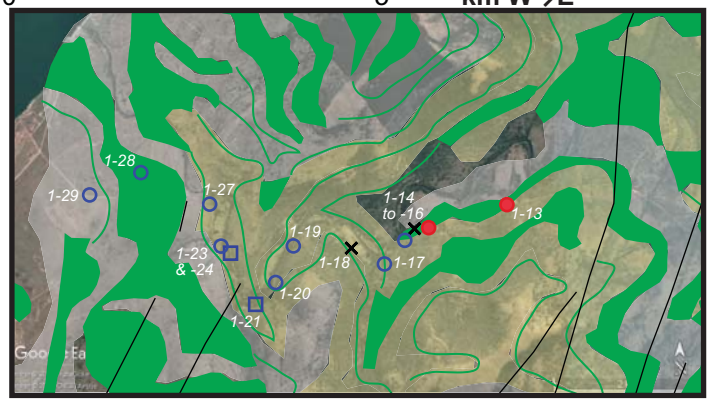
1-28
1-29
1-27
1-14 to -16
1-13
1-19
1-23 & -24
1-18
1-17
1-20
1-21


BCS1-29


BCS1-28

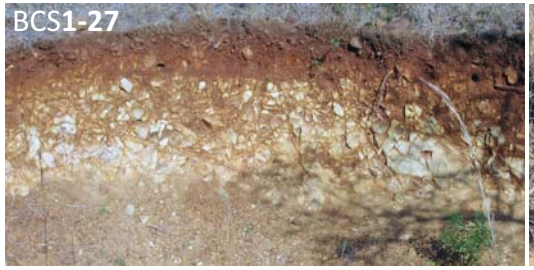
BCS1-27


BCS1-26


BCS1-25


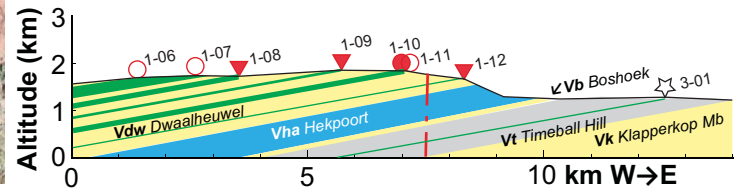




<BCS1-19


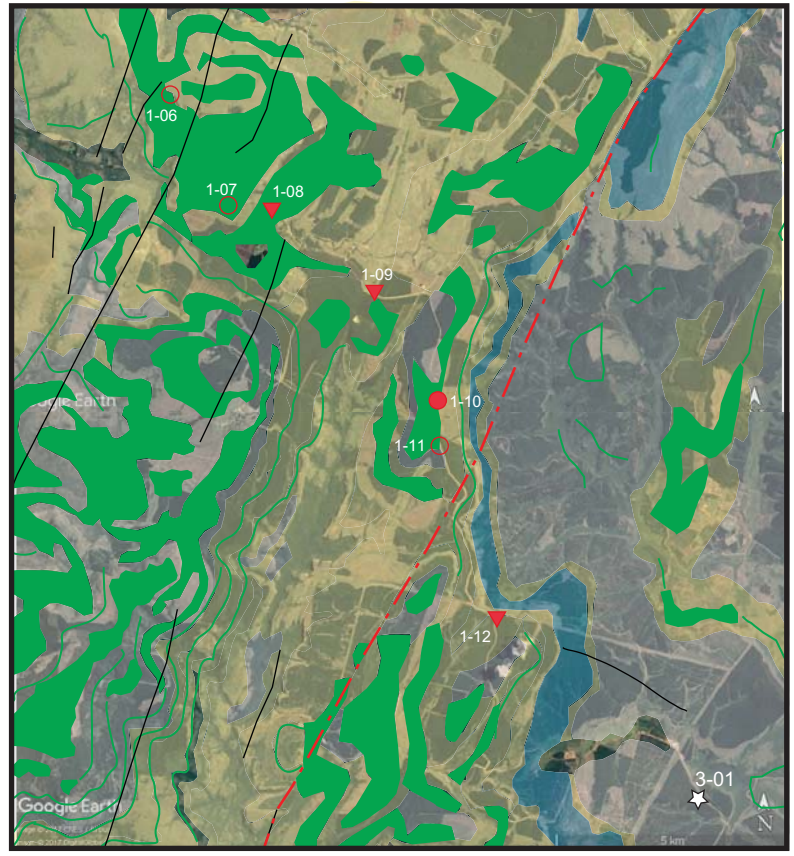


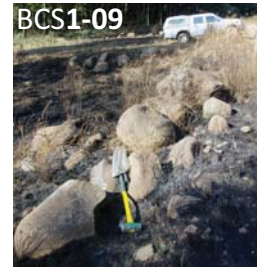




<BCS1-16 to -13




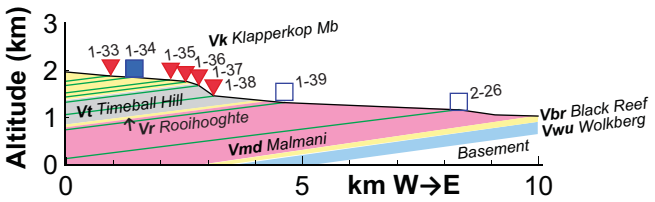


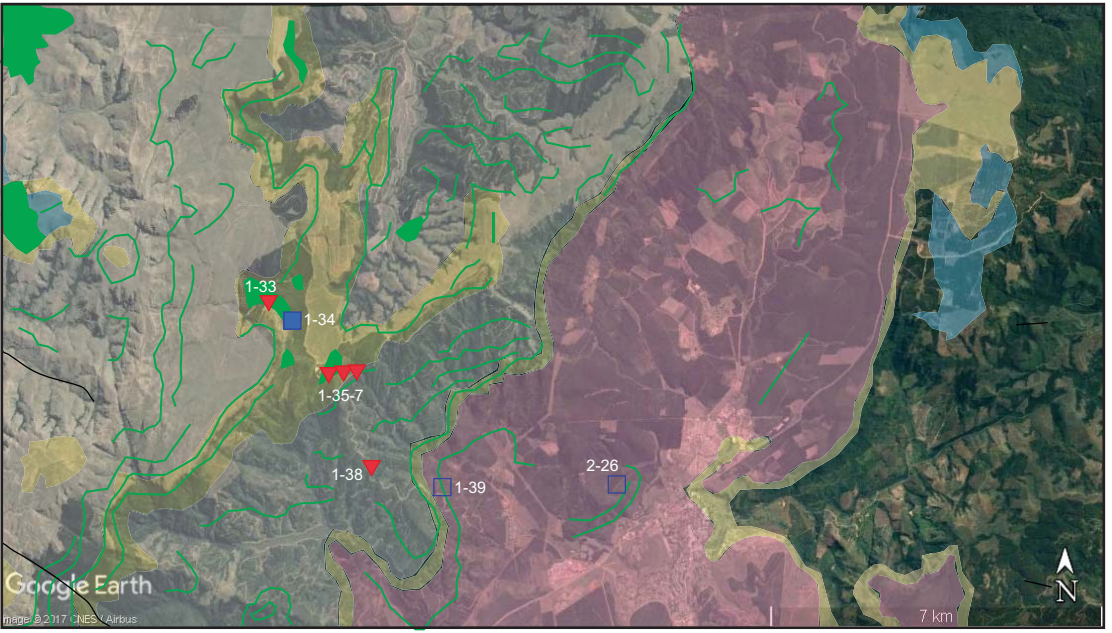





<BCS**1-38**


<BCS**2-46** to **-53** (Uitkomst/Nkomati drill core)



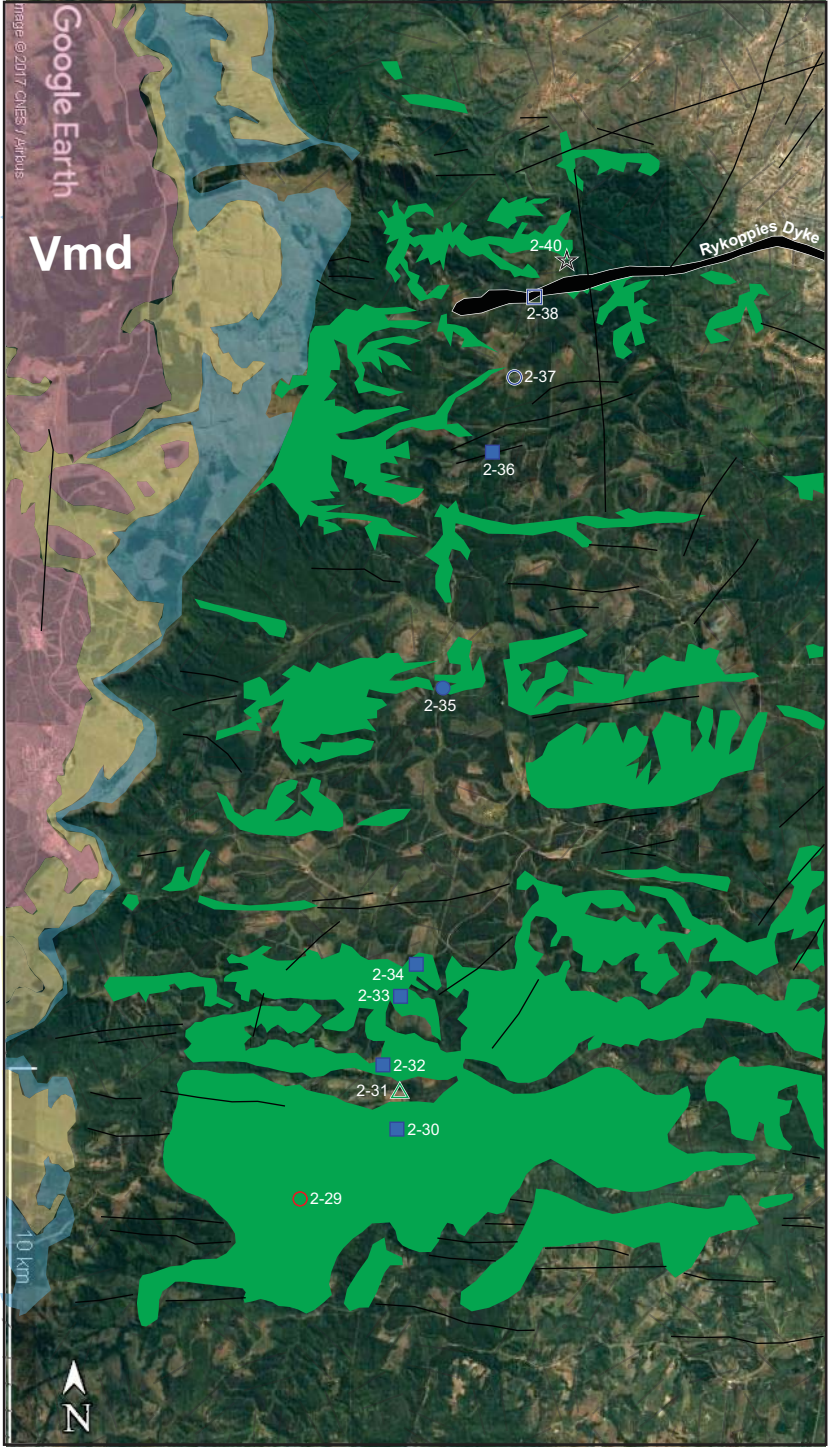


<BCS2-38 to -40



<BCS2-32 to -35




<BCS2-27 to -28

# Appendix A2

## Petrography and normative compositions

Available complete scans of cut blocks and/or thin sections.

Inserted squares indicate 1 mm (black) and 5 mm (white).

Shown together with pie charts based on normative mineral assemblages.

Samples are from localities that are sorted stratigraphically

from the top to bottom of the Traansvaal Supergroup.

Steenkampsberg Fm

Vermont Fm

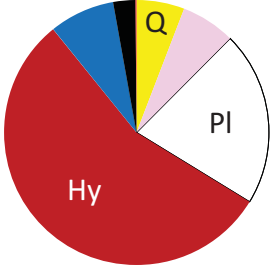


<1) BCS**1-03**

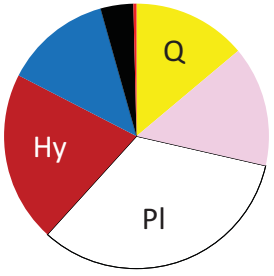


<2) BCS**1-04**

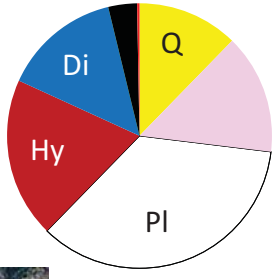


<3) BCS**1-05**

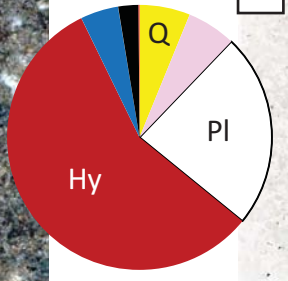


4) BCS**1-02**

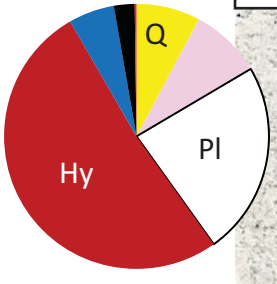


5) BCS**1-01**

Vermont Fm

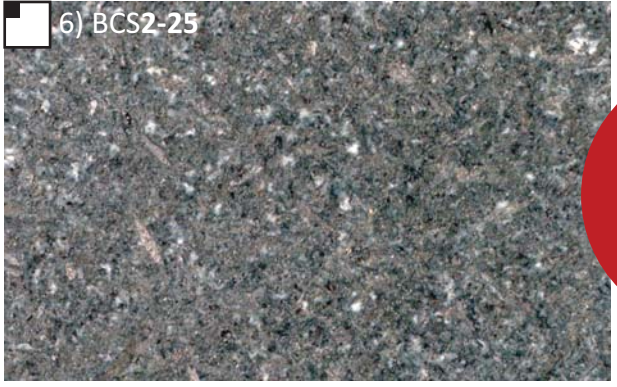
6) BCS2-25

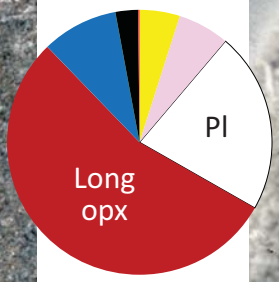
Pl
Long opx

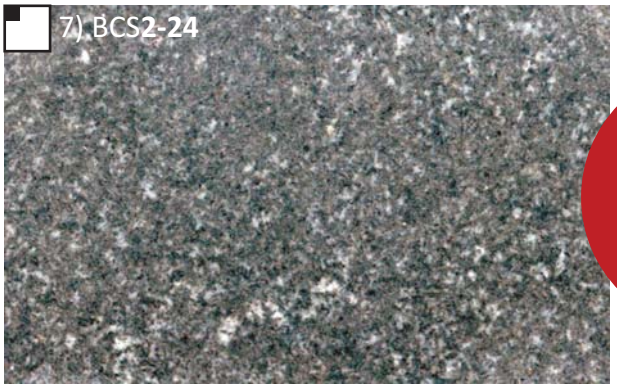
7) BCS2-24

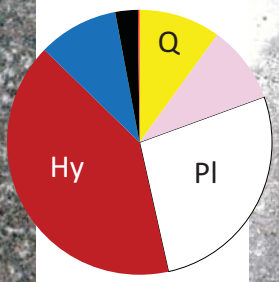
Q
Hy
Pl

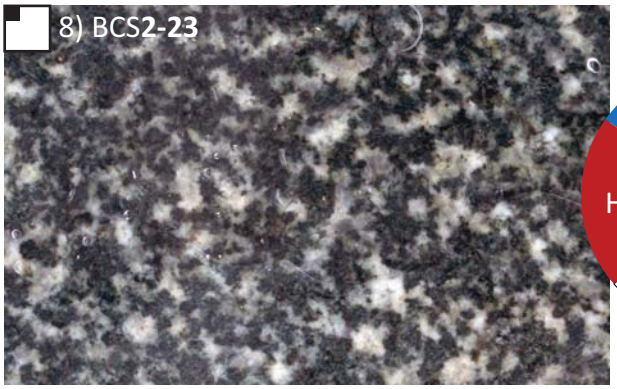
8) BCS2-23

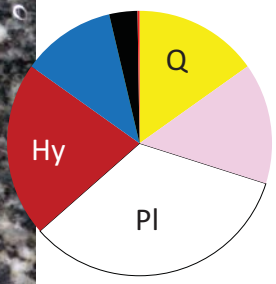
Q
Hy
Pl

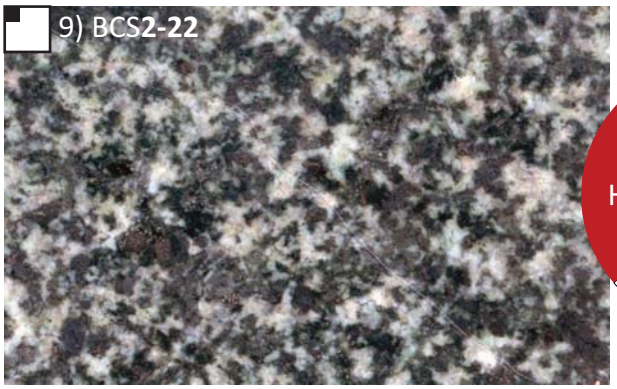
9) BCS2-22

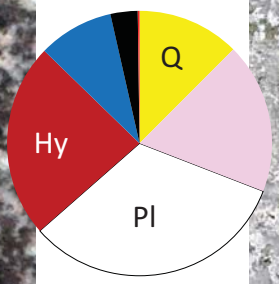
Q
Hy
Pl

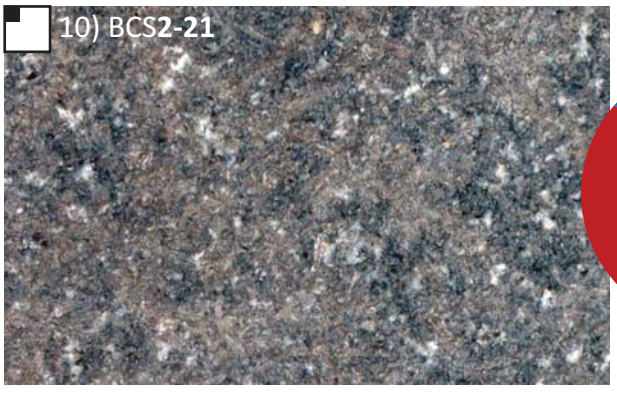
10) BCS2-21

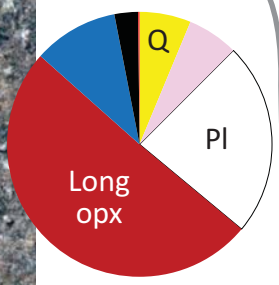
Q
Pl
Long opx

Vermont Fm

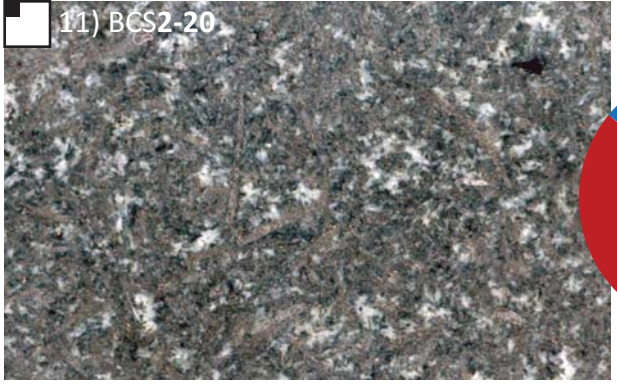
11) BCS2-20

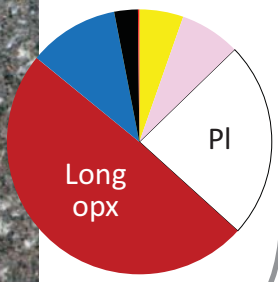
Pl
Long opx

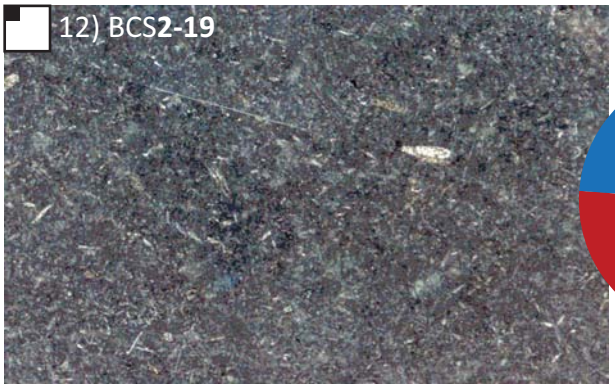
12) BCS2-19

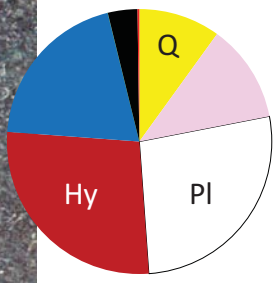
Q
Hy
Pl

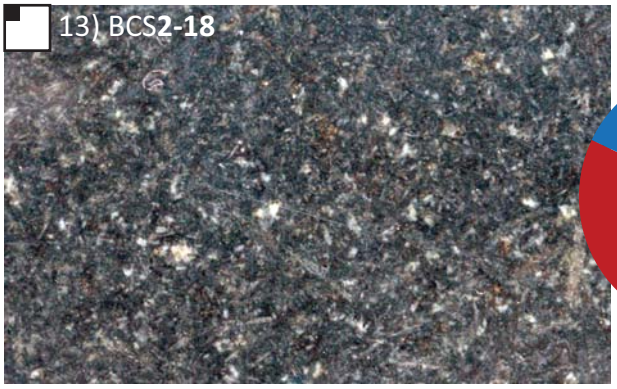
13) BCS2-18

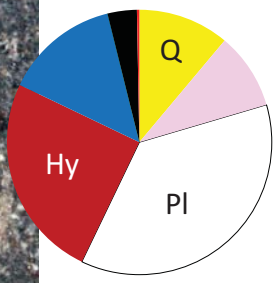
Q
Hy
Pl

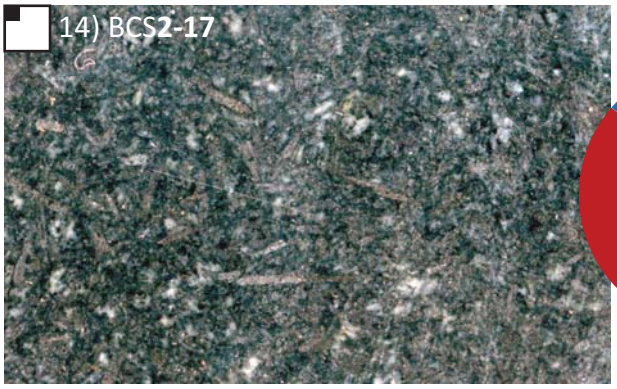
14) BCS2-17

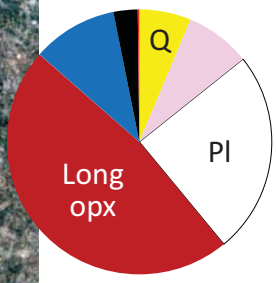
Q
Pl
Long opx

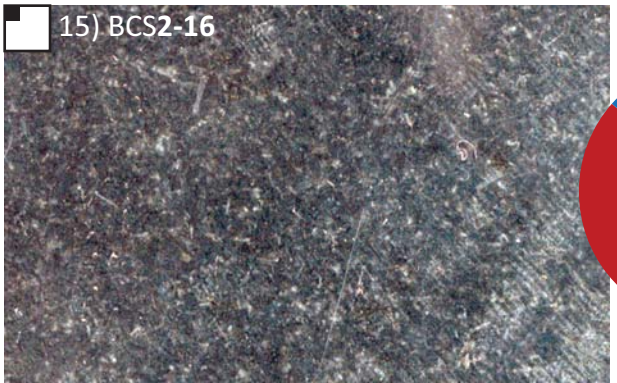
15) BCS2-16

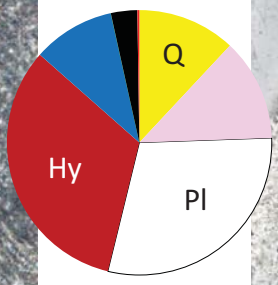
Q
Hy
Pl

Vermont Fm

16) BCS2-15

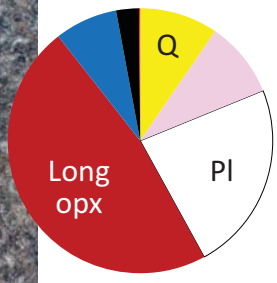


17) BCS2-14

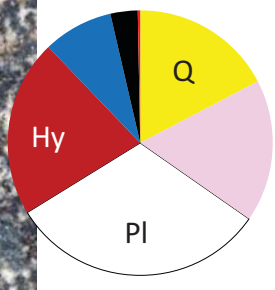


Magaliesberg Fm

18) BCS2-13

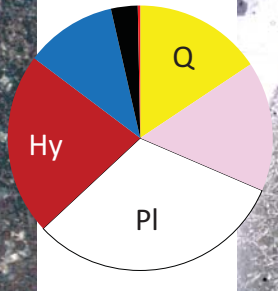


19) BCS2-12

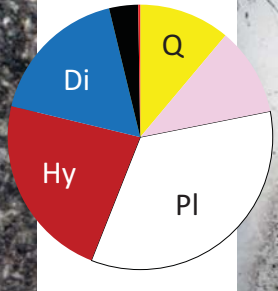


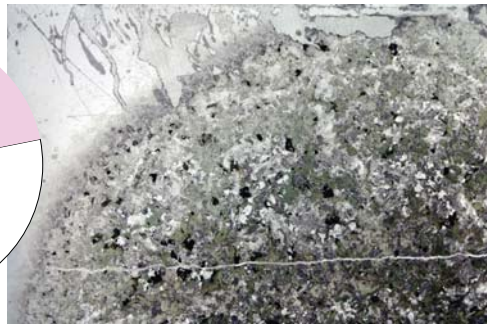

20) BCS2-11

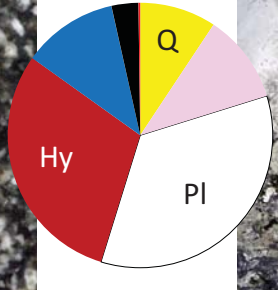


Magaliesberg>Silverton Silverton Lydenburg Mb

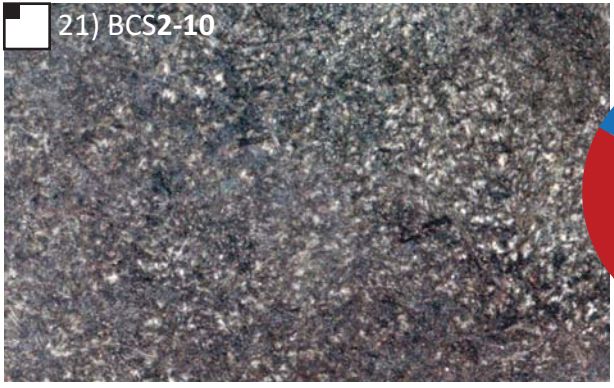


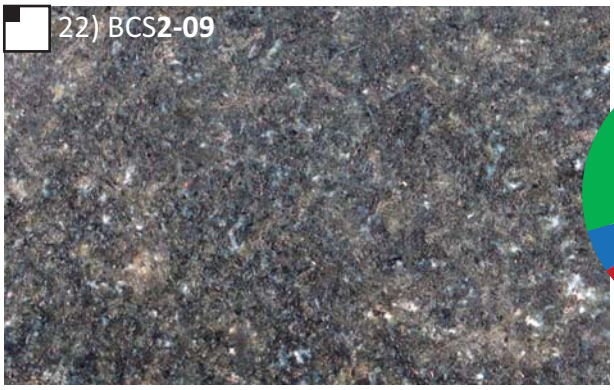


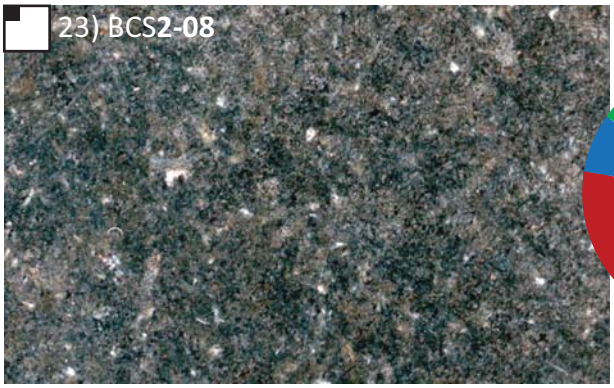


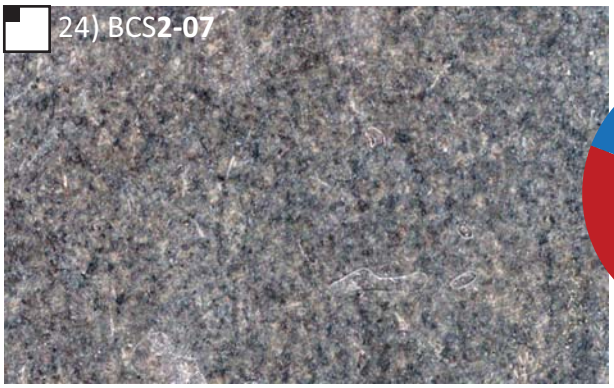


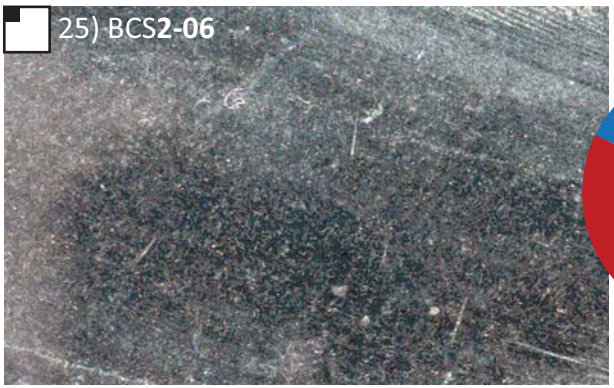

Silverton

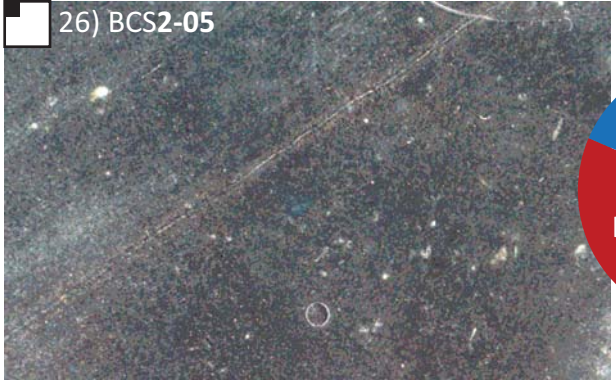


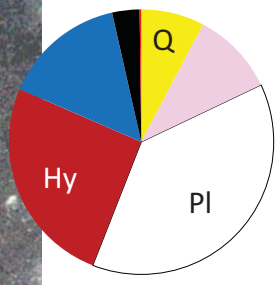


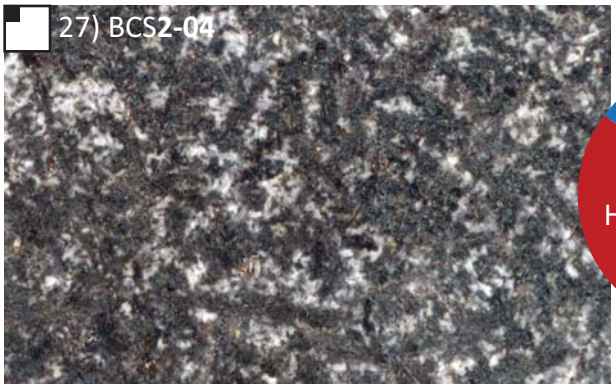


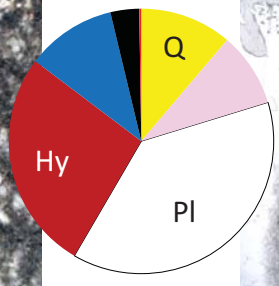


Lydenburg

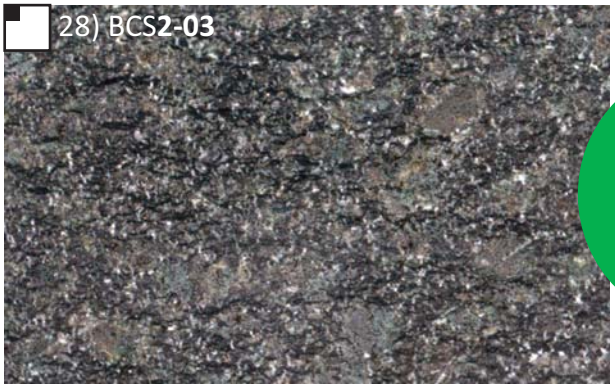


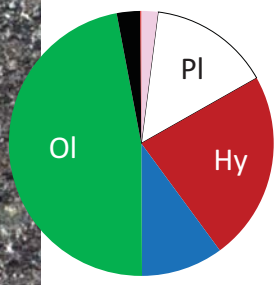


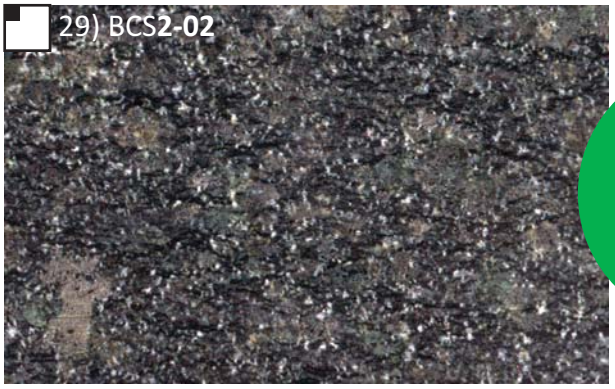


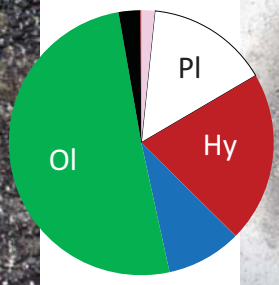


Mbg

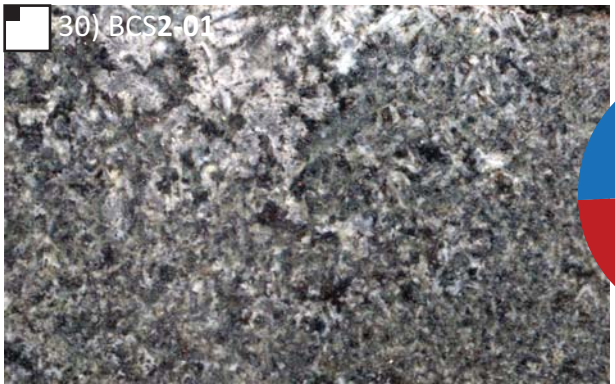


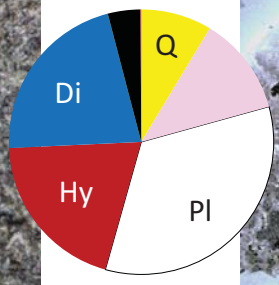


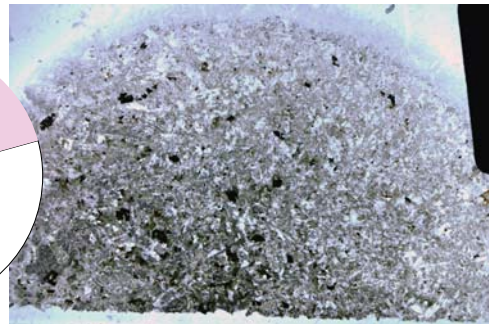

Silverton Lydenburg Mb

<31) BCS**1-30**

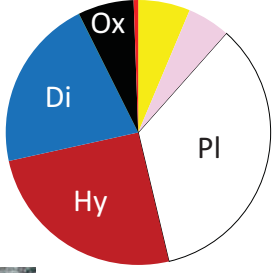


32) BCS**2-45**

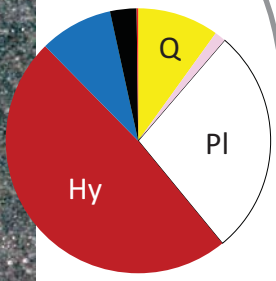


33) BCS**2-44**

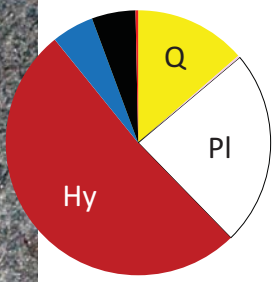


34) BCS**2-42**

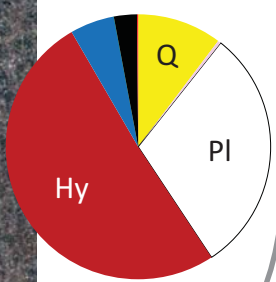


35) BCS**2-41**

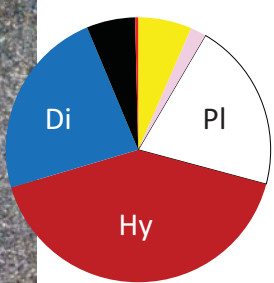

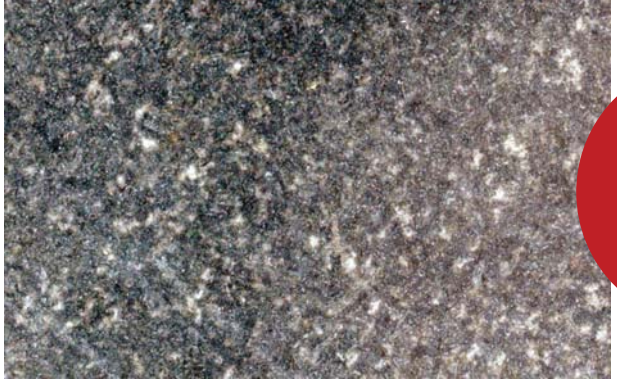

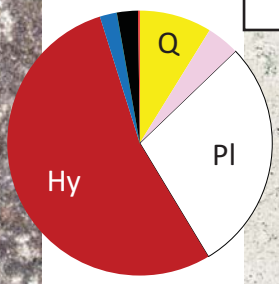


36) BCS**1-31**

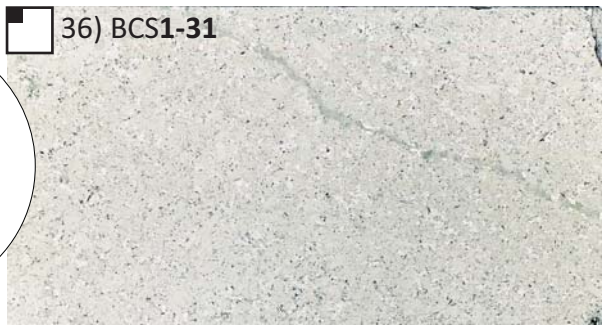

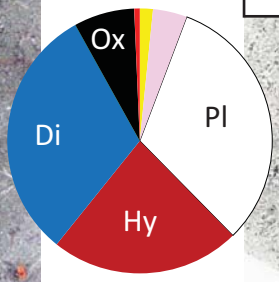


37) BCS**1-32**

38) BCS**1-29**

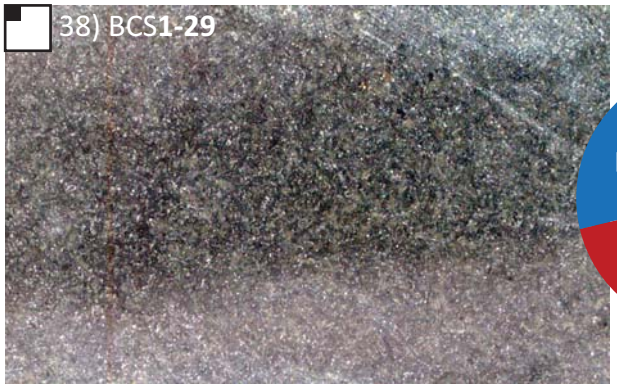

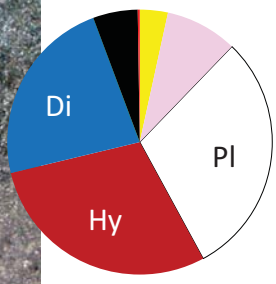


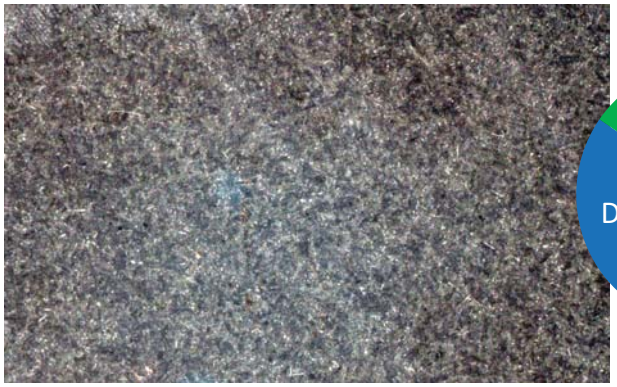

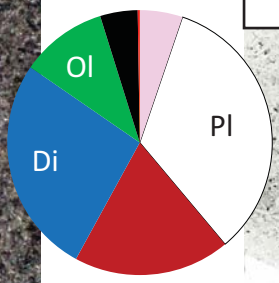


39) BCS**1-28**

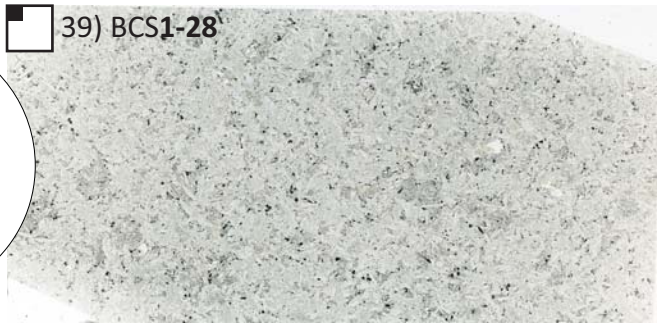

40) BCS**1-27**

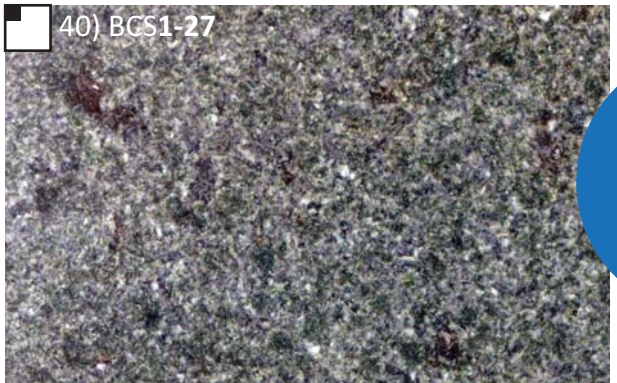

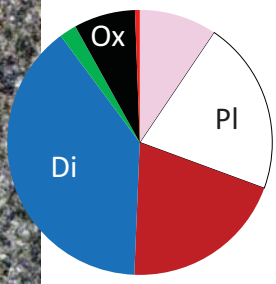

Silverton Bowen Mb

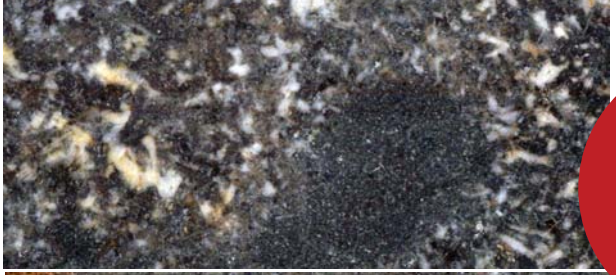

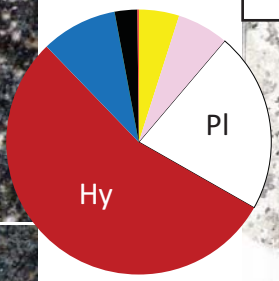


41) BCS**1-25**

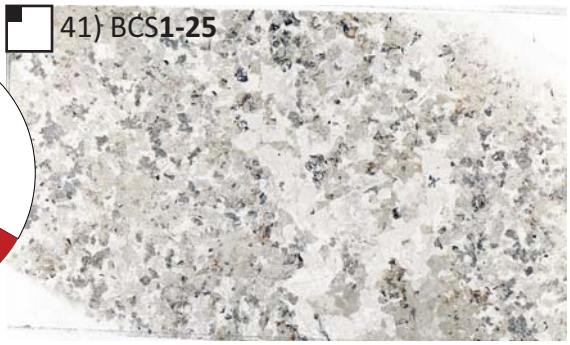

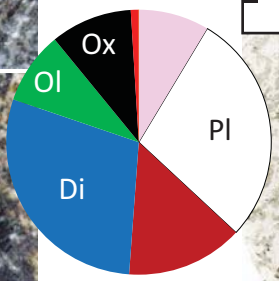


42) BCS**1-26**

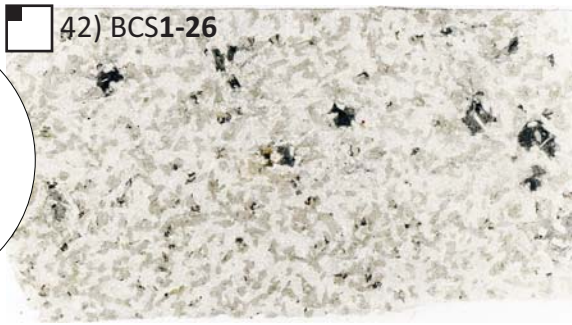

43) BCS**1-21**

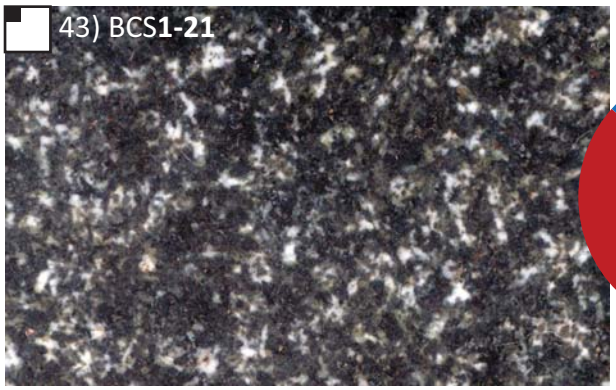

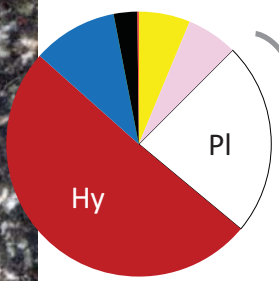


44) BCS**1-20**

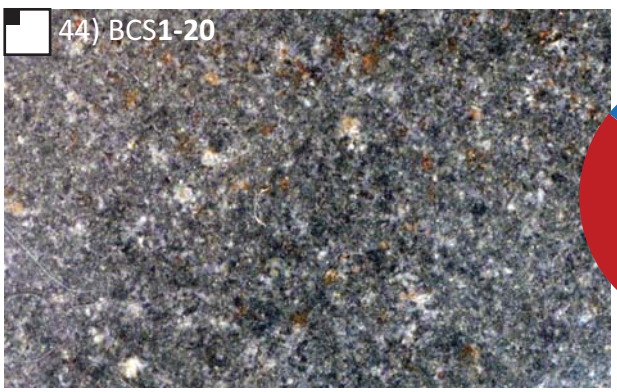

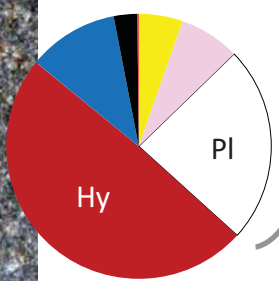


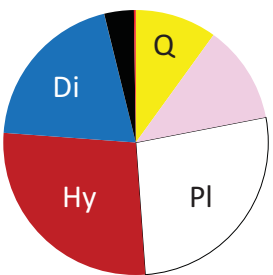


<45) BCS**1-19**

Silverton Bowen Mb

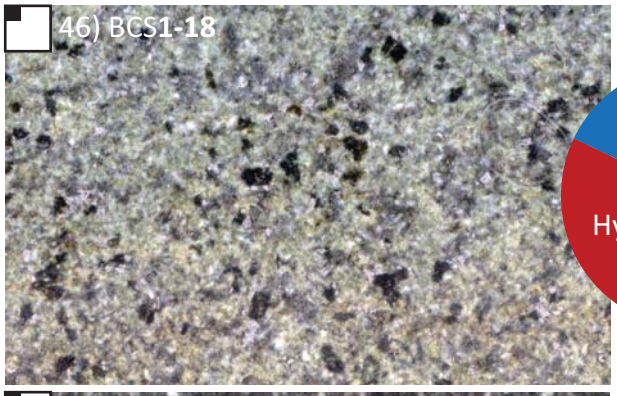


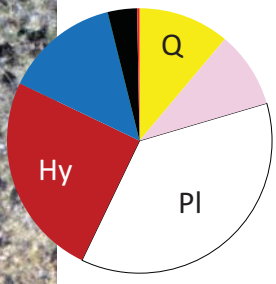


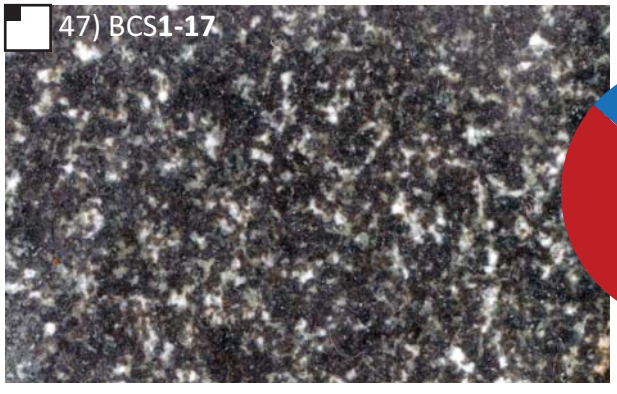


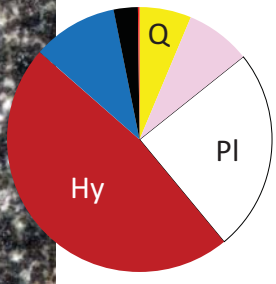


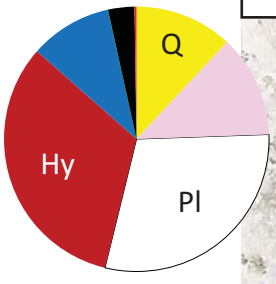


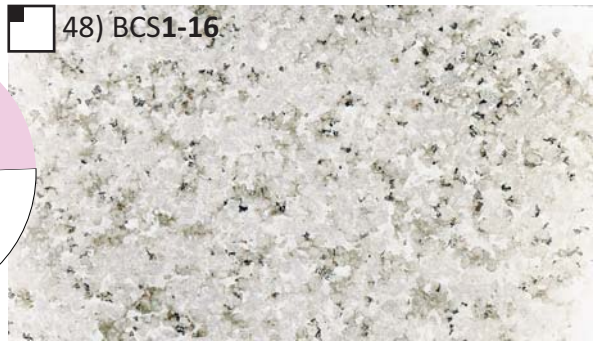


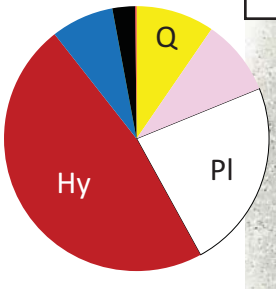


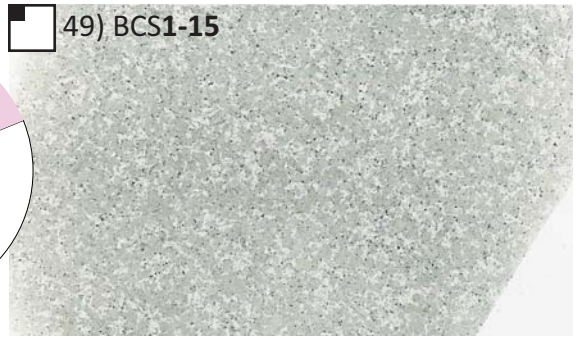


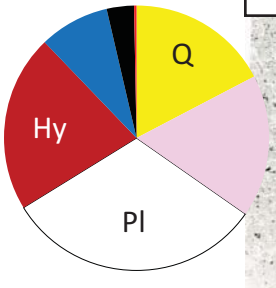


Silverton Bowen Mb

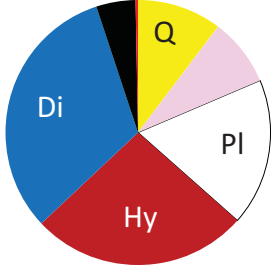


<51) BCS**1-13**

Daspoort Fm

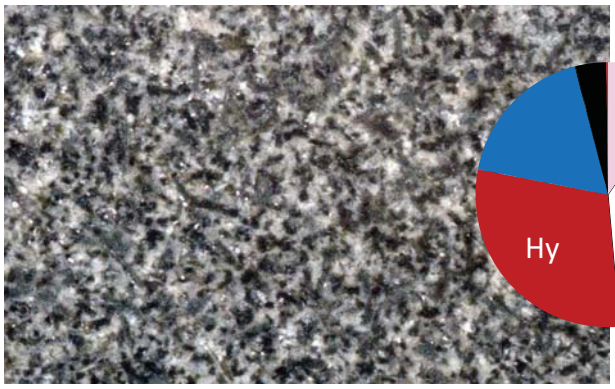


52) BCS**1-06**

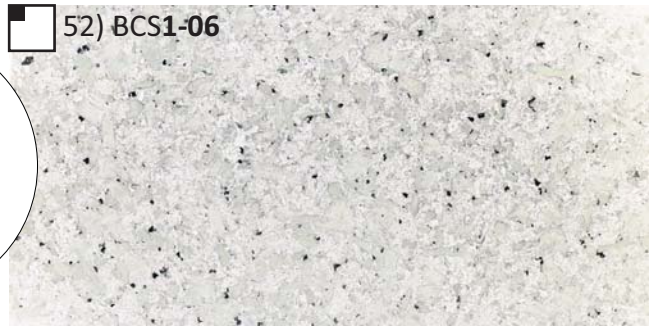

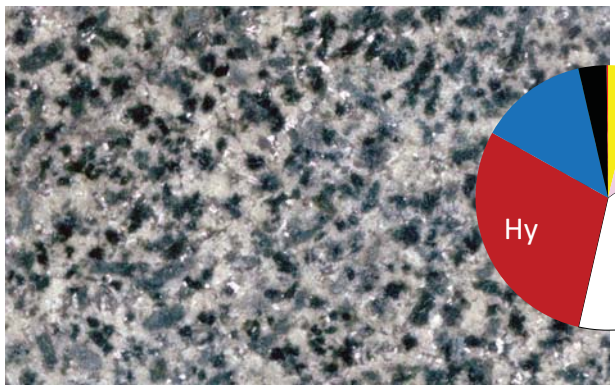


53) BCS**1-07**

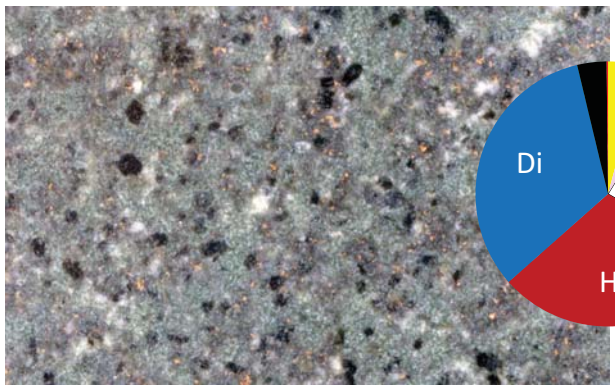


54) BCS**1-08**

Strubenkop Fm

55) BCS**1-09**

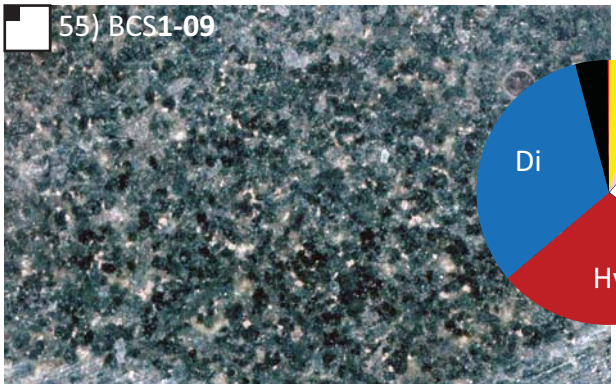

Strubenkop Fm

Timeball (klapperkop) Fm

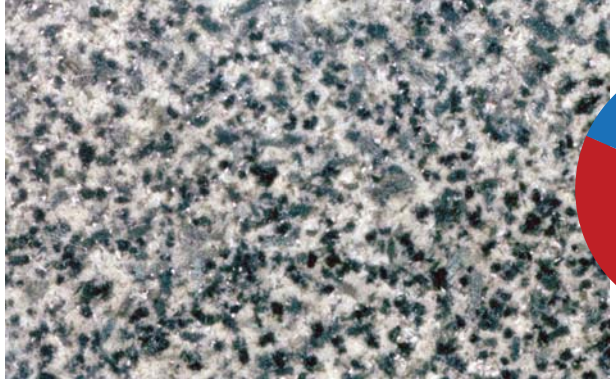

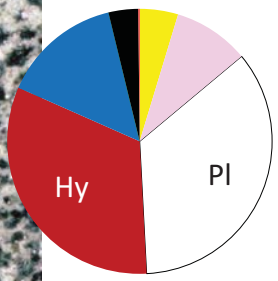


<56) BCS**1-10**

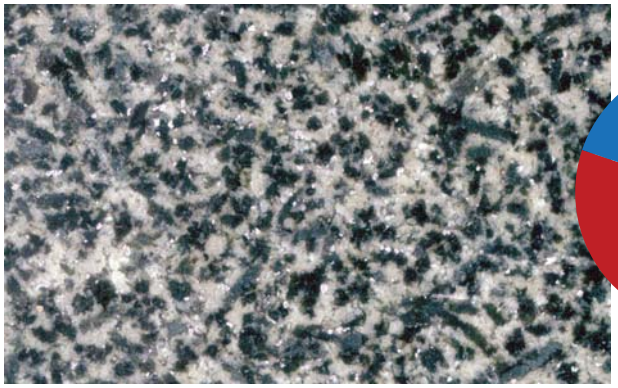

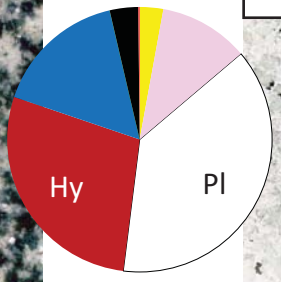


57) BCS**1-11**

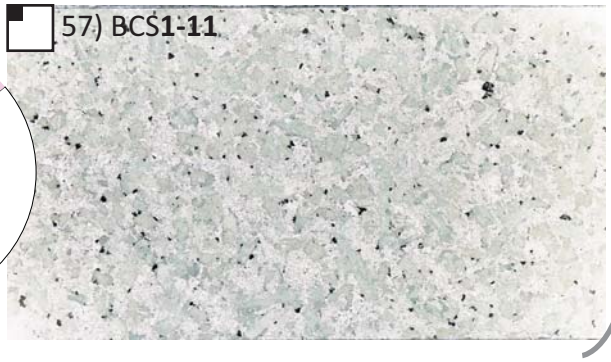

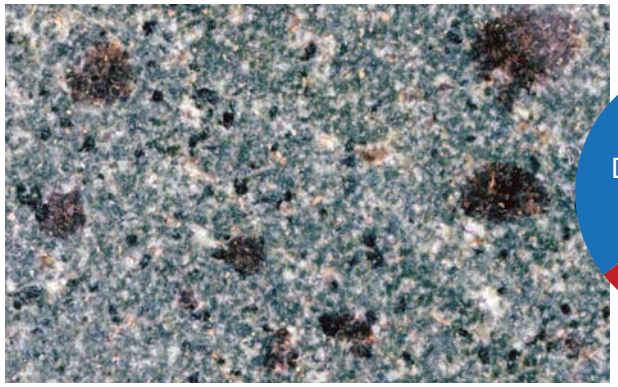

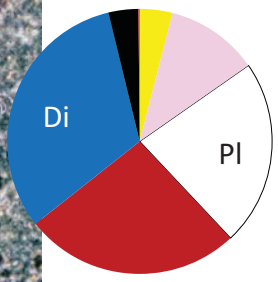


<58) BCS**1-12**

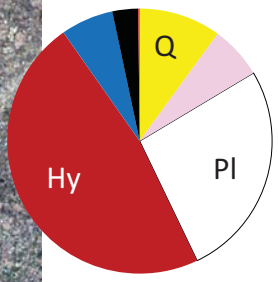


<59) BCS**1-33**

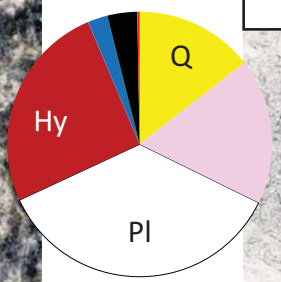


60) BCS**1-34**

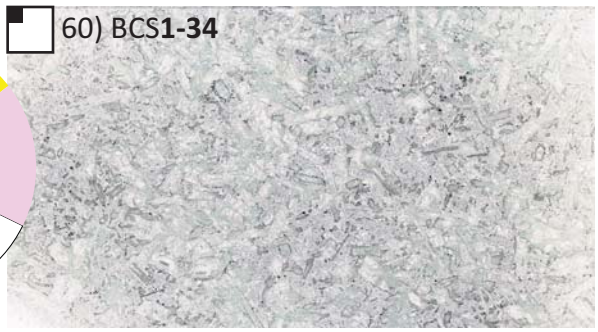

Timeball (klapperkop) Fm

Timeball Fm

Rooihoogte Fm

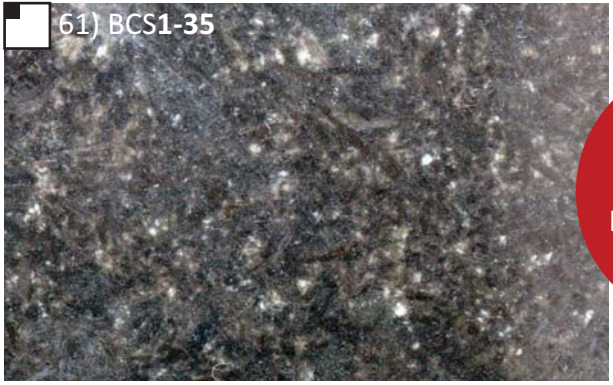


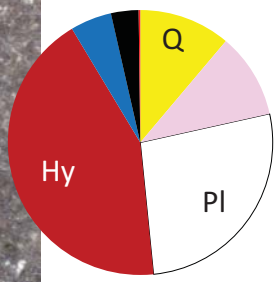


<61) BCS**1-35**

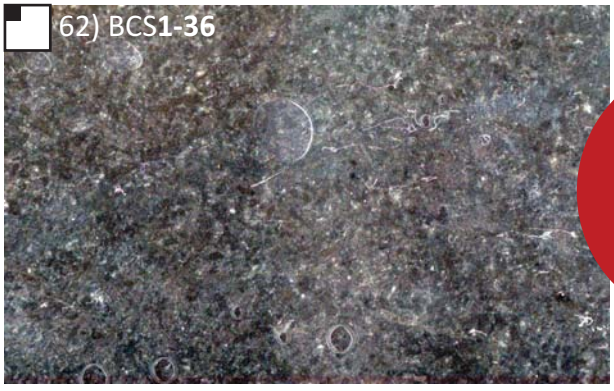


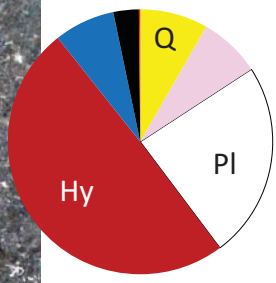


<62) BCS**1-36**

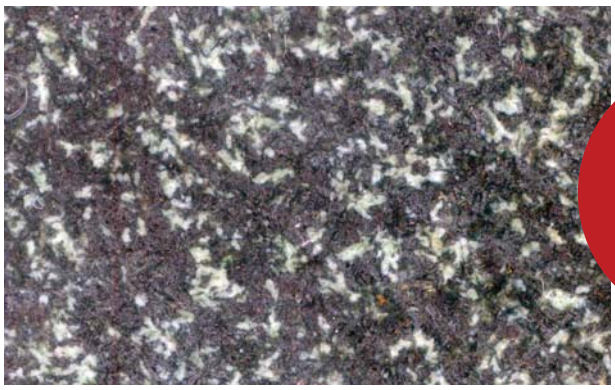

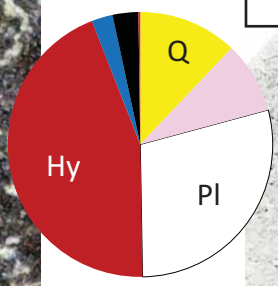



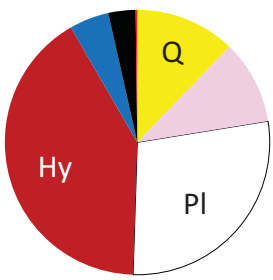


<64) BCS**1-38**

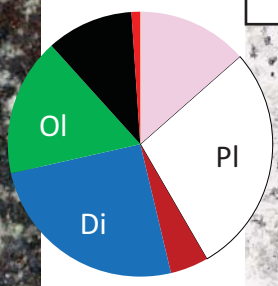


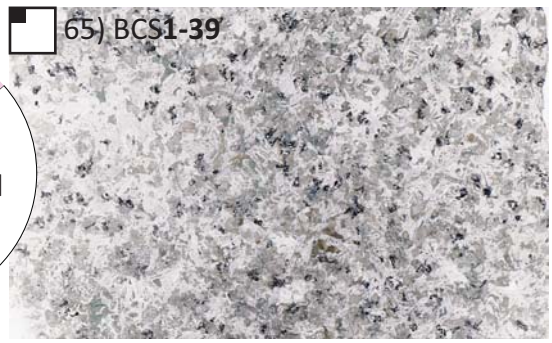

Malmani Fm (drill core BCS2-46 ff)

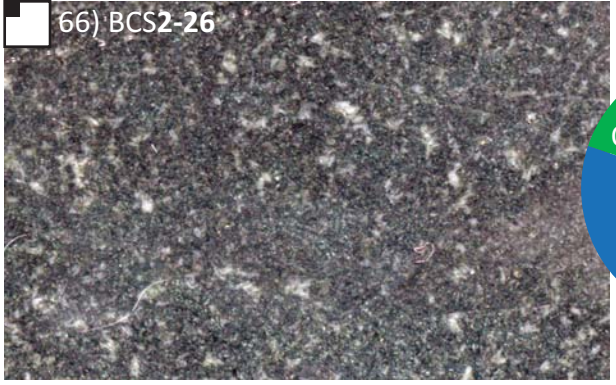


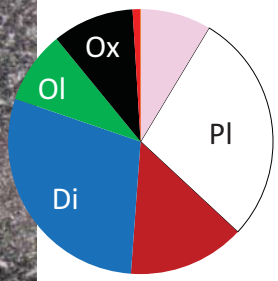


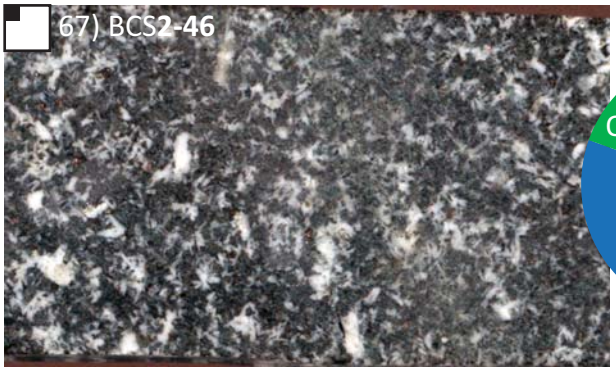


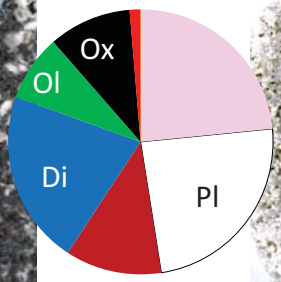


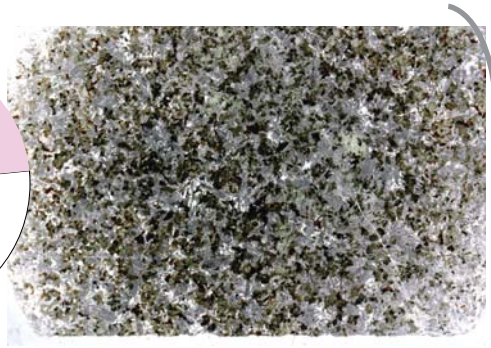

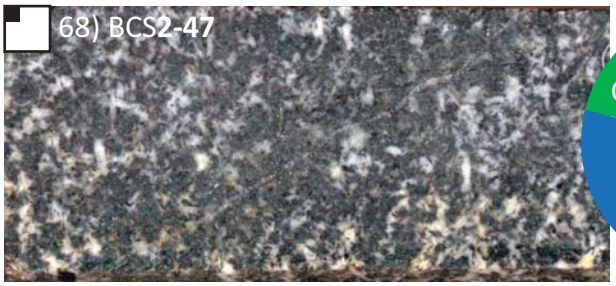


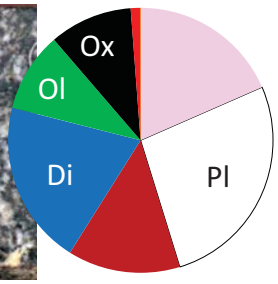


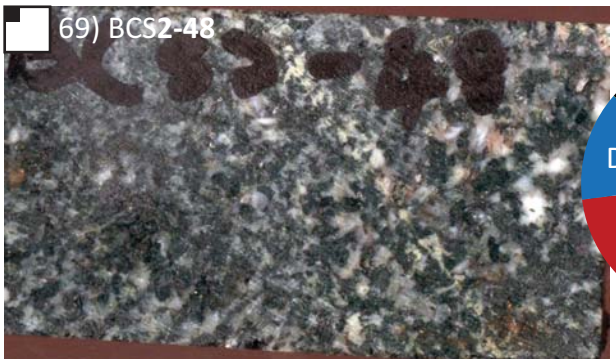


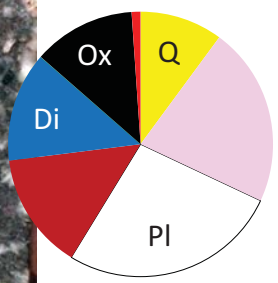



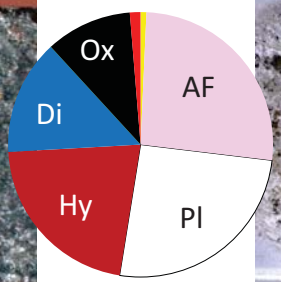


Malmani Fm (drill core) Basement

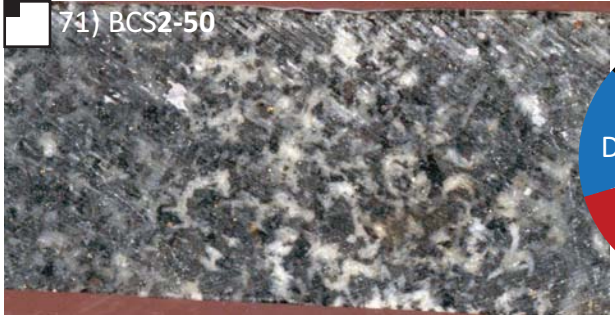


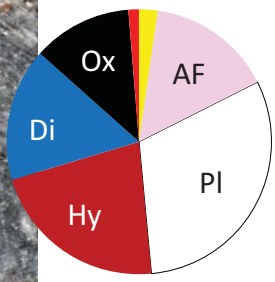


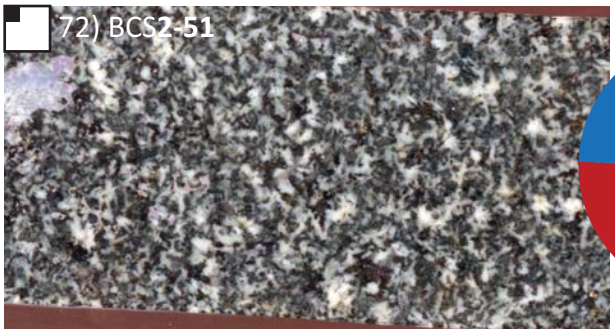


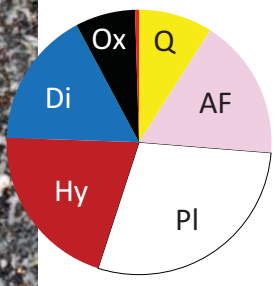



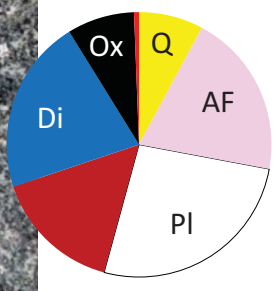


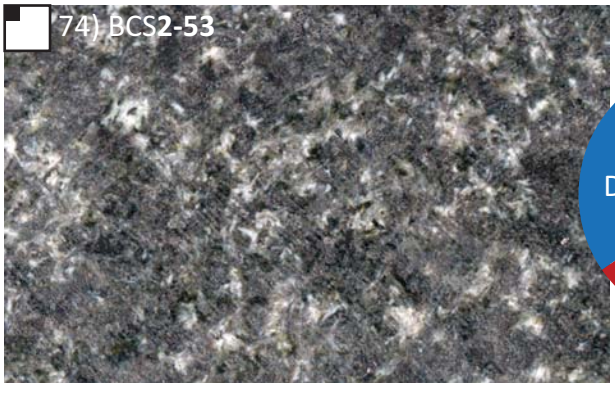


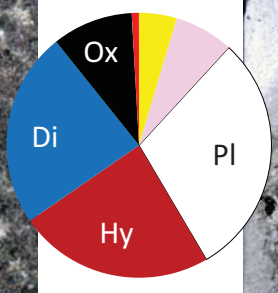


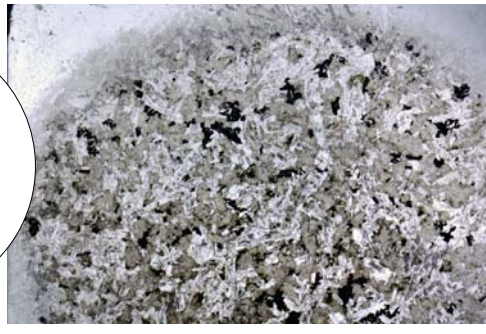

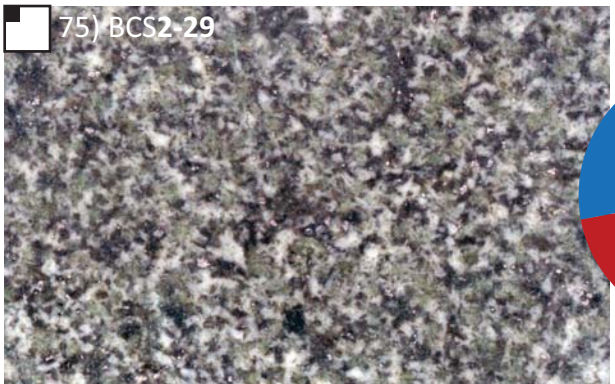


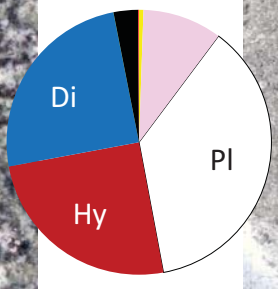


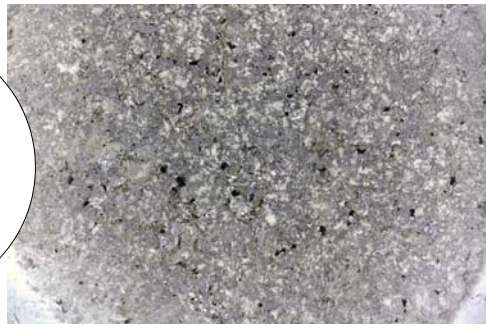

Precambrian Basement

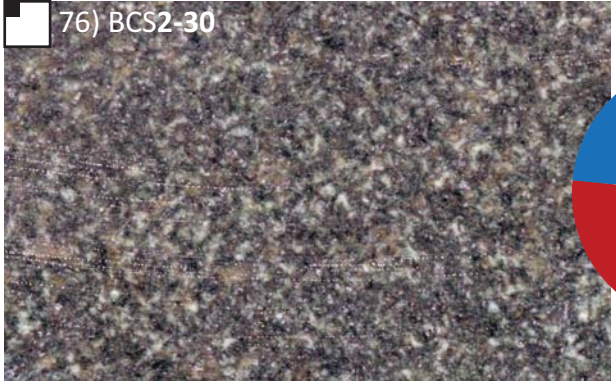


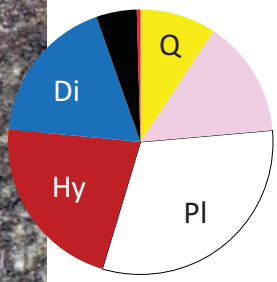


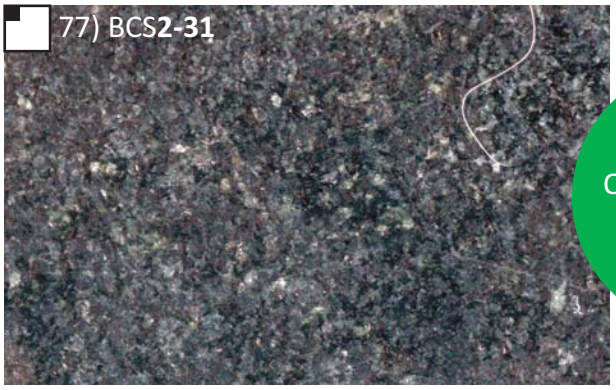


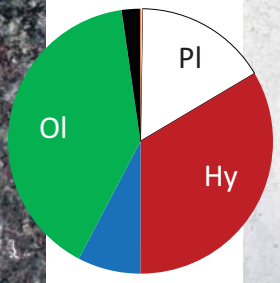


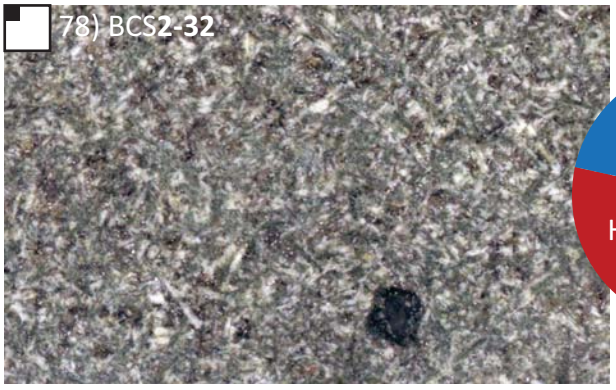


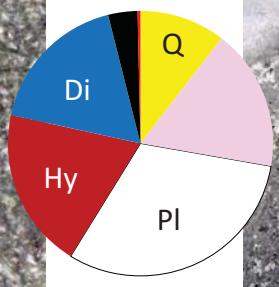


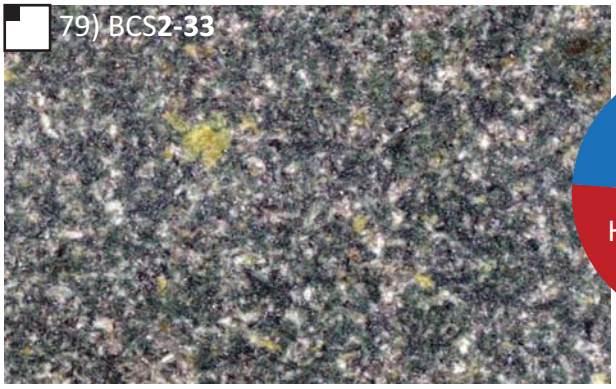


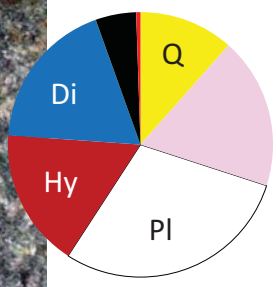



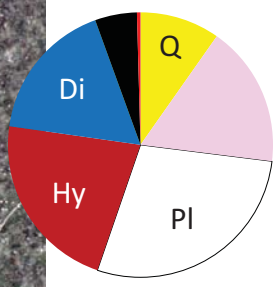

Precambrian Basement

81) BCS2-35

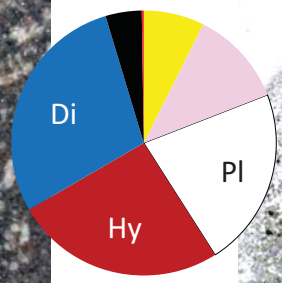


82) BCS2-36

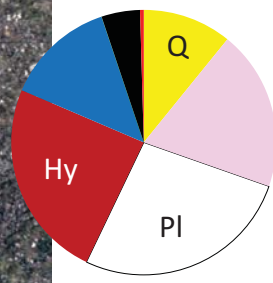


83) BCS2-37

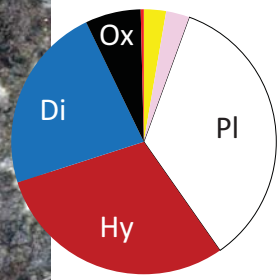


84) BCS2-38

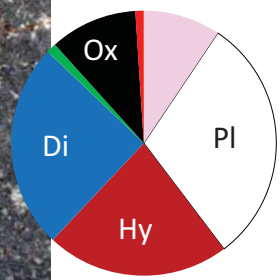


85) BCS2-40

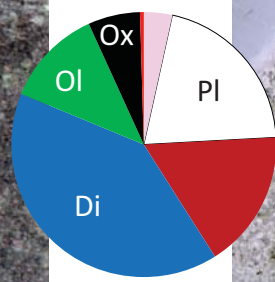


# APPENDIX A3

## PETROGRAPHY

Microphotographs of all BCS1 and BCS2 sample collection arranged stratigraphically, where the field of view in each image is ~5.2 mm, and the left and right column show paired photographs taken under plane and crossed polarized light, respectively.

## DASPOORT FM

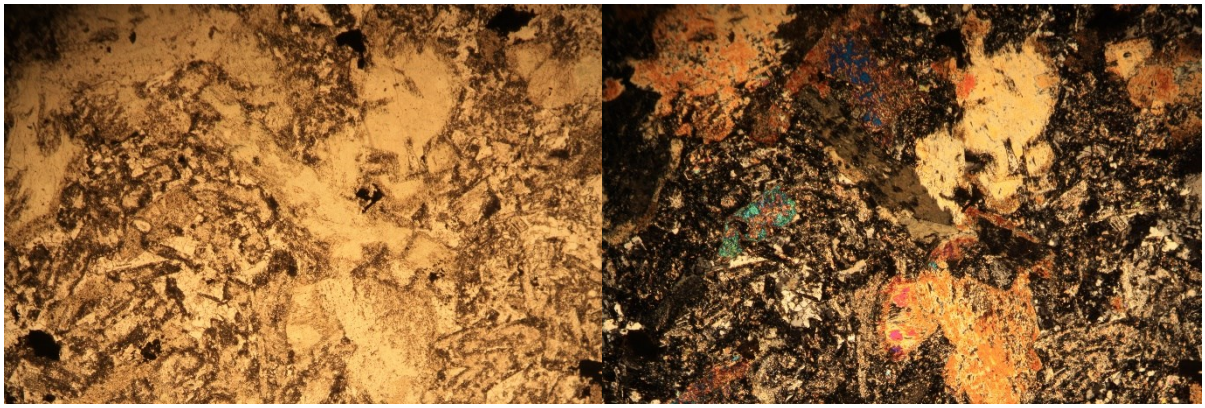

**BCS1-06:** Eu-subhedral ortho-amphibole, interstitial quartz & maybe plag? as well as moderate subhedral opaques.

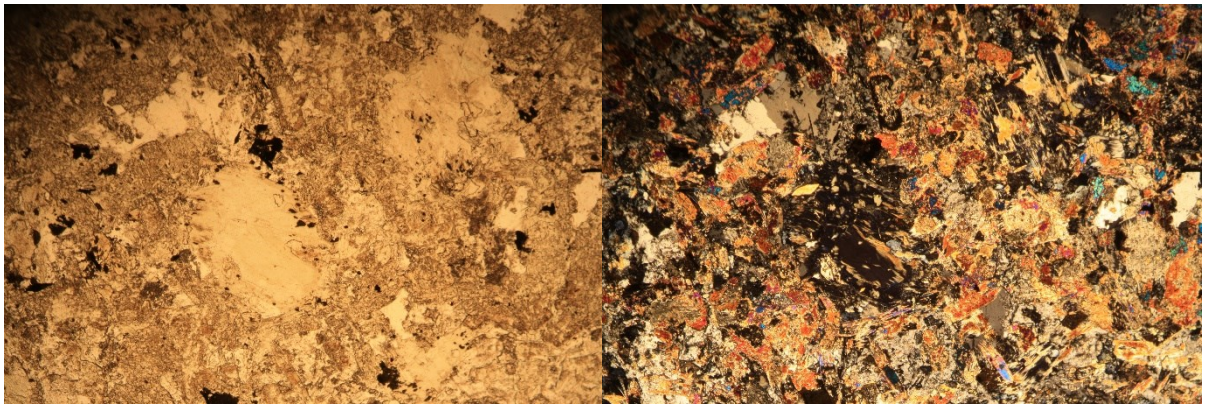

**BCS1-08:** euhedral ortho-amphiboles surrounded by chaotic 'matrix' of subhedral and altered plag and clino-amphibole, as well as interstitial quartz and opaques.

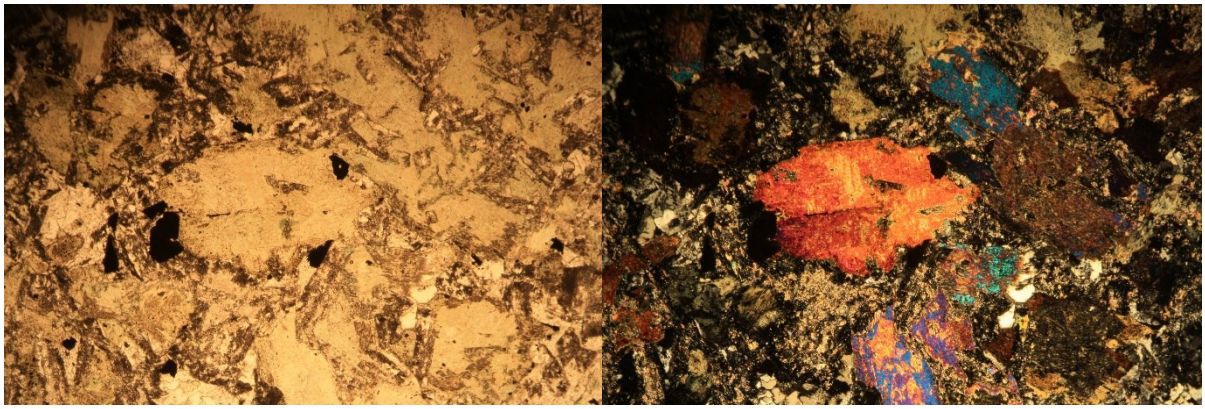

**BCS1-07:** Eu-subhedral ortho-amphibole, accessory quartz, much subhedral opaques

## STRUBENKOP FM

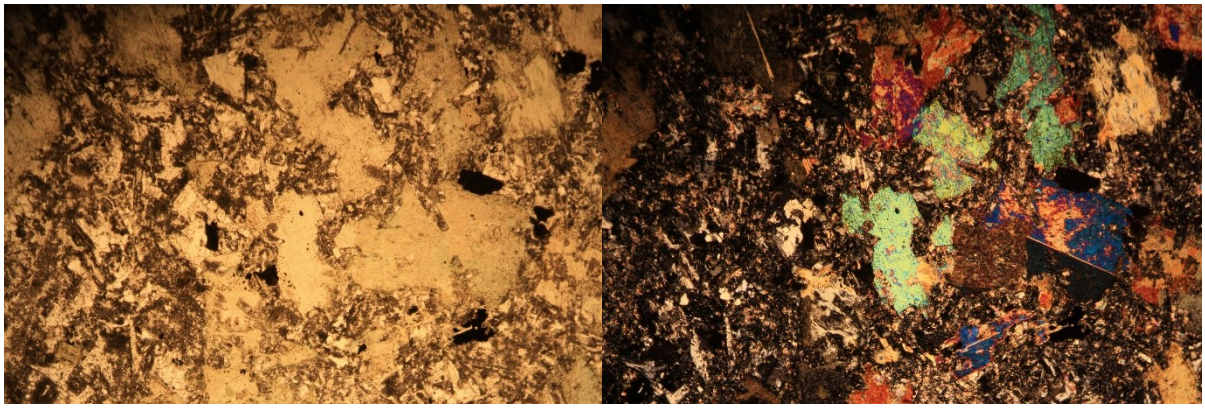

**BCS1-11:** Eu-subhedral ortho-amphibole, interstitial quartz & plag as well as moderate subhedral opaques.

**BCS1-14:** Eu-subhedral lath-shaped to elongated ortho-amphiboles, plag & quartz, as well as subhedral opaques.

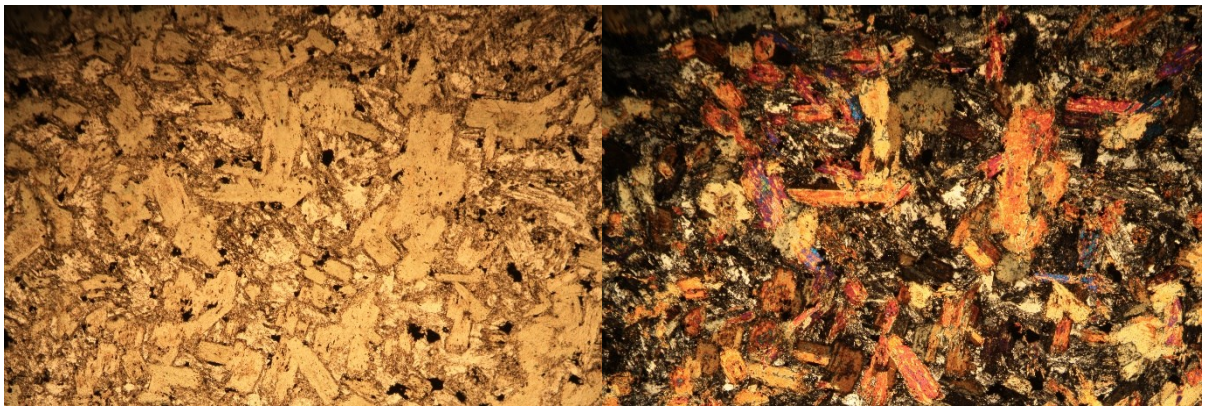

**BCS1-15:** Eu-subhedral orthoamphiboles and much altered subhedral plag laths.

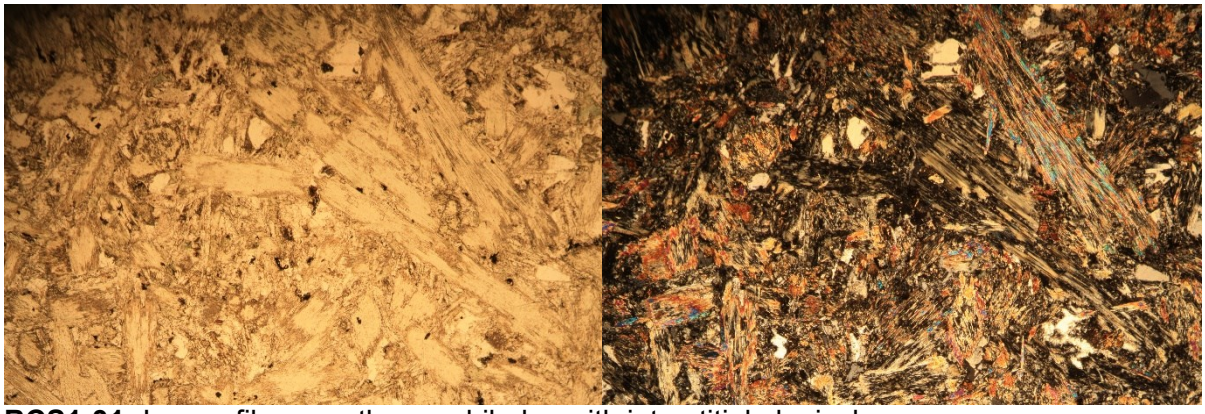

**BCS1-31:** Larger fibrous ortho-amphiboles with interstitial plagioclase.

**BCS1-32:** Euhedral fresh plag & subhedral greenish augite, mod interstitial opaques.

**TIMEBALL (KLAPPERKOP) FM**

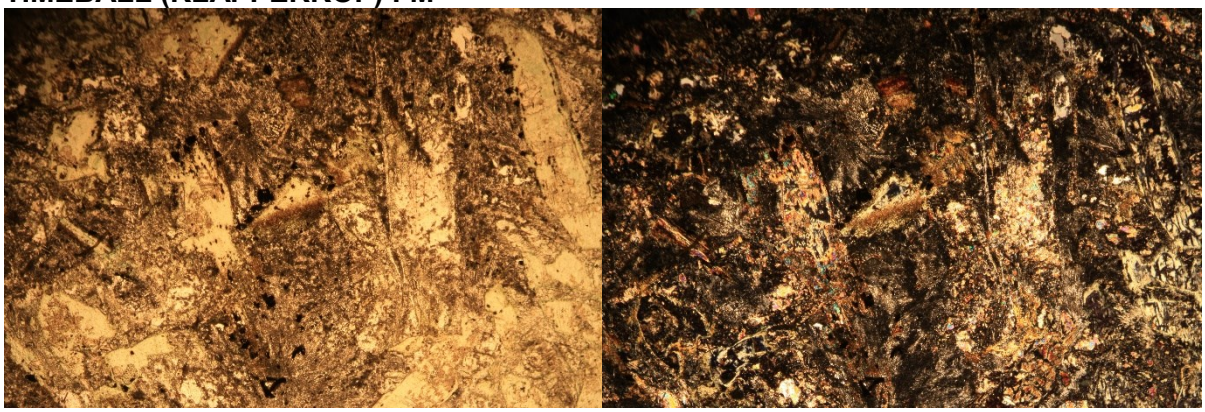

**BCS1-34:** Eu-subhedral orthoamphiboles (pseudomorph opx?), some **micrographic** quartz-fsp. Large subhedral opaques (slightly **skeletal**).

**SILVERTON FM**

**BCS2-01:** Euhedral and pale opx, cpx with higher interference colours and twins. Interstitial-subhedral plag with multiple and Interstitial quartz with 'myrmekitic' textures.

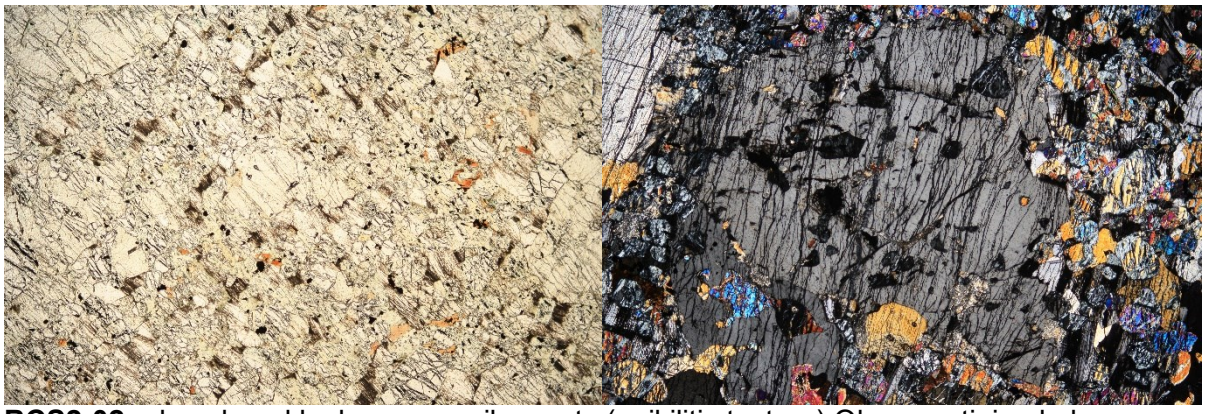

**BCS2-02:** ol enclosed by large opx oikocrysts (poikilitic texture) Ol serpentinised along fractures and some euhedral opaques.

**BCS2-11:** Eu-subhedral orthoamphiboles (pseudomorph opx), subhedral plag and micrographic quartz-fsp.

**BCS2-12:** Eu-subhedral greenish orthoamphiboles (pseudomorph opx), subhedral plag much micrographic quartz-fsp.

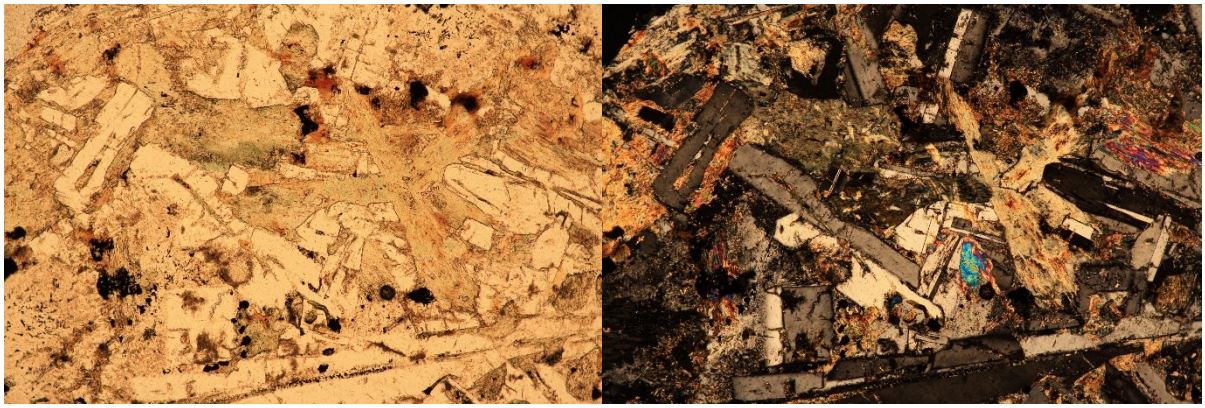

**BCS2:** Fresh euhedral plag, sub-euhedral greeninsh ortho-amphiboles. Biotite abundant.

**Basement Sills**

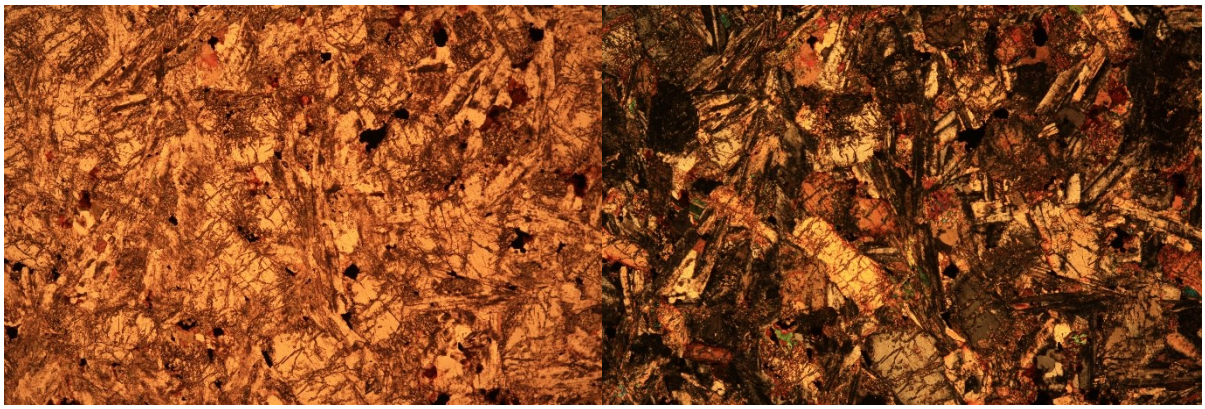

**BCS2-26:** Euhedral lath shaped opx surrounded by needle like plagioclase

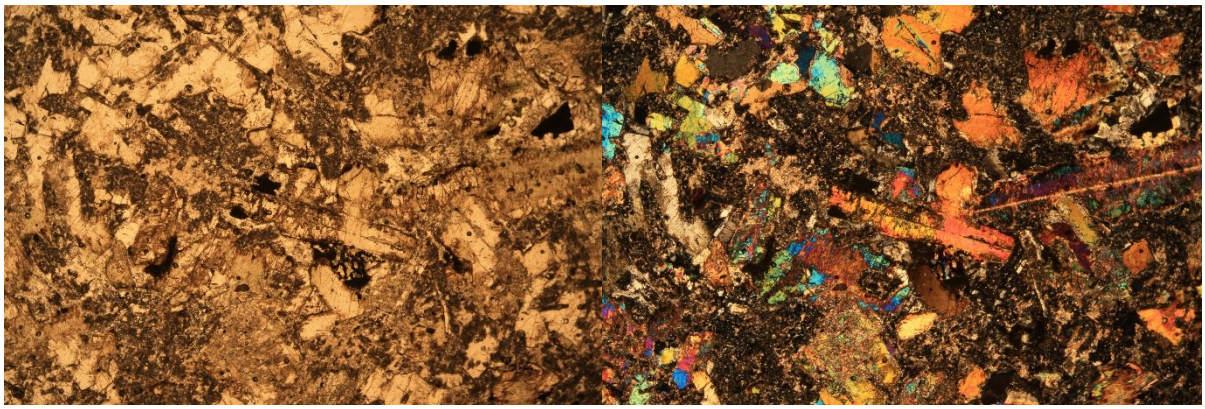

**BCS2-29:** Slightly skeletal opaques, eu-subhedral and elongated twinned amphiboles, and interstitial plagioclase

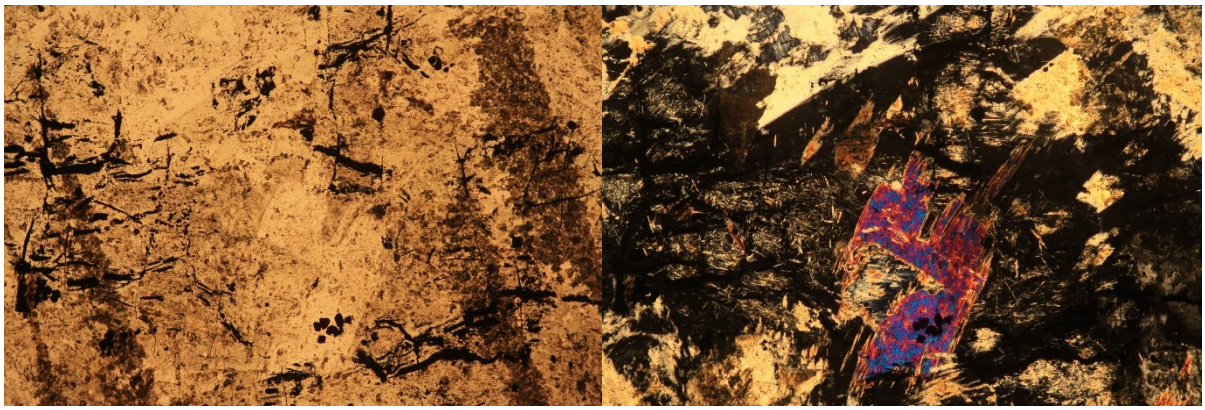

**BCS2-31:** Pseudomorph poikilitic texture like in BCS2-02. Totally serpentinsed olivines with opaque Fe-oxides strands along previous cracks.

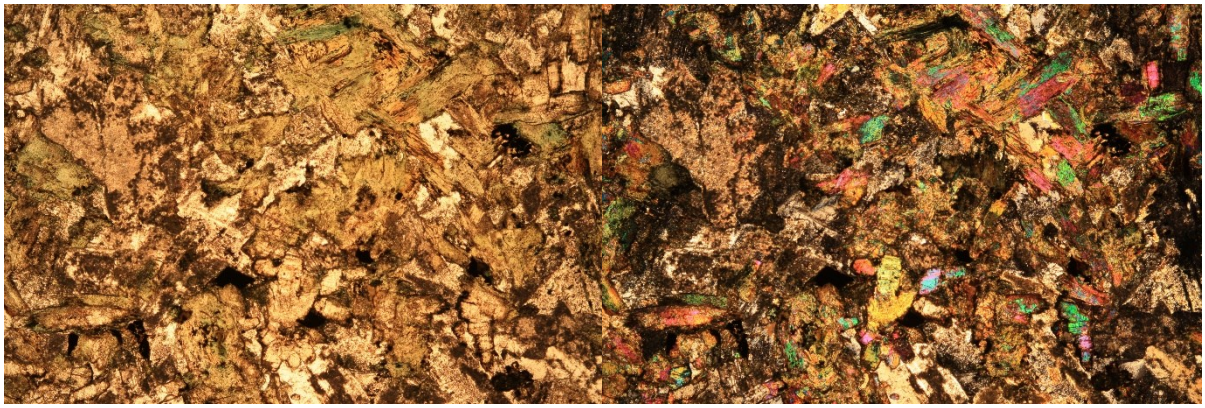

**BCS2-35:** Subheral cpx and inter plagioclase.

**Malmali (Chuniespoort)**

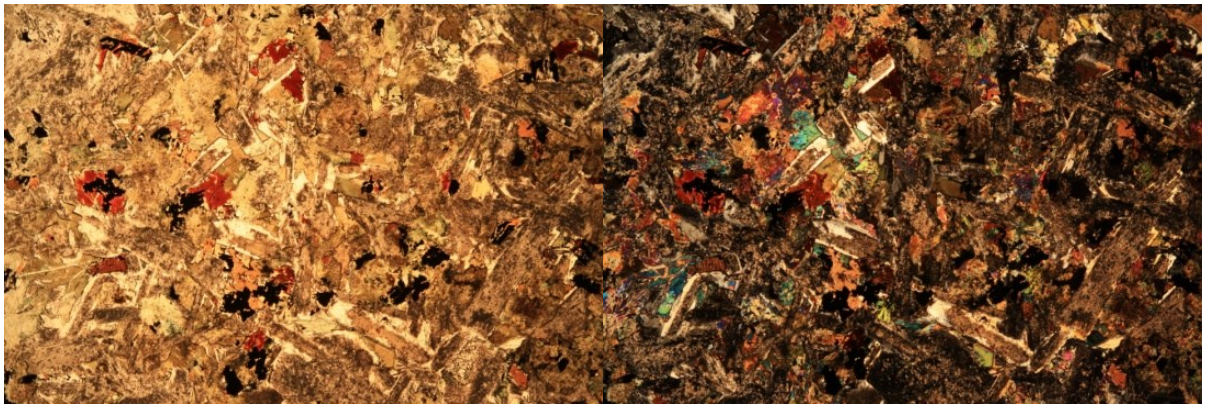

**BCS2-46:** Eu-subhedral plag with altered cores, interstitial hornblende and bio, skeletal opaques dominant.

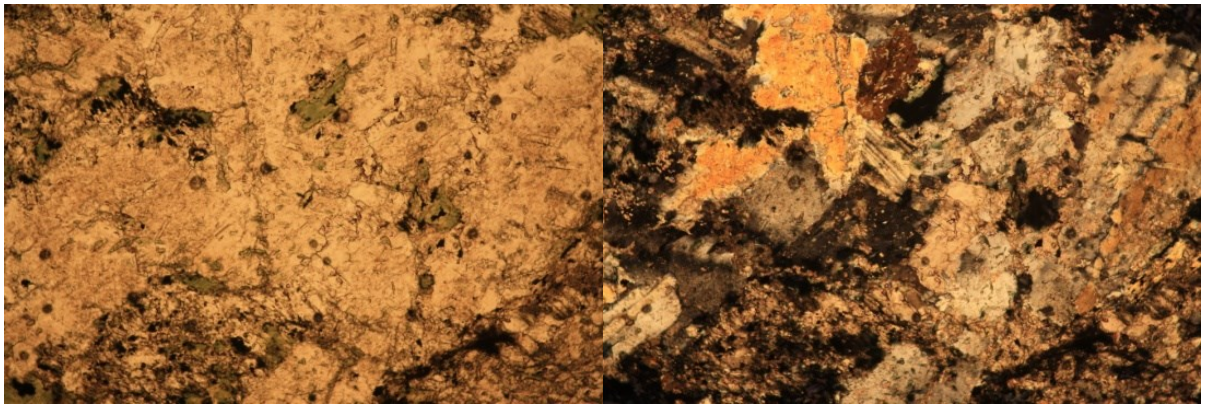

**BCS2-49:** Strongly altered greenish and isotropic (epidote?) microcrystalline matrix. Much opaques mainly concentrated in greenish alteration.

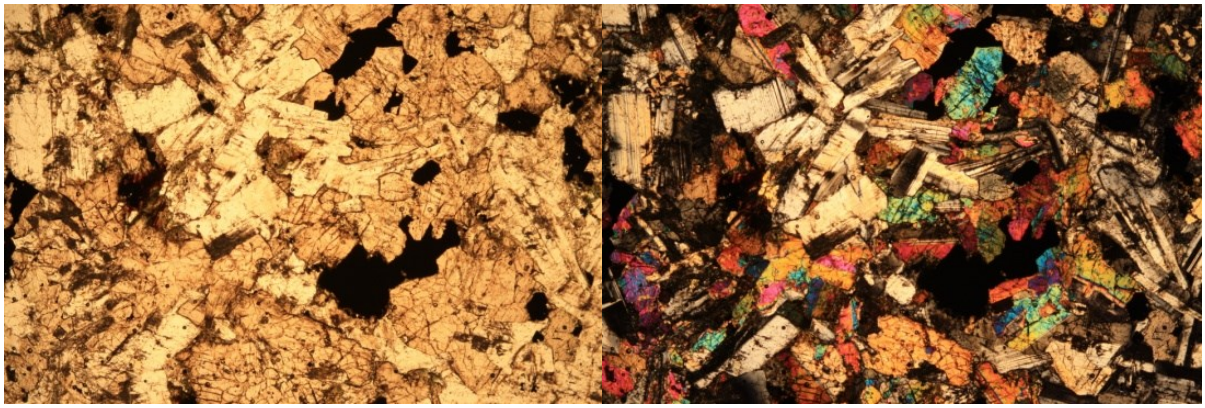

**BCS2-53:** Fresh sub-ophitic, with twinned augites around plag (much large interstitial opaques)

# APPENDIX A4

## WHOLE ROCK GEOCHEMISTRY ANALYSIS ON 85 MAFIC SILLS

| Sample ID | BCS1-01 | BCS1-02 | BCS1-03 | BCS1-04 | BCS1-05 | BCS1-06 | BCS1-07 | BCS1-08 | BCS1-09 | BCS1-10 | BCS1-11 |
|---|---|---|---|---|---|---|---|---|---|---|---|
| SiO2 | 56.999 | 56.014 | 56.312 | 58.038 | 57.177 | 53.251 | 53.795 | 54.110 | 54.540 | 54.460 | 53.494 |
| TiO2 | 0.255 | 0.274 | 0.344 | 0.619 | 0.504 | 0.495 | 0.496 | 0.590 | 0.705 | 0.554 | 0.506 |
| Al2O3 | 11.410 | 10.806 | 10.299 | 15.368 | 15.925 | 16.788 | 16.609 | 11.093 | 11.493 | 15.383 | 16.479 |
| FeO | 9.506 | 9.523 | 9.259 | 8.947 | 8.720 | 8.296 | 8.305 | 9.051 | 8.775 | 8.412 | 8.334 |
| MnO | 0.173 | 0.173 | 0.172 | 0.155 | 0.154 | 0.124 | 0.145 | 0.176 | 0.176 | 0.164 | 0.145 |
| MgO | 13.347 | 15.645 | 15.560 | 4.641 | 4.681 | 7.590 | 7.876 | 11.228 | 10.549 | 8.794 | 7.795 |
| CaO | 5.527 | 5.479 | 5.696 | 8.024 | 8.878 | 9.415 | 9.240 | 11.455 | 11.078 | 8.856 | 9.675 |
| Na2O | 1.642 | 1.250 | 1.497 | 2.548 | 2.212 | 3.052 | 2.170 | 1.697 | 1.907 | 2.288 | 2.272 |
| K2O | 1.050 | 0.783 | 0.809 | 1.516 | 1.636 | 0.918 | 1.302 | 0.528 | 0.715 | 1.026 | 1.239 |
| P2O5 | 0.092 | 0.051 | 0.051 | 0.144 | 0.113 | 0.072 | 0.062 | 0.072 | 0.062 | 0.062 | 0.062 |
| SUM | 100.000 | 100.000 | 100.000 | 100.000 | 100.000 | 100.000 | 100.000 | 100.000 | 100.000 | 100.000 | 100.000 |
| L.O.I. | 0.770 | 0.120 | 0.060 | 1.970 | 1.760 | 2.550 | 2.370 | 2.320 | 2.500 | 2.310 | 2.600 |
| Mg# | 60.940 | 64.608 | 65.125 | 36.564 | 37.360 | 50.410 | 51.306 | 57.954 | 57.188 | 53.738 | 50.964 |
| Fe# | 41.595 | 37.837 | 37.305 | 65.843 | 65.071 | 52.222 | 51.327 | 44.633 | 45.408 | 48.890 | 51.670 |
| Sc | 25 | 19 | 29 | 29 | 24 | 29 | 29 | 37 | 41 | 37 | 28 |
| V | 146 | 157 | 168 | 173 | 183 | 225 | 224 | 261 | 245 | 218 | 228 |
| Cr | 1026 | 875 | 1081 | 105 | 44 | 390 | 444 | 1146 | 1067 | 478 | 431 |
| Co | 59 | 62 | 65 | 38 | 35 | 38 | 39 | 44 | 41 | 40 | 39 |
| Ni | 323 | 290 | 310 | 59 | 72 | 128 | 132 | 165 | 151 | 152 | 131 |
| Cu | 42 | 26 | 31 | 62 | 98 | 67 | 68 | 75 | 78 | 66 | 66 |
| Zn | 79 | 63 | 68 | 87 | 69 | 64 | 68 | 81 | 78 | 66 | 66 |
| Rb | 36 | 28 | 26 | 44 | 60 | 31 | 41 | 14 | 27 | 34 | 34 |
| Sr | 186 | 148 | 137 | 263 | 266 | 92 | 81 | 75 | 85 | 74 | 82 |
| Y | 8 | 7 | 9 | 18 | 15 | 15 | 15 | 21 | 38 | 59 | 15 |
| Zr | 70 | 58 | 100 | 147 | 110 | 69 | 63 | 65 | 69 | 72 | 68 |
| Nb | 3.1 | 2.8 | 2.7 | 5.6 | 4.1 | 4.1 | 3.8 | 3.9 | 3.9 | 3.5 | 3.9 |
| Mo | | | 0.88 | 1.21 | | | | | 0.85 | 0.94 | |
| Cs | | | 0.88 | 1.08 | | | | | 0.67 | 1.24 | |
| Ba | 311 | 96 | 179 | 468 | 381 | 175 | 224 | 150 | 173 | 233 | 211 |
| La | 15.18 | 8.57 | 9.38 | 25.65 | 21.84 | 9.43 | 9.36 | 12.52 | 17.5 | 13.89 | 9.46 |
| Ce | 30.65 | 17.97 | 18.82 | 50.16 | 44.16 | 19.08 | 19.03 | 18.61 | 22.49 | 20.13 | 18.22 |
| Pr | 3.48 | 2 | 2.16 | 5.71 | 4.92 | 2.15 | 2.16 | 2.96 | 3.56 | 2.64 | 2.06 |
| Nd | 13.83 | 7.9 | 8.4 | 22.1 | 19.32 | 8.93 | 8.96 | 12.51 | 14.54 | 10.61 | 8.6 |
| Sm | 2.2 | 1.42 | 1.66 | 4.08 | 3.41 | 1.93 | 1.89 | 2.8 | 3.33 | 2.44 | 1.82 |
| Eu | 0.57 | 0.44 | 0.46 | 1.05 | 0.94 | 0.58 | 0.57 | 0.82 | 0.92 | 0.72 | 0.55 |
| Gd | 1.84 | 1.39 | 1.58 | 3.46 | 3.25 | 2.42 | 2.34 | 3.54 | 4.32 | 4.39 | 2.31 |
| Tb | 0.25 | 0.2 | 0.26 | 0.54 | 0.46 | 0.39 | 0.38 | 0.56 | 0.67 | 0.63 | 0.38 |
| Dy | 1.53 | 1.3 | 1.49 | 3.24 | 2.87 | 2.7 | 2.64 | 3.72 | 4.11 | 4 | 2.53 |
| Ho | 0.29 | 0.26 | 0.33 | 0.7 | 0.56 | 0.57 | 0.55 | 0.76 | 0.95 | 1 | 0.53 |
| Er | 0.82 | 0.75 | 0.98 | 1.88 | 1.59 | 1.71 | 1.66 | 2.21 | 2.6 | 2.74 | 1.59 |
| Tm | 0.12 | 0.11 | 0.14 | 0.28 | 0.23 | 0.25 | 0.24 | 0.31 | 0.36 | 0.34 | 0.23 |
| Yb | 0.8 | 0.73 | 1.02 | 1.83 | 1.47 | 1.62 | 1.59 | 2.01 | 2.32 | 1.91 | 1.5 |
| Lu | 0.13 | 0.11 | 0.15 | 0.27 | 0.22 | 0.25 | 0.25 | 0.31 | 0.35 | 0.31 | 0.23 |
| Hf | 1.7 | 1.38 | 1.37 | 3.19 | 2.6 | 1.7 | 1.6 | 1.65 | 1.82 | 1.95 | 1.61 |
| Ta | 0.190 | 0.170 | 0.190 | 0.360 | 0.260 | 0.280 | 0.260 | 0.250 | 0.250 | 0.270 | 0.260 |
| Pb | 10.650 | 2.760 | 2.690 | 6.630 | 13.590 | 4.650 | 4.040 | 4.120 | 5.610 | 4.020 | 3.940 |
| Th | 3.390 | 1.960 | 2.080 | 5.920 | 4.850 | 3.210 | 3.170 | 2.490 | 2.940 | 3.280 | 2.990 |
| U | 0.890 | 0.640 | 0.650 | 1.390 | 1.460 | 1.040 | 1.030 | 0.780 | 0.800 | 0.920 | 1.020 |

| Sample ID | BCS1-12 | BCS1-13 | BCS1-14 | BCS1-15 | BCS1-16 | BCS1-17 | BCS1-18 | BCS1-19 | BCS1-20 | BCS1-21 | BCS1-25 |
|---|---|---|---|---|---|---|---|---|---|---|---|
| SiO2 | 54.357 | 56.003 | 55.266 | 55.382 | 50.307 | 50.814 | 54.214 | 53.317 | 50.970 | 51.679 | 52.619 |
| TiO2 | 0.662 | 1.016 | 0.870 | 0.985 | 1.509 | 1.650 | 0.677 | 0.717 | 1.860 | 2.078 | 1.012 |
| Al2O3 | 11.300 | 9.234 | 10.414 | 11.883 | 11.884 | 11.111 | 16.630 | 15.288 | 12.376 | 14.268 | 16.752 |
| FeO | 8.567 | 11.881 | 12.007 | 12.078 | 11.885 | 12.024 | 9.348 | 11.513 | 12.474 | 12.718 | 9.139 |
| MnO | 0.176 | 0.197 | 0.195 | 0.185 | 0.185 | 0.197 | 0.188 | 0.187 | 0.197 | 0.197 | 0.134 |
| MgO | 10.731 | 8.871 | 9.503 | 7.943 | 8.621 | 8.984 | 7.700 | 7.390 | 7.783 | 5.113 | 5.553 |
| CaO | 11.279 | 10.166 | 9.093 | 8.753 | 12.346 | 11.827 | 5.898 | 6.392 | 10.495 | 8.490 | 9.486 |
| Na2O | 1.459 | 1.586 | 1.352 | 1.724 | 2.381 | 2.438 | 4.022 | 4.500 | 2.681 | 3.980 | 3.881 |
| K2O | 1.407 | 0.922 | 1.178 | 0.924 | 0.677 | 0.737 | 1.240 | 0.624 | 0.904 | 1.164 | 1.270 |
| P2O5 | 0.062 | 0.124 | 0.123 | 0.144 | 0.205 | 0.218 | 0.083 | 0.073 | 0.260 | 0.312 | 0.155 |
| SUM | 100.000 | 100.000 | 100.000 | 100.000 | 100.000 | 100.000 | 100.000 | 100.000 | 100.000 | 100.000 | 100.000 |
| L.O.I. | 2.360 | 1.510 | 1.460 | 1.420 | 1.300 | 2.100 | 2.650 | 2.300 | 1.830 | 1.680 | 1.900 |
| Mg# | 58.191 | 45.345 | 46.792 | 42.219 | 44.626 | 45.362 | 47.787 | 41.629 | 40.943 | 30.877 | 40.303 |
| Fe# | 44.393 | 57.251 | 55.820 | 60.328 | 57.960 | 57.235 | 54.833 | 60.906 | 61.578 | 71.325 | 62.204 |
| Sc | 44 | 30 | 24 | 12 | 32 | 35 | 28 | 49 | 30 | 24 | 13 |
| V | 249 | 229 | 223 | 47 | 278 | 269 | 228 | 296 | 277 | 265 | 131 |
| Cr | 1008 | 740 | 970 | 11 | 242 | 309 | 225 | 201 | 363 | 52 | 19 |
| Co | 41 | 55 | 59 | 34 | 54 | 60 | 34 | 46 | 60 | 52 | 35 |
| Ni | 149 | 183 | 186 | 4 | 195 | 255 | 104 | 124 | 232 | 84 | 120 |
| Cu | 73 | 105 | 108 | 20 | 134 | 178 | 28 | 86 | 139 | 138 | 76 |
| Zn | 65 | 94 | 105 | 74 | 109 | 99 | 73 | 83 | 110 | 216 | 70 |
| Rb | 41 | 28 | 44 | 29 | 20 | 22 | 27 | 13 | 29 | 28 | 32 |
| Sr | 70 | 114 | 145 | 177 | 282 | 251 | 162 | 151 | 308 | 297 | 436 |
| Y | 52 | 24 | 22 | 29 | 26 | 25 | 20 | 21 | 29 | 30 | 20 |
| Zr | 65 | 192 | 151 | 259 | 186 | 157 | 82 | 63 | 195 | 222 | 216 |
| Nb | 3.7 | 8.6 | 9.3 | 12.5 | 9.5 | 8.1 | 5 | 2.9 | 11 | 12.3 | 10.3 |
| Mo | 0.87 | 1.42 |  | 1.19 |  | 1.4 |  | 1.11 | 1.63 | 1.34 |  |
| Cs | 0.93 | 1.2 |  | 0.79 |  | 0.79 |  | 0.31 | 1.06 | 1.88 |  |
| Ba | 420 | 281 | 441 | 523 | 162 | 192 | 1009 | 194 | 213 | 279 | 274 |
| La | 16.62 | 22.84 | 22.15 | 48.35 | 17.66 | 17.2 | 12.66 | 8.33 | 22.45 | 26.35 | 20.25 |
| Ce | 18.74 | 43.53 | 43.93 | 92.22 | 40.68 | 38.8 | 22.99 | 15.92 | 49.91 | 57.42 | 45.52 |
| Pr | 3.21 | 5.18 | 5.01 | 10.19 | 5.17 | 5.04 | 2.86 | 1.87 | 6.47 | 7.35 | 5.38 |
| Nd | 13.34 | 20.55 | 20.58 | 38.06 | 23.99 | 21.86 | 12.51 | 7.49 | 27.19 | 30.24 | 23.2 |
| Sm | 3.27 | 4.53 | 4.04 | 7.15 | 5.38 | 5.31 | 2.43 | 2.02 | 6.41 | 6.8 | 4.74 |
| Eu | 1.01 | 1.06 | 1.1 | 1.53 | 1.63 | 1.57 | 0.61 | 0.59 | 1.9 | 2.03 | 1.49 |
| Gd | 4.88 | 4.61 | 4.42 | 6.14 | 5.93 | 5.35 | 3.29 | 2.53 | 6.11 | 6.84 | 4.72 |
| Tb | 0.81 | 0.74 | 0.67 | 0.9 | 0.84 | 0.82 | 0.53 | 0.51 | 0.98 | 1 | 0.69 |
| Dy | 5.41 | 4.44 | 4.21 | 5.55 | 5.15 | 4.71 | 3.5 | 3.37 | 5.69 | 5.94 | 4.29 |
| Ho | 1.24 | 0.91 | 0.82 | 1.09 | 0.97 | 1 | 0.72 | 0.77 | 1.14 | 1.16 | 0.8 |
| Er | 3.64 | 2.57 | 2.32 | 3.03 | 2.65 | 2.56 | 2.1 | 2.4 | 3.14 | 3.1 | 2.24 |
| Tm | 0.44 | 0.34 | 0.33 | 0.42 | 0.36 | 0.34 | 0.3 | 0.36 | 0.42 | 0.43 | 0.31 |
| Yb | 2.47 | 2.24 | 2.06 | 2.79 | 2.28 | 2.29 | 1.88 | 2.37 | 2.7 | 2.81 | 1.97 |
| Lu | 0.38 | 0.34 | 0.31 | 0.42 | 0.32 | 0.32 | 0.27 | 0.36 | 0.39 | 0.4 | 0.28 |
| Hf | 1.65 | 3.92 | 3.47 | 6.69 | 4.38 | 4.05 | 2.04 | 1.81 | 5.09 | 5.49 | 4.91 |
| Ta | 0.350 | 0.660 | 0.640 | 0.660 | 0.520 | 0.480 | 0.340 | 0.250 | 0.660 | 0.720 | 0.590 |
| Pb | 5.620 | 7.450 | 7.370 | 12.540 | 4.550 | 3.450 | 1.380 | 2.110 | 3.120 | 3.050 | 2.920 |
| Th | 2.680 | 7.020 | 7.060 | 7.830 | 1.660 | 1.630 | 3.190 | 2.650 | 2.180 | 2.580 | 2.070 |
| U | 0.780 | 2.070 | 2.210 | 1.140 | 0.490 | 0.460 | 1.000 | 0.780 | 0.560 | 0.670 | 0.660 |

| Sample ID | BCS1-26 | BCS1-27 | BCS1-28 | BCS1-29 | BCS1-30 | BCS1-31 | BCS1-32 | BCS1-33 | BCS1-34 | BCS1-35 | BCS1-36 |
|---|---|---|---|---|---|---|---|---|---|---|---|
| SiO2 | 50.439 | 51.272 | 52.608 | 52.746 | 52.071 | 56.662 | 52.272 | 56.308 | 57.927 | 57.305 | 56.102 |
| TiO2 | 1.511 | 1.740 | 0.610 | 1.074 | 1.536 | 0.252 | 1.386 | 0.507 | 0.579 | 0.535 | 0.507 |
| Al2O3 | 12.550 | 11.290 | 14.985 | 13.571 | 14.299 | 12.262 | 14.108 | 11.471 | 16.418 | 12.528 | 10.830 |
| FeO | 13.319 | 11.781 | 11.000 | 13.058 | 13.136 | 9.170 | 12.955 | 10.284 | 9.526 | 9.943 | 9.793 |
| MnO | 0.198 | 0.186 | 0.186 | 0.217 | 0.206 | 0.158 | 0.197 | 0.169 | 0.145 | 0.168 | 0.179 |
| MgO | 10.590 | 8.690 | 7.105 | 6.548 | 5.804 | 13.745 | 5.037 | 12.835 | 4.559 | 10.652 | 14.208 |
| CaO | 8.391 | 11.352 | 9.266 | 9.316 | 9.928 | 5.616 | 9.950 | 6.470 | 6.668 | 5.965 | 6.312 |
| Na2O | 1.960 | 2.621 | 3.764 | 2.510 | 2.268 | 1.556 | 3.568 | 0.994 | 1.954 | 1.531 | 0.950 |
| K2O | 0.782 | 0.849 | 0.393 | 0.868 | 0.546 | 0.494 | 0.310 | 0.888 | 2.109 | 1.290 | 1.045 |
| P2O5 | 0.261 | 0.218 | 0.083 | 0.093 | 0.206 | 0.084 | 0.217 | 0.074 | 0.114 | 0.084 | 0.074 |
| SUM | 100.000 | 100.000 | 100.000 | 100.000 | 100.000 | 100.000 | 100.000 | 100.000 | 100.000 | 100.000 | 100.000 |
| L.O.I. | 2.480 | 1.380 | 2.290 | 1.500 | 1.120 | 3.870 | 1.720 | 4.070 | 2.550 | 2.890 | 3.620 |
| Mg# | 46.907 | 45.043 | 41.782 | 35.782 | 32.929 | 62.483 | 30.167 | 58.101 | 34.716 | 54.343 | 61.716 |
| Fe# | 55.706 | 57.549 | 60.757 | 66.601 | 69.355 | 40.017 | 72.005 | 44.483 | 67.632 | 48.280 | 40.802 |
| Sc | 20 | 32 | 34 | 41 | 34 | 22 | 30 | 29 | 20 | 29 | 30 |
| V | 233 | 261 | 289 | 334 | 220 | 144 | 216 | 181 | 169 | 181 | 189 |
| Cr | 370 | 405 | 203 | 78 | 234 | 1327 | 219 | 1042 | 95 | 1082 | 1527 |
| Co | 67 | 55 | 41 | 47 | 40 | 55 | 30 | 55 | 34 | 51 | 57 |
| Ni | 416 | 254 | 113 | 76 | 103 | 384 | 66 | 277 | 68 | 225 | 319 |
| Cu | 132 | 187 | 79 | 157 | 178 | 38 | 129 | 58 | 70 | 48 | 62 |
| Zn | 122 | 98 | 76 | 108 | 123 | 77 | 129 | 82 | 76 | 88 | 87 |
| Rb | 29 | 25 | 8 | 30 | 15 | 32 | 7 | 38 | 86 | 57 | 57 |
| Sr | 298 | 272 | 142 | 151 | 94 | 160 | 77 | 67 | 130 | 106 | 50 |
| Y | 26 | 26 | 18 | 23 | 39 | 8 | 38 | 14 | 22 | 15 | 15 |
| Zr | 212 | 166 | 68 | 56 | 126 | 70 | 135 | 71 | 130 | 84 | 67 |
| Nb | 11.3 | 8.8 | 3.2 | 2.4 | 5.8 | 3.3 | 6.4 | 4.4 | 8 | 5.4 | 4.2 |
| Mo |  | 0.86 |  | 1.58 | 0.95 |  |  | 1.18 |  | 1.39 | 1.1 |
| Cs |  | 0.79 |  | 0.69 | 1.44 |  |  | 3.38 |  | 9.16 | 12.12 |
| Ba | 195 | 191 | 78 | 127 | 113 | 149 | 31 | 216 | 376 | 248 | 157 |
| La | 22.1 | 18.53 | 7.54 | 3.5 | 10.99 | 13.44 | 11.43 | 13.69 | 22.42 | 17.14 | 13.7 |
| Ce | 50.15 | 41.48 | 16.07 | 8.89 | 24.79 | 28.07 | 25 | 26.36 | 45.32 | 32.95 | 26.41 |
| Pr | 6.21 | 5.39 | 1.83 | 1.32 | 3.3 | 2.97 | 3.5 | 2.95 | 4.72 | 3.56 | 2.94 |
| Nd | 27.45 | 23.32 | 8.1 | 6.59 | 15.16 | 12.03 | 17.2 | 10.9 | 18.82 | 13.83 | 11.45 |
| Sm | 5.86 | 5.58 | 1.96 | 2.31 | 4.83 | 2.04 | 4.75 | 2.3 | 3.42 | 2.75 | 2.36 |
| Eu | 1.9 | 1.64 | 0.58 | 0.86 | 1.34 | 0.52 | 1.34 | 0.56 | 0.85 | 0.68 | 0.62 |
| Gd | 6.03 | 5.59 | 2.65 | 3.2 | 6.01 | 1.76 | 6.32 | 2.41 | 3.58 | 2.72 | 2.27 |
| Tb | 0.87 | 0.88 | 0.46 | 0.59 | 1 | 0.24 | 1.04 | 0.39 | 0.54 | 0.41 | 0.42 |
| Dy | 5.34 | 5.17 | 3.28 | 3.93 | 6.97 | 1.5 | 6.98 | 2.47 | 3.52 | 2.6 | 2.56 |
| Ho | 1 | 1 | 0.71 | 0.85 | 1.53 | 0.29 | 1.46 | 0.55 | 0.71 | 0.55 | 0.53 |
| Er | 2.76 | 2.91 | 2.18 | 2.52 | 4.22 | 0.83 | 4.29 | 1.64 | 2.07 | 1.68 | 1.57 |
| Tm | 0.37 | 0.38 | 0.32 | 0.34 | 0.62 | 0.12 | 0.6 | 0.22 | 0.3 | 0.25 | 0.22 |
| Yb | 2.38 | 2.49 | 2.12 | 2.49 | 4.31 | 0.79 | 3.96 | 1.53 | 1.95 | 1.62 | 1.49 |
| Lu | 0.34 | 0.36 | 0.32 | 0.37 | 0.62 | 0.12 | 0.57 | 0.23 | 0.28 | 0.24 | 0.25 |
| Hf | 4.83 | 4.45 | 1.78 | 1.61 | 3.56 | 1.71 | 3.46 | 1.99 | 3.16 | 2.4 | 1.92 |
| Ta | 0.630 | 0.550 | 0.230 | 0.150 | 0.380 | 0.220 | 0.400 | 0.430 | 0.790 | 0.610 | 0.450 |
| Pb | 2.910 | 3.990 | 2.530 | 3.860 | 2.530 | 8.990 | 6.000 | 6.930 | 15.220 | 8.010 | 5.130 |
| Th | 2.270 | 1.830 | 2.510 | 0.480 | 2.580 | 3.310 | 2.630 | 6.030 | 9.470 | 7.530 | 5.650 |
| U | 0.600 | 0.440 | 0.840 | 0.140 | 0.700 | 1.020 | 0.750 | 1.910 | 3.840 | 2.760 | 2.280 |

| Sample ID | BCS1-37 | BCS1-38 | BCS1-39 | BCS2-01 | BCS2-02 | BCS2-03 | BCS2-04 | BCS2-05 | BCS2-06 | BCS2-07 | BCS2-08 |
|---|---|---|---|---|---|---|---|---|---|---|---|
| SiO2 | 57.367 | 57.577 | 49.549 | 55.974 | 45.973 | 46.431 | 55.962 | 54.693 | 56.016 | 52.458 | 51.989 |
| TiO2 | 0.453 | 0.513 | 2.246 | 0.686 | 0.402 | 0.474 | 0.536 | 0.482 | 0.593 | 0.326 | 0.347 |
| Al2O3 | 12.882 | 12.862 | 14.410 | 15.192 | 6.947 | 6.975 | 15.911 | 16.081 | 15.402 | 9.547 | 9.306 |
| FeO | 10.218 | 9.868 | 14.252 | 7.393 | 11.903 | 12.078 | 9.239 | 9.321 | 9.951 | 9.711 | 9.696 |
| MnO | 0.168 | 0.168 | 0.241 | 0.143 | 0.201 | 0.190 | 0.196 | 0.195 | 0.245 | 0.173 | 0.184 |
| MgO | 10.451 | 10.013 | 5.552 | 6.946 | 28.199 | 27.225 | 6.282 | 6.389 | 5.580 | 20.349 | 21.142 |
| CaO | 5.799 | 6.117 | 8.522 | 10.090 | 5.287 | 5.436 | 8.785 | 9.609 | 8.922 | 5.579 | 5.510 |
| Na2O | 1.463 | 1.519 | 3.936 | 2.192 | 0.814 | 0.853 | 1.926 | 1.938 | 2.024 | 1.204 | 1.153 |
| K2O | 1.105 | 1.278 | 0.945 | 1.352 | 0.233 | 0.284 | 1.071 | 1.210 | 1.165 | 0.602 | 0.602 |
| P2O5 | 0.095 | 0.084 | 0.346 | 0.031 | 0.042 | 0.053 | 0.093 | 0.082 | 0.102 | 0.051 | 0.071 |
| SUM | 100.000 | 100.000 | 100.000 | 100.000 | 100.000 | 100.000 | 100.000 | 100.000 | 100.000 | 100.000 | 100.000 |
| L.O.I. | 3.340 | 2.900 | 1.760 | 1.180 | 4.090 | 4.020 | 1.490 | 0.670 | 0.330 | 0.390 | 0.140 |
| Mg# | 53.191 | 52.996 | 30.210 | 51.073 | 72.470 | 71.465 | 43.036 | 43.235 | 38.389 | 69.955 | 70.784 |
| Fe# | 49.438 | 49.635 | 71.964 | 51.560 | 29.681 | 30.731 | 59.526 | 59.330 | 64.070 | 32.305 | 31.442 |
| Sc | 22 | 29 | 21 | 34 | 20 | 22 | 36 | 38 | 37 | 28 | 27 |
| V | 185 | 187 | 272 | 243 | 128 | 147 | 191 | 205 | 206 | 161 | 158 |
| Cr | 1043 | 1040 | 14 | 170 | 3413 | 3198 | 154 | 115 | 99 | 2616 | 2746 |
| Co | 50 | 51 | 57 | 116 | 141 | 130 | 90 | 105 | 89 | 149 | 148 |
| Ni | 214 | 225 | 109 | 68 | 739 | 700 | 128 | 125 | 112 | 799 | 960 |
| Cu | 56 | 60 | 81 | 78 | 39 | 51 | 53 | 62 | 70 | 41 | 34 |
| Zn | 81 | 91 | 133 | 52 | 78 | 80 | 83 | 81 | 82 | 74 | 68 |
| Rb | 49 | 61 | 21 | 60 | 7 | 10 | 42 | 43 | 45 | 21 | 24 |
| Sr | 107 | 121 | 319 | 206 | 76 | 82 | 195 | 181 | 194 | 123 | 135 |
| Y | 20 | 16 | 46 | 11 | 7 | 9 | 16 | 13 | 17 | 9 | 8 |
| Zr | 93 | 93 | 253 | 57 | 31 | 40 | 85 | 69 | 98 | 45 | 45 |
| Nb | 5.9 | 6 | 13.6 | 3.4 | 1.5 | 2.1 | 4.3 | 3.6 | 5 | 2.3 | 2.1 |
| Mo |  | 1.52 | 0.98 | 0.59 | 0.47 | 0.57 | 0.69 | 1 | 1.22 | 0.74 | 0.89 |
| Cs |  | 8.3 | 0.88 | 3.94 | 0.31 | 0.55 | 3.6 | 4.3 | 4.18 | 2.17 | 3.16 |
| Ba | 213 | 291 | 754 | 335 | 82 | 101 | 195 | 266 | 278 | 172 | 174 |
| La | 16.27 | 19.06 | 28.33 | 10.37 | 4.42 | 5.73 | 18.73 | 15 | 21.76 | 9.37 | 9.76 |
| Ce | 32.27 | 36.4 | 59.23 | 20.63 | 9.58 | 12.22 | 36.89 | 30.24 | 41.85 | 18.82 | 19.6 |
| Pr | 3.4 | 4.12 | 8.29 | 2.33 | 1.2 | 1.5 | 4.27 | 3.51 | 4.86 | 2.23 | 2.27 |
| Nd | 13.81 | 14.81 | 36.9 | 9.58 | 4.98 | 6.49 | 15.65 | 13.32 | 19.23 | 8.43 | 8.47 |
| Sm | 2.54 | 3.14 | 8.39 | 2.02 | 0.94 | 1.69 | 3.5 | 2.52 | 3.68 | 1.98 | 1.78 |
| Eu | 0.62 | 0.75 | 2.67 | 0.54 | 0.42 | 0.44 | 0.82 | 0.81 | 0.87 | 0.49 | 0.46 |
| Gd | 2.7 | 3.08 | 8.84 | 1.7 | 1.42 | 1.5 | 3.13 | 2.61 | 3.33 | 1.5 | 1.66 |
| Tb | 0.41 | 0.47 | 1.32 | 0.29 | 0.13 | 0.27 | 0.4 | 0.42 | 0.53 | 0.27 | 0.27 |
| Dy | 2.7 | 2.92 | 7.66 | 1.88 | 1.32 | 1.84 | 2.81 | 2.5 | 3.26 | 1.64 | 1.6 |
| Ho | 0.56 | 0.63 | 1.52 | 0.42 | 0.29 | 0.39 | 0.62 | 0.52 | 0.59 | 0.34 | 0.31 |
| Er | 1.62 | 1.75 | 4.25 | 1.39 | 0.72 | 1.15 | 1.7 | 1.55 | 1.85 | 0.94 | 0.86 |
| Tm | 0.23 | 0.26 | 0.56 | 0.2 | 0.11 | 0.16 | 0.26 | 0.2 | 0.27 | 0.16 | 0.12 |
| Yb | 1.46 | 1.83 | 3.68 | 1.37 | 0.76 | 1.01 | 1.52 | 1.52 | 1.77 | 1.08 | 0.79 |
| Lu | 0.22 | 0.27 | 0.51 | 0.19 | 0.12 | 0.14 | 0.22 | 0.24 | 0.32 | 0.11 | 0.11 |
| Hf | 2.41 | 2.86 | 6.36 | 1.74 | 1.03 | 1.04 | 2.28 | 2.01 | 2.55 | 1.33 | 1.28 |
| Ta | 0.580 | 0.680 | 0.800 | 0.330 | 0.120 | 0.130 | 0.340 | 0.260 | 0.430 | 0.160 | 0.160 |
| Pb | 7.180 | 10.510 | 7.820 | 4.700 | 1.790 | 2.020 | 7.620 | 4.590 | 9.000 | 4.030 | 4.010 |
| Th | 6.810 | 8.580 | 2.630 | 3.970 | 1.050 | 1.100 | 4.520 | 3.810 | 5.220 | 2.160 | 2.390 |
| U | 2.780 | 3.070 | 0.680 | 1.020 | 0.170 | 0.170 | 1.050 | 0.850 | 1.310 | 0.490 | 0.530 |

| Sample ID | BCS2-09 | BCS2-10 | BCS2-11 | BCS2-12 | BCS2-13 | BCS2-14 | BCS2-15 | BCS2-16 | BCS2-17 | BCS2-18 | BCS2-19 |
|---|---|---|---|---|---|---|---|---|---|---|---|
| SiO2 | 50.226 | 55.869 | 56.096 | 56.436 | 59.303 | 60.221 | 57.609 | 58.079 | 55.734 | 56.142 | 56.947 |
| TiO2 | 0.267 | 0.445 | 0.435 | 0.495 | 0.420 | 0.423 | 0.347 | 0.409 | 0.409 | 0.534 | 0.570 |
| Al2O3 | 7.489 | 14.045 | 15.228 | 14.999 | 15.028 | 15.272 | 11.273 | 14.000 | 11.576 | 15.554 | 13.037 |
| FeO | 9.975 | 9.889 | 9.396 | 10.090 | 8.284 | 7.954 | 9.298 | 9.182 | 9.690 | 9.334 | 9.165 |
| MnO | 0.164 | 0.197 | 0.176 | 0.206 | 0.154 | 0.165 | 0.184 | 0.215 | 0.174 | 0.174 | 0.163 |
| MgO | 26.074 | 8.193 | 7.003 | 5.116 | 5.095 | 4.616 | 12.641 | 7.410 | 12.998 | 5.940 | 7.833 |
| CaO | 4.459 | 8.131 | 8.205 | 9.109 | 7.565 | 6.908 | 5.881 | 6.918 | 6.821 | 9.039 | 8.770 |
| Na2O | 0.863 | 1.999 | 2.155 | 2.300 | 2.327 | 2.509 | 1.583 | 2.385 | 1.534 | 2.114 | 2.108 |
| K2O | 0.431 | 1.160 | 1.222 | 1.155 | 1.712 | 1.817 | 1.123 | 1.310 | 0.982 | 1.057 | 1.314 |
| P2O5 | 0.051 | 0.073 | 0.083 | 0.093 | 0.113 | 0.114 | 0.061 | 0.092 | 0.082 | 0.113 | 0.092 |
| SUM | 100.000 | 100.000 | 100.000 | 100.000 | 100.000 | 100.000 | 100.000 | 100.000 | 100.000 | 100.000 | 100.000 |
| L.O.I. | 0.920 | 1.930 | 2.000 | 1.490 | 0.740 | 1.530 | 0.460 | 0.620 | 0.700 | 0.870 | 0.530 |
| Mg# | 74.388 | 47.932 | 45.298 | 36.038 | 40.596 | 39.202 | 60.168 | 47.276 | 59.846 | 41.423 | 48.706 |
| Fe# | 27.670 | 54.690 | 57.298 | 66.353 | 61.918 | 63.278 | 42.382 | 55.340 | 42.710 | 61.108 | 53.920 |
| Sc | 24 | 36 | 34 | 38 | 31 | 29 | 31 | 31 | 31 | 36 | 35 |
| V | 136 | 215 | 206 | 232 | 190 | 176 | 171 | 179 | 184 | 205 | 212 |
| Cr | 3736 | 409 | 239 | 58 | 113 | 84 | 1033 | 363 | 1119 | 151 | 405 |
| Co | 130 | 72 | 82 | 82 | 84 | 68 | 107 | 74 | 108 | 94 | 87 |
| Ni | 1231 | 184 | 146 | 97 | 95 | 79 | 261 | 143 | 335 | 107 | 133 |
| Cu | 36 | 61 | 64 | 70 | 48 | 54 | 47 | 63 | 53 | 57 | 63 |
| Zn | 69 | 88 | 72 | 83 | 78 | 79 | 71 | 78 | 79 | 92 | 75 |
| Rb | 15 | 55 | 62 | 45 | 62 | 66 | 37 | 44 | 34 | 35 | 48 |
| Sr | 103 | 242 | 281 | 232 | 285 | 280 | 166 | 268 | 180 | 212 | 188 |
| Y | 6 | 12 | 12 | 14 | 13 | 14 | 11 | 12 | 11 | 15 | 14 |
| Zr | 36 | 65 | 68 | 80 | 99 | 106 | 69 | 79 | 62 | 88 | 79 |
| Nb | 1.7 | 2.9 | 3 | 3.6 | 5.2 | 5.2 | 3.5 | 3.5 | 2.7 | 4.4 | 4.1 |
| Mo | 0.65 | 0.75 | 0.95 | 0.96 | 1.65 | 1.13 | 1.02 | 1.15 | 0.65 | 0.84 | 1.55 |
| Cs | 1.01 | 3.72 | 1.9 | 2.2 | 4.06 | 4.34 | 2.17 | 3.58 | 2.18 | 2.03 | 2.78 |
| Ba | 139 | 261 | 303 | 415 | 532 | 515 | 320 | 413 | 264 | 315 | 266 |
| La | 8.15 | 12.96 | 13.93 | 15.53 | 26.01 | 26.66 | 16.86 | 18.06 | 13.09 | 19.03 | 14.06 |
| Ce | 15.76 | 26.57 | 27.93 | 31.38 | 49.91 | 52.12 | 32.42 | 36.29 | 26.07 | 38.13 | 28.77 |
| Pr | 1.76 | 3.01 | 3.17 | 3.63 | 5.58 | 5.74 | 3.57 | 4.1 | 3.06 | 4.11 | 3.21 |
| Nd | 6.92 | 11.42 | 11.92 | 14.56 | 20.51 | 21.88 | 13.51 | 15.76 | 12.07 | 17.34 | 12.16 |
| Sm | 1.73 | 2.61 | 2.41 | 3.05 | 3.56 | 3.85 | 2.9 | 2.99 | 2.53 | 3.05 | 2.61 |
| Eu | 0.37 | 0.71 | 0.68 | 0.76 | 1.01 | 0.93 | 0.7 | 0.91 | 0.62 | 0.83 | 0.8 |
| Gd | 1.38 | 2.22 | 2.33 | 2.83 | 3.27 | 3.15 | 2.1 | 2.96 | 2.03 | 3.08 | 2.74 |
| Tb | 0.2 | 0.37 | 0.32 | 0.41 | 0.42 | 0.5 | 0.32 | 0.36 | 0.32 | 0.41 | 0.43 |
| Dy | 1.32 | 2.2 | 2.18 | 2.73 | 2.33 | 2.5 | 2.01 | 2.29 | 2.03 | 2.97 | 2.51 |
| Ho | 0.19 | 0.43 | 0.48 | 0.52 | 0.46 | 0.43 | 0.41 | 0.44 | 0.41 | 0.62 | 0.53 |
| Er | 0.7 | 1.32 | 1.26 | 1.54 | 1.37 | 1.48 | 0.96 | 1.4 | 1.18 | 1.94 | 1.51 |
| Tm | 0.08 | 0.2 | 0.21 | 0.21 | 0.21 | 0.24 | 0.15 | 0.23 | 0.17 | 0.27 | 0.22 |
| Yb | 0.71 | 1.24 | 1.39 | 1.64 | 1.27 | 1.29 | 1.11 | 1.13 | 1.2 | 1.83 | 1.6 |
| Lu | 0.1 | 0.2 | 0.21 | 0.26 | 0.18 | 0.23 | 0.2 | 0.17 | 0.21 | 0.3 | 0.23 |
| Hf | 1 | 1.8 | 1.93 | 2.36 | 2.73 | 2.99 | 1.88 | 2.33 | 1.68 | 2.75 | 2.06 |
| Ta | 0.110 | 0.220 | 0.220 | 0.220 | 0.380 | 0.380 | 0.220 | 0.260 | 0.150 | 0.320 | 0.270 |
| Pb | 3.160 | 4.840 | 5.540 | 7.680 | 6.360 | 12.100 | 7.550 | 7.500 | 6.810 | 9.170 | 8.090 |
| Th | 1.760 | 3.390 | 3.320 | 4.260 | 5.680 | 6.390 | 3.790 | 4.360 | 2.940 | 4.430 | 3.350 |
| U | 0.380 | 0.740 | 0.830 | 0.940 | 1.590 | 1.690 | 1.250 | 1.130 | 0.780 | 1.070 | 1.060 |

| Sample ID | BCS2-20 | BCS2-21 | BCS2-22 | BCS2-23 | BCS2-24 | BCS2-25 | BCS2-26 | BCS2-29 | BCS2-30 | BCS2-31 |
|---|---|---|---|---|---|---|---|---|---|---|
| SiO2 | 55.456 | 55.808 | 57.898 | 58.646 | 57.242 | 55.506 | 50.378 | 52.479 | 56.265 | 45.922 |
| TiO2 | 0.389 | 0.389 | 0.463 | 0.474 | 0.317 | 0.367 | 2.098 | 0.362 | 0.861 | 0.229 |
| Al2O3 | 11.261 | 10.938 | 15.655 | 15.422 | 12.615 | 10.376 | 13.835 | 15.848 | 14.883 | 7.392 |
| FeO | 9.830 | 9.861 | 8.932 | 8.645 | 9.366 | 9.639 | 13.299 | 8.117 | 9.883 | 12.234 |
| MnO | 0.205 | 0.205 | 0.175 | 0.144 | 0.174 | 0.183 | 0.241 | 0.176 | 0.176 | 0.153 |
| MgO | 13.532 | 13.857 | 5.112 | 4.763 | 10.419 | 15.488 | 6.230 | 8.317 | 5.092 | 27.954 |
| CaO | 6.802 | 6.586 | 7.447 | 7.927 | 6.905 | 6.211 | 9.262 | 11.483 | 8.390 | 6.073 |
| Na2O | 1.555 | 1.526 | 2.139 | 2.268 | 1.757 | 1.364 | 3.724 | 2.038 | 2.945 | -0.033 |
| K2O | 0.900 | 0.758 | 2.098 | 1.618 | 1.124 | 0.794 | 0.619 | 1.138 | 1.338 | 0.044 |
| P2O5 | 0.072 | 0.072 | 0.082 | 0.093 | 0.082 | 0.071 | 0.315 | 0.041 | 0.166 | 0.033 |
| SUM | 100.000 | 100.000 | 100.000 | 100.000 | 100.000 | 100.000 | 100.000 | 100.000 | 100.000 | 100.000 |
| L.O.I. | 0.730 | 0.210 | 1.650 | 1.910 | 0.620 | 0.510 | 2.850 | 2.070 | 1.780 | 6.840 |
| Mg# | 60.468 | 60.958 | 38.873 | 37.969 | 55.277 | 64.097 | 34.234 | 53.238 | 36.407 | 71.742 |
| Fe# | 42.076 | 41.576 | 63.599 | 64.480 | 47.340 | 38.362 | 68.097 | 49.392 | 65.996 | 30.442 |
| Sc | 31 | 31 | 30 | 29 | 34 | 30 | 25 | 43 | 27 | 24 |
| V | 180 | 176 | 203 | 195 | 181 | 169 | 275 | 194 | 191 | 120 |
| Cr | 1189 | 1232 | 62 | 55 | 719 | 1578 | 68 | 370 | 111 | 3428 |
| Co | 102 | 99 | 83 | 63 | 100 | 107 | 79 | 80 | 78 | 116 |
| Ni | 357 | 365 | 92 | 81 | 195 | 416 | 155 | 120 | 100 | 1405 |
| Cu | 53 | 50 | 77 | 70 | 44 | 46 | 125 | 50 | 92 | 26 |
| Zn | 73 | 83 | 73 | 79 | 80 | 76 | 138 | 80 | 92 | 154 |
| Rb | 28 | 25 | 86 | 59 | 38 | 27 | 9 | 57 | 34 | 4 |
| Sr | 166 | 163 | 283 | 266 | 207 | 156 | 465 | 170 | 296 | 6 |
| Y | 11 | 11 | 15 | 15 | 9 | 10 | 46 | 16 | 19 | 11 |
| Zr | 59 | 59 | 98 | 101 | 69 | 58 | 234 | 40 | 119 | 23 |
| Nb | 2.5 | 2.5 | 4.7 | 5.1 | 3.2 | 2.4 | 13.2 | 1.8 | 4.2 | 1.2 |
| Mo | 0.83 | 0.93 | 1.12 | 0.99 | 0.96 | 1.09 | 1.59 | 0.56 | 0.79 | 0.69 |
| Cs | 1.79 | 1.6 | 3.6 | 2.46 | 2.23 | 1.78 | 0.35 | 1.1 | 0.77 | 1.15 |
| Ba | 252 | 261 | 477 | 505 | 333 | 242 | 282 | 159 | 335 | 34 |
| La | 12.33 | 12.65 | 23.36 | 25.82 | 17.85 | 11.94 | 36.8 | 6.98 | 18.17 | 3.15 |
| Ce | 24.93 | 24.31 | 45.56 | 49.84 | 35.57 | 23.07 | 61.63 | 13.72 | 37.15 | 5.65 |
| Pr | 2.83 | 2.77 | 5.16 | 5.47 | 4.17 | 2.67 | 9.13 | 1.67 | 4.47 | 0.92 |
| Nd | 10.51 | 11.32 | 20 | 21.32 | 16.25 | 10.07 | 39.23 | 6.19 | 17.03 | 3.6 |
| Sm | 2.08 | 2.39 | 3.4 | 4.15 | 3.22 | 2.19 | 8.91 | 1.55 | 4.16 | 0.9 |
| Eu | 0.67 | 0.59 | 0.95 | 1.09 | 0.75 | 0.51 | 2.53 | 0.57 | 1.17 | 0.16 |
| Gd | 2.1 | 1.67 | 3.14 | 3.35 | 2.06 | 1.91 | 9.57 | 1.71 | 3.68 | 1.25 |
| Tb | 0.31 | 0.31 | 0.43 | 0.56 | 0.34 | 0.29 | 1.47 | 0.32 | 0.7 | 0.26 |
| Dy | 1.92 | 1.89 | 2.58 | 2.86 | 1.89 | 1.82 | 8.55 | 2.32 | 3.66 | 1.96 |
| Ho | 0.36 | 0.39 | 0.56 | 0.55 | 0.33 | 0.36 | 1.76 | 0.61 | 0.71 | 0.38 |
| Er | 1.25 | 1.29 | 1.63 | 1.61 | 1.07 | 1.15 | 4.57 | 1.79 | 2.13 | 1.22 |
| Tm | 0.21 | 0.15 | 0.22 | 0.25 | 0.15 | 0.16 | 0.59 | 0.28 | 0.29 | 0.19 |
| Yb | 1.21 | 1.08 | 1.4 | 1.97 | 0.92 | 1.15 | 3.61 | 1.95 | 2 | 1.61 |
| Lu | 0.18 | 0.18 | 0.24 | 0.28 | 0.16 | 0.19 | 0.58 | 0.31 | 0.28 | 0.19 |
| Hf | 1.63 | 1.57 | 2.41 | 3 | 1.76 | 1.56 | 6.19 | 1.14 | 3.2 | 0.66 |
| Ta | 0.200 | 0.170 | 0.330 | 0.340 | 0.230 | 0.180 | 0.750 | 0.100 | 0.230 | 0.080 |
| Pb | 5.760 | 6.390 | 11.160 | 11.370 | 8.620 | 6.070 | 2.490 | 3.050 | 4.710 | 0.640 |
| Th | 2.850 | 2.850 | 5.700 | 6.060 | 3.590 | 2.810 | 2.530 | 1.260 | 2.390 | 0.620 |
| U | 0.820 | 0.760 | 1.920 | 1.880 | 0.920 | 0.780 | 0.610 | 0.190 | 0.480 | 0.120 |

| Sample ID | BCS2-32 | BCS2-33 | BCS2-34 | BCS2-35 | BCS2-36 | BCS2-37 | BCS2-38 | BCS2-40 | BCS2-41 | BCS2-42 |
|---|---|---|---|---|---|---|---|---|---|---|
| SiO2 | 57.919 | 57.827 | 57.985 | 55.850 | 58.242 | 50.355 | 50.389 | 49.043 | 55.141 | 55.770 |
| TiO2 | 0.486 | 0.866 | 0.792 | 0.734 | 0.798 | 1.545 | 2.321 | 1.528 | 1.159 | 0.390 |
| Al2O3 | 15.361 | 15.003 | 14.972 | 11.776 | 14.540 | 13.925 | 14.262 | 9.730 | 10.460 | 11.651 |
| FeO | 7.172 | 8.530 | 8.778 | 12.238 | 8.440 | 14.323 | 14.029 | 12.777 | 11.912 | 10.257 |
| MnO | 0.145 | 0.165 | 0.144 | 0.255 | 0.145 | 0.234 | 0.240 | 0.249 | 0.198 | 0.190 |
| MgO | 5.727 | 4.482 | 4.857 | 6.219 | 5.886 | 6.749 | 5.176 | 11.996 | 10.304 | 13.821 |
| CaO | 8.528 | 8.120 | 7.162 | 9.064 | 6.861 | 10.266 | 8.951 | 12.328 | 7.746 | 6.921 |
| Na2O | 2.812 | 3.163 | 3.879 | 2.743 | 3.182 | 2.155 | 3.586 | 1.788 | 2.787 | 0.885 |
| K2O | 1.716 | 1.659 | 1.286 | 1.030 | 1.741 | 0.305 | 0.711 | 0.374 | 0.157 | 0.053 |
| P2O5 | 0.134 | 0.185 | 0.144 | 0.092 | 0.166 | 0.142 | 0.335 | 0.187 | 0.136 | 0.063 |
| SUM | 100.000 | 100.000 | 100.000 | 100.000 | 100.000 | 100.000 | 100.000 | 100.000 | 100.000 | 100.000 |
| L.O.I. | 1.940 | 1.390 | 1.410 | 0.330 | 1.960 | -0.190 | 1.980 | 1.670 | 2.400 | 4.070 |
| Mg# | 47.013 | 36.862 | 38.072 | 36.087 | 43.661 | 34.364 | 29.075 | 51.056 | 49.009 | 59.956 |
| Fe# | 55.601 | 65.554 | 64.379 | 66.306 | 58.911 | 67.972 | 73.049 | 51.578 | 53.619 | 42.598 |
| Sc | 29 | 23 | 24 | 27 | 25 | 43 | 23 | 37 | 26 | 33 |
| V | 155 | 175 | 180 | 204 | 171 | 367 | 297 | 272 | 203 | 191 |
| Cr | 242 | 148 | 80 | 123 | 191 | 139 | 25 | 680 | 1037 | 1331 |
| Co | 76 | 74 | 74 | 102 | 64 | 92 | 86 | 99 | 93 | 75 |
| Ni | 122 | 127 | 107 | 159 | 121 | 106 | 96 | 455 | 362 | 293 |
| Cu | 49 | 86 | 51 | 155 | 79 | 175 | 94 | 167 | 138 | 65 |
| Zn | 86 | 134 | 72 | 103 | 119 | 125 | 132 | 160 | 114 | 72 |
| Rb | 52 | 53 | 40 | 29 | 54 | 9 | 22 | 10 | 17 | 2 |
| Sr | 385 | 390 | 382 | 208 | 446 | 143 | 459 | 247 | 342 | 94 |
| Y | 27 | 28 | 18 | 26 | 26 | 29 | 42 | 66 | 20 | 11 |
| Zr | 129 | 144 | 115 | 114 | 141 | 92 | 256 | 129 | 104 | 47 |
| Nb | 8.1 | 4.9 | 4.5 | 6.5 | 7.2 | 4.3 | 13.2 | 6.7 | 9.8 | 2.3 |
| Mo | 0.78 | 1.18 | 0.64 | 1.13 | 0.92 | 0.65 | 1.23 | 0.88 | 0.87 | 0.75 |
| Cs | 0.57 | 0.74 | 0.84 | 0.96 | 3.16 | 1.89 | 2.58 | 2.54 | 8.5 | 1.32 |
| Ba | 361 | 435 | 413 | 289 | 411 | 98 | 149 | 145 | 103 | 37 |
| La | 33.65 | 23.96 | 19.45 | 22.68 | 29.02 | 8.22 | 39.91 | 31.87 | 24.14 | 12.56 |
| Ce | 67.2 | 45.09 | 38.15 | 37.48 | 59.24 | 19.19 | 66.79 | 34.3 | 46.87 | 21.07 |
| Pr | 7.76 | 5.58 | 4.46 | 4.66 | 7.17 | 2.63 | 10.5 | 8.59 | 5.8 | 2.62 |
| Nd | 28.55 | 22.21 | 17.55 | 18.5 | 26.53 | 13.23 | 43.51 | 38.6 | 22.91 | 10.2 |
| Sm | 5.54 | 4.99 | 4.2 | 4.92 | 5.48 | 3.9 | 9.39 | 9.4 | 5.16 | 2.25 |
| Eu | 1.14 | 1.41 | 1.14 | 1.23 | 1.46 | 1.38 | 2.92 | 3.24 | 1.38 | 0.57 |
| Gd | 5.24 | 4.29 | 3.44 | 4.46 | 5.5 | 4.27 | 9.01 | 11.76 | 4.75 | 2.18 |
| Tb | 0.8 | 0.74 | 0.55 | 0.73 | 0.82 | 0.85 | 1.43 | 1.69 | 0.64 | 0.35 |
| Dy | 4.94 | 4.32 | 3.4 | 4.56 | 4.65 | 5.26 | 8.07 | 10.61 | 3.75 | 1.91 |
| Ho | 0.96 | 0.93 | 0.62 | 0.97 | 1.05 | 1.18 | 1.62 | 2.15 | 0.71 | 0.47 |
| Er | 2.95 | 2.22 | 1.87 | 2.57 | 2.83 | 3.46 | 4.65 | 5.36 | 2.23 | 1.27 |
| Tm | 0.44 | 0.3 | 0.24 | 0.35 | 0.39 | 0.47 | 0.52 | 0.7 | 0.26 | 0.16 |
| Yb | 3.29 | 1.99 | 1.54 | 2.31 | 2.56 | 3.6 | 3.47 | 4.32 | 1.85 | 1.19 |
| Lu | 0.4 | 0.31 | 0.24 | 0.33 | 0.32 | 0.46 | 0.51 | 0.68 | 0.23 | 0.21 |
| Hf | 3.13 | 3.45 | 3.01 | 3 | 3.77 | 2.54 | 6.37 | 3.39 | 3.09 | 1.34 |
| Ta | 0.460 | 0.330 | 0.290 | 0.420 | 0.440 | 0.260 | 0.820 | 0.450 | 0.740 | 0.210 |
| Pb | 4.460 | 5.720 | 4.050 | 7.540 | 6.170 | 2.330 | 4.800 | 12.880 | 5.030 | 4.620 |
| Th | 4.670 | 2.670 | 2.930 | 5.820 | 3.310 | 1.490 | 2.800 | 1.130 | 3.300 | 2.240 |
| U | 0.620 | 0.450 | 0.810 | 1.040 | 0.550 | 0.370 | 0.760 | 0.230 | 0.880 | 0.630 |

| Sample ID | BCS2-44 | BCS2-45 | BCS2-46 | BCS2-47 | BCS2-48 | BCS2-49 | BCS2-50 | BCS2-51 | BCS2-52 | BCS2-53 |
|---|---|---|---|---|---|---|---|---|---|---|
| SiO2 | 56.436 | 56.951 | 51.381 | 50.455 | 53.981 | 51.647 | 50.926 | 55.715 | 56.541 | 50.048 |
| TiO2 | 1.237 | 0.418 | 2.226 | 2.264 | 3.008 | 2.472 | 2.817 | 1.507 | 1.598 | 2.489 |
| Al2O3 | 9.822 | 11.940 | 14.538 | 14.548 | 14.695 | 15.041 | 15.134 | 14.721 | 14.898 | 13.014 |
| FeO | 12.491 | 9.549 | 12.728 | 13.212 | 12.249 | 12.858 | 12.518 | 11.034 | 9.343 | 15.621 |
| MnO | 0.211 | 0.167 | 0.176 | 0.208 | 0.177 | 0.142 | 0.164 | 0.146 | 0.134 | 0.235 |
| MgO | 12.803 | 12.118 | 5.126 | 5.888 | 3.466 | 4.683 | 5.372 | 4.426 | 4.268 | 5.487 |
| CaO | 5.519 | 6.566 | 7.704 | 7.902 | 6.785 | 7.003 | 7.883 | 7.491 | 7.434 | 9.751 |
| Na2O | 1.311 | 2.070 | 3.997 | 3.707 | 3.497 | 3.518 | 3.505 | 3.338 | 4.227 | 2.305 |
| K2O | 0.032 | 0.146 | 1.678 | 1.412 | 1.769 | 2.178 | 1.245 | 1.454 | 1.361 | 0.724 |
| P2O5 | 0.137 | 0.073 | 0.445 | 0.405 | 0.375 | 0.457 | 0.437 | 0.167 | 0.196 | 0.326 |
| SUM | 100.000 | 100.000 | 100.000 | 100.000 | 100.000 | 100.000 | 100.000 | 100.000 | 100.000 | 100.000 |
| L.O.I. | 3.770 | 3.080 | 1.150 | 1.390 | 1.850 | 6.060 | 6.700 | 1.720 | 1.700 | -0.400 |
| Mg# | 53.246 | 58.506 | 30.913 | 33.116 | 23.917 | 28.810 | 32.288 | 30.827 | 33.671 | 28.074 |
| Fe# | 49.383 | 44.073 | 71.291 | 69.174 | 77.947 | 73.302 | 69.971 | 71.373 | 68.640 | 74.004 |
| Sc | 28 | 32 | 24 | 25 | 21 | 23 | 26 | 22 | 23 | 44 |
| V | 220 | 187 | 263 | 277 | 207 | 283 | 332 | 211 | 218 | 468 |
| Cr | 1524 | 970 | 55 | 62 | 9 | 34 | 33 | 38 | 39 | 126 |
| Co | 101 | 81 | 80 | 86 | 60 | 68 | 64 | 96 | 74 | 92 |
| Ni | 708 | 283 | 99 | 144 | 9 | 84 | 91 | 803 | 81 | 78 |
| Cu | 159 | 65 | 75 | 93 | 38 | 69 | 52 | 1636 | 58 | 241 |
| Zn | 103 | 97 | 96 | 112 | 85 | 43 | 48 | 77 | 44 | 153 |
| Rb | 1 | 11 | 45 | 35 | 53 | 93 | 33 | 51 | 38 | 20 |
| Sr | 124 | 198 | 404 | 444 | 662 | 308 | 265 | 411 | 376 | 159 |
| Y | 26 | 12 | 42 | 39 | 32 | 42 | 41 | 24 | 26 | 37 |
| Zr | 99 | 64 | 348 | 316 | 200 | 339 | 320 | 192 | 189 | 155 |
| Nb | 7.3 | 2.8 | 15 | 14 | 15.2 | 14.7 | 14.7 | 11.1 | 11.5 | 9 |
| Mo | 0.76 | 0.64 | 1.6 | 1.4 | 1.22 | 0.74 | 0.54 | 0.98 | 0.83 | 1.11 |
| Cs | 0.59 | 3.53 | 2.06 | 1.85 | 4.25 | 11.77 | 3.56 | 1.96 | 1.05 | 0.54 |
| Ba | 32 | 110 | 509 | 552 | 331 | 432 | 328 | 390 | 309 | 220 |
| La | 28.88 | 13.48 | 36.03 | 31.89 | 26.66 | 34.63 | 30.45 | 26.06 | 24.91 | 15.64 |
| Ce | 35.49 | 26.69 | 79.29 | 71.51 | 61.29 | 76.71 | 71.75 | 54.44 | 55.19 | 36.27 |
| Pr | 6.32 | 3.03 | 10.05 | 9.04 | 8.47 | 9.61 | 9.58 | 6.68 | 7.07 | 4.71 |
| Nd | 25.58 | 11.51 | 42.87 | 39.24 | 37.31 | 40.42 | 40.93 | 28.1 | 29.29 | 22.3 |
| Sm | 5.49 | 2.45 | 9.33 | 9.3 | 8.93 | 9.66 | 9.72 | 5.76 | 6.31 | 6.2 |
| Eu | 1.5 | 0.6 | 2.96 | 2.54 | 3.1 | 2.52 | 2.54 | 1.83 | 2.05 | 1.85 |
| Gd | 5.61 | 2.22 | 9.14 | 8.79 | 8.27 | 8.91 | 8.57 | 5.79 | 6.44 | 6.16 |
| Tb | 0.82 | 0.34 | 1.38 | 1.31 | 1.29 | 1.27 | 1.3 | 0.82 | 0.87 | 1.01 |
| Dy | 5.03 | 2.19 | 8.71 | 7.58 | 6.94 | 7.48 | 8.13 | 4.86 | 5.36 | 6.77 |
| Ho | 1 | 0.42 | 1.56 | 1.6 | 1.33 | 1.61 | 1.73 | 0.91 | 1.15 | 1.35 |
| Er | 2.67 | 1.25 | 4.53 | 4.22 | 3.31 | 4.26 | 4.4 | 2.84 | 2.93 | 4 |
| Tm | 0.35 | 0.16 | 0.65 | 0.59 | 0.44 | 0.59 | 0.59 | 0.36 | 0.39 | 0.65 |
| Yb | 2.26 | 1.3 | 4.55 | 3.92 | 2.62 | 4.3 | 4.01 | 2.4 | 2.75 | 4.21 |
| Lu | 0.33 | 0.24 | 0.57 | 0.54 | 0.36 | 0.56 | 0.55 | 0.34 | 0.38 | 0.57 |
| Hf | 2.6 | 1.69 | 8.72 | 8.21 | 5.56 | 8.55 | 7.85 | 5.06 | 4.91 | 4 |
| Ta | 0.430 | 0.180 | 1.030 | 0.860 | 1.020 | 0.890 | 0.890 | 0.740 | 0.710 | 0.470 |
| Pb | 14.570 | 5.720 | 5.600 | 6.780 | 4.490 | 2.260 | 2.580 | 8.200 | 3.630 | 5.420 |
| Th | 1.760 | 3.240 | 3.550 | 3.150 | 3.430 | 3.250 | 3.250 | 3.820 | 3.460 | 2.690 |
| U | 0.480 | 0.700 | 0.940 | 0.910 | 0.890 | 1.130 | 0.940 | 1.020 | 1.040 | 0.790 |

## CIPW NORM CALCULATIONS

| Sample ID | BCS1-01 | BCS1-02 | BCS1-03 | BCS1-04 | BCS1-05 | BCS1-06 | BCS1-07 | BCS1-08 | BCS1-09 | BCS1-10 | BCS1-11 | BCS1-12 | BCS1-13 | BCS1-14 | BCS1-15 | BCS1-16 | BCS1-17 | BCS1-18 | BCS1-19 | BCS1-20 | BCS1-21 | BCS1-25 |
|---|---|---|---|---|---|---|---|---|---|---|---|---|---|---|---|---|---|---|---|---|---|---|
| %AN | 58.368 | 65.762 | 58.554 | 53.220 | 59.101 | 51.754 | 61.955 | 58.061 | 54.720 | 58.255 | 60.403 | 60.577 | 51.891 | 60.862 | 58.656 | 48.011 | 44.002 | 39.587 | 32.748 | 44.200 | 33.037 | 41.325 |
| Q | 6.772 | 5.557 | 5.143 | 11.039 | 10.114 | 0.000 | 3.136 | 3.599 | 3.998 | 3.800 | 2.335 | 3.539 | 8.998 | 7.747 | 8.845 | 0.000 | 0.000 | 0.000 | 0.000 | 0.000 | 0.000 | 0.000 |
| or | 6.137 | 4.550 | 4.699 | 9.060 | 9.777 | 5.370 | 7.665 | 3.106 | 4.209 | 6.029 | 7.290 | 8.293 | 5.538 | 7.051 | 5.545 | 4.027 | 4.379 | 7.220 | 3.646 | 5.391 | 6.935 | 7.457 |
| ab | 14.581 | 11.048 | 13.212 | 23.138 | 20.094 | 27.147 | 19.415 | 15.180 | 17.059 | 20.433 | 20.313 | 13.068 | 14.471 | 12.300 | 15.730 | 21.516 | 22.030 | 35.593 | 39.986 | 24.297 | 36.046 | 34.645 |
| an | 20.442 | 21.220 | 18.665 | 26.323 | 29.037 | 29.121 | 31.617 | 21.015 | 20.616 | 28.514 | 30.986 | 20.079 | 15.608 | 19.128 | 22.318 | 19.870 | 17.310 | 23.323 | 19.471 | 19.246 | 17.784 | 24.401 |
| di | 4.872 | 4.165 | 7.026 | 10.397 | 11.829 | 13.346 | 10.923 | 28.109 | 26.998 | 11.825 | 13.134 | 28.271 | 27.870 | 20.628 | 16.692 | 32.347 | 32.250 | 3.985 | 9.154 | 25.281 | 18.122 | 17.109 |
| hy | 44.810 | 51.128 | 48.768 | 16.576 | 16.033 | 21.993 | 24.294 | 25.790 | 23.659 | 26.328 | 22.971 | 23.391 | 23.081 | 29.108 | 26.489 | 11.718 | 15.038 | 21.943 | 13.438 | 18.953 | 10.492 | 5.262 |
| ol | 0.000 | 0.000 | 0.000 | 0.000 | 0.000 | 0.075 | 0.000 | 0.000 | 0.000 | 0.000 | 0.000 | 0.000 | 0.000 | 0.000 | 0.000 | 4.768 | 2.849 | 4.526 | 10.812 | 0.062 | 3.208 | 6.742 |
| mt | 1.845 | 1.851 | 1.912 | 2.290 | 2.166 | 2.114 | 2.131 | 2.231 | 2.353 | 2.176 | 2.139 | 2.309 | 2.731 | 2.550 | 2.682 | 3.207 | 3.373 | 2.308 | 2.355 | 3.608 | 3.835 | 2.661 |
| il | 0.351 | 0.376 | 0.471 | 0.872 | 0.710 | 0.683 | 0.688 | 0.819 | 0.978 | 0.768 | 0.702 | 0.920 | 1.438 | 1.229 | 1.395 | 2.115 | 2.312 | 0.930 | 0.989 | 2.615 | 2.920 | 1.401 |
| ap | 0.190 | 0.105 | 0.104 | 0.305 | 0.239 | 0.149 | 0.129 | 0.151 | 0.130 | 0.128 | 0.129 | 0.129 | 0.264 | 0.260 | 0.305 | 0.432 | 0.458 | 0.172 | 0.151 | 0.548 | 0.657 | 0.322 |
| AF2.7 | 11.538 | 8.642 | 9.592 | 17.630 | 17.220 | 15.425 | 14.856 | 8.728 | 10.527 | 13.596 | 14.813 | 13.133 | 10.898 | 11.606 | 11.371 | 11.996 | 12.538 | 20.402 | 18.455 | 14.389 | 20.286 | 20.288 |
| PL2.7 | 29.622 | 28.176 | 26.983 | 40.891 | 41.688 | 46.214 | 43.842 | 30.573 | 31.357 | 41.379 | 43.776 | 28.307 | 24.720 | 26.872 | 32.222 | 33.417 | 31.181 | 45.734 | 44.648 | 34.544 | 40.479 | 46.215 |

| Sample ID | BCS1-26 | BCS1-27 | BCS1-28 | BCS1-29 | BCS1-30 | BCS1-31 | BCS1-32 | BCS1-33 | BCS1-34 | BCS1-35 | BCS1-36 | BCS1-37 | BCS1-38 | BCS1-39 | BCS2-01 | BCS2-02 | BCS2-03 | BCS2-04 | BCS2-05 | BCS2-06 | BCS2-07 | BCS2-08 |
|---|---|---|---|---|---|---|---|---|---|---|---|---|---|---|---|---|---|---|---|---|---|---|
| %AN | 56.808 | 41.274 | 40.318 | 50.734 | 57.209 | 64.158 | 40.228 | 73.076 | 62.944 | 63.107 | 72.245 | 65.845 | 64.250 | 34.805 | 58.391 | 66.659 | 65.210 | 64.641 | 64.490 | 61.888 | 63.589 | 64.045 |
| Q | 0.000 | 0.000 | 0.000 | 2.698 | 5.092 | 7.668 | 1.097 | 9.193 | 12.251 | 9.792 | 7.673 | 10.632 | 10.724 | 0.000 | 7.124 | 0.000 | 0.000 | 9.395 | 6.478 | 9.388 | 0.000 | 0.000 |
| or | 4.640 | 5.046 | 2.311 | 5.199 | 3.294 | 2.884 | 1.856 | 5.238 | 12.653 | 7.624 | 6.128 | 6.545 | 7.572 | 5.637 | 7.996 | 1.299 | 1.595 | 6.387 | 7.203 | 6.977 | 3.437 | 3.430 |
| ab | 17.678 | 23.663 | 33.643 | 22.857 | 20.783 | 13.801 | 32.448 | 8.909 | 17.817 | 13.755 | 8.467 | 13.168 | 13.678 | 35.699 | 19.703 | 6.912 | 7.274 | 17.454 | 17.535 | 18.417 | 10.448 | 9.984 |
| an | 23.250 | 16.631 | 22.728 | 23.538 | 27.785 | 24.704 | 21.839 | 24.181 | 30.265 | 23.528 | 22.040 | 25.387 | 24.583 | 19.058 | 27.650 | 13.819 | 13.634 | 31.909 | 31.847 | 29.907 | 18.246 | 17.783 |
| di | 13.494 | 30.869 | 17.998 | 18.185 | 16.889 | 1.816 | 21.378 | 5.911 | 2.065 | 4.437 | 6.856 | 2.271 | 4.249 | 17.098 | 17.811 | 8.577 | 9.317 | 9.181 | 12.523 | 11.431 | 6.556 | 6.505 |
| hy | 34.895 | 15.798 | 12.915 | 23.027 | 20.245 | 46.717 | 15.857 | 43.521 | 21.627 | 37.739 | 45.812 | 39.037 | 36.115 | 3.152 | 16.369 | 19.467 | 21.524 | 22.531 | 21.436 | 20.574 | 50.607 | 48.530 |
| ol | 0.151 | 1.636 | 7.138 | 0.000 | 0.000 | 0.000 | 0.000 | 0.000 | 0.000 | 0.000 | 0.000 | 0.000 | 0.000 | 11.429 | 0.000 | 47.349 | 43.885 | 0.000 | 0.000 | 0.000 | 8.285 | 11.265 |
| mt | 3.230 | 3.463 | 2.249 | 2.782 | 3.289 | 1.889 | 3.110 | 2.185 | 2.261 | 2.205 | 2.169 | 2.129 | 2.186 | 4.035 | 2.326 | 1.965 | 2.039 | 2.195 | 2.128 | 2.253 | 1.876 | 1.893 |
| il | 2.115 | 2.438 | 0.846 | 1.518 | 2.184 | 0.347 | 1.955 | 0.706 | 0.819 | 0.745 | 0.701 | 0.632 | 0.717 | 3.161 | 0.957 | 0.529 | 0.627 | 0.753 | 0.677 | 0.837 | 0.440 | 0.466 |
| ap | 0.547 | 0.457 | 0.172 | 0.197 | 0.440 | 0.174 | 0.460 | 0.154 | 0.241 | 0.176 | 0.153 | 0.199 | 0.176 | 0.732 | 0.064 | 0.084 | 0.105 | 0.196 | 0.173 | 0.217 | 0.103 | 0.144 |
| AF2.7 | 11.187 | 13.810 | 14.771 | 13.664 | 10.991 | 7.995 | 13.874 | 8.538 | 19.252 | 12.718 | 9.264 | 11.422 | 12.638 | 18.859 | 15.294 | 3.859 | 4.289 | 12.851 | 13.698 | 13.798 | 7.307 | 7.127 |
| PL2.7 | 34.380 | 31.529 | 43.910 | 37.930 | 40.870 | 33.394 | 42.269 | 29.791 | 41.483 | 32.188 | 27.372 | 33.678 | 33.195 | 41.535 | 40.055 | 18.170 | 18.214 | 42.899 | 42.888 | 41.503 | 24.825 | 24.069 |

| Sample ID | BCS2-09 | BCS2-10 | BCS2-11 | BCS2-12 | BCS2-13 | BCS2-14 | BCS2-15 | BCS2-16 | BCS2-17 | BCS2-18 | BCS2-19 | BCS2-20 | BCS2-21 | BCS2-22 | BCS2-23 | BCS2-24 | BCS2-25 | BCS2-26 | BCS2-29 | BCS2-30 | BCS2-31 | BCS2-32 |
|---|---|---|---|---|---|---|---|---|---|---|---|---|---|---|---|---|---|---|---|---|---|---|
| %AN | 66.367 | 59.092 | 59.372 | 56.831 | 54.972 | 52.643 | 58.870 | 52.466 | 61.288 | 61.123 | 54.010 | 60.176 | 60.241 | 58.357 | 57.118 | 59.546 | 61.829 | 36.492 | 62.685 | 46.986 | 101.476 | 48.972 |
| Q | 0.000 | 7.009 | 7.664 | 8.989 | 12.758 | 13.935 | 8.371 | 9.675 | 5.536 | 9.138 | 8.289 | 4.700 | 5.485 | 10.415 | 12.401 | 8.544 | 4.378 | 0.000 | 0.448 | 7.070 | 0.000 | 8.177 |
| or | 2.422 | 6.881 | 7.259 | 6.920 | 10.217 | 10.845 | 6.586 | 7.767 | 5.749 | 6.305 | 7.799 | 5.262 | 4.431 | 12.531 | 9.678 | 6.626 | 4.619 | 3.687 | 6.689 | 7.975 | 0.245 | 10.140 |
| ab | 7.362 | 18.022 | 19.447 | 20.940 | 21.107 | 22.757 | 14.104 | 21.489 | 13.654 | 19.165 | 19.021 | 13.815 | 13.559 | 19.419 | 20.612 | 15.746 | 12.060 | 33.713 | 18.208 | 26.685 | -0.280 | 25.254 |
| an | 14.526 | 26.032 | 28.419 | 27.567 | 25.768 | 25.297 | 20.188 | 23.718 | 21.616 | 30.132 | 22.338 | 20.876 | 20.544 | 27.212 | 27.456 | 23.178 | 19.534 | 19.371 | 30.587 | 23.651 | 19.231 | 24.236 |
| di | 4.938 | 11.198 | 9.564 | 14.109 | 9.126 | 6.860 | 6.703 | 8.104 | 9.124 | 11.533 | 16.624 | 9.649 | 9.061 | 7.677 | 9.397 | 8.391 | 8.276 | 19.915 | 20.669 | 13.809 | 7.412 | 13.770 |
| hy | 43.282 | 27.984 | 24.772 | 18.413 | 18.127 | 17.389 | 41.493 | 26.441 | 41.573 | 20.550 | 22.733 | 43.024 | 44.244 | 19.802 | 17.453 | 34.975 | 48.536 | 9.761 | 20.819 | 16.701 | 32.462 | 15.335 |
| ol | 25.219 | 0.000 | 0.000 | 0.000 | 0.000 | 0.000 | 0.000 | 0.000 | 0.000 | 0.000 | 0.000 | 0.000 | 0.000 | 0.000 | 0.000 | 0.000 | 0.000 | 6.072 | 0.000 | 0.000 | 38.705 | 0.000 |
| mt | 1.796 | 2.098 | 2.090 | 2.165 | 2.068 | 2.083 | 1.949 | 2.040 | 2.014 | 2.188 | 2.204 | 1.990 | 1.992 | 2.120 | 2.138 | 1.929 | 1.949 | 3.870 | 1.991 | 2.549 | 1.856 | 2.130 |
| il | 0.354 | 0.623 | 0.609 | 0.699 | 0.591 | 0.596 | 0.480 | 0.572 | 0.565 | 0.751 | 0.798 | 0.536 | 0.536 | 0.652 | 0.669 | 0.440 | 0.503 | 2.947 | 0.502 | 1.210 | 0.304 | 0.677 |
| ap | 0.102 | 0.152 | 0.174 | 0.197 | 0.238 | 0.240 | 0.127 | 0.193 | 0.170 | 0.238 | 0.193 | 0.148 | 0.148 | 0.174 | 0.196 | 0.171 | 0.147 | 0.663 | 0.086 | 0.350 | 0.065 | 0.281 |
| AF2.7 | 5.148 | 13.556 | 14.461 | 14.675 | 18.034 | 19.273 | 11.809 | 15.726 | 10.806 | 13.403 | 14.844 | 10.379 | 9.452 | 19.723 | 17.313 | 12.458 | 9.085 | 16.173 | 13.433 | 17.858 | 0.142 | 19.494 |
| PL2.7 | 19.161 | 37.379 | 40.664 | 40.752 | 39.058 | 39.625 | 29.068 | 37.248 | 30.213 | 42.199 | 34.315 | 29.574 | 29.081 | 39.439 | 40.434 | 33.092 | 27.127 | 40.598 | 42.052 | 40.453 | 19.054 | 40.136 |

| Sample ID | BCS2-33 | BCS2-34 | BCS2-35 | BCS2-36 | BCS2-37 | BCS2-38 | BCS2-40 | BCS2-41 | BCS2-42 | BCS2-44 | BCS2-45 | BCS2-46 | BCS2-47 | BCS2-48 | BCS2-49 | BCS2-50 | BCS2-51 | BCS2-52 | BCS2-53 |
|---|---|---|---|---|---|---|---|---|---|---|---|---|---|---|---|---|---|---|---|
| %AN | 43.469 | 36.059 | 40.529 | 41.485 | 58.636 | 39.152 | 52.041 | 38.353 | 77.690 | 63.887 | 55.152 | 31.854 | 36.201 | 37.919 | 37.335 | 41.020 | 41.080 | 31.753 | 52.667 |
| Q | 8.713 | 6.781 | 5.768 | 8.240 | 2.195 | 0.000 | 0.000 | 4.932 | 9.501 | 12.009 | 8.131 | 0.000 | 0.000 | 7.422 | 0.532 | 1.642 | 6.648 | 5.300 | 3.699 |
| or | 9.869 | 7.605 | 6.172 | 10.300 | 1.837 | 4.265 | 2.215 | 0.926 | 0.310 | 0.189 | 0.858 | 9.986 | 8.410 | 10.672 | 13.037 | 7.441 | 8.699 | 8.064 | 4.407 |
| ab | 28.602 | 34.859 | 24.983 | 28.608 | 19.735 | 32.700 | 16.087 | 25.056 | 7.915 | 11.849 | 18.442 | 36.165 | 33.554 | 32.057 | 31.999 | 31.847 | 30.341 | 38.067 | 21.320 |
| an | 21.993 | 19.658 | 17.026 | 20.282 | 27.976 | 21.040 | 17.456 | 15.588 | 27.561 | 20.962 | 22.678 | 16.905 | 19.040 | 19.581 | 19.065 | 22.149 | 21.154 | 17.711 | 23.722 |
| di | 13.884 | 11.970 | 22.393 | 10.178 | 18.426 | 17.469 | 34.092 | 17.602 | 4.989 | 4.558 | 7.336 | 14.947 | 14.255 | 9.836 | 10.487 | 11.637 | 12.297 | 14.398 | 19.134 |
| hy | 12.796 | 15.277 | 20.025 | 18.468 | 24.059 | 15.558 | 14.263 | 31.145 | 47.000 | 45.440 | 39.765 | 8.271 | 9.762 | 10.478 | 16.073 | 15.676 | 15.125 | 10.520 | 19.118 |
| ol | 0.000 | 0.000 | 0.000 | 0.000 | 0.000 | 0.846 | 10.128 | 0.000 | 0.000 | 0.000 | 0.000 | 5.681 | 6.919 | 0.000 | 0.000 | 0.000 | 0.000 | 0.000 | 0.000 |
| mt | 2.538 | 2.444 | 2.401 | 2.463 | 3.273 | 4.129 | 3.234 | 2.852 | 2.052 | 2.971 | 2.060 | 3.982 | 4.027 | 4.877 | 4.349 | 4.713 | 3.256 | 3.297 | 4.328 |
| il | 1.214 | 1.105 | 1.037 | 1.113 | 2.195 | 3.283 | 2.133 | 1.616 | 0.541 | 1.734 | 0.578 | 3.125 | 3.179 | 4.278 | 3.489 | 3.971 | 2.125 | 2.233 | 3.571 |
| ap | 0.391 | 0.301 | 0.195 | 0.347 | 0.303 | 0.710 | 0.392 | 0.284 | 0.132 | 0.289 | 0.152 | 0.938 | 0.854 | 0.800 | 0.969 | 0.924 | 0.354 | 0.411 | 0.703 |
| AF2.7 | 20.462 | 20.515 | 15.425 | 20.896 | 9.147 | 16.376 | 8.173 | 10.206 | 3.241 | 4.577 | 7.688 | 23.381 | 20.838 | 22.545 | 24.888 | 19.236 | 19.936 | 22.162 | 12.303 |
| PL2.7 | 40.002 | 41.606 | 32.756 | 38.294 | 40.402 | 41.629 | 27.584 | 31.363 | 32.545 | 28.422 | 34.290 | 39.675 | 40.167 | 39.765 | 39.213 | 42.200 | 40.258 | 41.679 | 37.145 |